UNIVERSITI TEKNOLOGI MARA

STUDY OF NANOFILLER-PALM KERNEL SHELL-DERIVED CARBON-GRAPHITE-COPPER FORMULATION FOR RAIL PANTOGRAPH SLIDE MATERIAL USING WARM COMPACTION PROCESS

FAZIRA SURIANI
BINTI MOHAMED FADZIL

PhD

May 2026

UNIVERSITI TEKNOLOGI MARA

STUDY OF NANOFILLER-PALM KERNEL SHELL-DERIVED CARBON-GRAPHITE-COPPER FORMULATION FOR RAIL PANTOGRAPH SLIDE MATERIAL USING WARM COMPACTION PROCESS

FAZIRA SURIANI
BINTI MOHAMED FADZIL

Thesis submitted in fulfilment
of the requirements for the degree of
Doctor of Philosophy
(Mechanical Engineering)

Faculty of Mechanical Engineering

May 2026

CONFIRMATION BY PANEL OF EXAMINERS

I certify that a Panel of Examiners has met on 10 February 2026 to conduct the final examination of Fazira Suriani binti Mohamed Fadzil on her Doctor of Philosophy thesis entitled "Study of Nanofiller-Palm-Kernel Shell-Derived Carbon-Graphite-Copper Formulation for Rail Pantograph Slide Material using Warm Compaction Process" in accordance with Universiti Teknologi MARA Act 1976 (Akta 173). The Panel of Examiners recommends that the student be awarded the relevant degree. The Panel of Examiners was as follows:

Hamid Yusoff, PhD
Associate Professor
Faculty of Mechanical Engineering
Universiti Teknologi MARA
(Chairman)

Aidah Jumahat, PhD
Professor
Faculty of Mechanical Engineering
Universiti Teknologi MARA
(Internal Examiner)

Jaharah A. Ghani, PhD
Professor
Fakulti Kejuruteraan dan Alam Bina
Universiti Kebangsaan Malaysia
(External Examiner)

PROFESSOR DR HJH ZURAEDA IBRAHIM
Dean
Institute of Postgraduates Studies
Universiti Teknologi MARA

Date: 19 May 2026

AUTHOR'S DECLARATION

I declare that the work in this thesis was carried out in accordance with the regulations of Universiti Teknologi MARA. It is original and is the result of my own work, unless otherwise indicated or acknowledged as referenced work. This thesis has not been submitted to any other academic institution or non-academic institution for any degree or qualification.

I, hereby, acknowledge that I have been supplied with the Academic Rules and Regulations for Postgraduate, Universiti Teknologi MARA, regulating the conduct of my study and research.

Name of Student	:	Fazira Suriani Binti Mohamed Fadzil
Student ID. No.	:	2023127521
Programme	:	Doctor of Philosophy (Mechanical Engineering) – CEEM950
Faculty	:	Mechanical Engineering
Thesis Title	:	Study of Nanofiller-Palm Kernel Shell-Derived Carbon-Graphite-Copper Formulation for Rail Pantograph Slide Material using Warm Compaction Process
Signature of Student	:	
Date	:	May 2026

ABSTRACT

Pantograph slides are important components in electric railway systems, ensuring uninterrupted electrical contact between the pantograph and the overhead catenary wire. In Malaysia, these components are entirely imported, leading to heavy dependence on foreign suppliers that limits operational efficiency and restricts local industry growth and technological development. Therefore, this study aims to study the formulation of carbon-copper composites using locally available raw materials, specifically palm kernel shell (PKS)-derived carbon fabricated using a warm compaction method. Various PKS-derived carbon-graphite ratios were studied to achieve a balance between mechanical strength and electrical conductivity. Comprehensive testing was conducted to characterise the developed composites, such as X-ray diffraction (XRD), scanning electron microscopy (SEM), energy-dispersive X-ray spectroscopy (EDX), and Raman spectroscopy. The optimum formulation at 65 wt% carbon (80% graphite and 20% PKS-derived carbon), 20 wt% copper, and 15 wt% phenolic resin was identified. The effect of filler type (graphene oxide, carbon nanotubes, and copper-coated carbon nanotubes) and content (from 1 wt% to 3 wt%) were investigated. 1 wt% of carbon nanotubes (CNT) was identified as the most effective filler in enhancing both conductivity and strength. The optimum condition of the warm compaction process was determined using Taguchi L_9 orthogonal array based on three parameters: temperature, time, and pressure. It is identified that the pressure is the dominant factor, followed by compaction time and temperature. Signal-to-noise (S/N) ratio and analysis of variance (ANOVA) resulted in two distinct optimum samples: one optimised for the lowest electrical resistivity (OPT2) and another for the highest transverse rupture strength (OPT1). Eliminating the post-baking step still preserved the properties of the composites, keeping them within the range and comparable to those of commercial pantograph slides. Electrical resistivity measurements showed that OPT2 compacted at 200°C, 50 tonnes and 5 minutes recorded the lowest value at 14.2 μΩ.m, meeting requirements for efficient electrical conduction. Tribological behaviour was evaluated using the pin-on-disc test against a copper disc to simulate pantograph-catenary interaction. The results showed that both OPT1 and OPT2 exhibited comparable wear rates. However, OPT2 achieved significantly lower coefficient of friction (0.1761) and friction force (1.7607 N) compared to OPT1 (0.2936 and 2.9361N, respectively). SEM and EDX analysis of the work pins revealed that OPT2 developed a stable and compact tribofilm with minimal debris, resulting in smoother wear scars. The optimum OPT2 showed compatible performance with density of 1.898 g/cm^3, hardness of 94.5 HRR, and transverse rupture strength (TRS) of 45.6 MPa. This study demonstrated that the optimised PKS-derived carbon-graphite-copper composites, in terms of composition, filler type, and processing parameters, can meet the performance of commercialised pantograph slides. The novelty of this study lies in the integration of a new natural PKS-derived carbon-graphite-copper with advanced nanomaterial (CNT) reinforcement and phenolic resin as a binder to produce a railway component through the warm compaction method without post-baking. The findings support pantograph slide fabrication using local material (PKS-derived carbon), promote sustainability using palm oil wastes, and enhance the understanding of wear mechanisms in natural-carbon-based composites under dry sliding conditions.

ACKNOWLEDGEMENT

I would like to express my sincere gratitude to all those who have contributed to the successful completion of this research. Without their support, guidance, and encouragement, this work would not have been possible.

First and foremost, I would like to thank my supervisor, Assoc. Prof. Ir. Dr. Koay Mei Hyie, for her invaluable guidance, patience, and unwavering support throughout my PhD journey. Her expertise and insightful feedback were very helpful in shaping this research.

I am also grateful to my co-supervisor, Ts. Dr. Mohd. Asri Selamat for his valuable support and assistance. His expertise and advice were essential in forming the direction of this research.

I would like to extend my thanks to the Advanced Materials Research Centre (AMREC) SIRIM Berhad and the Mechanical Engineering Studies, UiTM Cawangan Pulau Pinang and UiTM Shah Alam for providing me with excellent research facilities and a conducive research environment. I am also grateful to the technical staff for their assistance in conducting the lab work.

Special appreciation to SIRIM Berhad for the financial assistance by granting a full-time study leave and a research grant under SIRIM Industrial Research Fund (SR230004), in making this journey to be realised. Also, I would like to express my full gratitude to IPSIS and the Postgraduate support group of UiTM for their constant support throughout the study.

I would like to acknowledge the contributions of the management team, researchers and supporting staff in AMREC, who provided valuable discussions, feedback, and support. I am also particularly grateful to my colleagues and Road to PhD team members for their unwavering encouragement.

Finally, I would like to thank my family, especially my other half, Tengku Mohamad Albaijure, my mother, my siblings, family members, and dear friends for their everlasting love, support, and understanding. Their sacrifices and tremendous encouragement have been a persistent source of strength throughout my academic journey.

May this humble thesis bring benefit in some way to those who read it.

Thank you.

TABLE OF CONTENTS

		Page
CONFIRMATION BY PANEL OF EXAMINERS		**ii**
AUTHOR'S DECLARATION		**iii**
ABSTRACT		**iv**
ACKNOWLEDGEMENT		**v**
TABLE OF CONTENTS		**vi**
LIST OF TABLES		**xi**
LIST OF FIGURES		**xiii**
LIST OF PLATES		**xvi**
LIST OF SYMBOLS		**xix**
LIST OF ABBREVIATIONS		**xx**
CHAPTER 1 INTRODUCTION		**1**
1.1	Overview	1
1.2	Research Background	2
1.3	Problem Statement	5
1.4	Research Question	7
1.5	Research Objectives	8
1.6	Scope of Study	8
1.7	Significance of Study	10
CHAPTER 2 LITERATURE REVIEW		**13**
2.1	Introduction	13
2.2	Electric Railway Advancement	13
	2.2.1 Electric Railway in Southeast Asia	14
	2.2.2 Electric Railway Systems in Malaysia	14
2.3	Pantograph-Catenary System	16
2.4	Development of Pantograph Slide	20
	2.4.1 Overview	20
	2.4.2 Properties Requirement	26

2.5 Pantograph Slide Materials 29
2.5.1 Graphite-Copper Composite 30
2.5.2 Carbon-Graphite Composite 31
2.5.3 Carbon-Copper Composite 32
2.5.4 Carbon-Carbon Composite 32
2.5.5 Carbon Source 33
2.5.6 Binder 36
2.5.7 Additives and Fillers 37
2.6 Pantograph Slide Processing Methods 41
2.6.1 Powder/Metal Impregnation 41
2.6.2 Powder Metallurgy 42
2.6.3 Development of Green Body 42
2.6.4 Warm Compaction 43
2.6.5 Post Treatment 43
2.6.6 Summary of Methods 44
2.7 Pantograph Slide Processing Factor 45
2.7.1 Warm Compaction Temperature 45
2.7.2 Warm Compaction Time 45
2.7.3 Warm Compaction Pressure 46
2.8 Determination of Optimum Condition 46
2.8.1 Design of Experiment 46
2.8.2 Full-Factorial Method 47
2.8.3 Taguchi Method 47
2.9 Testing and Characterisation 49
2.9.1 Physical 50
2.9.2 Mechanical 50
2.9.3 Electrical 50
2.9.4 Wear 51
2.10 Research Gap 52
2.11 Summary 57

CHAPTER 3 RESEARCH METHODOLOGY 58
3.1 Introduction 58
3.2 Raw Materials Description 59

3.3 Methodology of the Research Study and Design of Experiment (DOE) 61
3.4 Fabrication of Carbon-Copper Composite 63
3.4.1 Mixing of Materials (Dry Mixing) 63
3.4.2 Development of Preform (Cold Pressing) 64
3.4.3 Development of Carbon-Copper Composite (Warm Compaction) 65
3.4.4 Post-baking of Carbon-Copper Composite 66
3.5 Phase 1: Formulation of Carbon-Copper Composite 67
3.6 Phase 2: Effects of Filler Type and Composition 71
3.7 Phase 3: Optimum Condition of Process Flow and Parameter 73
3.8 Phase 4: Wear Characterisation of the Carbon-Copper Composite 77
3.9 Preparation of Specimen for Testing and Characterisation 81
3.10 Testing and Characterisation 82
3.10.1 Scanning Electron Microscopy (SEM) and EDX 82
3.10.2 X-Ray Diffraction (XRD) 83
3.10.3 Raman Spectroscopy 85
3.10.4 ImageJ Software for Powder Particle Analysis 86
3.10.5 Density 87
3.10.6 Hardness 89
3.10.7 Transverse Rupture Strength (TRS) 89
3.10.8 Electrical Resistivity 90
3.10.9 Confocal Microscopy 92

CHAPTER 4 RESULTS AND DISCUSSION 94
4.1 Introduction 94
4.2 Raw Materials Characterisation and Analysis 94
4.2.1 Powder Structure and Particle Size Analysis 95
4.2.2 Powder Phase Composition 100
4.3 Effects of PKS-derived Carbon Content on the Properties of Carbon-Copper Composite 107
4.3.1 Formation of the Carbon-Copper Composite 107
4.3.2 Characterisation of the Carbon-Copper Composite 111
4.4 Effects of Graphite/PKS-derived Carbon Ratio on the Properties of Carbon-Copper Composite 116
4.4.1 Density 117

4.4.2 Hardness 120
4.4.3 Transverse Rupture Strength 123
4.4.4 Electrical Resistivity 126
4.5 Effects of Different Filler Addition on the Properties of Carbon-Copper Composite 130
4.5.1 Density 131
4.5.2 Hardness 132
4.5.3 Transverse Rupture Strength (TRS) 134
4.5.4 Electrical Resistivity 135
4.6 Effects of CNT Addition on the Properties of Carbon-Copper Composite 139
4.6.1 Density 139
4.6.2 Hardness 142
4.6.3 Transverse Rupture Strength (TRS) 144
4.6.4 Electrical Resistivity 146
4.7 Effects of Post-baking Process 147
4.8 Optimum Condition of Warm Compaction Process Parameter using the Taguchi Method 153
4.8.1 Experimental Data 154
4.8.2 Data Analysis 154
4.8.3 Main Effects and S/N Ratio Analysis 155
4.8.4 ANOVA for Factor Significance 159
4.8.5 Experimental Data Validation 162
4.9 Tribological Characterisation on the Carbon-Copper Composite 167
4.9.1 Wear Rate 167
4.9.2 Coefficient of Friction 168
4.9.3 Friction Force 169
4.9.4 Morphology of Pin and Disc Worn Surface 170
4.10 Summary 179

CHAPTER 5 CONCLUSION AND RECOMMENDATION 184
5.1 Conclusion 184
5.2 Recommendation 186

REFERENCES **188**

AUTHOR'S PROFILE **214**

LIST OF TABLES

Tables	Title	Page
Table 2.1	Top-running Electric Train in Southeast Asia (In Operation)	14
Table 2.2	Top-running Electric Train in Southeast Asia (Under Construction)	14
Table 2.3	Current Collector Type in Rail Systems in Malaysia	16
Table 2.4	Summary of Research in Pantograph Slide Development for the Past 10 Years	24
Table 2.5	Technical Data of Commercial Pantograph Carbon Slides of Different Manufacturers	26
Table 2.6	Comparison of Different Filler Types	38
Table 2.7	Summary of Pantograph Slide Processing Methods	44
Table 2.8	Previous Studies of Carbon-Copper Composite for Current Collector Application Using Warm Compaction Method	55
Table 3.1	List of Powder Materials Used in the Experimental Work	59
Table 3.2	Shaker Mixer Specification	64
Table 3.3	Automatic Hydraulic Press Specification	65
Table 3.4	Hydraulic Compression Moulding Press Specification	66
Table 3.5	Raw Material Composition for Phase 1	69
Table 3.6	Graphite to PKS-derived carbon ratio for Phase 1	70
Table 3.7	Filler Type and Composition for Phase 2	72
Table 3.8	Best Filler Composition Study in the Carbon-Copper Composite	73
Table 3.9	Setting of Warm Compaction Parameter for Phase 3	76
Table 3.10	Orthogonal Array L_9 for Experimental Runs in Phase 3	76
Table 3.11	Pin-on-Disk Parameter Setting for Wear Characterisation	80
Table 4.1	Properties of Carbon-Copper Composite Samples in Phase 1 (Effect of Carbon Composition)	111
Table 4.2	Hardness Values of Carbon-Copper Composite at Different Graphite/PKS-derived carbon Ratios	120

Table 4.3	TRS of Carbon-Copper Composite at Different Graphite/PKS-derived carbon Ratios	124
Table 4.4	Characterisation of Carbon-Copper Composites With and Without Post-baking Process	148
Table 4.5	Experimental Data from Taguchi Design	154
Table 4.6	Response Table for Mean Resistivity	155
Table 4.7	Response Table for S/N Ratio	157
Table 4.8	ANOVA for Resistivity	159
Table 4.9	Optimum Condition for Smaller is Better for Resistivity	160
Table 4.10	Analysis of Variance (ANOVA) for TRS	161
Table 4.11	Optimum Condition for Larger is Better for TRS	161
Table 4.12	Comparison of TRS and Resistivity of Optimised Samples with Commercial Pantograph Slide Data	162
Table 4.13	New Formulation of Carbon-Copper Composite at a Graphite/PKS-derived carbon Ratio of 80:20	179
Table 4.14	Wear Test Results	182
Table 4.15	Comparison of Properties of Developed Carbon-Copper Composite and Commercial Pure Carbon Pantograph Slide	183

LIST OF FIGURES

Figures	Title	Page
Figure 1.1	Pantograph-Catenary System	2
Figure 2.1	Function of Pantograph-catenary System	18
Figure 2.2	Development of Pantograph Processes and Materials in Asia	21
Figure 2.3	Previous Research and Gap on Process, Main Material, and Additional Material for the Development of Pantograph Carbon Slide	52
Figure 3.1	Methodology of Research Work	62
Figure 3.2	Schematic Diagram of Fabrication Process Flow of Carbon-Copper Composite	63
Figure 3.3	Post-baking Temperature Profile	67
Figure 3.4	Flowchart for the Study of Formulation of Carbon-Copper Composite (Phase 1)	68
Figure 3.5	Flowchart for the Study of Filler Type and Composition (Phase 2)	71
Figure 3.6	Flowchart for the Study of Filler Type and Composition (Phase 3)	74
Figure 3.7	Flowchart of the Taguchi Method Experimental Set-Up	75
Figure 3.8	Process Flow for Wear Characterisation Study (Phase 4)	78
Figure 3.9	Schematic Diagram of Pin-on-Disk Wear Test System	80
Figure 3.10	Schematic X-Ray diffraction	84
Figure 3.11	Electrical Resistivity Measurement by Two-Probe Method	91
Figure 4.1	Size Distribution of Copper Powder	97
Figure 4.2	XRD Pattern of PKS-derived Carbon Powder	101
Figure 4.3	XRD Pattern of Graphite Powder	102
Figure 4.4	XRD Pattern of Copper Powder	103
Figure 4.5	XRD Pattern of Phenolic Resin	104
Figure 4.6	XRD Pattern of GO Powder	104
Figure 4.7	XRD Pattern of Cu-CNT Powder	105
Figure 4.8	XRD Pattern of CNT	106

Figure 4.9	Schematic Illustration of (a) PKS, (b) Copper, (c) Resin, and (d) the Mixtures	109
Figure 4.10	Density of Carbon-Copper Composite at Different Graphite to PKS-derived Carbon Ratio	117
Figure 4.11	Electrical Resistivity of Carbon-Copper Composite at Different Graphite to PKS-derived carbon Ratios	127
Figure 4.12	Density of Carbon-Copper Composites with Different Types of Fillers	132
Figure 4.13	Hardness of Carbon-Copper Composite with Different Type of Fillers	133
Figure 4.14	TRS of Carbon-Copper Composite with Different Types of Fillers	135
Figure 4.15	Resistivity of Carbon-Copper Composite	136
Figure 4.16	EDX Line Scanning for Carbon-Copper Composite without CNT	138
Figure 4.17	EDX Line Scanning for Carbon-Copper Composite with CNT Addition	138
Figure 4.18	Density of Carbon-Copper Composite at Different CNT Contents	140
Figure 4.19	XRD Pattern of Carbon-Copper Composites with Different CNT Contents	141
Figure 4.20	Hardness Carbon-Copper Composites with Different CNT Contents	142
Figure 4.21	TRS of Carbon-Copper Composites with Different CNT Contents	145
Figure 4.22	Resistivity of Carbon-Copper Composite at Different CNT Contents	146
Figure 4.23	Raman Spectra of Carbon-Copper Composite	148
Figure 4.24	XRD Spectrum of Carbon-Copper Composite	149
Figure 4.25	Altered Process Route for Developing Carbon-Copper Composite	152
Figure 4.26	Main Effects Plot for S/N Ratio in Resistivity	156
Figure 4.27	Main Effects Plot for S/N Ratio in TRS	157
Figure 4.28	XRD spectra for OPT1 and OPT2	164

Figure 4.29	Raman Spectra of OPT1 and OPT2	166
Figure 4.30	Wear Rates for OPT1 and OPT2	168
Figure 4.31	Coefficient of Friction for OPT1 and OPT2	169
Figure 4.32	Friction Force of OPT1 and OPT2	170
Figure 4.33	Roughness Profile for OPT1	178
Figure 4.34	Roughness Profile for OPT2	178

LIST OF PLATES

Plates	Title	Page
Plate 1.1	Pantograph Slides Fixed to a Pantograph Head on Top of the Train	3
Plate 2.1	Pantograph Slide Set-Up on KTMB Komuter	17
Plate 3.1	Mixing of Powders: (a) Turbula Shaker Mixer, and (b) Mixing Container	64
Plate 3.2	Cold Pressing: (a) Balance to Weigh Mixed Powder, (b) Mould, (c) Automatic Hydraulic Press for Preforming, and (d) Preform Ejected from Mould	65
Plate 3.3	Warm Compaction: (a) Four-Cavity Mould and (b) Hydraulic Compression Moulding Press	66
Plate 3.4	Microprocessor-Controlled Oven for Post-baking Process	67
Plate 3.5	Magnum Pin on Disk Wear and Friction Test System	79
Plate 3.6	Struers Secotom Cutter with Alumina Blade	81
Plate 3.7	Preparation of Sample Before Testing (a) Sample Before Cutting (b) Sample After Cutting	81
Plate 3.8	HITACHI Tabletop SEM for Micrograph of Raw Materials	82
Plate 3.9	Leo SEM/EDX for Micrograph of Raw Materials	83
Plate 3.10	XRD Analysis: (a) Powder in Sample Holder, (b) Bruker D8 XRD	84
Plate 3.11	Renishaw Raman Microscope	85
Plate 3.12	ImageJ Software Interface used to Measure Particle Size of Powder Samples	86
Plate 3.13	ImageJ Software Interface used to Measure Irregular Shape Powder Particles	87
Plate 3.14	Densitometer for Density Measurement of the Composite	88
Plate 3.15	Rockwell Hardness Tester	89
Plate 3.16	INSTRON Series IX/s Automated Materials for TRS Tests	90
Plate 3.17	Automotive Meter for Electrical Resistance Test	92
Plate 3.18	Confocal Laser Scanning Microscope	93

Plate 4.1	Particle Morphology of PKS-derived carbon at magnifications of (a) 100x and (b) 2500x	95
Plate 4.2	Particle Morphology of Graphite at magnification of 100x	96
Plate 4.3	Particle Morphology of Copper Powder at magnifications of (a) 100x and (b) 2000x	96
Plate 4.4	Particle Morphology of Phenolic Resin (a) 100x magnification and (b) 500x magnification	97
Plate 4.5	Particle Morphology of Graphene Oxide at (a) 100x Magnification	98
Plate 4.6	Particle Morphology of Cu-CNT at (a) 100x Magnification	98
Plate 4.7	Particle Morphology of CNT	99
Plate 4.8	Successful Cold-Pressed Powder for 65 wt% PKS-derived carbon and 70 wt% PKS-derived carbon	107
Plate 4.9	Failed Cold-Pressed Powder for A01, A02, and A05	107
Plate 4.10	SEM Micrograph of Carbon-Copper Composite Cross-Section at 50X Magnification: (a) 65 wt% PKS-derived carbon and (b) 70 wt% PKS-derived carbon	113
Plate 4.11	EDX image of Sample A03 (65 wt% PKS-derived Carbon, 20 wt% Copper, 15 wt% Resin)	114
Plate 4.12	EDX image of Sample A04 (70 wt% PKS, 15 wt% Copper, 15 wt% Resin)	115
Plate 4.13	SEM Micrographs for Carbon-Copper Composite Sample (a) B05 (20:80 Graphite/PKS-derived carbon ratio) and (b) B01 (80:20 Graphite/PKS-derived carbon ratio)	119
Plate 4.14	SEM Micrograph of Carbon-Copper Composite with Graphite to PKS-derived carbon Ratios of (a) 20:80 and (b) 80:20	123
Plate 4.15	SEM Micrograph of Cross-Section of Developed Composite	126
Plate 4.16	Micrograph of Carbon-Copper Composites with Graphite-to-PKS-derived carbon Ratios of (a) 20:80 and (b) 80:20	129
Plate 4.17	SEM Micrographs of Carbon-Copper Composite with (a) 1 wt% CNT and (b) 3 wt% CNT	143
Plate 4.18	SEM Micrographs of Carbon-Copper Composite	151
Plate 4.19	SEM Micrographs of OPT1 (Mag. 50x)	163
Plate 4.20	SEM Micrographs of OPT2 (Mag. 50x)	164

Plate 4.21	SEM Micrograph of Worn Surface of Pin Specimen	171
Plate 4.22	EDX Spots and Spectrum for Pin Surface of Sample OPT1 (a,b) and OPT2 (c,d) on Bright Area and Dark Area	173
Plate 4.23	Wear Track on Copper Disk	174
Plate 4.24	SEM micrograph of the Wear Track on the Copper Disk for the Sample (a) OPT1 and (b) OPT2	175
Plate 4.25	EDX Spots and Spectrums for Disk Surface of OPT1 (a,b) and OPT 2 (c,d)	176

LIST OF SYMBOLS

Symbols

A	Cross-sectional Area of Sample
b	Width of the Specimen
d_{hkl}	Interplanar Distance
h	Thickness of the Specimen
I	Current
L	Span between the Supports
l	Length of Sample
λ	Wavelength of the Incoming Wave
m	Mass of Specimen
n_r	Order of Reflection
P	Maximum Load Applied
R	Resistance
R_a	Roughness
ρ	Density
ρ_E	Electrical Resistivity
θ	Angle of Reflection
V	Voltage

LIST OF ABBREVIATIONS

Abbreviations

ANOVA	Analysis of Variance
ASTM	American Standard Testing Method
ATS	Autonomous Rapid Transit
C/C	Carbon-Carbon
CFRP	Carbon Fibre Reinforced Polymer
CNT	Carbon Nanotubes
CVD	Chemical Vapour Deposition
DOE	Design of Experiment
EDX	Electron Dispersive X-Ray Spectroscopy
ERL	Express Rail Link
ETS	Electric Train Service
GO	Graphene Oxide
KLIA	Kuala Lumpur International Airport
KTMB	Keretapi Tanah Melayu Berhad
MITI	Ministry of Investment, Trade, and Industry
MRT	Mass Rapid Transit
MWCNT	Multi-walled Carbon Nanotube
NIMP	New Industrial Master Plan
NKEA	National Key Economic Areas
PKS	Palm Kernel Shell
PM	Powder Metallurgy
RTS	Rapid Transit System
SDG	Sustainable Development Goals
SEM	Scanning Electron Microscopy
SG	Sulfonated Graphene
TRS	Transverse Rupture Strength
XRD	X-Ray Diffraction

CHAPTER 1
INTRODUCTION

1.1 Overview

The performance of the pantograph slides to transfer electrical power from the substation to the moving trains has been discussed globally. Research has been done actively worldwide to improve its properties and performance. The main properties of a good pantograph slide include its wear resistance and electrical resistivity. These properties could be enhanced by studying the materials and optimising the consolidation process. The utilisation of natural carbon in developing carbon-copper composites has been an area of interest for the past years. It has been proven that palm kernel shells (PKS)-derived carbon-copper composite material can be used in many applications, including as current collectors in a third rail system. The use of carbon composite as a material for pantograph slides in railway applications has also been widely established. Currently, the demand for the use of natural carbon from PKS and coconut shells has been explored as an alternative replacement for conventional carbon or graphite to benefit the environment and enhance sustainability. Although the properties of natural carbon may have drawbacks in terms of its properties compared to those of conventional carbon or graphite, the incorporation of copper and graphene or carbon nanotubes (CNT) into the composite is suggested to improve the electrical properties and mechanical strength, making it appropriate for the application. This study was conducted to further investigate the mechanical performance, electrical performance, and physical properties of the newly developed composite using the warm compaction method, as explained in the following subchapters.

1.2 Research Background

In the development of electrified railways, the performance of the pantograph is important, which is to ensure the consistency of electric energy transmission from the catenary system to the moving train [1]. The pantograph is positioned on the roofs of train cars, while the catenary, a configuration of cable, is positioned above the tracks. The pantograph slide serves as a device for transmitting electric energy [2][3]. It is a crucial component of electrical rail systems, ensuring dependable and efficient electrical energy transfer from traction substations to moving trains [4].

In Malaysia, several electrical railway systems are in operation, including Keretapi Tanah Melayu Berhad (KTMB) Electric Train Service (ETS), Kuala Lumpur International Airport (KLIA) Terminal Express Rail Link (ERL), and KTMB Komuter. These are the top-running railways, which refers to trains operating with electrification through a pantograph-catenary system. KTM ETS, KTM Komuter, and ERL run on a 25 kV 50 Hz electrification system using an overhead pantograph-catenary setup [5]. Figure 1.1 illustrates the pantograph-catenary system. This system significantly contributes to facilitating intracity and intercity transportation within Malaysia [6].

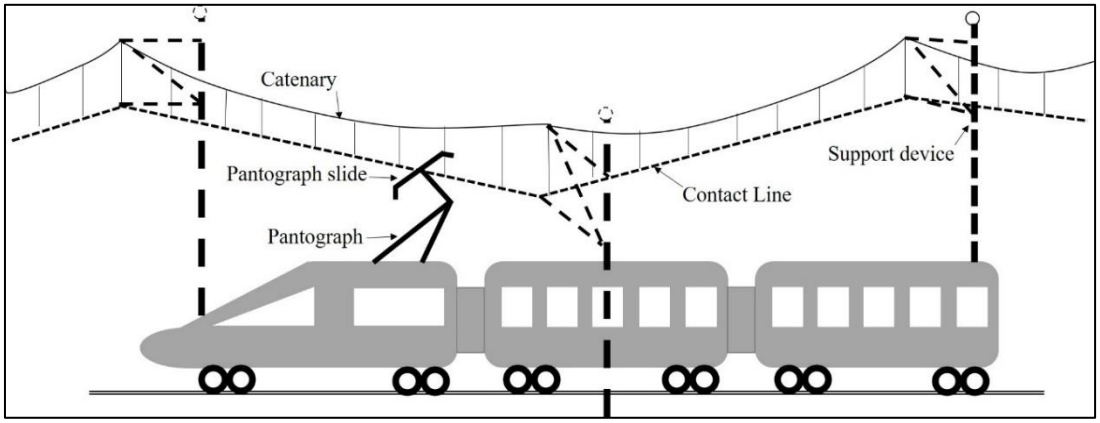

Figure 1.1 Pantograph-Catenary System

Plate 1.1 illustrates a pantograph slide installed on the pantograph head of a train for current collection from the overhead contact line.



Plate 1.1 Pantograph Slides Fixed to a Pantograph Head on Top of the Train

The pantograph slides require particular characteristics, including resistance to wear, good lubricating properties, high mechanical strength and sufficient electric conductivity [7]. This attribute not only enhances energy transmission during contact between the pantograph carbon strip and the current-carrying overhead catenary but also minimises energy loss. The wear resistance of the materials, which is also important for a pantograph slide, determines the lifespan of the parts and the frequency of changing them. Another key characteristic of pantograph carbon strips is their ability to self-lubricate, and researchers have recently experimented with various lubricants, including graphite [4].

This study was initiated due to the necessity of localising the production of pantograph slides for electrified rails in Malaysia. Currently, these slides are imported, but since they are wear-prone components that require regular replacement during operation, there is a crucial need to produce them locally. To establish a domestic manufacturing line, it is essential first to identify suitable local materials and available processes, ensuring the feasibility of the objective. This study addresses the need to enhance the overall performance, durability, and reliability of pantograph slides while ensuring their compatibility with operational requirements, particularly in Malaysia.

Carbon composites have become widely used as they offer excellent electrical conductivity, high strength, and good wear resistance [1]. In addition to carbon composites, copper-based composites have also been investigated as potential materials for pantograph slides. These composites exhibit good electrical conductivity, thermal conductivity, and corrosion resistance. Copper-matrix composite materials shall be added with graphite so that they possess excellent anti-friction properties and meet the requirements for pantograph slide usage [4]. Graphite is a naturally occurring form of carbon with excellent lubrication properties. In addition, incorporating graphene and CNT into pantograph slide materials could enhance their conductivity, reduce wear and tear, and improve the sliding contact between the pantograph and the overhead wires. Hence, using carbon-copper composites, graphene, CNT, and graphite in the development of materials for pantograph slides can offer several benefits due to their unique properties. This study focused on further enhancing the mechanical properties, lubrication, anti-friction effects, and overall performance by incorporating these materials.

The fabrication of a carbon-copper composite may be difficult due to the low solubility of carbon and copper. Hence, the use of an external binder adapted to facilitate the interactions between particles is a strategy frequently used in carbon granular technology [7]. Binders such as epoxy resin and phenolic resin are good binders due to their low cost, good wettability to carbon, and their capacity for generating matrices with distinct microstructures in carbon-copper composites.

Although there has been a lot of research on the materials and processes to develop pantograph slides or carbon strips, few studies have been conducted to investigate the effect of using carbon from natural materials in the formation of materials for pantograph slides. It is beneficial to understand the effect of these materials on the density, hardness, resistivity, and wear properties of the resulting materials. This understanding will lead to a better knowledge of the materials, which could promote the utilisation of natural materials that are abundant in Malaysia and can be obtained at low cost. Thus, the focus of this study is to investigate the processing and properties of carbon-copper composites for pantograph slides using different types and compositions of carbon, namely natural carbon from natural materials and conventional synthetic graphite. It is suggested that using natural materials might eventually replace traditional carbon powder in carbon-copper composite applications for current collectors.

In addition, this study investigated the effects of graphene oxide (GO), CNT, and copper-coated CNT as fillers on the physical, mechanical, and electrical properties of the developed composites. The warm compaction technique was employed to heat the carbon-copper composite to approximately 250°C, a temperature sufficient to liquefy the resin and facilitate effective bonding between the carbon and copper constituents [8]. Furthermore, the effects of both the warm compaction process and post-baking processes on the resulting material properties were examined.

Warm compaction of powder is a powder metallurgy technique that involves pressing a preheated powder mixture, comprising metal powder and high-temperature lubricant, at a temperature above room temperature to obtain high-density products. This technology has been established over the past few decades [9]. It is recognised as a cost-effective and efficient method for producing high-performance powder metallurgy parts. In numerous powder metallurgy applications, achieving highly sintered dense powder is needed to achieve the desired mechanical strength. However, such densities are often challenging to realise through conventional compaction and sintering techniques. Warm compaction addresses this limitation by enabling the production of higher-density powder metallurgy parts via a single compaction process [10].

Several techniques can be employed to determine the optimum process parameters in the warm compaction method to achieve output quality. Among these, the Taguchi approach is notable for its emphasis on designing processes and products to be robust against sources of variation, thereby minimising variability in the process or product through parameter design [11]. In this study, this approach was utilised to improve the quality of the warm compaction process and to reduce the production cost of the carbon-copper composite. Specifically, efforts were made to improve the electrical and mechanical properties of the carbon-copper composite by optimising the warm compaction parameters, including temperature, time, and pressure.

1.3 Problem Statement

The utilisation of palm kernel shells (PKS) aligns with government policies promoting the "waste to wealth" concept and fostering research into the efficient use of waste materials to reduce waste accumulation [12]. Despite increasing interest in the application of sustainable materials in railway systems [13], there remains a shortage of

comprehensive research on the characterisation and wear resistance of PKS-derived carbon-based composites specifically tailored for pantograph slide applications. PKS-derived carbon offers several advantages as a renewable and low-cost material for composite fabrication [12]. Characterisation data and wear resistance evaluation are crucial to provide deeper insight into the viability of natural carbon in developing efficient and sustainable transportation systems that benefit both the nation and the environment. The specific microstructure and composition of PKS-derived carbon could contribute to increased resistance to deformation and enhanced hardness. However, organic-based materials typically exhibit higher electrical resistivity compared to conductive materials such as graphite. Factors such as the specific chemical composition, presence of impurities, and structural arrangement of carbon within PKS-derived carbon affect its electrical conductivity. Previous studies have demonstrated that PKS-derived carbon, when incorporated with copper, has the potential to be used as a current collector in third rail systems. These composites exhibit similar properties and wear characteristics to those of commercial current collectors [8][14]. Nonetheless, knowledge gaps remain regarding the performance of such materials in top-running electrical rail systems. Therefore, optimisation of the composition between natural carbon and copper is crucial to achieve the required properties for the pantograph slide applications.

The development of PKS-derived carbon composites for pantograph slide materials using the warm compaction method requires a comprehensive understanding of the interactions between PKS-derived carbon particles, binders, and processing parameters during the fabrication stages, including mixing, cold pressing, warm compaction, and post-baking. Therefore, further research is needed to optimise these processing parameters to improve the mechanical properties and wear resistance of the resulting composites.

Due to their efficient self-lubricating properties, pure carbon pantograph slides or contact strips have been frequently employed. However, the limited mechanical strength and comparatively poor conductivity of pure carbon pantograph slides make them insufficient for use in electrical locomotives travelling at speeds exceeding 100 km/h [2][3]. Thus, improvements to pure carbon pantograph slides are necessary. Literature has shown that the addition of copper [15][16] and GO [17][18] into carbon can produce composite materials with improved electrical conductivity, mechanical strength, wear resistance, and thermal stability, making them more suitable for high-

performance railway applications. This study leverages the self-lubricating properties of carbon, the conductivity of copper, and the strength of graphene and CNT to create composite pantograph slides. These composites aim to achieve an optimal balance between performance and durability, effectively addressing the limitations of current materials used in electric train systems.

Several techniques have been used to consolidate the materials for pantograph slides, including the metal impregnation process and powder metallurgy route, such as sintering and hot forging. However, these processes involve complex procedures and high temperatures. Carbon-based composites require thermal treatment up to 2500℃, making them not economical due to the low solubility of carbon in copper. As a result, liquid copper is unable to adequately wet carbon, even during liquid-phase sintering, leading to carbon-copper composites with weak interfacial bonding and poor mechanical properties [14]. In contrast, warm compaction offers a more energy-efficient process as it requires lower temperatures (around 150℃ to 250℃) and shorter processing times compared to conventional sintering [9]. Previous studies have demonstrated the successful application of this method in consolidating PKS-derived carbon-copper composites [8][14]. However, there is still a lack of detailed insights into the effects of warm compaction pressure and duration on the properties of the resulting materials. Therefore, identification of the optimum condition of the warm compaction method, particularly in terms of temperature, pressure, and time, remains a promising area for further exploration.

The effectiveness and durability of pantograph slides in railway systems heavily rely on their wear resistance under dynamic operating conditions, with commercial pantograph materials exhibiting wear rates ranging from 0.1 to 0.5 mm^3/km [19]. However, there is limited understanding of the wear mechanisms and long-term performance of PKS-derived carbon composite materials in such applications. Therefore, gaining insight into these aspects is crucial for optimising their potential as durable and efficient pantograph slides.

1.4 Research Question

Several research questions have been formulated to address the problem statement in this study:

a) What is the optimum composition of PKS-derived carbon, graphite, copper, and resin for use in the composite system for pantograph applications?
b) Does the addition of fillers improve the properties of PKS-derived carbon-copper composite materials fabricated through the warm compaction method?
c) Which parameters in the warm compaction process significantly affect the consolidation and resulting properties of the carbon-copper composite?
d) Can the optimised composite material meet the wear performance standards required for pantograph slide applications?

1.5 Research Objectives

The main objective of this study is to develop a PKS-derived carbon-copper composite for use as a pantograph slide in railway applications by optimising the processes involved in the powder metallurgy route. The processes include material mixing, cold pressing, warm compaction, and post-baking. The specific objectives are:

a) To evaluate the effect of graphite/PKS-derived carbon ratio in carbon-copper composites on the mechanical and electrical performance of pantograph slides.
b) To investigate the effects of different filler types and contents on the physical and electrical properties of the composite material.
c) To investigate the optimum condition in the warm compaction process (temperature, time, and pressure), with and without post-baking, on the mechanical and electrical properties of the composite materials using the Taguchi L_9 orthogonal array.
d) To analyse the tribological properties of the optimised carbon-copper composite under dry sliding conditions.

1.6 Scope of Study

This study focuses on the development and performance evaluation of carbon-copper composite material for use as a pantograph slide in railway electrification systems. The key aspect of this study is the use of PKS-derived carbon as a carbon source within the composite. This study investigates various PKS-derived carbon-to-graphite ratios, ranging from 20:80 to 80:20, to evaluate how different combinations affect the strength and electrical conductivity of the final material. In addition, phenolic

resin is proposed as an alternative binder to the epoxy resin commonly used in previous studies. The resin content is kept constant at 15 wt% throughout the experiments. The findings from this initial phase determine the optimal PKS-to-graphite ratio, which will serve as the foundation for the subsequent phases of this study.

In the second phase, this study is extended to incorporate advanced fillers at 1% loading, specifically GO, CNT, and carbon-coated carbon nanotubes (Cu-CNT). The most promising filler is further investigated at varying percentages, ranging from 1 wt% to 3 wt%, to evaluate its synergistic effects when combined with different carbon sources and binders. This phase aims to enhance the overall performance of the composite material for demanding pantograph slide applications. The best-performing fillers and composition identified in this phase are carried forward for further testing and evaluation in the subsequent phase of this study.

Processing parameters, including warm compaction temperature (ranging from 150℃ to 250℃), compaction pressure (40 to 60 tons), compaction time (2.5 to 10 minutes), and post-baking conditions (with and without post-baking at 200℃), are varied to optimise the properties of the composites using the Taguchi method. This study investigated the influence of thermal treatments on the wear resistance, mechanical strength, and electrical conductivity of the final composite materials. Identifying the optimal processing conditions is essential for the successful fabrication of high-performance pantograph slide materials.

In this study, BS EN 50405:2016 [20] is used as a reference framework to guide the laboratory characterisation and performance evaluation of the developed composites for pantograph contact slide applications. The standard is intended for testing full-scale pantograph contact strips and their specified test configurations. In the present research, only small laboratory-scale specimens are produced, and the objective is to evaluate the essential material and processing performance of the developed composites rather than the functional performance of a complete pantograph strip. Therefore, established material characterisation and tribological standards are more appropriate and technically consistent with the scope of this work. Thus, the selected test methods and benchmarking approach are aligned, where applicable, with the requirements and intent of this standard. Subsequently, the developed composites are tested for density (ASTM D792), hardness (ASTM D785), transverse rupture strength (ASTM D790), and electrical resistance (ASTM B193). The microstructure and phase composition of the materials are analysed using scanning electron microscopy (SEM), energy dispersive

X-ray spectroscopy (EDS), and X-ray diffraction (XRD). These analyses provide valuable insights into how the material composition and processing parameters influence the final properties of the composites. The same characterisation method is also applied to the raw materials before consolidation to better understand their initial properties and behaviour.

Finally, the performance of the newly developed composites is evaluated in the final phase through wear testing (ASTM G99), with the results compared against commercial pantograph materials reported in the literature. SEM and confocal microscopy analyses are conducted to further investigate and interpret the wear characteristics. The wear test outcomes validate the effectiveness of the optimised processing conditions established in earlier phases, providing a comprehensive understanding of the performance of the material under dry sliding operating conditions. These final wear test results serve as a benchmark for assessing the potential of PKS-based composites in railway applications, contributing to the development of sustainable and efficient pantograph slide materials.

1.7 Significance of Study

The findings of this study contribute to the development of carbon-copper composites through the utilisation of carbon materials derived from PKS and the addition of GO and CNT using a combination of warm compaction and post-baking processes. Few studies have been conducted using other powder metallurgy routes for carbon-copper and carbon-carbon composites. However, research on the development of hybrid natural carbon and graphite composites using the warm compaction method for pantograph slide applications remains limited. Investigation into the effects of adding GO and CNT into the composite through this method is also scarce. Previous studies have primarily focused on the utilisation of PKS-derived carbon as the base material for producing current collectors. Therefore, this study presents novel insights into enhancing composite materials by incorporating natural carbon sources and introducing fillers, such as CNT, Cu-CNT, and GO, through the warm compaction method.

This research not only provides insights into the potential applicability of the developed materials as pantograph slides but also emphasises the novelty of producing

them locally. Currently, pantograph slides are largely imported, which increases dependency on foreign suppliers, elevates costs, and limits opportunities for local industry growth. By utilising locally available raw materials and adapting established processing routes, this research demonstrates the feasibility of developing pantograph slides in Malaysia. This approach introduces a significant step towards self-reliance in railway component manufacturing, creates new paths for local technological advancement, and reduces import dependency.

The development and improvement of materials for pantographs play a significant role in the overall development of railway applications, particularly in the context of overhead electrification systems. The contribution of this study is significant, as its outcomes can serve as a valuable reference for industry, given that the primary objective is to fabricate low-cost pantograph slides from natural materials using a low-temperature process route. This research provides new insights into the development of materials for pantograph slides with the addition of natural carbon sources. The performance of these materials is important to ensure the uniform and optimum transfer of current from the traction substation to the moving train.

On top of that, this research also increases awareness about the use of natural materials, which is in line with the Malaysian Government's policy on the National Key Economic Areas (NKEA) — Oil, Gas and Energy; Communications, Content and Infrastructure; Palm Oil and Rubber; and Business Services. It also aligns with Malaysia's Sustainable Development Goals (SDG) by supporting SDG 9 (Industry, Innovation, and Infrastructure) through the localisation of pantograph slide production, fostering innovation, and reducing dependence on imports. Furthermore, it contributes to SDG 12 (Responsible Consumption and Production) by using sustainable materials such as PKS, turning agricultural waste into valuable resources, and minimising environmental impact. Additionally, this study supports SDG 13 (Climate Action) by promoting energy-efficient manufacturing processes that reduce carbon emissions, while also potentially contributing to SDG 8 (Decent Work and Economic Growth) by creating local job opportunities and strengthening the manufacturing sector in Malaysia. It also aligns with the Ministry of Investment, Trade, and Industry's (MITI) New Industrial Master Plan (NIMP) 2030 vision. Rail is one of the sectors highlighted in the plan. Based on the global trends, rail transport is expected to become the preferred mode of commuting and travel. Enhancing the rail network, including the construction of new lines and the upgrading of existing lines, will be crucial to meet this demand. The

growing population in Malaysia is expected to lead to an increase in rail passengers in the coming years. Major rail projects in Malaysia include the East Coast Rail Link (ECRL), Klang Valley MRT3 Circle Line, Johor Bahru – Singapore Rapid Transit System (RTS Link), Light Rapid Transit (LRT) Penang, and Sarawak Autonomous Rapid Transit (ART). Hence, the demand for current collectors, including pantographs, is projected to rise, and local production will be crucial to meet this growing demand.

In conclusion, the development of materials for pantograph slides in rail applications is crucial for optimising energy efficiency, safety, reliability, and overall performance. By utilising advanced materials and engineering techniques, the railway industry can develop more efficient and sustainable transportation systems that benefit both passengers and the environment.

CHAPTER 2
LITERATURE REVIEW

2.1 Introduction

This chapter reviews the advancement of electric railway systems with emphasis on Southeast Asia and Malaysia, followed by an overview of the pantograph–catenary system and the development and functional requirements of pantograph slides. The chapter then critically examines the main pantograph slide material systems, including graphite–copper, carbon–graphite, carbon–copper and carbon–carbon composites, together with the roles of carbon sources, binders, additives and fillers. Subsequently, the major processing methods, namely powder and metal impregnation routes, powder metallurgy, green body development, warm compaction and post-treatment processes, are reviewed, along with the influence of key processing factors such as compaction temperature, time and pressure. The chapter further discusses process optimisation approaches, including design of experiment, full-factorial and Taguchi methods, as well as commonly used physical, mechanical, electrical and wear testing techniques for pantograph slides. Based on this critical review, the limitations of existing materials, processing strategies and evaluation methods are identified, leading to the formulation of the research gap addressed in this study.

2.2 Electric Railway Advancement

Electric railways have revolutionised the way people travel, bringing about significant changes in global transportation modes. These rail systems have not only stimulated economic activity but have also contributed to reducing congestion on roads and highways congestion [21]. In Southeast Asia, the expansion of electric train lines represents a notable development of the transportation sector in the region. With the rapid pace of urbanisation and population growth, concerns regarding environmental sustainability have become more pronounced. Consequently, electric trains have emerged as a viable solution for promoting efficient and eco-friendly public transportation [22].

2.2.1 Electric Railway in Southeast Asia

Southeast Asia has witnessed the implementation of several electric railway projects, with many others currently under construction. These initiatives aim to enhance transportation connectivity, improve travel efficiency, and promote sustainable mobility. Table 2.1 presents an overview of the fastest train lines currently in operation within the region. The speed ranges from 120 km/h to a maximum speed of 160 km/h. Table 2.2 summarises the fastest train lines still under construction, which are expected to operate at speeds of up to 250 km/h upon completion. These projects span across various Southeast Asian countries, including Malaysia, Thailand, Laos, Indonesia, and the Philippines. These electrical railways are expected to significantly enhance transportation connectivity and operational efficiency in the region.

Table 2.1
Top-running Electric Train in Southeast Asia (In Operation)

Line	Country	Operating Speed
KLIA Ekspres	Malaysia	160 km/h
Airport Rail Link (Bangkok)	Thailand	160 km/h
Boten-Vientiane Railway	Laos	160 km/h
KTM ETS (Gemas – Padang Besar)	Malaysia	140 km/h
Sprinter	Thailand	120 km/h
Jakarta-Bandung HSR	Indonesia	200 km/h
Trans-Sulawesi Railway	Indonesia	120 km/h

Table 2.2
Top-running Electric Train in Southeast Asia (Under Construction)

Line	Country	Operating Speed	Schedule for Opening
Bangkok-Nong Khai High-Speed Railway	Thailand	250 km/h	2026
Don Mueang – Suvarnabumi – U-Tapao HSR	Thailand	250 km/h	2029
East Coast Rail Link	Malaysia	160 km/h	2026
North-South Commuter Railway	Philippines	120 – 160 km/h	2029

2.2.2 Electric Railway Systems in Malaysia

Several electric railway systems are currently in operation in Malaysia, including services provided by Keretapi Tanah Melayu Berhad (KTMB), Express Rail Link Sdn Bhd (ERL), Rapid Rail Sdn Bhd, and Mass Rapid Transit Corporation Sdn

Bhd. Although these systems are not classified as high-speed railways, they form the backbone of intercity and intracity public transport in the country [6]. The selection of current collection systems in Malaysia reflects operational and network requirements rather than train speed alone, with different solutions adopted for intercity and urban transit applications. As summarised in Table 2.3, KTMB ETS, KTMB Komuter and ERL employ an overhead pantograph–catenary system, while the LRT and MRT networks adopt a track-mounted conductor rail (third rail) system.

In the Malaysian intercity and airport rail networks, namely KTMB ETS, KTMB Komuter and ERL, electrical power is supplied through an overhead contact line using a top-running pantograph system. In this configuration, a roof-mounted pantograph presses its carbon slide strip upward against the underside of the contact wire and maintains continuous sliding contact during operation. Traction power is delivered through a 25 kV, 50 Hz AC electrification system [5]. The contact wire is laterally staggered along the track so that the pantograph slide traverses different regions of the strip surface, thereby reducing localised wear and improving current collection stability. This top-running arrangement is widely adopted for longer-distance and higher-capacity routes, where operational flexibility, higher voltage transmission and reduced trackside equipment are advantageous [21].

In contrast, the Malaysian LRT and MRT systems employ a third-rail current collection system, in which electrical power is supplied through a conductor rail installed alongside the running rails [23]. A collector shoe mounted on the train bogie maintains sliding contact with the conductor rail as the vehicle moves. In a side-running configuration, the collector shoe is loaded laterally and slides against the side surface of the conductor rail to collect current. Hence, unlike the pantograph–catenary arrangement, the sliding interface is formed between the collector shoe and a track-mounted conductor rail rather than an overhead wire [5].

The term ‘side-running’ is commonly used in the literature to describe third-rail systems in which the contact occurs on the lateral face of the conductor rail; however, third-rail designs may also employ top-contact or bottom-contact geometries depending on the protection and support arrangement. For the Malaysian LRT and MRT networks, traction power is supplied at low-voltage DC using protected conductor rails and bogie-mounted collector shoes [5]. This configuration is particularly suited to dense urban environments because it avoids overhead structures, simplifies tunnel and via duct construction, and supports frequent station spacing and rapid acceleration.

Overall, the evolution of current collection systems in Malaysia is driven primarily by transportation need, namely intercity and airport connectivity versus high frequency intracity service, rather than by operating speed alone. The overhead top-running pantograph system is preferred for longer routes and higher-voltage transmission, whereas third-rail side-running systems are adopted for compact urban rail networks such as the LRT and MRT [23].

Table 2.3 summarises the current collector systems adopted by the major electric rail services in Malaysia and shows a clear distinction between intercity and urban rail operations. The intercity and airport-linked services operated by Keretapi Tanah Melayu Berhad (KTM ETS and KTM Komuter) and Express Rail Link Sdn Bhd (KLIA Transit) employ a top-running pantograph–catenary system, with operating speeds ranging from 120 to 160 km/h [24][25]. In contrast, the urban rail networks operated by Rapid Rail Sdn Bhd (LRT) and Mass Rapid Transit Corporation Sdn Bhd (MRT) utilise side-running third-rail current collection systems at comparatively lower operating speeds of 80 to 100 km/h [26]. This comparison indicates that the choice of current collector in Malaysia is primarily influenced by the functional and infrastructural requirements of intercity versus intracity rail services, such as route length, station spacing, urban constraints and power supply architecture rather than by operating speed alone.

Table 2.3
Current Collector Type in Rail Systems in Malaysia

Line	**Service Provider**	**Operating Speed km/h**	**Current Collector Type**
KTM ETS	Keretapi Tanah Melayu Berhad	140	Top running
KLIA Transit – ERL	Express Rail Link Sdn. Bhd.	160	Top running
KTM Komuter	Keretapi Tanah Melayu Berhad	120	Top running
Light Rapid Transit (LRT)	Rapid Rail Sdn. Bhd. (Prasarana)	80	Side running
Mass Rapid Transit (MRT)	Mass Rapid Transit Corporation	100	Side running

2.3 Pantograph-Catenary System

The pantograph slide serves as a critical component of electric railway systems, responsible for transferring electrical power from the overhead wires to the power collection system of the train. Its primary function is to establish and maintain stable

and efficient contact with the overhead wires, ensuring the seamless transmission of power to the propulsion system of the train. Plate 2.1 shows an example of a pantograph with its pantograph slide placed on the roof of a train car.



Plate 2.1 Pantograph Slide Set-Up on KTMB Komuter

The performance and reliability of electric trains heavily rely on the efficiency of the power transfer process. Over the years, substantial advancements in materials processing and engineering have led to the development of innovative pantograph slide designs and improved manufacturing techniques, aimed at addressing the challenges associated with conventional pantograph slides [27], [28], [29].

To begin with, this section outlines the fundamental functions and requirements of pantograph slides within electric railway systems. It examines the power transmission process, emphasising the critical role played by pantograph slides in maintaining a stable and efficient connection with the overhead wires. This review then focuses on recent advancements in processing techniques employed in pantograph slide manufacturing. Precision machining, surface treatment, and coating technologies are discussed in detail, as these techniques have proven instrumental in enhancing the performance and durability of pantograph slides. The impacts of these processing

techniques on wear resistance and other property requirements are analysed, along with their implications for the overall system efficiency.

Furthermore, the role of materials in pantograph slide development is thoroughly investigated. Various material choices, ranging from traditional metals to advanced composites and alloys, are evaluated based on their mechanical properties, electrical conductivity, and tribological characteristics. The influence of material selection on wear resistance, contact forces, and noise generation is explored to identify materials that offer improved performance and reliability for pantograph slide applications [28], [30], [31].

Figure 2.1 illustrates the pantograph-catenary system [32]. The function of each part is explained as follows.

a) Catenary

The catenary is mainly composed of contact wires. It is a specialised power supply line built along the railway track to provide electrical energy to high-speed trains. It is arranged above the tracks, while the pantograph is mounted on the roof of the train cars. It forms the sliding contact current collection system [2].

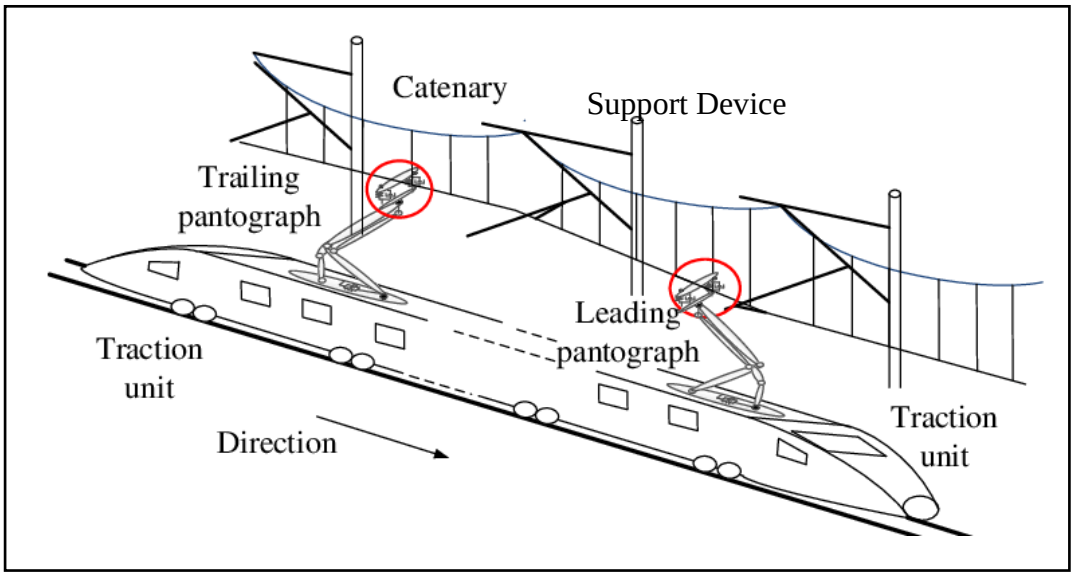

Figure 2.1 Function of Pantograph-catenary System

b) Contact line

The contact line, or contact wire, part of the overhead catenary, is the electrical cable used to transmit electrical energy to the electric trains. It is situated over rail tracks and raised to a high electrical potential by connection to feeder stations at regular intervals. It is the one in contact with the pantograph slide. The feeder stations are usually fed from a high-voltage electrical grid. This wire is attached to the contact wire at regular intervals by vertical wires known as "droppers" or "drop wires." It is supported regularly at structures by a pulley, link, or clamp. The whole system is then subjected to mechanical tension [33].

c) Support device

The support device refers to a structure that provides the necessary support for the overhead lines [32] .

d) Pantograph

The pantograph is the device used in electric trains to efficiently acquire electrical energy from the catenary system, which is an overhead power supply system installed along the train tracks [34]. This innovative mechanism enables the train to draw power from the catenary, allowing it to operate efficiently and sustain high speeds [28]. The pantograph is mounted on the roof of the train and features a hinged arm that can be raised or lowered as needed [35]. When the train is in motion, the pantograph extends upward and makes physical contact with the catenary wires, establishing an electrical connection [30]. Through this contact, electrical energy is transmitted from the catenary wires to the power systems of the train, providing the necessary power to drive the train's motors and other electrical equipment [36]. As the train moves along the tracks, the pantograph maintains a constant connection with the catenary, ensuring a continuous and reliable supply of electricity [37]. This ingenious technology has revolutionised the way high-speed electrical trains are powered, allowing them to operate efficiently and sustainably, contributing to modern and environmentally friendly transportation systems.

e) Pantograph slide

The pantograph slide is the sliding current collecting component attached to the pantograph. The pantograph is used to carry out the transmission of electric energy

[38][39]. It is the key subsystem of a high-speed railway that transmits the electrical energy from the traction substations to the moving train [36]. It maintains the efficiency and reliability of power transmission for the trains. Its performance is an important factor restricting the development of electrified railways towards high speed [40]. As the pantograph travels beneath the contact wire, its carbon insert gradually wears down over time. To ensure even wear and prevent notches, the contact wire is slightly zigzagged on straight tracks, alternating between the left and right sides of the centre from one support to the next. However, on curves, the "straight" wire segments between the supports cause the contact point to sweep across the pantograph's surface as the train navigates the bend. This movement of the contact wire over the pantograph's head is known as the "sweep".

The zig-zag movement of pantograph slides happens because the overhead catenary wire is installed with a slight lateral stagger, making the pantograph move side-to-side instead of straight. These spreads contact over the entire surface of the pantograph, preventing grooves and reducing stress that could cause faster wear. By distributing friction across a wider area, the zig-zag motion helps maintain good electrical contact and extends the life of both the pantograph and the wire [41]. For wear resistance studies, simulating this zig-zag motion is important to reflect real operating conditions and accurately test material performance [41].

2.4 Development of Pantograph Slide

2.4.1 Overview

The development of pantograph slides has progressed through several stages involving various material selections, such as metal slide plates, pure carbon slide plates, powder metallurgy, slide plates, metal-impregnated slide plates, and composite slide plates [15]. The development of pantograph slide materials dan processes has undergone a significant transformation over the past several decades.

Figure 2.2 reveals the evolution of pantograph processes and materials in Asia [2]. The transition from pure metal to carbon-based, powder-metallurgy and finally composite pantograph slides occurred mainly to reduce wear on both the slide and overhead wire, improve electrical contact stability and arcing resistance, and meet the increasing speed and current demands of modern rail systems, while extending service

life and lowering maintenance cost. At the same time, advances in powder metallurgy and composite engineering enabled tailored combinations of strength, conductivity and self-lubrication that could not be achieved with single-material slides.

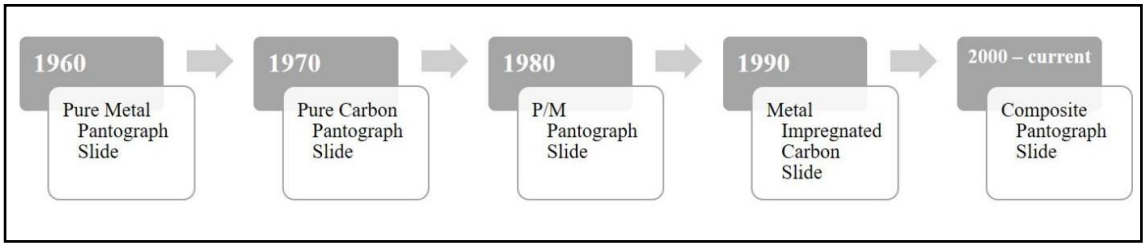

Figure 2.2 Development of Pantograph Processes and Materials in Asia

According to Wu et. al [2], the development of pantograph slides in Asia began in the 1960s, when pantograph slides were primarily manufactured using pure metals. While metallic slides exhibited good electrical conductivity, they suffered from excessive wear, high contact forces, and increased damage to the overhead catenary wires. The operational limitations of metallic slides highlighted the need for alternative materials that could balance conductivity with mechanical compatibility [2]. By the 1970s, pure carbon pantograph slides were introduced as an alternative to metallic counterparts. Carbon offered excellent self-lubricating characteristics, reduced wear on contact wires, and the ability to operate under fluctuating current loads. However, the relatively low mechanical strength and brittleness of pure carbon slides limited their durability, particularly under high-speed or high-current applications [2]. To address these shortcomings, the 1980s saw the introduction of powder metallurgy pantograph slides. The powder metallurgy technique enabled the tailoring of microstructures and the incorporation of different additives, which improved density, hardness, and wear resistance while maintaining acceptable electrical conductivity. Despite these improvements, further enhancement in service performance was required to cope with the rapid development of electrified railway systems [2]. In the 1990s, metal-impregnated carbon slides emerged as a hybrid solution that combined the superior conductivity of metals with the lubricating and wear-resistant properties of carbon. Metal impregnation significantly enhanced current-carrying capacity and mechanical integrity, allowing for better performance under high-speed and high-load conditions [2]. From the 2000s to the present, the focus has shifted towards composite pantograph slides. These materials integrate carbon with copper, graphite, polymers, and various

fillers to achieve an optimised balance between electrical and mechanical properties. Composite slides demonstrate superior durability, thermal stability, and adaptability to diverse operating environments [2]. The ongoing research and development in composite materials reflect the increasing demand for sustainable, high-performance pantograph systems.

Table 2.4 provides a structured and comparative overview of pantograph slide research published over approximately the last decade (≈2015–2025) and is intended to highlight both the dominant technical trends and the remaining research gaps addressed in this study. Each row represents a selected and representative publication, while the columns summarise the major experimental and material design elements reported in each work. Specifically, the table distinguishes the primary fabrication routes employed—namely impregnation-based processing, chemical vapour deposition (CVD), conventional powder metallurgy, and warm compaction—together with any supplementary or post-processing treatments such as hot pressing, spark plasma sintering, post-baking and heat treatment. These processing routes are important because they directly govern the densification behaviour, microstructural development and interfacial bonding of carbon-based sliding materials, which in turn control their mechanical integrity and electrical performance under pantograph operating conditions.

In addition, the table records the material systems adopted in the literature, which are predominantly carbon or graphite matrices combined with copper or copper-alloy constituents to balance electrical conductivity with mechanical strength and wear resistance. The use of additives and reinforcements, including nanocarbons such as carbon nanotubes (CNTs), graphene and other functional modifiers, is also explicitly indicated. These reinforcements are commonly introduced to improve load transfer, stabilise frictional behaviour, suppress arc erosion and enhance the durability of the sliding interface. The reported performance improvements claimed by the respective authors—such as reduced wear rate, improved resistance to electrical arcing, and enhanced current-carrying stability—are summarised to allow a direct comparison of the functional benefits associated with different processing routes and material designs.

Furthermore, the table compiles the key properties evaluated in each study, including density, transverse rupture strength (TRS), electrical resistivity, hardness, friction coefficient and wear rate. The use of check marks provides a clear visual indication of which processing parameters, material variables and characterisation methods were considered in each work, thereby revealing the extent and focus of

existing investigations. From this consolidated comparison, it is evident that most previous studies emphasise either advanced densification routes or imported and commercially available raw materials, while systematic studies combining alternative, locally sourced carbon materials with practical manufacturing routes remain limited.

The final row of Table 2.4 summarises the processing strategy, material constituents, additives and characterisation parameters adopted in the present research. By positioning this study alongside the existing literature, the table demonstrates that the current work differs from previous approaches by integrating locally derived carbon sources with a scalable powder-based and warm compaction route, and by evaluating a comprehensive set of mechanical, physical and electrical properties relevant to railway pantograph applications. This comparison clearly establishes the novelty of the present study and its contribution towards the localisation and sustainable development of pantograph slide materials.

Table 2.4
Summary of Research in Pantograph Slide Development for the Past 10 Years

Authors / Theme	**Year**	**Process**			**Additional Process**		**Materials**					**Additives**				**Improvement Highlight**				**Properties Assessment**						
Sub-theme		Im	CVD	PM	AT	OT	GrCu	CG	CCu	CC	Ni	Gt	CF	AM	Gn	IFB	AF/W	UCC	MS	D	TRS	R	H	FC	W
Yang et. al [42]	2015			✓						✓															✓
Zhang et. al [43]	2015			✓	✓				✓													C	✓		
Selvakumar et. al. [44]	2016			CPS					✓					CNT					✓						✓
Ibrahim et. al. [14]	2016			WC		PB			✓					Re					✓	✓	✓	✓	✓	✓	✓	✓
Selamat et. al. [8]	2016			WC		PB			✓					Re					✓	✓	✓	✓	✓	✓	✓	✓
Budin et. al. [45]	2016			WC		PB			✓					Re					✓		✓		✓			
Nurulhadi et. al. [46]	2016			WC		PB			✓					Re					✓	✓	✓	✓	✓			
Mou et. al. [47]	2017			✓	✓	WH			✓										✓				✓		✓
Yin et. al. [48]	2017	✓	✓						✓			✓	✓												✓
Fu et. al. [40]	2017			VHP					✓					Al						✓		✓	✓	✓	✓
Ma et. al. [38]	2018	✓								✓				Al					✓					✓	✓
Wu et. al [49]	2018	✓							✓					Cu											
Wang et. al. [50]	2019		✓						✓			✓								✓		C		✓	
Xu et. al. [51]	2019			✓			✓				✓	✓		Cr						✓	IT	✓	✓	✓	✓
Huang et. al. [52]	2020			✓					✓			✓					✓							✓	✓
Wang et. al. [31]	2021			✓	✓	HPF	✓										✓			✓		✓	✓	✓	✓
Deng et. al. [53]	2021	✓							✓					Cu							CS			✓	
Liao et. al. [54]	2021	✓							✓		✓					✓					✓	✓			
Li et. al. [55]	2021	✓							✓			✓						✓	✓					✓	✓
Wang et. al. [56]	2021	✓	✓						✓				✓						✓			C			✓
Wang et. al. [57]	2021			HP				✓				✓	✓								✓				✓
Wei et. al. [34]	2021	✓								✓				Al,Cu		✓						C			
Morimoto et. al. [58]	2022	✓							✓					Cu							✓	✓			
Zou et. al. [59]	2022			SPS		HT	✓													✓		✓		✓	✓
Li et. al. [29]	2022			✓						✓											✓	✓		✓	✓
Wu et. al. [60]	2023			✓		HPF	✓							Bi		✓					✓			✓	✓
Wang et. al [61]	2023	✓								✓				Cu										✓	✓
Li et. al. [62]	2023			HPS			✓					✓					✓			✓			✓	✓	✓
Zhang et. al. [63]	2023			✓						✓		✓			✓				✓						✓
Wang et. al [64]	2024			HPS					✓				✓						✓			C	✓		✓
Li et. al [65]	2025			✓				✓	✓					Zr,B					✓			C			✓
Fazira Fadzil	**2025**			**WC**					✓			✓		**Re**	✓	✓	✓		✓	✓	✓	✓	✓	✓	✓

Legend:

Process	Additional Process	Materials	Additives	Improvement Highlight	Properties Assessment
Im: Powder/Metal Impregnation	HPF: Hot Powder Forging	GrCu: Graphite Copper Matrix	Ni: Nickel	IFB: Interfacial	D: Density
CVD: Chemical Vapor Deposition	AT Aging Treatment,	CG: Carbon Graphite Matrix	Gt: Graphite	Bonding/Wettability	TRS: Transverse Rupture Strength
PM: Powder Metallurgy	HT: Hydrophobic treatment	CCu: Carbon Copper Matrix	CF: Carbon Fiber	AF/W: Anti Friction/ Self-lubricating / Wear	CS: Compressive Strength
HP: Hot Pressing	WH: Water hardening	CC: Carbon/carbon Matrix	Gn: Graphene	IT: Impact Toughness	
HPS: Hot Press Sintering	PB: Post-baking		Cr: Chromium	UCC: Uniform Copper Contribution	R: Resistivity C: Conductivity
VHP: Vacuum Hot Pressing	HC: Heat curing		Al: Aluminium		H: Hardness
CPS: Cold Press Sintering	OT: Other Processes		CNT: Carbon nanotube	MS: Mechanical Strength	FC: Friction Coefficient
WC: Warm Compaction			Re: Resin		W: Wear
			Cu: Copper		

2.4.2 Properties Requirement

The pantograph contact slide, or pantograph slide, is necessary for current collection by friction and must possess good anti-friction, corrosion resistance, wear resistance, and self-lubrication, in addition to good density, resistivity or electrical conductivity, thermal stability, and impact resistance [52][66]. Table 2.5 compares the properties of several commercial pantograph slides [67]. According to the table, most commercial pantograph slides are manufactured using the metal-impregnated method. This process involves incorporating metal or metal-based materials into the composition of the pantograph slide to enhance its mechanical and electrical properties. The focus on achieving specific properties is essential to optimise the performance of the pantograph slide and extend its operational life. The properties highlighted are resistance, density, hardness, or flexural strength (or transverse rupture strength). Metallised carbon graphite showed the best resistance value and flexural strength. However, the density and hardness are slightly lower when compared to metal impregnated copper and impregnated carbon. These values are referred from the product specification flyers from the mentioned manufacturers.

Table 2.5
Technical Data of Commercial Pantograph Carbon Slides of Different Manufacturers

Manufacturer (Product code)	**Material/ Process**	**Properties**			
		Resistance ($\mu\Omega$)	**Density (g/cm^3)**	**Hardness (HRB)**	**Flexural Strength (N/mm^2)**
Morganite (MY259)	Metallised pressed carbon graphite	<1	2.80	90	90
PanTrac GmbH (RH83M6)	Impregnated carbon	7	3.40	105	102
Elekrokarbon a.s. (SK162)	Metal Impregnated (Cu)	5	2.30	110	60
Mersen (P5696)	Metal Impregnated (22% Cu)	7	2.30	90	85

a) Wear resistance

The wear resistance of materials depends upon the hardness of the material, though there are exceptions. When there is strong bonding between the main material and the reinforcing phases, as well as dispersion strengthening, the wear rate tends to decrease. Wear statistics show that higher applied loads lead to greater volume loss and a greater wear rate [68].

The wear resistance of a pantograph slide is a highly desirable characteristic as it offers several advantageous outcomes. One primary benefit is the extension of the overall service life of pantograph slides, leading to cost savings by reducing the frequency of replacements and maintenance requirements. Moreover, improved wear resistance also contributes to lowering operational costs, as it minimises the need for frequent repairs and replacements [2]. Previous research has reported on wear studies of pantograph slide materials using different test methods, including pin-on-disk [69], ball-on-disk [62][70] and block-on-ring [71].

b) Electrical conductivity

In addition to wear resistance, another vital property that warrants attention in the design of a pantograph slide is high electrical conductivity. A pantograph slide with excellent electrical conductivity ensures efficient energy transmission during its operation. This is crucial, as it helps to minimise energy loss during the transfer of electrical power from the overhead contact wire to the pantograph slide and further down to the train or vehicle it serves. By optimising energy transmission, a high level of electrical conductivity contributes to improved energy efficiency and reduced power consumption in the overall system [2]. Previous studies have also highlighted the importance of having good electrical conductivity or resistivity in pantograph slide materials [8] [43][46].

c) Density

Furthermore, the pantograph slide should exhibit good density to ensure good hardness and wear resistance. Commercial pantograph slides show density values between 2.30 and 3.4 g/cm^3. On the other hand, Wu et al. [2] reported that pure carbon commercial pantograph slides from different countries, Germany, Japan, France, and China, have a density value of 1.65 – 1.70 g/cm^3. Xu et al. [51] reported decrease of density as the graphite content is increased due to the reason that copper and graphite

have poor wettability. Fu et. al. [40] reported that increased density correlates with improved hardness and flexural strength, as porosity reduction allows better load transfer between the matrix and reinforcement phases.

d) Hardness

Hardness reflects the ability of pantograph slides to resist deformation under an applied load. For commercial pure carbon pantograph slides, hardness values typically fall between 90 and 110 HRB, as depicted in Table 2.5. Higher hardness generally correlates with improved wear resistance and service life; however, excessive hardness may increase brittleness and reduce impact resistance. Heat treatment of carbon-copper composite has been shown to enhance hardness and wear resistance by improving the microstructure and bonding at the carbon-metal interface [72].

e) Flexural Strength

Flexural strength, or transverse rupture strength, is often measured as one of the key properties of commercial pantograph slides. It reflects the ability of the pantograph slide to withstand bending and transverse loading during service. Commercial pure carbon pantograph slides record flexural strengths of 60 to 102 N/mm^2, as shown in Table 2.5. Kuznar et al. [73] reported that for several pantograph slide materials (carbon composites), higher transverse bend (flexural) strength corresponds to better resistance to damage under dynamic contact.

The evaluation and characterisation of pantograph slides involve the use of analytical equipment to assess their desired properties. As mentioned, the key properties commonly measured include density, resistivity/conductivity, hardness, and flexural strength. These parameters play a crucial role in determining the overall performance and reliability of pantograph slides in practical applications. By ensuring that pantograph slides meet these specifications, manufacturers can produce reliable and efficient components that are essential for smooth and sustainable rail or transportation systems.

In conclusion, achieving good wear resistance, high electrical conductivity, and strength in a pantograph slide are crucial objectives in its design and development. These properties not only contribute to long-lasting performance and reliability but also lead to overall cost savings and enhanced energy efficiency in the electrified railway or

transportation systems where pantograph slides are utilised. Through identification of the optimum condition, the pantograph slides are ensured to operate effectively and sustain their performance over an extended period, benefiting both the transportation industry and the environment.

2.5 Pantograph Slide Materials

Research on pantograph slides, especially their materials, has been conducted extensively worldwide. Since the 1920s, countries such as Japan, France, and Germany have conducted numerous studies on pantographs. The development of pantograph slide materials has experienced different phases, including metal slide plates, pure carbon slide plates, powder metallurgy slide plates, metal-impregnated slide plates, and composite slide plates [2][74]. However, there has been limited research in Southeast Asia, particularly in Malaysia, aimed at enhancing the properties of pantograph slides. Currently, the pantograph slides used for KTM ETS are imported from China and Korea. While the exact economic break-even point is not yet calculated, the technical and strategic feasibility justifies the work. It builds the foundation for a domestic Maintenance, Repair, and Overhaul (MRO) ecosystem, transforming Malaysia from a technology consumer into a technology contributor in the ASEAN rail market, as stated in the National Transportation Policy (NTP) 2019 - 2030.

Electric locomotives are developing towards higher speeds, and their operating environments are becoming increasingly complicated and diversified; consequently, stricter performance requirements for pantograph contact slides have gradually emerged. Therefore, the development of new contact slide materials that combine various superior properties has become a key research focus in many countries [3].

Since 2001, research on pantograph slide development has explored the use of various materials to improve the properties and performance of pantograph slides, specifically composite materials. As shown in Table 2.4, the most common materials used are graphite-copper matrix, carbon-graphite matrix, carbon-copper matrix, and carbon-carbon matrix.

These matrices have been further enhanced through the incorporation of additional materials such as nickel, graphite, carbon fibre, graphene, chromium, aluminium, carbon nanotubes (CNT), resin, and copper.

2.5.1 Graphite-Copper Composite

Graphite-copper (Gr-Cu) composites combine the high electrical and thermal conductivity of copper with the solid lubrication and high-temperature stability of graphite, making them ideal for pantograph slide applications. In this matrix, graphite provides low friction and self-lubricating properties, thereby reducing wear under sliding electrical contact, while copper enhances the overall conductivity and mechanical integrity. This structure allows the composite to maintain stable contact under arcing and current-carrying conditions, with graphite forming a lubricating film and copper aiding in heat dissipation.

Previous studies have reported that hybrid composites exhibited lower wear rates than pure cast copper [68]. An increase in the amount of graphite not only improves the wear resistance of the composite but also results in a lower coefficient of friction compared to pure cast copper. The presence of graphite particles enhances the wear resistance of both composites and counterparts by providing a lubricating film on both surfaces [68].

In the study done by Guo et. al. [75], graphite particles of two different sizes, namely 295 μm and 495 μm, were used. The mass fraction of carbon in the pantograph slider samples was increased to 8%. The effects of graphite particle size and copper-coated graphite on the material's performance were also investigated. The results showed that larger graphite particle sizes led to lower resistivity, reduced antifriction performance, and increased hardness. Copper-coated graphite can improve the sintering process of the copper matrix pantograph slider material, decrease its porosity and resistivity, and enhance antifriction performance and hardness, but it did not alter the abrasion mechanism.

To further investigate the lubrication behaviour of graphite/Cu composites, Li et al. [62] studied their tribological properties with different graphite contents using ball-on-disk wear tests. The tribological results showed that the friction coefficient and wear rate of the 7 wt.% graphite/Cu composite decreased by 7.7% and 12.7%, respectively, compared with 5 wt.% graphite/Cu. However, both the friction coefficient and wear rate increased when the graphite content exceeded 7 wt.%. The excellent tribological performance of the composites was mainly attributed to the synergistic action of the oxidative tribo-layer and graphite lubricant film, composed of graphite, copper (Cu), copper oxide (CuO), and iron (III) oxide (Fe_2O_3). The wear mechanism of

the graphite/Cu composites was mainly abrasive wear, accompanied by adhesion and oxidation wear.

In a study conducted by Wu et. al [60], Bi-containing graphite/copper-matrix composites with different bismuth contents were manufactured via hot powder forging. The bonding between copper and graphite was improved through modifications in the preparation process. The tensile strength initially increased and then decreased with increasing bismuth content, reaching a maximum tensile strength of 137.62 MPa. The friction coefficient initially increased and then decreased as the current density increased, while the wear rate continued to rise. Meanwhile, the friction mechanism changed from an adhesive wear mechanism to an electrical wear mechanism [60]. Although bismuth-containing graphite/copper-matrix composites exhibited lower friction coefficients and higher wear rates compared to carbon-based composites, they offered advantages in terms of mechanical strength and conductivity [55].

2.5.2 Carbon-Graphite Composite

Research on carbon-graphite composites for pantograph slides focused on improving wear resistance, electrical conductivity, and thermal stability to enhance performance and longevity. A novel pantograph slide composed of a copper-mesh modified carbon fibre-reinforced polymer (CFRP) composite was studied by Wang et al. [57] using a resin mixture of carbon fibre and flaky graphite. The results showed that the composite exhibited much lower electrical resistance than that of the pure carbon slide used in high-speed railways in China. The addition of carbon fibre significantly improved impact strength and wear resistance but had little effect on anti-friction performance. The electric resistance and tribological performances were dependent on the graphite content: reduced electrical resistance and friction coefficient were observed as the flaky graphite content increased from 0 to 15 wt%, while negligible changes occurred in impact strength and wear rate. However, further increasing the flaky graphite content to 20 wt% caused a dramatic rise in wear rate. The high content of flaky graphite contributed to the formation of a thick tribolayer with an unconsolidated structure. The tribo-layer tended to curl and wear off from the wear surface, leading to severe wear of the composite during current-carrying friction tests.

2.5.3 Carbon-Copper Composite

Carbon-copper composites are widely used in pantograph slides due to their combination of excellent electrical conductivity and wear resistance. The carbon phase provides the necessary mechanical strength and thermal stability, while copper enhances the electrical conductivity required for efficient power transmission between the train and the overhead catenary. Liao et al. [54] reported that carbon/copper composites are widely used in collector brushes, pantograph sliders, collector shoes, and other applications due to their excellent mechanical friction, wear resistance, thermal conductivity, and electrical conductivity. However, the interfacial bonding in these composites is typically weak due to the natural non-wettability between copper and carbon-graphite matrix, which restricts their comprehensive mechanical and electrical properties. In their study, nickel was doped into the carbon-graphite matrix during the preparation process. The results showed that the nickel-modified carbon matrix was denser, and the nickel was evenly distributed throughout the carbon matrix. The porosity of the modified carbon/copper composites was significantly reduced, and the interfacial bonding mechanism changed from a simple mechanical interlock to solid solution bonding, improving the interfacial state. It was found that with a nickel content of 3 wt%, the compressive strength and flexural strength increased by nearly 52% and 58%, respectively, while electrical conductivity increased by nearly 35% [54].

In another study, Selamat et. al. [8] investigated carbon-copper (C-Cu) composites that combined the positive characteristics of Cu, such as high thermal and electrical conductivity, with the low thermal expansion coefficient and lubricating properties of conventional graphite. Due to economic and environmental concerns, activated carbon produced from Malaysian Palm Oil Board (MPOB)'s oil palm kernel shell (OPKS) was studied as a replacement for conventional graphite to enhance the properties of the composite. In their study, OPKS served as the only carbon source for the composite.

2.5.4 Carbon-Carbon Composite

Carbon-carbon (C/C) composites consist of carbon fibres embedded within a carbon matrix, offering excellent thermal stability, lightweight characteristics, and high strength-to-weight ratios. The carbon matrix serves as the binding phase, providing

structural integrity and electrical conductivity, while the reinforcement fibres enhance mechanical strength and wear resistance. In pantograph slide applications, the C/C matrix enables components to withstand high frictional heat and repeated arcing under current-carrying conditions. Its inherent self-lubricating property reduces friction, while its low thermal expansion maintains dimensional stability during operation. Modifications, such as copper alloy impregnation or fibre reinforcement, further enhance conductivity and surface durability, making C/C composites highly suitable for high-performance electrical contact components.

Wang et al. [61] studied copper fibre-reinforced carbon/carbon composite (C/C-Cuf) and copper alloy impregnating carbon/carbon (C/C-Cu) composite as materials for pantograph slides. Both C/C-Cuf and C/C-Cu composites offered more advantages over pure carbon slides in terms of electrical conductivity and mechanical performance. During current-carrying friction tests, the C/C-Cu composite exhibited the lowest arc discharge energy and the smoothest worn surface. Yin et al. [48] also prepared a carbon/carbon composite using chemical vapour infiltration (CVI) with propene (C_3H_6), followed by impregnation and carbonisation.

2.5.5 Carbon Source

Carbon materials, such as graphite and coke, are commonly used components in friction materials. Carbon materials for developing pantograph slides can be sourced from both natural and synthetic sources [76]. These materials are crucial for ensuring the efficiency and performance of pantograph slides, which are integral to railway electrification systems.

(a) Synthetic Carbon Source

Synthetic carbon sources are man-made materials that offer the advantage of precise control over their properties, which is essential for high-performance applications such as pantograph slides [77]. Synthetic carbon sources, including synthetic graphite, carbon black, CNT, and graphene, provide several advantages in pantograph slide materials. They provide greater control over their properties, such as particle size, purity, and structure. This consistency is crucial for ensuring the performance of pantograph slides, which are subjected to high-speed friction, electrical

currents, and wear. Synthetic graphite is one of the primary materials used in the production of pantograph slides. It is produced by heating petroleum coke or coal tar pitch at high temperatures to form a highly conductive and stable material. It has high electrical conductivity, which is essential for efficient power transmission between the pantograph and the overhead catenary system. It also has high thermal stability, which can withstand the heat generated during the high-speed operation of trains. Synthetic graphite is durable and has a relatively low wear rate, which is critical for the longevity of pantograph slides. It is often used in the form of carbon composite materials or graphite-impregnated carbon composites for pantograph slides.

Carbon black is also used as a raw material in the development of pantograph slides. It is a fine black powder produced from the incomplete combustion of hydrocarbons and is commonly used as a reinforcing filler in composite materials for pantograph slides. Carbon black has high electrical conductivity, which improves the efficiency of the pantograph slide material in conducting electricity [78]. It also enhances the strength and durability of the composite materials due to its improved mechanical properties.

(b) Natural carbon

Natural carbon materials are derived from organic matter, including plant and animal sources, as well as geological carbons such as graphite and coal. They are widely regarded as sustainable and cost-effective carbon sources due to their abundance, renewability, and relatively low environmental impact compared to synthetic carbons. Common natural carbon sources include wood, biomass, palm kernel shells (PKS), coal, anthracite, and natural graphite [79][80]. The structural and functional properties of natural carbon depend on their origin and processing. Biomass-derived carbons, such as PKS, are typically produced via pyrolysis, which removes non-carbon elements and generates a carbonaceous structure with varying degrees of porosity and graphitisation [79]. While these carbons are generally amorphous with heterogeneous morphologies, natural graphite exhibits a highly ordered layered structure, offering superior electrical conductivity and mechanical stability [81].

Advantages of natural carbon materials include sustainability, low cost, and environmental benefits. Biomass-derived carbons utilize agricultural by-products, reducing waste and promoting circular resource use. Furthermore, these carbons can be tailored through activation and surface modification to adjust porosity, surface

chemistry, and mechanical properties [79][81]. Despite these advantages, natural carbons present certain limitations, particularly in applications requiring high conductivity and wear resistance, such as pantograph current collectors. Biomass carbons often have inconsistent quality, reduced electrical conductivity, and lower wear resistance due to structural irregularities and amorphous carbon content [82]. To mitigate these limitations, natural carbons are typically blended with metals (e.g., copper) and resin binders, or combined with synthetic conductive carbons. Several studies have investigated PKS-derived carbon as a key component in carbon–metal composites for current collectors Selamat et. al. [8], Ibrahim et. al. [14], Budin et. al. [45], employed a composite of 65% carbon, 20% copper, and 15% epoxy resin, while Nurulhadi et al. [46] explored different carbon-to-copper ratios. Their results indicated that a formulation of 55% carbon, 30% copper, and 15% epoxy resin provided the best combination of electrical conductivity and transverse rupture strength (TRS). These findings highlight the importance of optimising metal content to compensate for the lower conductivity of natural carbons while maintaining tribological performance.

Other natural biomass sources have also been applied in electrical and tribological composites. For example, coconut shell carbon and bamboo charcoal have been explored for electrodes and electrical brushes due to their moderate hardness and structural versatility [83][84]. Hybridisation strategies, such as blending natural carbons with graphite or synthetic carbons, further enhance conductivity and mechanical stability [85]. Additionally, chemical or thermal activation of biomass carbons can improve surface functionality and graphitic content, thereby increasing electrical performance [86].

In conclusion, natural carbon materials offer sustainable and cost-effective alternatives for carbon sources in pantograph current collector composites. Their successful implementation relies on careful processing, composite design, and hybridisation with metals or conductive fillers to overcome inherent limitations in conductivity and wear resistance. Future research should focus on optimising carbon-metal-resin ratios, surface activation methods, and hybrid composite strategies to meet the stringent requirements of electrical and tribological applications.

2.5.6 Binder

For the warm compaction method applied in this research, a resin is used in the formation of the composite as a binder. Since the warm compaction temperature is much lower than the melting temperature of carbon and copper, and to promote wetting between carbon and copper, resin is used to ensure that the particles remain intact to form the block [8]. Phenolic powder resins are commonly used as binders in powder metallurgy processes due to their excellent thermal stability, good adhesion properties, and resistance to heat and chemicals [87]. They can effectively bind metal powders together during compaction, contributing to the formation of green compacts. When phenolic resin in powder form is used for warm compaction, it is typically mixed with the metal powders to form a homogeneous blend. During the compaction process, at a pressure of 50 tonnes and a temperature between 150℃ and 250℃, heat and pressure cause the phenolic powder resin to soften and flow, effectively bonding the metal particles together. Subsequent curing or solidification processes further strengthen the resin binder, resulting in compacted parts with adequate mechanical properties for further processing or use [88]. Li et. al [29] reported the use of pitch coke as a binder in the development of copper-carbon composite through a pressure infiltration process. The carbon matrix was warm compacted at 150℃ and then sintered and carbonised at 1200℃. Research conducted by Selamat et al. [8], Ibrahim et al. [14], Budin et al. [45], and Nurulhadi et al. [46] employed epoxy resin as the binder for carbon-copper composites through the warm compaction and post-baking process. The temperatures for both warm compaction and post-baking were set at 200℃.

(a) Epoxy Resin

Epoxy resins are a class of thermosetting polymers formed by the reaction of epoxide-functional monomers with curing agents such as amines, anhydrides, or thiols [89]. Once cured, the epoxy network undergoes an irreversible cross-linking reaction, producing a rigid three-dimensional structure with high mechanical strength, excellent chemical resistance, and strong adhesion to a wide range of substrates [90]. As binders in powder metallurgy and composite processing, epoxy resins function primarily to improve green strength and handling, enabling uniform dispersion of particulate phases and preventing powder segregation during shaping operations [90]. Because epoxy is a thermoset, it does not soften upon subsequent heating; instead, it

remains dimensionally stable up to its decomposition temperature, which can be advantageous in maintaining shape during post-processing steps such as debinding and sintering [89]. However, the irreversible nature of epoxy cross-linking also limits its ability to be reshaped or recycled once cured, and careful control of cure kinetics and binder removal is required to avoid residual stresses or cracking in the final part [90]. Overall, the thermosetting characteristic of epoxy resins makes them excellent for applications requiring high green strength and stable preform integrity, but it also imposes constraints on thermal processing windows and debinding strategies [89].

(b) Phenolic Resin

Phenolic resins are another widely used class of thermosetting polymers, synthesized through the condensation of phenol with formaldehyde under acid or basic catalysis [91]. The resulting network contains a high density of phenolic cross-links, which confer excellent thermal stability, flame resistance, and char yield compared to many other binders [92]. In powder metallurgy and composites, phenolic resins serve as binders that not only improve green strength and powder cohesion but also act as carbon precursors in applications where controlled carbonization is desirable, for example, carbon–carbon composites or metal–ceramic systems [93]. As thermosets, phenolic binders undergo irreversible curing, resulting in a rigid matrix that maintains shape under mechanical stress and elevated temperatures prior to final heat treatments [92]. During thermal debinding, phenolic resins decompose in a relatively predictable manner, producing a carbonaceous char that can influence porosity and microstructure if retained in the product [91]. This behaviour contrasts with thermoplastic binders, which typically melt and flow out of the green body; phenolic binders instead thermally degrade, influencing both binder removal strategy and final part properties. The thermosetting nature of phenolic resins makes them particularly suitable for high-temperature applications and for systems where partial carbonisation contributes to functional performance, but it also necessitates careful debinding and thermal management to prevent defects [92].

2.5.7 Additives and Fillers

The performance of carbon-copper composites, particularly for electrical contact applications such as pantograph slides, is significantly influenced by the type

and nature of nano-fillers incorporated into the matrix. Friction modifiers and anti-wear additives are used to reduce the coefficient of friction and to improve lubricity [94]. However, their effectiveness is closely linked to dispersion quality, interfacial bonding, and processing technique used.

Table 2.6
Comparison of Different Filler Types

Filler Type	**Advantages**	**Disadvantages**
Graphene	High conductivity, high strength, solid lubrication	Agglomeration risk, weak interfacial Cu bonding, very high cost
Graphene Oxide	Good dispersion, better bonding, oxides surface improves adhesion	Lower conductivity, thermally unstable functional groups
CNT	High strength, enhances wear/electrical properties, self-lubricating	Agglomeration, poor wettability, damage during processing
Cu-CNT	Excellent bonding, good dispersion, synergistic reinforcement	Complex processing, higher cost

Table 2.6 shows the comparison of different filler types, including graphene oxide (GO), graphene, CNT, and copper-coated CNT (Cu-CNT) [13][63][95]. These fillers have gained attention due to their ability to improve mechanical strength, electrical conductivity, thermal stability, and wear resistance.

Graphene is one of the solid materials suitable for use as a solid lubricant. It, along with its various derivatives and graphene-based materials, has garnered significant attention from researchers [13]. In terms of mechanical properties, graphene has been confirmed as an exceptionally robust material, possessing a high Young's modulus and fracture strength [14,15]. Remarkably, this outstanding mechanical performance, which is vital for its function as a lubricant additive, remains intact in graphene derivatives such as GO, even in the presence of structural defects [16].

Zhang et. al. [63] designed and prepared a pantograph carbon slider (PCS-1) using sulfonated graphene (SG) as an additive. The results showed that PCS-1 demonstrated enhanced mechanical strength and wear performance compared to the carbon slider in the absence of SG (PCS-0). For example, the current-carrying wear test indicated that the flexural strength of PCS-1 was 41.8% higher than that of PCS-0. The wear rate of PCS-1 was reduced by 51.0% and 50.0% under wet and normal conditions,

respectively. Moreover, the presence of SG can markedly decrease the number of random cracks, increase the compactness of the fracture surface, and inhibit the electro-erosion of the slider materials, thereby improving the mechanical strength and wear resistance significantly.

GO is suggested as a reinforcing material to enhance the physical properties of the carbon-copper composites [63]. This includes improving mechanical, electrical, and thermal properties, with particular emphasis on enhancing wear resistance [96]. However, ensuring proper dispersion of GO is crucial, as its particles tend to agglomerate due to strong Van der Waals forces [97]. This dispersion challenge can be mitigated through the use of a tubular mixer to thoroughly blend all powders before cold compaction, followed by consolidation through the warm compaction process [8], [14], [46].

The integration of CNT into carbon-copper composites has drawn significant attention due to their potential to improve mechanical and electric properties, especially in applications such as railway pantographs. Recent studies have indicated that the addition of CNT, even in modest weight percentages such as 1wt%, leads to marked improvements in mechanical properties. Cantürk et al. [95] highlighted the role of CNT in enhancing the resistance and fracture of the tenacity of copper/carbon composites, stressing that microstructural integrity can be improved through the infiltration technique. This fundamental understanding supports in-depth exploration of hot compacted composites, where the dispersion of CNT can considerably influence the final properties. Selvakumar et. al [44] used multi-walled carbon nanotubes (MWCNT) as reinforcement elements at 2 wt% and reported improvements in density, porosity, hardness, wear, and electrical conductivity of the copper hybrid composite for pantograph slide applications.

At higher CNT incorporation, such as 2wt% and 3wt%, significant improvements in electrical properties have also been reported. A study conducted by Sun et al. [98] demonstrated that the inclusion of CNT contributes to an improvement in electrical conductivity due to their highly conductive nature, which facilitates electron transport through the composite. This finding is particularly relevant to the rail sector, where efficient electrical conduction is essential for the operational reliability of pantograph systems.

Microstructural analysis plays a crucial role in understanding the improvements provided by CNT integration. Chen et al. [99] investigated the microstructure of carbon-

graphite composites reinforced with carbon nanofibers, establishing correlations between microstructural characteristics and improved mechanical performance. The study also clarified the operational advantages associated with varying CNT concentrations in carbon composites.

Copper–carbon nanotube (Cu-CNT) composites are engineered materials in which carbon nanotubes (CNTs) are integrated with a copper matrix to combine CNTs' high mechanical strength and excellent electrical potential with copper's superior conductivity and ductility. In synthesis, CNTs can be pre-coated with copper layers via electroless or molecular deposition and then mixed with copper powders using techniques like ball milling, ultrasonication, and spark plasma sintering (SPS) to promote homogeneous dispersion and strong interfaces between CNTs and Cu matrix [100]. These processes aim to overcome wettability and bonding challenges, improving load transfer and electrical pathways in the composite [101]. As a result, Cu-CNT composites often exhibit enhanced mechanical hardness, increased tensile strength, and competitive electrical conductivity compared with pure copper, making them promising for advanced conductors, connectors, and thermal management components in electronics and energy applications [102]. Recent studies continue to explore how CNT alignment, coating quality, and processing routes affect performance, including improvements in current carrying capacity and mechanical behaviour in brush-coated Cu-CNT conductor architectures [102].

Other fillers reported by researchers include Fe_2O_3 and nickel (Ni). Wei et al. [34] reported that the addition of 5 wt% Fe_2O_3 improved the TRS and electrical conductivity of the carbon matrix pantograph slide. Typically, TRS improved in range of 15% to 25%. The electrical resistivity, on the other hand, reduces by 10% to 12%.. Similarly, the addition of 3wt% Ni through the doping method into the carbon-copper composite successfully improved the compressive strength, flexural strength, and electrical conductivity of the composite [54]. They reported that while adding a second metal usually creates more scattering, the improved density of the composite (reduced porosity) often leads to a net gain in conductivity of about 5% to 8% compared to a standard carbon-copper base. The compressive and flexural strength often see a significant improvement of 20% to 30%. The addition of fillers is expected to further improve the performance and durability of carbon-copper composites. Fillers contribute to superior mechanical strength, enhanced electrical conductivity, better lubrication, and reduced friction [103].

The amount of filler is normally set low (0.1–5 wt%), which may be due to the high cost, which may render higher additions economically unfeasible. Optimising the composite formulation with the appropriate amount of filler may help tailor the properties of carbon-copper composites to meet the specific requirements of railway applications, resulting in improved performance, extended lifespan, and reduced maintenance costs [104].

2.6 Pantograph Slide Processing Methods

Pantograph slides require materials with excellent conductivity, wear resistance, and mechanical strength. Several fabrication techniques are employed to manufacture these slides, including metal impregnation, powder metallurgy, infiltration, and warm compaction. Recently, the development of novel materials, such as graphene-reinforced composites and MAX-phase ceramics, has also been reported [2][105].

2.6.1 Powder/Metal Impregnation

The powder or metal impregnation method has emerged as a significant technology in the processing of pantograph slides. This method involves the infiltration of a metal matrix with powder materials [38]. The primary advantage of powder or metal impregnation is its ability to improve the hardness of the material, thereby improving performance, mechanical strength, and wear resistance of sliding surfaces [106]. This manufacturing technique implies the production of components from metallic powders through processes such as pressure and sintering. Powder preparation techniques, including drying and atomisation by spraying, ensure a uniform distribution of metal particles, which subsequently improves the properties in the finished products [107]. The impregnation process generally involves the infiltration of molten metal into a porous matrix. It is a specialised treatment in which reinforcing acrylic resins penetrate the porous structure of the metal. Impregnation reinforces the structure, increases hardness, and improves the mechanical properties of the final product [108].

Several studies have highlighted the advantages of using the powder and metal impregnation method for producing a pantograph slide. This method improves wear resistance, as evidenced by the synergistic effect of steam and sand particles on the sliding wear properties of metal-impregnated pantograph slides [109]. Metal

impregnation, particularly with copper or similar metals, significantly increases the electrical conductivity of carbon-based pantograph slides, as reported by Wang et al. [61]. This is crucial for efficient current collection in railway systems. Despite these advantages, the powder and metal impregnation method also presents challenges and inherent limitations. A notable disadvantage is the complexity of the manufacturing process, which can increase production costs and time. In addition, maintaining a uniform porosity in the sintered body is essential, as irregularities can lead to incoherent impregnation and compromise the mechanical integrity of the final product [2]. The choice of metal for impregnation also directly impacts wear resistance and overall performance, making in-depth testing and optimisation necessary to achieve desirable results. Moreover, carbon-metal wettability is generally poor in this method, requiring high pressure, vacuum, or alloy modification, such as boron doping, to improve infiltration [15].

2.6.2 Powder Metallurgy

Powder metallurgy involves blending metal and reinforcement powders, followed by die compaction and sintering. It is a key method for producing high-density copper-carbon composites used in pantograph slides. The core steps—powder blending, pressing, and sintering—determine the microstructure, density, and mechanical performance of the material [110]. Typical compaction pressure ranges from 150 MPa up to 700 MPa, depending on the material and part geometry. Higher compaction pressures generally reduce porosity and improve density, hardness, and strength, and optimal sintering schedules, including temperature and time, further influence diffusion and the final properties [111]. Powder metallurgy routes employed for producing pantograph slides include hot forging [60], hot pressing and sintering [62], cold pressing and sintering [54], and warm compaction [8][14][45][46],

2.6.3 Development of Green Body

The green body, or preform, is the compacted but non-sintered form of the composite material, and it plays a vital role in determining the quality and performance of the final pantograph slide. This stage often involves cold compaction. To form a uniform green body, the powder materials, typically a mixture of metal, such as copper,

and carbon-based reinforcements, must be blended thoroughly. Lubricants and binders, such as zinc stearate or phenolic resin, are added to improve flowability, reduce die friction, and enhance green strength before sintering [112]. Proper mixing ensures consistent particle contact and prevents agglomeration, which is particularly important when nano-fillers are incorporated [113]. Wu et. al [60] reported the development of a graphite-copper matrix through a hot forging process, where the powders were first mixed and cold-pressed at 600 -800 MPa to form the green body before sintering and forging. In studies conducted by Selamat et al. [8], Ibrahim et al. [14], Budin et al. [45], and Nurulhadi et al. [46], the powders were compacted at 18 tonnes using an automated hydraulic press.

2.6.4 Warm Compaction

Warm compaction of powder is a technology in which preheated mixed powders (metal powder and high-temperature lubricant) are pressed at temperatures above room temperature to obtain high-density products. This powder metallurgy technique typically preheats the powder to 100℃ to 150℃ and involves simultaneous heating and compacting. The process is mainly used in the steel mould pressing of iron-based, high-density powder metallurgy green compacts. A proper warm compaction process can increase the green density of iron-based parts to 7.30 g/cm^3 under room-temperature compaction (600 -800 MPa), which is 0.15–0.25 g/cm^3 higher than that achieved by traditional room-temperature compaction [114]. In the research by Selamat et al. [8], Ibrahim et al. [14], Budin et al. [45], and Nurulhadi et al. [46], warm compaction was conducted at temperatures between 150℃ and 250℃ under a pressure of 50 tonnes. In another research by Wang et al. [115], powder prepared for the production of soft magnetic composites was warm compacted at 1600 MPa by heating the mould to 130℃ prior to heat treatment.

2.6.5 Post Treatment

Post-treatment processes are essential for enhancing the final properties of pantograph slide materials after sintering or impregnation. These treatments aim to improve mechanical strength, thermal stability, electrical conductivity, and resistance to environmental degradation. Aging treatments, either at room temperature or under

controlled conditions, allow internal stresses to relax and moisture content to stabilise, thereby improving dimensional stability and long-term performance [31]. Water hardening is applied in some formulations to induce rapid cooling after heating, increasing surface hardness through phase transformation or binder densification [43]. Post-baking is typically conducted between 200℃ and 250℃ to remove residual volatiles and reinforce carbon bonding within the composite [14]. It also facilitates further carbonisation of the binder, improving structural cohesion and reducing electrical resistance. In carbon-metal systems, post-baking can relieve internal stresses generated during compaction and sintering, contributing to better dimensional stability [116]. According to the literature [8], [14], [45], [46], the post-baking process is employed following warm compaction as a curing process. The carbon-copper composite was baked in an oven at 200℃ for four hours.

2.6.6 Summary of Methods

Table 2.7 summarises the methods for producing pantograph slides, comparing their key benefits and key limitations. Metal impregnation provides excellent electrical conductivity and strength; however, it relies on good metal-carbon wetting, requires costly equipment, and involves multi-step control, making it complex and capital-intensive. Powder metallurgy with subsequent infiltration offers highly tunable compositions and good wear resistance; however, residual porosity and the need for additional post-processing can limit conductivity and structural integrity. Warm compaction offers lower energy demand and compatibility with sustainable carbon sources; nevertheless, it typically attains lower green density and remains a developing route that requires parameter optimisation to bridge the performance gap.

Table 2.7
Summary of Pantograph Slide Processing Methods

Method	Key Benefits	Key Limitations
Metal Impregnation	High conductivity and strength	Poor wettability, costly equipment. Complex process
Powder Metallurgy and Infiltration	Customisable properties, high wear resistance	Residual porosity, additional processing required
Warm Compaction	Energy efficient, sustainable material sources	Lower density, still maturing process

2.7 Pantograph Slide Processing Factor

The performance and reliability of pantograph slides depend not only on the choice of materials but also on the processing parameters. Key factors influencing fabrication include compaction temperature, time, and pressure, all of which play vital roles in determining the final material properties, such as density, conductivity, wear resistance, and structural integrity [46].

2.7.1 Warm Compaction Temperature

Warm compaction involves pressing powder materials or green body at elevated temperatures, typically 150–200℃, to enhance particle bonding. The increased temperature [14] improves the plastic deformation of ductile particles, such as copper, leading to better green density and interparticle contact. However, if the temperature exceeds the optimal range, it may cause binder degradation or premature curing [117]. Selamat et al [8], Ibrahim et al. [14], and Budin et al. [45] studied the effects of warm compaction at 150℃, 200℃, and 250℃. Ibrahim et al. [14] reported that warm compaction at 150℃ is the most suitable temperature for producing carbon-copper composite and requires further post-baking treatment. Selamat et al. [8] found that 200℃ is the best warm compaction temperature, but also required further post-baking treatment at 200℃. Budin et al. [45] concluded that 200℃ is the optimised temperature for achieving the best hardness and TRS value for the composite, with subsequent post-baking treatment at 220℃.

2.7.2 Warm Compaction Time

In the powder metallurgy route, the duration of the mixing process and the sintering dwell time are among the most critical time-related parameters. A longer mixing period enhances powder homogeneity and interfacial bonding. Similarly, prolonged sintering dwell time at elevated temperatures allows sufficient diffusion and neck formation between particles, directly influencing the mechanical integrity and conductivity of the composite. Selamat et. al. [8], Ibrahim et. al. [14], Budin et. al. [45], and Nurulhadi et. al. [46] reported that a soaking time of 5 minutes yielded the best

results. Therefore, lower and higher levels of 2.5 minutes and 10 minutes, respectively, were selected. Longer processing time is not preferred due to reduced feasibility and process efficiency in terms of time and cost.

2.7.3 Warm Compaction Pressure

Compaction pressure influences the green density and porosity of the composite. Higher pressure improves particle packing and bonding, thereby reducing voids and enhancing load-bearing capacity. However, excessive pressure may cause tool wear or lead to excessive densification, which can hinder infiltration during subsequent processing steps. Selamat et. al. [8], Ibrahim et. al. [14], and Nurulhadi et. al. [46] employed a compaction pressure of 50 tonnes. On the other hand, Budin et. al. [45] investigated the effect of warm compaction pressure on the properties of the composites using pressures of 40, 50, and 60 tonnes. They concluded that 60 tonnes is the optimum warm compaction pressure for producing the carbon-copper composite for the current collector application.

2.8 Determination of Optimum Condition

In determining the optimum condition of a process, where efficiency forms the foundation, the utilisation of systematic methodologies is essential [118]. One of the most crucial approaches is the application of Design of Experiments (DOE), a structured and scientific technique aimed at identifying the optimal settings within a complex system [119].

The selection of an appropriate experimental design plays a key role in the success of process optimisation activities. Among the numerous options available, two methodologies are notable for their effectiveness and flexibility: the full factorial method and the Taguchi method [120]. Each approach has its unique advantages and offers distinct tools for managing the complexity of process optimisation.

2.8.1 Design of Experiment

Numerous experiments involve studying the effects of two or more factors, and factorial designs are the most efficient for this type of experiment. A factorial design,

in this context, refers to the examination of all conceivable combinations of factor levels in each complete trial or replication of the experiment [121]. When factors are arranged in a factorial design, they are said to be crossed. The effect of a factor is defined as the change in response produced by a change in the level of the factor. This is frequently referred to as the main effect, as it represents the primary factors of interest in the experiment [121]. Unlike the one-factor-at-a-time optimisation approach, the DOE technique allows all important parameters of a specific process to be evaluated simultaneously. This approach enables a better understanding of the interactions between parameters and allows the identification of the most significant variables influencing the response under study.

2.8.2 Full-Factorial Method

The full factorial design is useful in the early stages of experimental work, especially when the number of process parameters or factors is less than or equal to four. This was reported by Ravindran et al. [122]. Numerous experiments require the examination of the combined effects of two or more variables. Factorial designs are typically the most effective for such investigations. In a factorial design, every potential combination of factor levels is explored in each trial or replication of the experiment [121].

2.8.3 Taguchi Method

Various techniques are available to study the effects of parameters and interactions, such as the Taguchi method, Taguchi-Grey relational analysis, and fuzzy logic technique [123]. The Taguchi approach is commonly used to improve quality with minimal testing and without increasing production costs. It provides a simple, effective, and systematic approach to optimising process parameters for enhanced performance [124]. Chouhan et al [11] employed the Taguchi method with an L_9 design matrix in their experiment to optimise the impact behaviour of functionally graded materials produced through the hot compaction powder metallurgy process.

The Taguchi method is an effective method for enhancing the performance of a process or product [125]. The primary objective of the Taguchi method is to apply a methodical statistical experimental design, also known as robust design, to minimise

variability around the target value of product attributes [121]. Robust design serves as a key strategy for achieving long-term product life and manufacturing viability. Taguchi simplified the setup of experimental designs through the use of orthogonal arrays, thereby reducing both time and costs [126]. Additionally, Taguchi introduced the concept of the signal-to-noise (S/N) ratio as a measure of robustness [127]. The S/N ratio quantifies the effect of uncontrollable factors (noise) on performance characteristics and guides the identification of factor settings that minimize variability. Depending on the type of quality characteristic, the S/N ratio is calculated differently:

(a) Smaller-the-better (for minimizing undesirable characteristics, e.g., defects, wear):

$$S/N = -10\, log_{10}\left(\frac{1}{n}\sum_{i=1}^{n} y_i^2\right) \tag{2.1}$$

(b) Larger-the-better (for maximizing desirable characteristics, e.g., strength, output):

$$S/N = -10\, log_{10}\left(\frac{1}{n}\sum_{i=1}^{n} \frac{1}{y_i^2}\right) \tag{2.2}$$

(c) Nominal-the-best (for targeting a specific value with minimal deviation):

$$S/N = -10\, log_{10}\left(\frac{\bar{y}^2}{s^2}\right) \tag{2.3}$$

where y_i is the observed value, n is the number of observations, $\bar{y}$ is the mean, and s^2 is the variance [128].

To statistically assess the influence of each factor on the response, Analysis of Variance (ANOVA) is commonly used in conjunction with the Taguchi method. ANOVA helps identify and quantify the sources of variation among results from different trial runs [121]. ANOVA decomposes the total variability of the response into

contributions from each factor and experimental error, allowing the identification of statistically significant factors. The general ANOVA model can be expressed as:

$$Y_{ij} = \mu + \tau_i + \epsilon_{ij} \tag{2.4}$$

where Y_{ij} is the observed response for the ith factor at the jth level, μ is the overall mean, τ_i represents the effect of the ith factor, and ϵ_{ij} is the random error [129].

By combining orthogonal array experimentation, S/N ratio analysis, and ANOVA, the Taguchi method provides a powerful framework for optimizing process parameters. This integrated approach allows engineers to improve product quality, reduce variability, and efficiently allocate resources to the most critical factors, making it widely applied in industries such as automotive, electronics, and material processing. Therefore, the Taguchi method is a robust experimental design that aims to achieve the best combination of factor levels at the lowest possible cost while maintaining the desired product quality.

An L_9 Taguchi orthogonal array is selected because the study focuses on screening and identifying the most influential processing factors with a minimal number of experimental runs, which is more efficient and robust against noise compared to Response Surface Methodology (RSM). In contrast, RSM is more suitable for detailed modelling and optimisation of factor interactions after key factors have already been identified and would require substantially more experiments for the same number of factors and levels.

2.9 Testing and Characterisation

Comprehensive testing and characterisation are critical in the development of pantograph slide materials, as these components operate under harsh mechanical, electrical, and environmental conditions. To ensure reliability, durability, and optimal performance in electrical rail systems, materials must undergo physical, mechanical, electrical, and tribological evaluations that closely simulate real-world service environments. The data obtained from these tests guide material selection, composition optimisation, and process refinement, supporting both laboratory research and industrial-scale production.

2.9.1 Physical

Physical characterisation typically involves the evaluation of density, porosity, microstructure, and surface morphology. Density and porosity are important parameters as they influence the strength, conductivity, and wear life of the material. For example, Shiju et al. [114] reported that warm-compacted and infiltrated Cu-graphite composites exhibited increased density (up to 6.5 g/cm^3) and reduced porosity, resulting in improved electrical conductivity and wear resistance. Scanning electron microscopy (SEM) coupled with energy dispersive X-ray spectroscopy (EDS) is often used to evaluate the distribution of carbon and metal phases, particle bonding, and filler dispersion. Furthermore, studies by Selamat et al. [8], Ibrahim et al. [14], Budin et al. [45], and Nurulhadi et al. [46] stated that the density value of carbon-copper composite is important for their current collector applications. Density test is conducted using an electronic densitimeter following the Archimedes drainage method.

2.9.2 Mechanical

Mechanical testing assesses the hardness, flexural strength, and compressive strength of pantograph slide materials, which are critical for resisting deformation under sliding contact loads. Vickers or Rockwell hardness tests provide insight into surface hardness, which correlates with wear resistance. Flexural strength, often evaluated via three-point bending tests, indicates the ability of the material to resist fracture under bending stress, while compressive strength measures resistance to crushing forces during operation. Copper-graphite composites, particularly those reinforced with nano-fillers such as CNT or GO, have demonstrated improved mechanical performance due to improved stress transfer and stronger matrix-filler bonding [130]. Selamat et al. [8], Ibrahim et al. [14], Budin et al. [45], and Nurulhadi et al. [46] reported hardness test conducted using a Rockwell hardness tester at 60 kgf with ½ ½-inch ball indenter.

2.9.3 Electrical

Electrical characterisation involves measuring the bulk electrical resistivity or conductivity of the material. Since pantograph slides are responsible for efficient current collection from the catenary, low electrical resistivity is essential to minimise

energy losses. The four-point probe method is commonly used to obtain accurate resistivity measurements. Hybrid composites containing copper and well-dispersed conductive carbon fillers, such as GO or CNT, can achieve significantly improved electrical conductivity [131]. Selamat et al. [8], Ibrahim et al. [14], Budin et al. [45], and Nurulhadi et al. [46] reported that resistivity testing was performed using a digital resistivity meter.

2.9.4 Wear

Tribological testing evaluates the wear resistance and coefficient of friction of pantograph slide materials under simulated operating conditions. The pin-on-disc method is widely used, where a composite pin is slid against a rotating metallic disc under controlled load and speed. Other methods include ball-on-disk and block-on-ring. Measurements of wear rate and friction provide critical insights into the durability and stability of the material during long-term use. Factors such as carbon content, particle distribution, porosity, and bonding quality significantly influence wear performance [132]. The addition of lubricating phases, such as graphite or molybdenum disulfide (MoS_2), and optimisation of microstructural features have been shown to reduce wear rate and extend operational lifespan [133]. Li et al. [134] examined the wear behaviour of copper-sintered carbon composites using a dry sliding wear test. Shibata et al. [135] investigated the friction and wear properties of copper/carbon/RB ceramic composites for pantograph slides application under dry sliding conditions. Similarly, Shibata et al. [136] conducted a wear test on the same material under water-lubricated conditions. Zhang et al. [63] also conducted wear tests in normal (dry) and wet conditions, calculating the current-carrying wear rate for each sample.

2.10 Research Gap

Figure 2.3 shows the research gap addressed in this study, focusing on the processing methods commonly used for the development of pantograph slides.

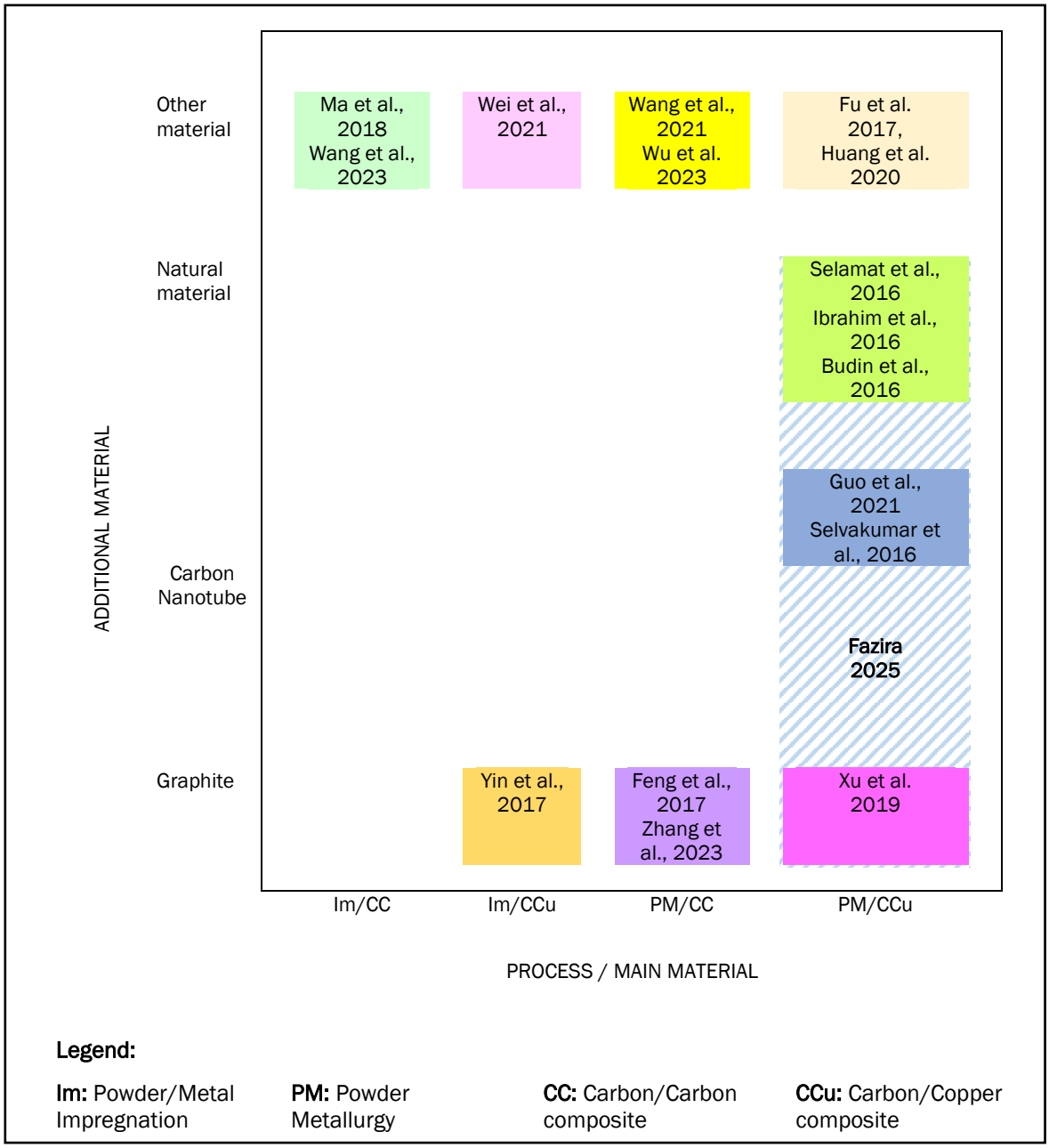

Figure 2.3 Previous Research and Gap on Process, Main Material, and Additional Material for the Development of Pantograph Carbon Slide

The comparison between previous studies and current research focuses on the processing method, main materials, and additive materials used in composite fabrication. Impregnation and powder metallurgy are the most frequently applied

processing techniques. In terms of material composition, carbon-carbon and carbon-copper composites have emerged as the two most promising candidates for further investigation. Furthermore, a range of additive materials is chosen to be incorporated into the composite, including graphite, graphene, carbon fibre, natural carbon, and other materials such as aluminium, copper, and chromium.

In the development of carbon–carbon composites via impregnation, Ma et al. [38] studied sintered carbon materials infiltrated with aluminium. Cylindrical samples of carbon composites impregnated with aluminium alloy were obtained following rapid cooling and solidification processes. More recently, in 2023, Wang et al. [137] compared the performance of copper fibre-reinforced C/C composite and copper alloy-impregnated C/C composite with that of conventional pure carbon pantograph slides used in rail applications. Both types of composites demonstrated superior electrical conductivity and mechanical performance than the pure carbon slidees.

In addition, regarding the impregnation of carbon-copper composites, Yin et al. [48] investigated the wear behaviour of these materials under varying electric current loads, emphasising the influence of copper content and applied load on wear resistance. The copper mesh-modified carbon composites in their study were prepared using an impregnation-carbonisation process. Similarly, Wei et al. [34] studied the arc erosion characteristics of copper copper-impregnated carbon slides. These composites were fabricated by infiltrating molten copper into the carbon substrate under high temperature and pressure conditions.

Moving on to the powder metallurgy route for C/C composite, Feng et al. [96] consolidated the carbon materials through the dispersion of sulfonated graphene oxide (SGO) and graphite in a phenolic resin alcohol solution, followed by drying, hot rolling, pulverisation, cold pressing, and solidification by heat treatment. The results showed that the flake graphite particles were bridged by the SGO, and the ground surface of the brush exhibited an interconnected carbon structure. Zhang et al. [63] investigated the use of sulfonated graphene (SG) to enhance the wear resistance of pantograph carbon slide materials under both normal and wet conditions. The composites were prepared by hot extrusion and roasting before machining to obtain the shape of a pantograph slide.

On the other hand, in 2021, Wang et al. [31] explored copper mesh modified carbon fibre reinforced polymer (CFRP) composite fabricated using copper foam impregnation and hot-pressing technology. Their approach aimed to improve the impact

strength, electrical resistance, and wear resistance of the pantograph slide, highlighting the synergy between the lubricating properties of graphite and the conductivity of copper. Wu et al. [60] investigated Bi-containing graphite/copper matrix composites with different bismuth content. The composites were manufactured via hot powder forging.

Xu et. al. [51] reported that copper-based composites with high graphite content for pantograph sliders were manufactured via the powder metallurgy method. Large-sized clustered graphite was added into the matrix as a solid lubricant to optimise the mechanical and wear performance of the composites. Fu et al. [40] examined the effect of reinforcement content on the properties of Ti_3SiC_2/Al_2O_3 hybrid-reinforced copper matrix pantograph slides. The study highlighted the potential of using ceramic reinforcements to enhance the mechanical and tribological properties of the composites. Meanwhile, Huang et al. [52] fabricated chromium-containing copper matrix composites with different flake graphite contents through the powder metallurgy method, and the mechanical properties, friction properties, and microstructure of the graphite/copper matrix composites were studied.

Guo et al. [138] reported that under the combined actions of CNT and TiB_2, the composite presented better arc resistance stability, and lower arc duration and energy. The formulated composites were prepared through mixing and compacting before being sintered at 900–950℃. Selvakumar et al. [44] also reported that the even distribution of multi-walled carbon nanotubes (MWCNT) and B_4C, coupled with good relative density, enhanced the hardness and wear resistance and decreased the porosity of the copper hybrid composite.

Focusing on natural material-based composites, the research by Ibrahim et al. [14], Selamat et al. [8], and Budin et. al [45] investigated the use of natural carbon materials, specifically PKS, for fabricating carbon-copper composites. They employed a warm compaction process to create composites intended for electrical and electronic applications. The warm compaction process is an inexpensive route that uses a lower processing temperature to consolidate the carbon-copper composite. The use of natural materials, such as PKS-derived carbon, presents an eco-friendly and cost-effective alternative to commercial carbon materials [12]. .

Based on the analysis of existing research, there is a significant gap in the understanding of the influence of natural material variability and the detailed mechanical and electrical performance of carbon-copper composites under actual

conditions. While previous studies have explored various processing methods, such as powder metallurgy and impregnation, to enhance the wear resistance and conductivity of carbon-copper composites, and have examined materials such as carbon-carbon and carbon-copper composites with additives like graphite, graphene, and natural carbon, research on using natural carbon sources like one from PKS and combining with graphite through the warm compaction method remains limited. Most of the research has utilised only PKS-derived carbon or only graphite as their source of carbon for the composite.

Table 2.8
Previous Studies of Carbon-Copper Composite for Current Collector Application Using Warm Compaction Method

Authors	Binder	Effect of Composition	Effect of Carbon Powder Size	Effect of Addition of Filler	Effect of Warm Compaction Temperature	Effect of Post-baking Temperature
Selamat [8]	Epoxy resin	Not studied	Not studied	Not studied	150 °C 200 °C 250 °C	Not studied
Ibrahim [14]	Epoxy resin	Not studied	<90µm, <150µm	Not studied	150 °C 200 °C 250 °C	Without post-baking 150 °C 200 °C 250 °C
Budin [45]	Epoxy resin	Not studied	Not studied	Not studied	150 °C 200 °C 250 °C	180 °C 200 °C 220 °C
Fazira, 2025	Phenolic resin	Effect of PKS, carbon/graphite ratio, with and without different fillers	Not studied	Addition of Graphene Oxide, CNT, and Cu-CNT as filler	150 °C 200 °C 250 °C	Without and with post-baking 200 °C

Previous studies on warm-compacted current collectors have primarily focused on epoxy resin as the binder, as shown in Table 2.8, with key contributions from Selamat et. al. [8], Ibrahim et. al. [14], and Budin et. al. [45]. These investigations have provided valuable insights into processing parameters such as warm compaction temperature and post-baking conditions. Further details on these parameters are explained in Section 2.7. However, they have not explored alternative binder systems that may offer superior thermal stability, wear resistance, and bonding characteristics. Specifically, phenolic resin, known for its heat resistance and mechanical integrity in tribological applications, remains unstudied in the context of warm-compacted carbon-

based composites.

In addition, the tribological characteristics of the carbon-copper composite under dry sliding conditions are investigated in this study. Previous studies have not conducted any wear analysis on carbon-copper composites developed from PKS-derived carbon through the warm compaction method.

Furthermore, the potential of PKS-derived carbon as a sustainable and cost-effective carbon source, as well as the influence of varying PKS-derived carbon-to-graphite ratios, remains unexplored. Such compositional variations could significantly impact the mechanical strength, electrical stability, and wear behaviour of the composite, yet they have not been systematically studied.

Another significant limitation of previous works lies in the absence of advanced filler technology. None of the earlier studies examined the incorporation of nanostructured additives such as GO, CNT, which are known to enhance thermal and electrical conductivity, mechanical strength, and tribological performance. The synergistic effects of these fillers, in combination with different carbon sources and binder types, remain unknown, representing a substantial knowledge gap in the development of new friction materials.

Although warm compaction temperatures ranging from 150℃ to 250℃ have been studied, these investigations were limited to epoxy resin systems and did not evaluate the interaction between temperature, pressure, and time during the warm compaction process. Similarly, while post-baking conditions have been partially addressed in some studies, no research has systematically examined the role of post-baking in phenolic resin-based composites reinforced with fillers. The combined influence of binder type, filler type, and thermal treatment, therefore, remains insufficiently understood.

To address these gaps, this study investigated the development of warm-compacted materials using phenolic resin as the binder, PKS-derived carbon with varying PKS-derived carbon-to-graphite ratios, and different fillers, while systematically evaluating the effects of warm compaction temperature, pressure, time, and post-baking temperatures on their mechanical, electrical, and tribological performance.

2.11 Summary

A review of previous studies reveals several critical research gaps. First, there is limited evidence regarding the suitability of locally sourced carbon, particularly PKS-derived carbon, when hybridised with graphite and copper, in meeting the performance requirements for electrical rail service demand, specifically pantograph slides. Second, the warm compaction process, with or without post-baking treatment, has not been thoroughly investigated with respect to its potential to concurrently optimise the electrical conductivity and mechanical strength of the composite. These gaps provide the basis and motivation for this research, which seeks to develop and optimise a locally produced carbon-copper composite incorporating PKS-derived carbon, graphite, copper, phenolic resin, and selected fillers. The proposed material system is processed via the warm compaction method and benchmarked against the performance of commercial pantograph slides reported in the literature.

The hybridisation of PKS-derived carbon and graphite is highlighted as it allows the combination of the fibrous strengthening characteristics of PKS-derived carbon with the lubricating and electrically conductive properties of graphite. Furthermore, the role of additional fillers is elaborated to establish their influence on the physical and functional properties of the carbon-copper composite.

Pantograph slides are usually manufactured using impregnation or powder metallurgy, with warm compaction being one of the powder metallurgies routes. However, there are very few studies that focus on the process parameters of warm compaction for PKS-derived carbon-based composites. To address this gap, this study investigates the effects of compaction time, temperature, and pressure. The resulting composites from all stages are tested for density, hardness, electrical resistivity, and transverse rupture strength (TRS).

Finally, the composite from the optimum condition identification stage is tested under dry sliding conditions to evaluate its wear rate and coefficient of friction. This provides a direct measure of its suitability for pantograph slide applications. Overall, this review reveals clear gaps in current knowledge, and this study is designed to address them. The findings from the literature form the foundation for the experimental methodology presented in Chapter 3.

CHAPTER 3
RESEARCH METHODOLOGY

3.1 Introduction

This chapter presents detailed information on the materials, equipment, and fabrication techniques employed in the development of the carbon-copper composite. The methodology of the research study is designed to achieve all research objectives is also presented. To gain a comprehensive understanding of the raw materials, a series of characterisation techniques was employed, including Raman spectroscopy, X-ray diffraction (XRD), and scanning electron microscopy (SEM). The selection of materials and their optimal composition was based on a thorough review of existing literature and experimental data obtained from laboratory investigations. The aim was to identify the most suitable combination of materials that would yield carbon-copper composites with the desired properties. This chapter outlines the specific procedures involved in fabricating the carbon-copper composites using the warm compaction method and the identification of the optimum condition of the process using the Taguchi L9 orthogonal array. Once fabricated, the composites were subjected to a range of tests to evaluate their physical, mechanical, electrical, and wear properties. The research framework comprised four phases. Phase 1 focused on identifying the composition of carbon, copper, and resin to develop the carbon-copper composite from PKS-derived carbon. A combination of PKS-derived carbon and graphite was also studied to obtain a composite with acceptable properties for the intended application. In Phase 2, the effects of adding filler on the properties of the composites were investigated. For each of these phases, the tests included measurements of density, hardness, electrical resistivity, and transverse rupture strength (TRS). Furthermore, SEM, XRD, and Raman spectroscopy analyses were conducted to support the findings and discussions. The data obtained were analysed, and the compositions with the best properties were selected. In Phase 3, the identification of the optimum condition of the warm compaction process was conducted using the Taguchi L_9 orthogonal array, and the data were analysed using analysis of variance (ANOVA). The properties evaluated were electrical resistivity and TRS. Finally, the optimised composites were tested for their wear characteristics under dry sliding conditions in Phase 4.

3.2 Raw Materials Description

The study investigated the properties of carbon-copper composites; hence, the main materials used were carbon and copper. The carbon sources consisted of PKS-derived carbon and graphite. Mixtures of both carbon materials at various ratios were prepared and examined in this research. Other materials used in the fabrication of the carbon-copper composites were phenolic resin, which served as a binder, as well as graphene oxide (GO), CNT, and copper-CNT, acting as filler or additive. The raw materials used in this study are listed in Table 3.1. All received raw materials were utilised directly without any further treatment.

Table 3.1
List of Powder Materials Used in the Experimental Work

Materials	Colour and shape	Size	Manufacturer/Supplier
PKS-derived carbon	Black	200 mesh	Tan Meng Keong Sdn. Bhd.
Graphite	Black, chips	< 500 µm	AFI Brake Manufacturing
Copper (Purity: 98%)	Brown, spheroidal	10 – 25 µm	Sigma Aldrich / PLT Scientific Sdn. Bhd.
Phenolic Resin (Purity: 89.6%)	Yellow	< 100 µm	AFI Brake Manufacturing Sdn. Bhd.
Graphene Oxide (Purity: 100%)	Black, flaky powders	200 – 500 µm	UM Innovations Sdn. Bhd.
Carbon Nanotube	Black, rolled sheets	Diameter 8-15nm Length 30-50nm Layer 8-15	Ugent Tech Sdn. Bhd.
Copper-CNT	Blake, spheroidal	Diameter 20µm Length 10µm	Applied Carbon Nanotechnology Co. Ltd.

a) Palm kernel shell (PKS) derived carbon

The activated natural carbon (PKS-derived carbon) was obtained from a local company, Tan Meng Keong Sdn. Bhd. For this study, fine PKS-derived carbon powder with a particle size of 200 mesh was selected. The PKS-derived carbon appeared as a fine black powder. It was used as a carbon source and bio-based reinforcement to partially substitute graphite, thereby enhancing the sustainability of the composite while improving its hardness, wear resistance, and thermal stability.

b) Graphite

Graphite powder was obtained from a local company, AFI Brake Manufacturing Sdn. Bhd. The graphite powder appeared as black chips with a particle size of less than 500 μm. It was used as a carbon source and reinforcement phase, providing excellent electrical and thermal conductivity, as well as acting as a solid lubricant. These characteristics enhanced the tribological performance and stability of the composite.

c) Copper

Copper powder used in this research had a particle size of less than 90 μm and appeared as a spheroidal-shaped brown powder. It was manufactured under the brand Sigma-Aldrich and supplied by a local company, PLT Scientific Sdn. Bhd. Copper was used as the functional phase to enhance the electrical conductivity of the composite while also acting as a co-matrix with the phenolic resin to ensure good interfacial bonding with the carbon-based constituents [139].

d) Phenolic resin

Phenolic resin in powder form was used in this study as a binder. It appeared as a yellowish powder with a particle size of less than 100 μm. The resin was cured during the warm compaction process dan further cured during the post-baking process. Phenolic resin acted as the primary matrix material, binding the carbon, copper, and filler phases together to provide structural integrity and dimensional stability.

e) CNT

CNT powder was used as a nanofiller in the composite for Phase 2. CNT is known for its outstanding mechanical and electrical properties. The CNT used in this study consisted of 8 – 15 multi-walled layers, with diameters ranging from 8 to 15 nm and lengths between 30 and 50 nm. CNT was used as a nanoscale reinforcement filler to enhance the mechanical strength and electrical efficiency of the composite.

f) Graphene oxide

GO appeared as a black, flaky powder with a particle size of 200 – 500 μm. It was used as a nanoscale reinforcement filler in Phase 2 to enhance the mechanical strength and electrical efficiency of the composite.

g) Copper-CNT

Copper-CNT (Cu-CNT) powder was used as a filler in the composite for Phase 2. It served as a reinforcement material to enhance the mechanical strength and electrical efficiency of the composite, as it combined the properties of both copper and CNT.

3.3 Methodology of the Research Study and Design of Experiment (DOE)

The methodology of the research study was designed to investigate in a systematic manner. The conceptual research method, as shown in Figure 3.1, was designed to attain all the key aspects required to achieve the research objectives. The framework was divided into four phases. Phase 1 focused on studying the composition of PKS-derived carbon and the effects of the PKS-derived carbon-to-graphite ratio on the properties of the carbon-copper composite. Different compositions of PKS-derived carbon were analysed, and the ratio of PKS-derived carbon to graphite was also investigated. The best combination of carbon (PKS-derived carbon and graphite), copper, and resin identified in Phase 1 was then used in Phase 2, where the effects of adding fillers were studied. Three types of fillers were examined: GO, CNT, and Cu-CNT. The addition of filler is expected to enhance the properties of the carbon-copper composite. In Phase 3, the warm compaction process parameters were optimised using the Taguchi method to achieve the best properties of the carbon-copper composite. ANOVA was employed to identify the optimal composite, which was then carried forward to Phase 4. In the final phase, the tribological properties of the optimised carbon-copper composite were evaluated under dry sliding conditions. Each phase had a designated purpose, accompanied by experiments to fabricate and produce the carbon-copper composite from PKS-derived carbon and graphite for pantograph slide applications in rail systems. Technical replicates were performed in the study to reduce human error in conducting the experiments.

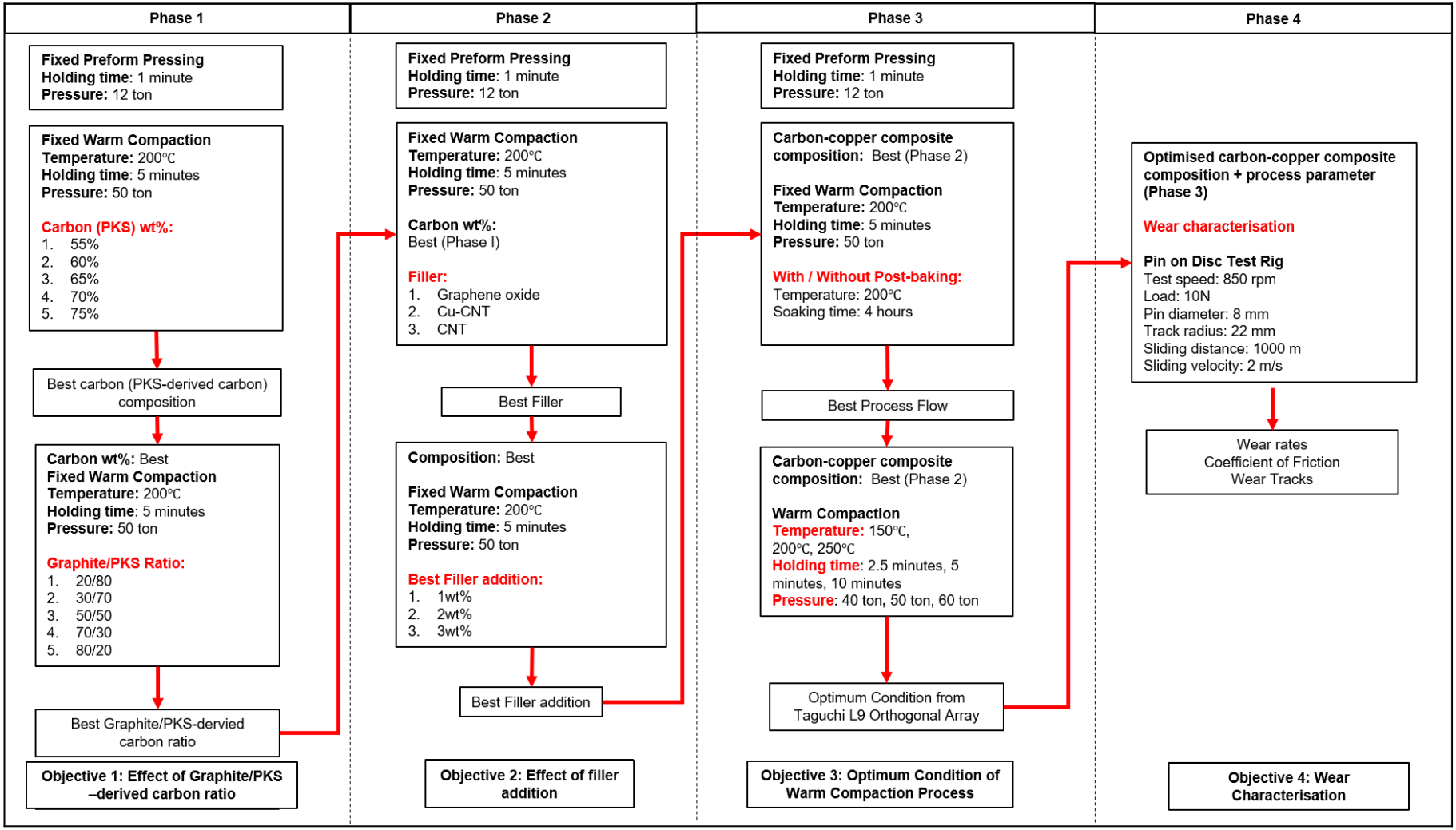

Figure 3.1 Methodology of Research Work

3.4 Fabrication of Carbon-Copper Composite

The carbon-copper composite was fabricated using the powder metallurgy route, which consists of the development of the preform (cold pressing), a warm compaction process, and a post-baking process. The schematic flow of the process is shown in Figure 3.2. The process involved several steps, including mixing, cold pressing, warm compaction, and post-baking. The fabrication of the carbon-copper composite was the main procedure throughout the research and was applied in Phases 1 to 3.

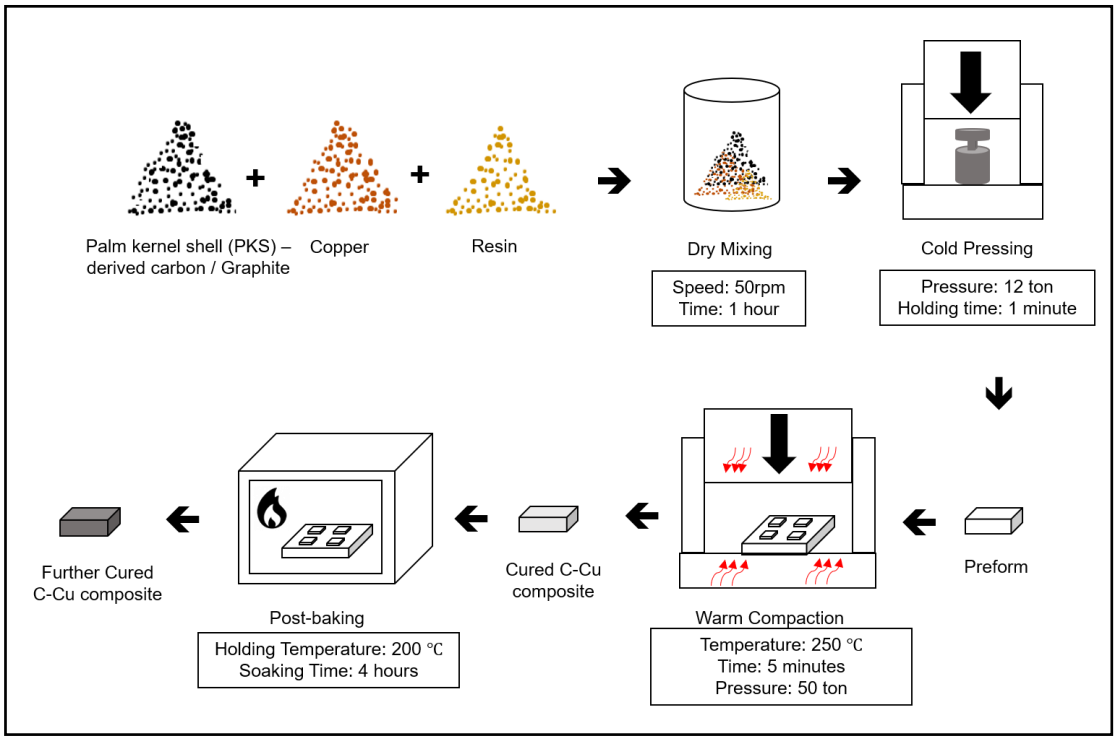

Figure 3.2 Schematic Diagram of Fabrication Process Flow of Carbon-Copper Composite

3.4.1 Mixing of Materials (Dry Mixing)

A shaker mixer (Plate 3.1(b)) was employed to mix the powder through a dry mixing procedure. The specifications of the mixer are shown in Table 3.2. Powders with the specified composition, as discussed in the research phases, were placed into the mixing container (Plate 3.1(a)) and secured within the bracket inside the mixer. The duration and speed of the mixing operation were preconfigured via the control panel. A total of 100 g of powder was mixed for each batch. This process was applied in Phases

1, 2, and 3. The speed and mixing time were kept constant across all phases.

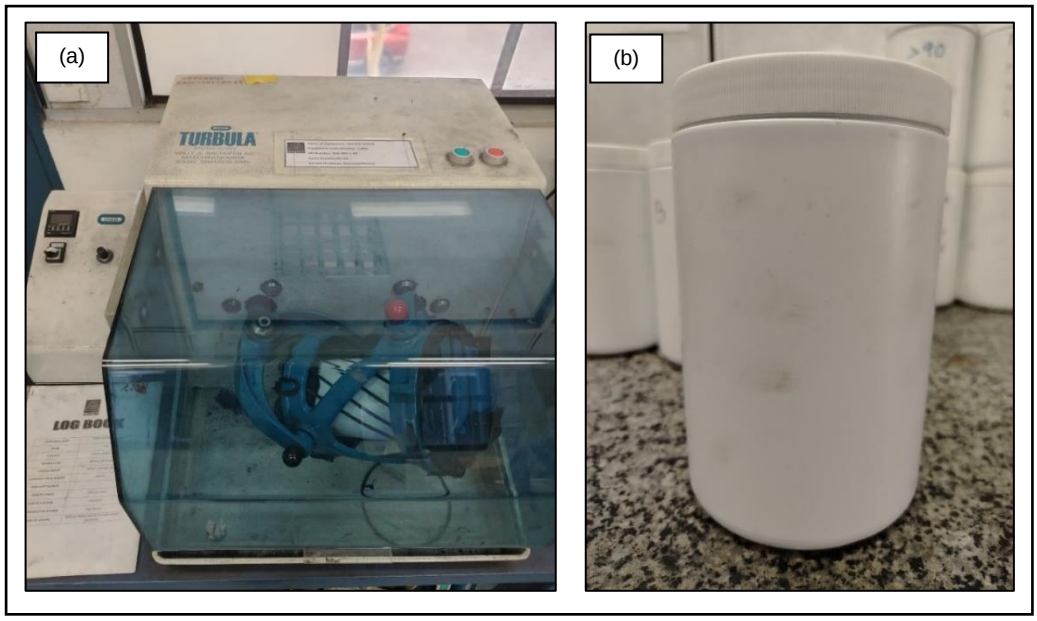

Plate 3.1 Mixing of Powders: (a) Turbula Shaker Mixer, and (b) Mixing Container

Table 3.2
Shaker Mixer Specification

Equipment	Brand	Origin	Model	Speed
Shaker Mixer	WAB	Switzerland	Turbula T 2 G	22 – 96 rpm

3.4.2 Development of Preform (Cold Pressing)

An automatic hydraulic press was employed to create the green body of the preform (Plate 3.2). The specifications of the machine are presented in Table 3.12. Once the mixed powder was prepared, it was weighed and poured into the mould to shape it into a 1-inch by 1-inch block with a thickness of approximately 1 cm. Due to the limitations of the cold press machine, a maximum tonnage of 12 tonnes was applied for all stages. The holding time was fixed at 1 minute. The applied pressure and soaking duration were kept constant at 12 tonnes across all phases. This procedure was applied in Phases 1 to 3.

Table 3.3
Automatic Hydraulic Press Specification

Equipment	Brand	Origin	Model	Maximum Compression Force
Automatic Hydraulic Press	Carver	USA	3890	25 Tons

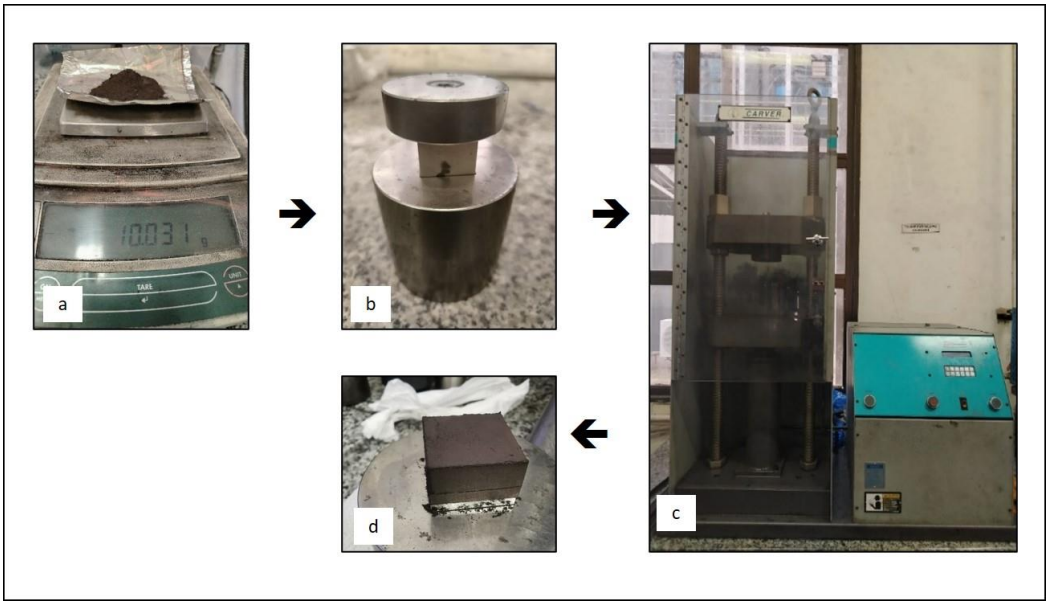

Plate 3.2 Cold Pressing: (a) Balance to Weigh Mixed Powder, (b) Mould, (c) Automatic Hydraulic Press for Preforming, and (d) Preform Ejected from Mould

3.4.3 Development of Carbon-Copper Composite (Warm Compaction)

The warm compaction process was conducted using a hydraulic compression moulding press machine. The specifications of the press machine are shown in Table 3.4. Preforms were positioned within a mould with cavities as shown in Plate 3.3(a). This step is applied in Phases 1, 2, and 3. Based on previous studies [8], [14], [45], [46], the warm compaction temperature was fixed at 200 °C, holding time was 5 minutes, and pressure was 50 tonnes. The parameters of the warm compaction process (temperature, time, pressure) were kept constant in Phases 1 and 2. However, in Phase 3, the optimum condition is determined using the Taguchi method at three levels for each factors to achieve the best properties of the carbon-copper composite.

Table 3.4
Hydraulic Compression Moulding Press Specification

Equipment	Brand	Origin	Compression Force	Temperature
Hydraulic Compression Moulding Press	Santec	India	200 Tons	250 ℃

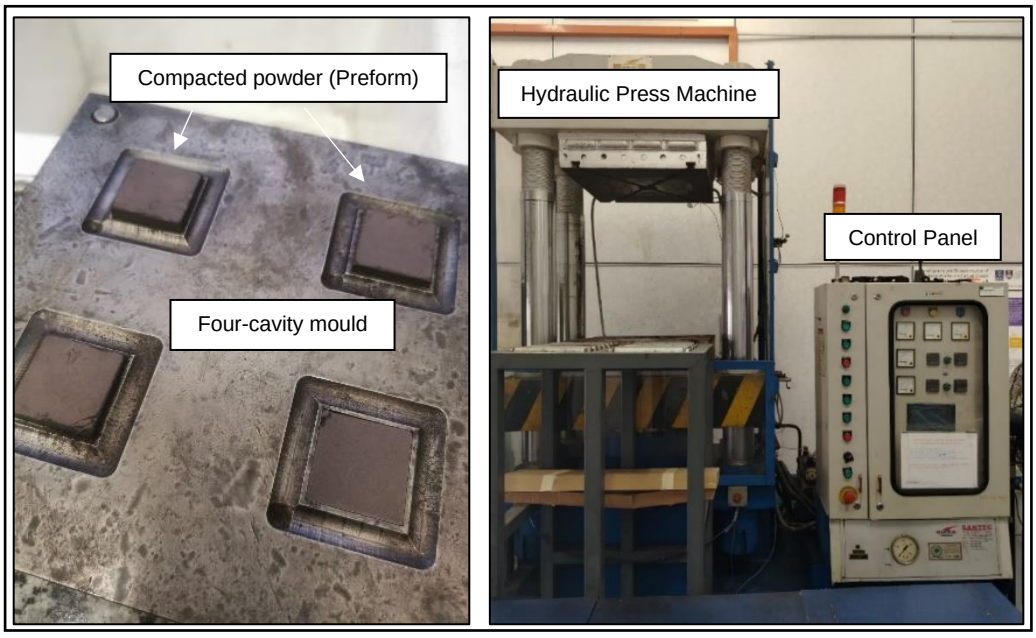

Plate 3.3 Warm Compaction: (a) Four-Cavity Mould and (b) Hydraulic Compression Moulding Press

3.4.4 Post-baking of Carbon-Copper Composite

The samples went through a post-baking treatment in the oven for further curing. Temperature and time for the post-baking process are shown in the heating profile, as in Figure 3.3. The temperature profile was referred to a previous work done by Ibrahim et. al. [14]. The Shel Lab microprocessor-controlled oven was utilised for this purpose, shown in Plate 3.4. This step is applied in Phase 1 to Phase 3. The temperature is kept constant at 200℃ throughout the investigation. In Phase 3, the composite is also developed without the post-baking process to identify the necessity of this step.

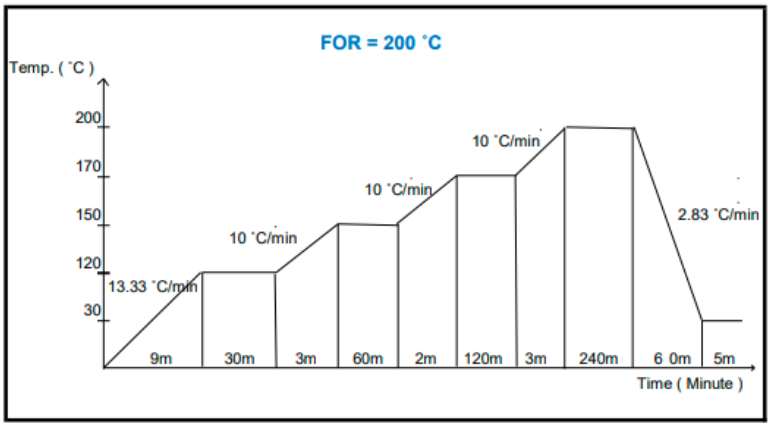

Figure 3.3 Post-baking Temperature Profile

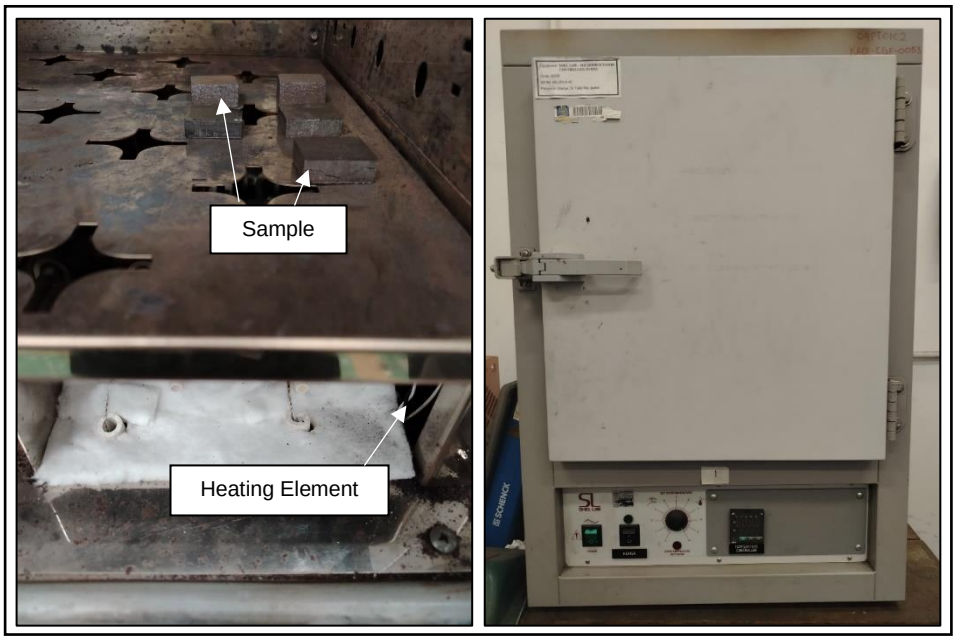

Plate 3.4 Microprocessor-Controlled Oven for Post-baking Process

3.5 Phase 1: Formulation of Carbon-Copper Composite

In Phase 1, the aim was to determine the optimal formulation of carbon, copper, and phenolic resin for the development of the carbon-copper composite. This process was conducted in two sequential steps, as shown in Figure 3.4. The first step examined the effect of carbon content in the composite by varying the proportion of carbon and copper while maintaining a fixed amount of resin. Only activated carbon derived from PKS was used as the carbon source in this step.

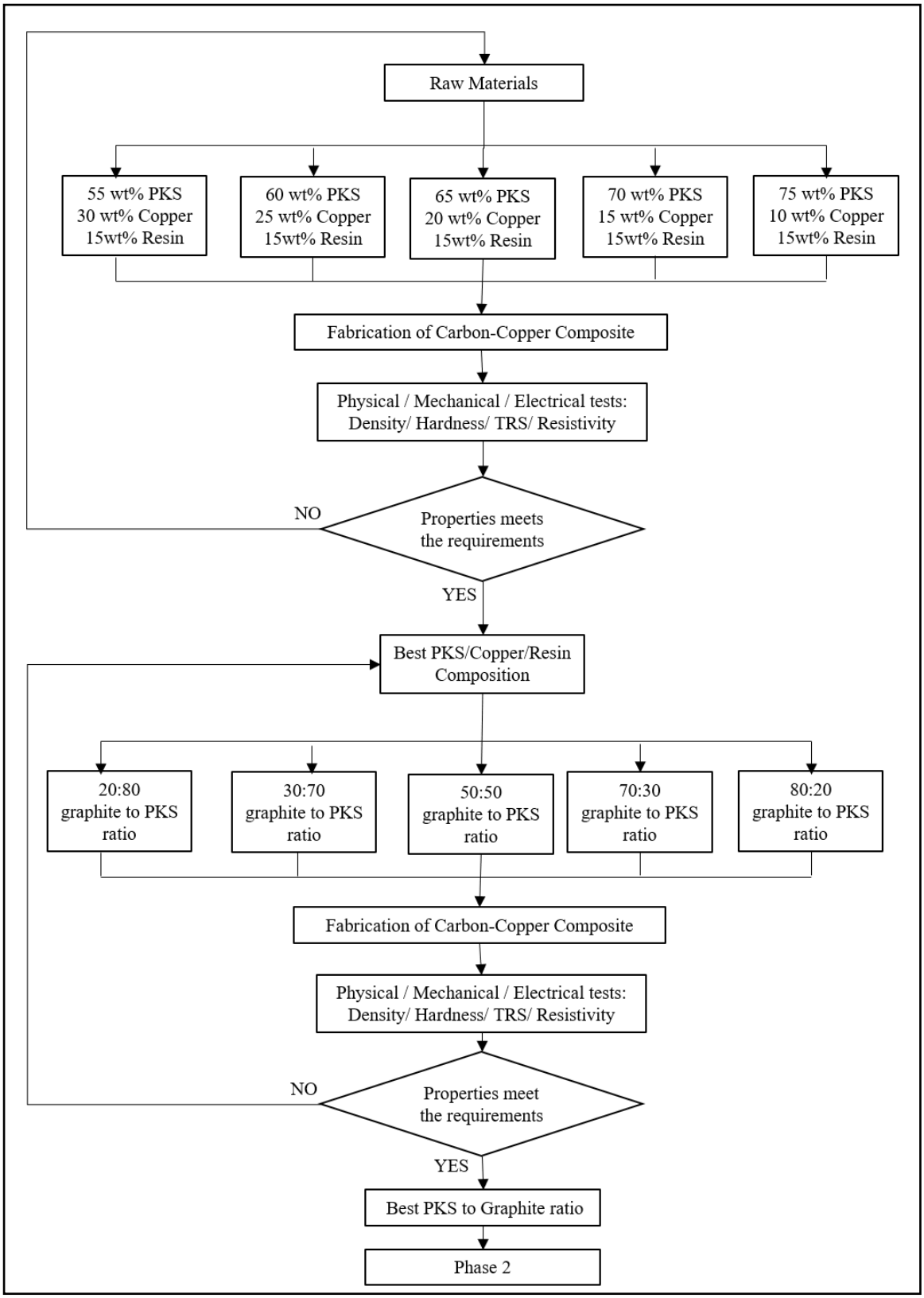

Figure 3.4 Flowchart for the Study of Formulation of Carbon-Copper Composite (Phase 1)

To identify the most suitable formulation, different PKS-derived carbon contents were investigated, namely 55, 60, 65, 70, and 75 wt%. As the resin was fixed at 15 wt%,

the content of copper was adjusted to ensure the total composite composition summed to 100 wt%. The material compositions are presented in Table 3.5. The resin content of 15 wt% was selected based on previous studies by Selamat et al. [8], Ibrahim et al. [14], Budin et al. [45], and Nurulhadi et al. [46] as this amount was sufficient to bind the carbon and copper powders. Additionally, increasing the resin content generally reduces conductivity and shifts the composite towards more insulating behaviour [140], which is not favoured for this application.

After the fabrication of the composites was completed, they were tested for density, hardness, electrical resistivity, and TRS. SEM and XRD analyses were conducted to support the findings and discussions. The performance of these compositions was benchmarked against commercial pantograph slides reported in the literature to identify the best formulation, or at least those that met the requirements for the intended application.

Table 3.5
Raw Material Composition for Phase 1

Sample identification	**Raw material composition (wt%)**		
	PKS-derived carbon	**Copper**	**Phenolic resin**
A01	55	30	15
A02	60	25	15
A03	65	20	15
A04	70	15	15
A05	75	10	15

In this study, activated carbon derived from PKS was used as the carbon source. The aim was to determine the best composition of carbon for developing the carbon-copper composite to be used in the subsequent phase of this study. The phenolic resin content was maintained at 15 wt%, while the proportions of PKS-derived carbon and copper were varied, as presented in Table 3.5.

To investigate the influence of carbon content in this phase, the pressing pressure was adjusted to 12 tonnes (118 kN) with a holding period of one minute. The warm compaction process parameters were set to a temperature of 200℃, a holding duration of 5 minutes, and a pressure of 50 tonnes (490 kN). The post-baking temperature was conducted at 200°C for a soaking time of four hours. These parameters were selected based on previous studies reported by Selamat et al. [8] and Ibrahim et.al [14]. This set of optimised parameters was used to produce the carbon-copper composite intended for

use as a current collector in third-rail applications, which is similar in function to a pantograph slide [2]. However, due to the limitations of the machine during the experimental work, the maximum achievable pressure for the cold pressing process was restricted to 12 tonnes (118 kN) instead of 18 tonnes (176 kN) as recommended in previous research.

The composite exhibiting the best properties was selected for further investigation in the next step, which studied the incorporation of graphite with PKS-derived carbon to enhance the properties of the composite. In this step, the total carbon content was fixed at 65 wt%, while the copper and resin contents were maintained at 20 wt% and 15 wt%, respectively. The carbon fraction was then adjusted by varying the graphite-to-PKS-derived carbon ratio at 20:80, 30:70, 50:50, 70:30, and 80:20, as shown in Table 3.6. After the fabrication of the carbon-copper composites was completed, they were tested for density, hardness, electrical resistivity, and TRS. The composition demonstrating the best properties, or at least meeting the requirements for the intended application, was selected for continuation into the subsequent phase.

Table 3.6
Graphite to PKS-derived carbon ratio for Phase 1

Sample identification	**Graphite/PKS-derived carbon ratio**	
	Graphite	**PKS-derived carbon**
B01	20	80
B02	30	70
B03	50	50
B04	70	30
B05	80	20

3.6 Phase 2: Effects of Filler Type and Composition

In Phase 2, the aim was to determine the type of filler and its weight percentage (amount) to be added to the carbon-copper composite. The flow of this study is depicted in Figure 3.5.

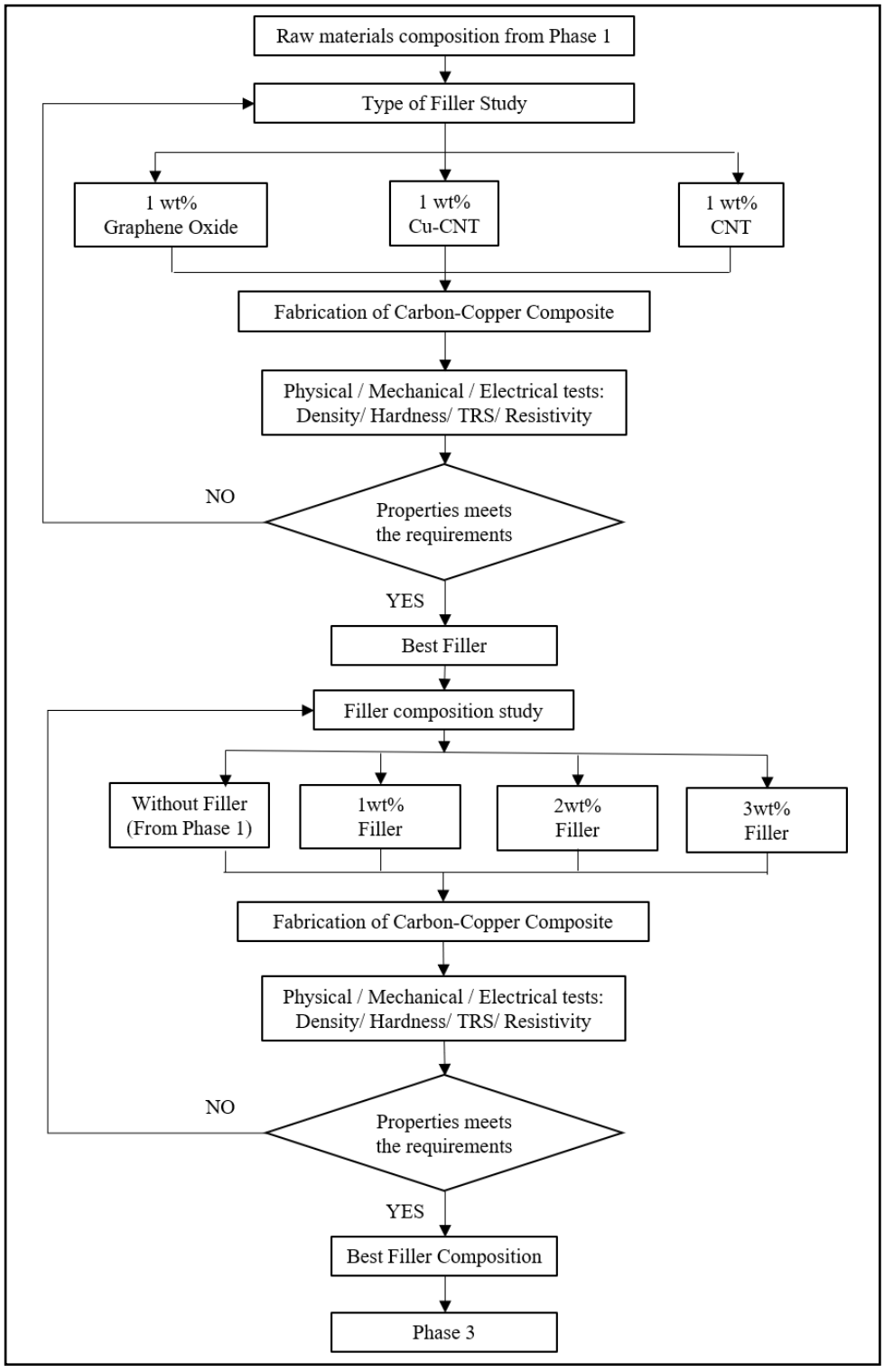

Figure 3.5 Flowchart for the Study of Filler Type and Composition (Phase 2)

Table 3.7 presents the type of filler and its composition added to the carbon-copper composite based on the selected formulation from Phase 1. The powders underwent the same fabrication process, which included mixing, preform development, warm-compaction, and post-baking to produce the carbon-copper composites. The resulting composites were then tested for density, hardness, electrical resistivity, and TRS. The results were analysed to identify the most suitable filler for the carbon-copper composite. The optimal filler for the composite was selected based on its performance in comparison to the commercial pantograph slide reported in the literature.

Table 3.7
Filler Type and Composition for Phase 2

Sample identification	**Filler**	
	Material	**Composition (wt%)**
C01	Graphene Oxide	1
C02	Cu-CNT	1
C03	CNT	1

The second step in this phase was carried out to investigate the effect of different compositions of the optimal filler identified in the first step on the physical and electrical properties of the carbon-copper composite. The overall process for this phase is shown in Figure 3.2 in the previous section. The preparation of raw materials involved varying the filler content at 1 wt%, 2 wt%, and 3 wt%, as shown in Table 3.8. To maintain the stoichiometric coefficient, the amounts of PKS-derived carbon and graphite were adjusted accordingly. The same fabrication process, comprising powder mixing, preform development, warm compaction, and post-baking, was employed, as shown in Figure 3.5. The resulting composites were tested for density, hardness, electrical conductivity, and TRS. The results were analysed to determine the optimum filler composition for the carbon-copper composite. The optimal filler composition was selected based on its performance relative to commercial pantograph slides reported in the literature.

Table 3.8
Best Filler Composition Study in the Carbon-Copper Composite

Sample identification	Filler Composition (wt%)
D01	0
D02	1
D03	2
D04	3

3.7 Phase 3: Optimum Condition of Process Flow and Parameter

In Phase 3, the objective was to investigate the optimum conditions for the warm compaction temperature, time, and pressure, both with and without the post-baking process. The flow of this study is illustrated in Figure 3.6. The first step was to investigate the effects of the post-baking process. The optimal formulation obtained from Phase 2, comprising carbon, copper, resin, and filler, underwent the same fabrication process. The first step aimed to investigate the necessity of the post-baking process. Subsequently, the warm compaction process parameters were optimised using the Taguchi method. The resulting composites were tested for density, hardness, electrical resistivity, and TRS. The results were analysed to compare composites with and without the post-baking step and to identify the optimal process flow for producing the carbon-copper composite. It was selected based on its performance relative to commercial pantograph slides reported in the literature.

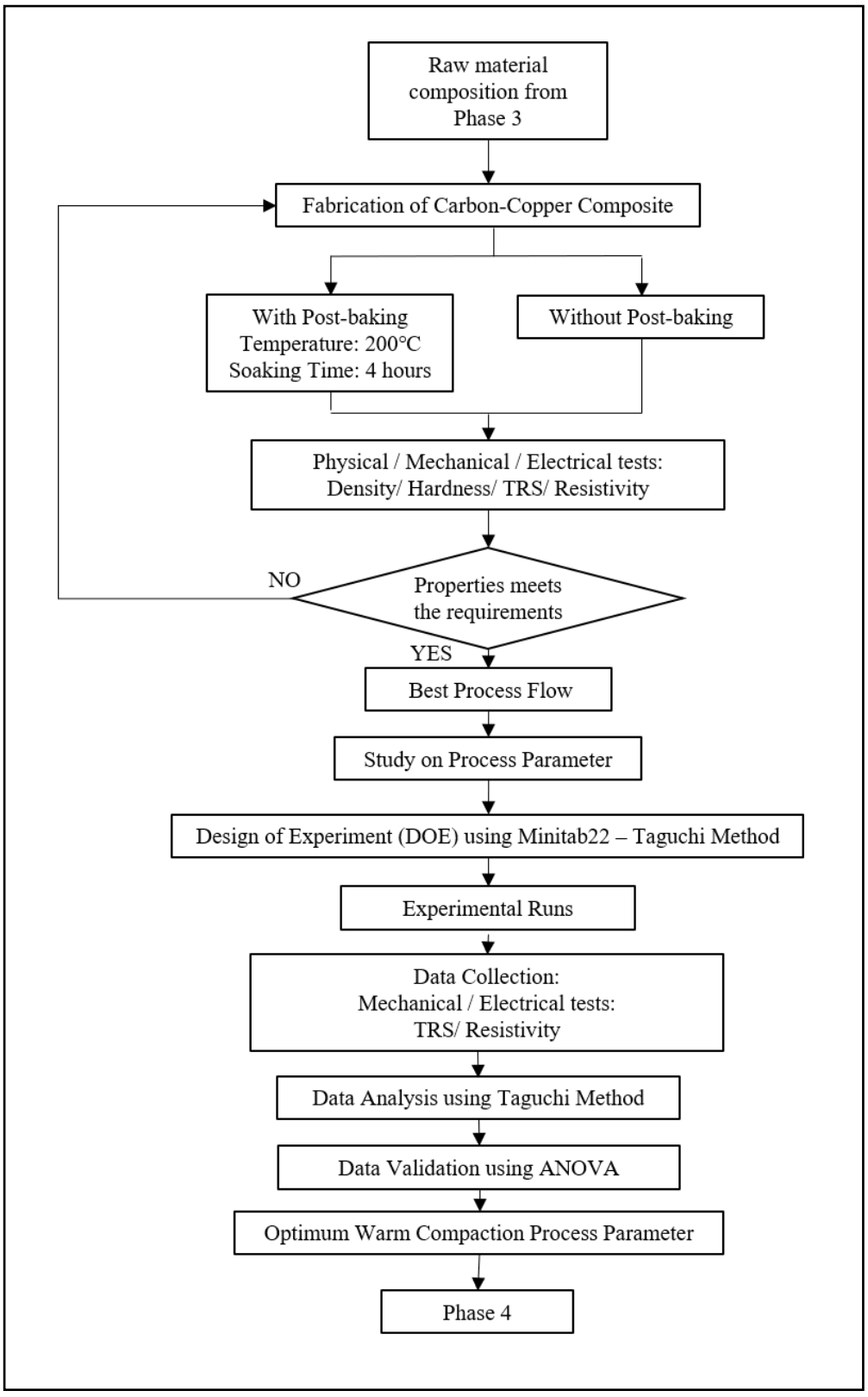

Figure 3.6 Flowchart for the Study of Filler Type and Composition (Phase 3)

In this study, three parameters and their interactions were investigated: temperature, time, and pressure.

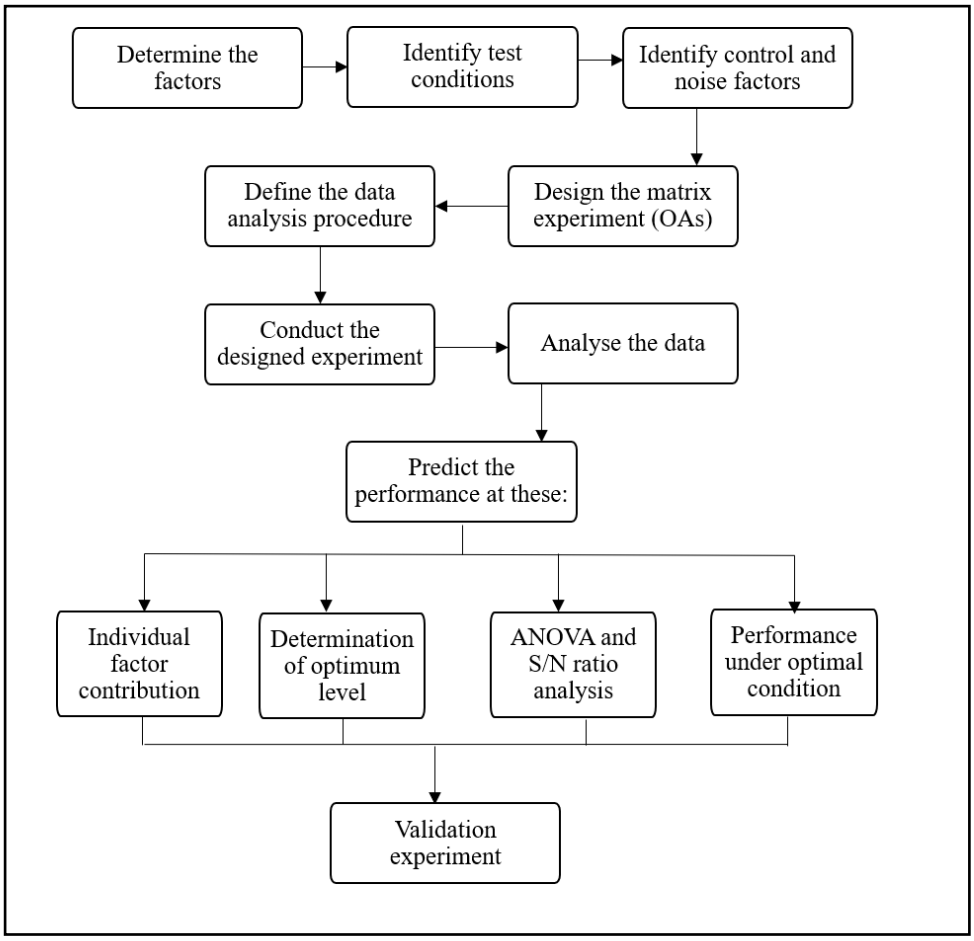

Figure 3.7 Flowchart of the Taguchi Method Experimental Set-Up

The Taguchi technique was used to optimise the process parameters by evaluating the results obtained for electrical resistivity and transverse rupture strength (TRS). The design of experiments (DOE) technique was employed to optimise the warm compaction process parameters. The Taguchi method was selected to design the experiment, as shown in Figure 3.7. Different warm compaction parameter settings were used to fabricate the carbon-copper composite. Based on previous studies, the critical process parameters were identified, as shown in Table 3.9. By varying the warm compaction parameters, their effects on the electrical resistivity and TRS of the composites were determined. The parameters studied were temperature, time, and pressure. each set at three levels. Table 3.9 summarises the setting of the warm compaction parameters used in this study.

Table 3.9
Setting of Warm Compaction Parameter for Phase 3

Factor	Level	L1	L2	L3
A	Warm compaction temperature (℃)	150	200	250
B	Warm compaction soaking time (minutes)	2.5	5	10
C	Warm compaction pressure (ton)	40	50	60

From Table 3.9, three variables were selected for this study, and each variable was tested at three levels. The warm compaction temperature was set at 150℃, 200℃, and 250℃. The warm compaction time was set at 2.5 minutes, 5 minutes, and 10 minutes. The warm compaction pressure was set at 40 tonnes, 50 tonnes, and 60 tonnes.

Table 3.10
Orthogonal Array L_9 for Experimental Runs in Phase 3

Sample identification	Run	A	B	C
E01	R1	1	1	1
E02	R2	1	2	2
E03	R3	1	3	3
E04	R4	2	1	2
E05	R5	2	2	3
E06	R6	2	3	1
E07	R7	3	1	3
E08	R8	3	2	1
E09	R9	3	3	2

The parameter settings were transferred into the Minitab 22 software to design the Taguchi orthogonal array for this study. Using three warm compaction parameters as the factors, the L_9 (3^2) orthogonal array was used. The settings of the L_9 (3^2) orthogonal array are shown in Table 3.10. The carbon-copper composites were produced through the warm compaction method using the parameters listed in Table 3.10. The powders with the best composition from the previous phase underwent the same fabrication process; however, during the warm compaction step, the parameters followed the orthogonal arrays setting, with nine trial runs. The resulting composites were then tested for their electrical resistivities and TRS.

All statistical analyses were conducted using Minitab 22 software. The workflow comprised data preparation and quality checks, followed by Taguchi mean-

based analysis to identify factor levels that minimised electrical resistivity and, separately, maximised TRS. The optimised conditions were then validated by benchmarking the results against commercial pantograph slides reported in the literature.

Raw measurements of resistivity and TRS were imported with a unique run ID, and the randomised run order used during fabrication and testing was maintained. Density and hardness were monitored as supporting quality indicators (constraints) but were not included as optimum condition responses.

A Taguchi orthogonal array (OA) was executed and analysed using the response means. Response tables for the means were used to identify the optimal level of each factor for each response separately (resistivity "smaller", TRS "larger"). Main-effects plots were used to visualise trends and assess practical significance. To establish practical relevance, no model-prediction comparison was performed; instead, validation was performed by benchmarking the optimised samples against commercial pantograph slide data reported in the literature. A statistical performance measurement known as the S/N ratio was employed to analyse results in this approach. The experimental data were converted into S/N ratios and subsequently evaluated. The signal factor shows the real values obtained from the system, while the noise factor denotes factors that are not part of the experimental parameters but still affect the experimental results. Noise sources are variables that cause deviations in the desired performance characteristics from the target value. In addition, analysis of variance (ANOVA) was used to evaluate the response magnitude, expressed in percentage (%), of each parameter in the orthogonal experiments.

3.8 Phase 4: Wear Characterisation of the Carbon-Copper Composite

In Phase 4, the objective was to investigate the wear characterisation of the developed carbon-copper composite. Since pantograph slides in rail applications are frequently in contact with overhead copper lines during operation, it is important to examine their wear characteristics to assess the viability of the carbon-copper composite formulation developed in this study. Figure 3.8 presents the process flow for the wear characterisation study. The pin-on-disk method was employed to evaluate the wear characterisation of the carbon-copper composite.

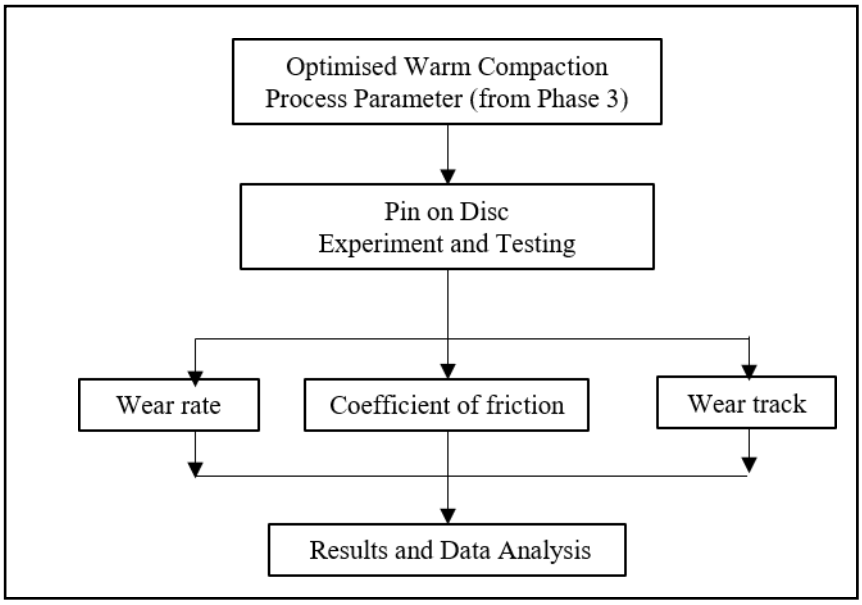

Figure 3.8 Process Flow for Wear Characterisation Study (Phase 4)

The wear test on the sample was conducted in accordance with ASTM G99 (Standard Test Method for Wear and Friction Testing with a Pin-on-Disk Apparatus). This test allowed the evaluation and comparison of the wear resistance of the composites, supporting the selection of the most suitable material and process parameter. The Magnum Pin-on-Disk Wear and Friction Test Rig was utilised for this test. It was conducted at room temperature (27.5°C). The optimised sample from Phase 3 was tested under the settings depicted in Figure 3.8 and Table 3.11, under dry sliding conditions.

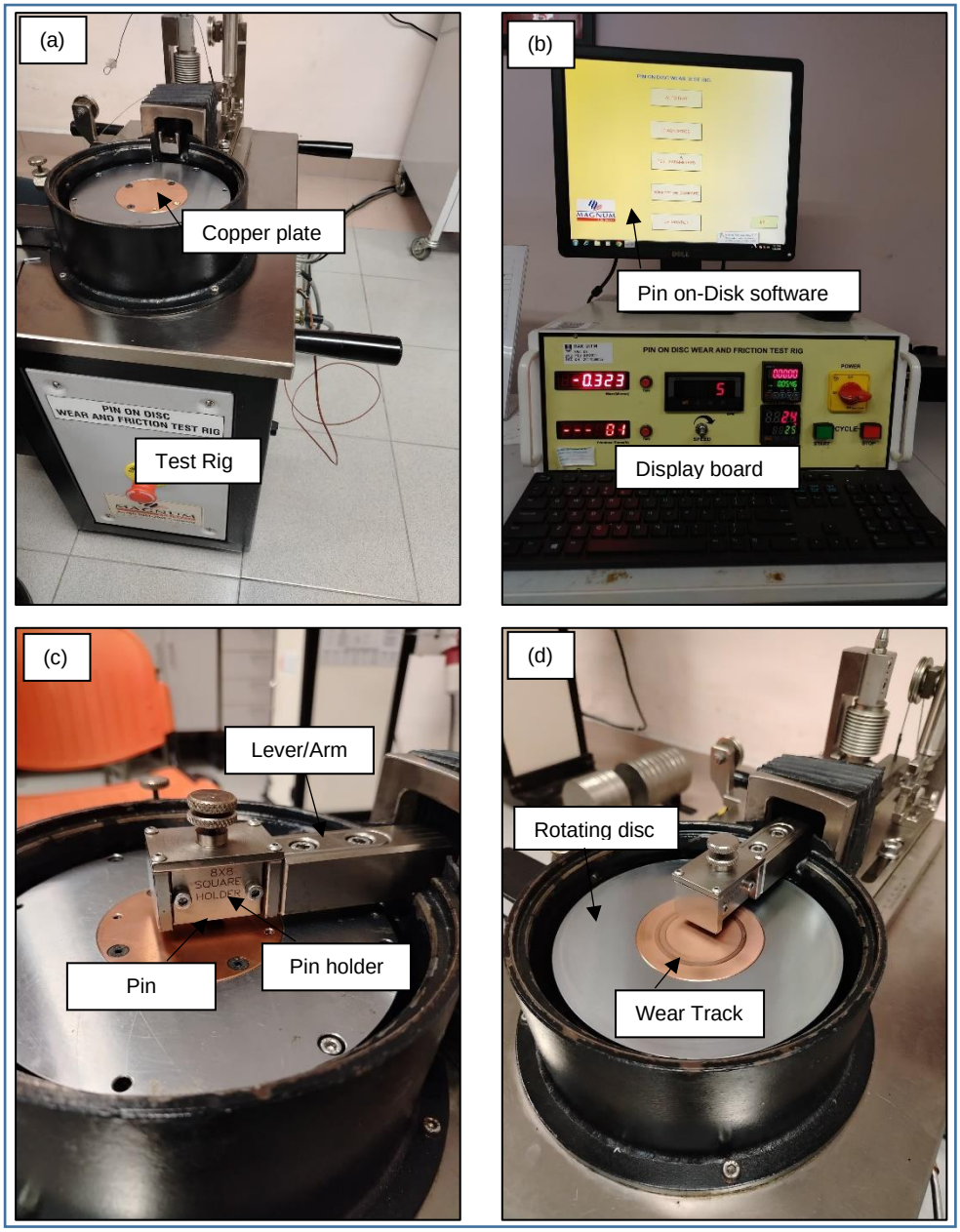

Plate 3.5 Magnum Pin on Disk Wear and Friction Test System

The Pin-on-Disk Wear and Friction Test Rig and its experimental setup are illustrated in Plate 3.5 (a-d). The system includes the main rig with its components (Plate 3.5 (a)), as well as a computer running the Pin-on-Disk software (Plate 3.5 (b)). Figure 3.9 shows a schematic of the pin-on-disk wear test system. It consists of a driven spindle and chuck to hold the revolving disk, a lever-arm device to hold the pin, and an attachment to allow the pin specimen to be forced against the revolving disk specimen with a controlled load.

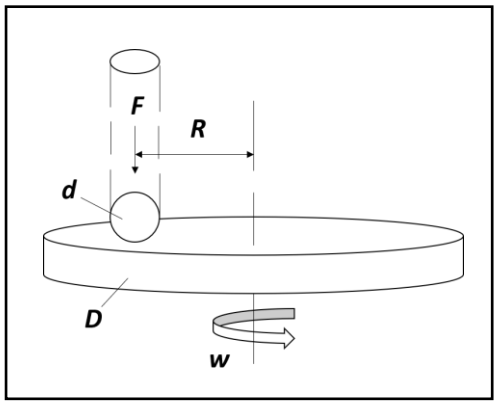

Figure 3.9 Schematic Diagram of Pin-on-Disk Wear Test System

The pantograph slider continuously slides against overhead wires; thus, pantograph slider materials were used as the pin specimen in this wear test, while a copper plate serves as the disk under dry conditions. The developed carbon-copper composite from Phase 3 was sliced into three smaller pieces to produce the pin, each measuring 8 mm x 8mm (square end) and 25.5 mm in length. Details of the cutting process are explained in Section 3.9. The pin was fitted in the square holder (Plate 3.5 (c)). A pure industrial copper (99.9%) plate (75 mm ± 0.5 mm diameter, 4.0 mm ± 0.5 mm thickness) was fabricated and fitted onto the base rotating disk (230 mm diameter). During the test, the pin was slid against the copper plate.

The test setup parameters were fixed, as shown in Table 3.11. The test speed was set at 850 rpm, corresponding to a sliding velocity of around 2 m/s (rotation radius = 22 mm). The pin specimen was pressed against the disk using a lever with an attached weight, applying a load of 10 N. Wear results were reported as volume loss, measured in cubic millimetres, for both the pin and the disk separately.

Table 3.11
Pin-on-Disk Parameter Setting for Wear Characterisation

Parameter	Set Value
Test Speed	850 rpm
Normal Load	10 N
Pin Diameter	8 mm
Track Radius	22 mm
Sliding Distance	1000 m
Sliding Velocity	2 m/s

3.9 Preparation of Specimen for Testing and Characterisation

Cutting of the sample was necessary to conduct the electrical resistivity and TRS tests. The 1 inch x 1 inch sample was sliced into three approximately equal parts using Struers Secotom (Plate 3.6 and Plate 3.7) equipped with an alumina blade. For density and hardness tests, the sample remained unsliced (Plate 3.7 (a)).

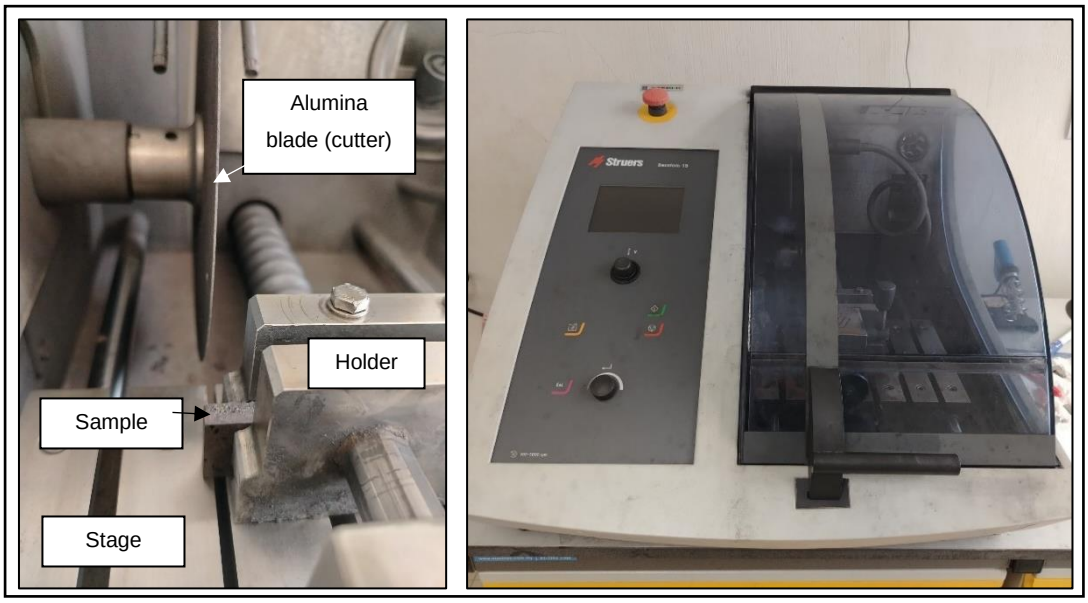

Plate 3.6 Struers Secotom Cutter with Alumina Blade

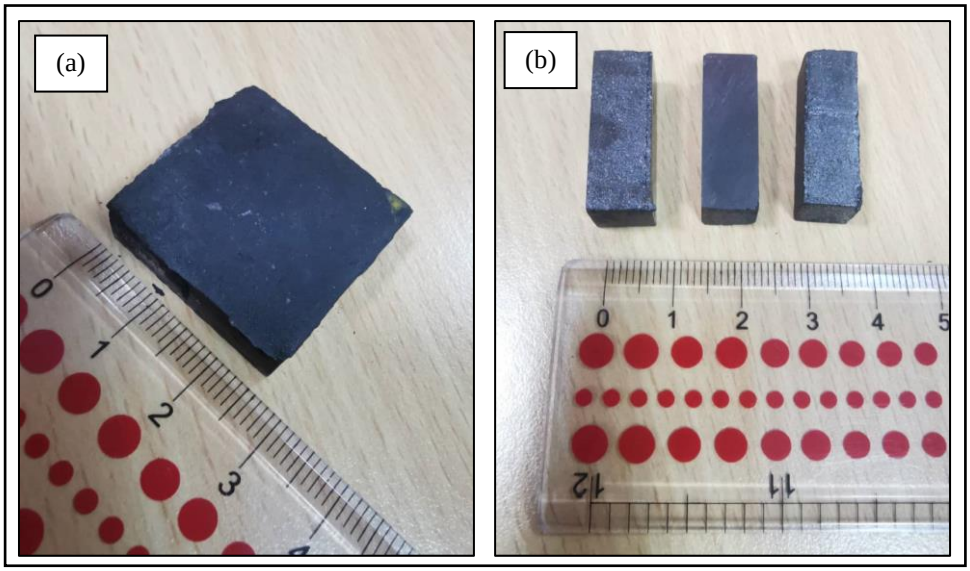

Plate 3.7 Preparation of Sample Before Testing
(a) Sample Before Cutting (b) Sample After Cutting

3.10 Testing and Characterisation

To gain a comprehensive understanding of the raw materials, a series of characterisation techniques was employed. Raman spectroscopy was used to analyse the vibrational properties of the materials, while X-ray diffraction (XRD) was utilised to determine their crystalline structure. Scanning electron microscopy (SEM) provided insights into the surface morphology and microstructure of the materials.

3.10.1 Scanning Electron Microscopy (SEM) and EDX

SEM imaging provides high-resolution visualisations of the surface morphology of the raw materials, including details of particle size, shape, and distribution. In warm compaction studies, understanding the morphology is crucial as it directly influences the compaction behaviour, powder packing density, and the resulting mechanical properties of the material [10]. SEM also reveals the presence of agglomerates, surface irregularities, and the overall microstructure, thereby aiding researchers in optimising the powder compaction process [141].



Plate 3.8 HITACHI Tabletop SEM for Micrograph of Raw Materials

SEM imaging of the raw materials was performed to view the morphology of the powder, surface, and cross-section of the developed carbon-copper composites. Hitachi TM3030Plus Tabletop Microscope (Plate 3.8) and Leo (Plate 3.9) were utilised for this purpose. Energy dispersive X-ray (EDX) was also conducted to obtain information on

the elemental composition of the powder and composite materials through line scans, mapping, and point scans. The powder sample was prepared by scattering it onto the carbon tape affixed to a stub. The stub was then mounted on the stage and transferred into the chamber for imaging. Particle size analysis was conducted using ImageJ software.

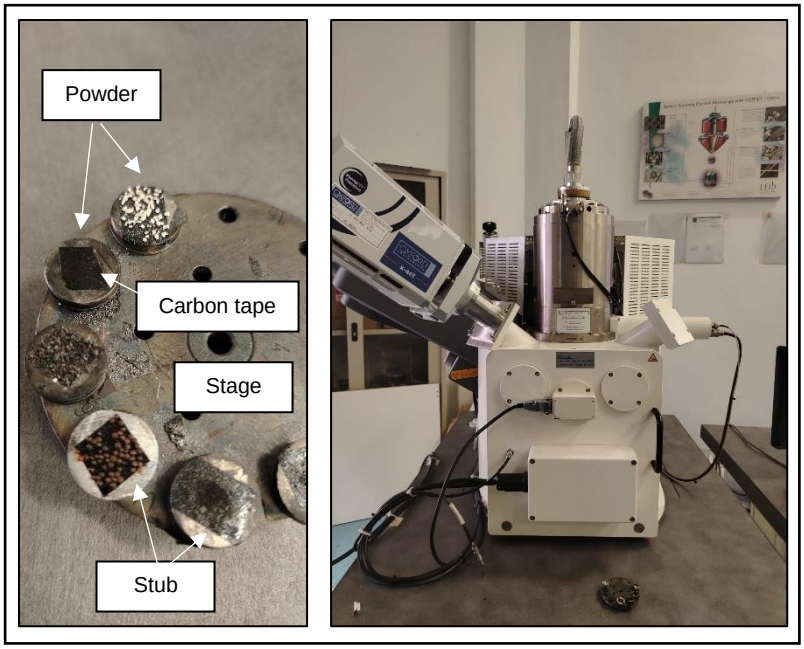

Plate 3.9 Leo SEM/EDX for Micrograph of Raw Materials

3.10.2 X-Ray Diffraction (XRD)

XRD provides information on the phases present in the raw materials. It is a crucial technique for determining the structural parameters of materials, particularly in the characterisation of crystalline materials. Based on the XRD analysis, information on the crystallographic structure, orientation, and degree of crystallinity was acquired.

A schematic diagram of XRD is shown in Figure 3.10, which illustrates Bragg's Law shown in Equation 3.1.

$$2d_{hkl}sin\theta = n_r\lambda \tag{3.2}$$

where

d_{hkl} = interplanar distance
θ = angle of reflection
n_r = order of reflection
λ = wavelength of the incoming wave

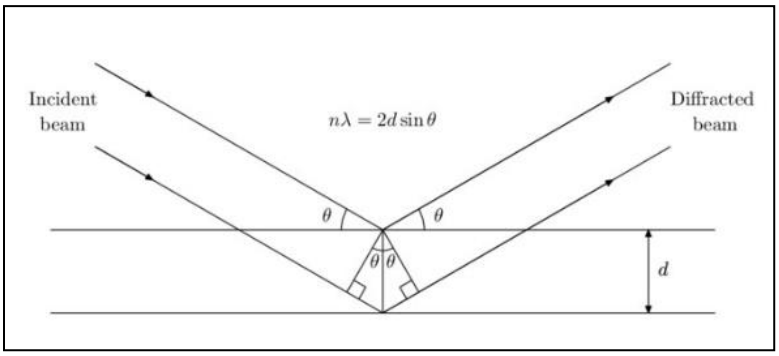

Figure 3.10 Schematic X-Ray diffraction

XRD analysis for all powders in this study was conducted using Bruker D8 X-ray diffractometer (Plate 3.10). The same XRD instrument was also used for the analysis of the developed carbon-copper composite samples. Cu K_α radiation with a wavelength of 1.540 Å was applied. The incident angle was maintained at 2°, and the 2θ range was set between 10° and 70°, with a step size of 0.02°.

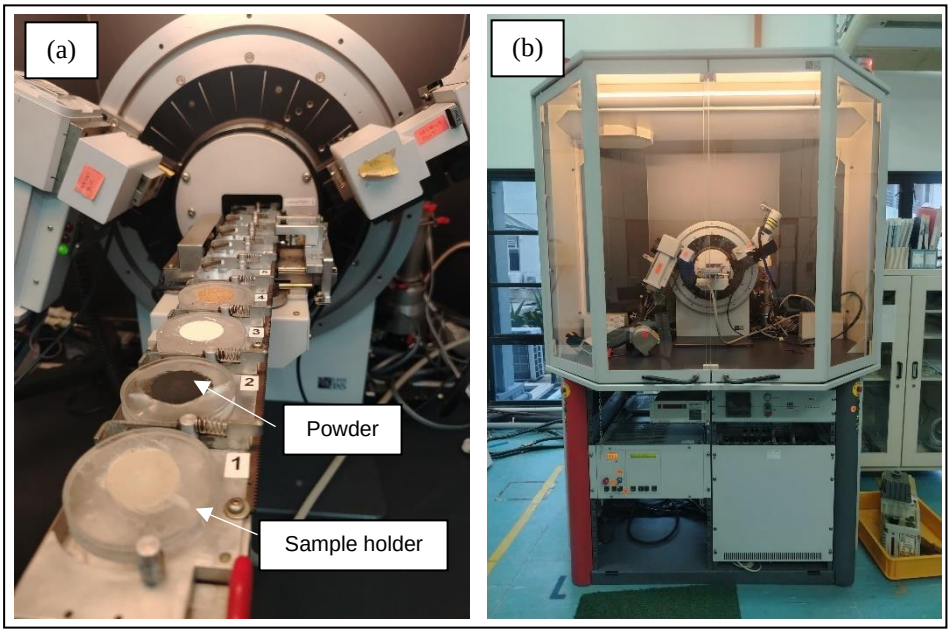

Plate 3.10 XRD Analysis: (a) Powder in Sample Holder, (b) Bruker D8 XRD

3.10.3 Raman Spectroscopy

Raman spectroscopy is commonly used in chemistry to identify molecules by producing a structural fingerprint, in which it observes vibrational, rotational, and other low-frequency modes in a system. It relies on Raman scattering of monochromatic light (usually from a laser), which interacts with the molecules and is scattered at different frequencies due to the interaction between light oscillation and molecular vibration. The laser light interacts with molecular vibrations, phonons, and other excitations in the system, resulting in a shift in the energy of the laser photons. The energy shift provides information about the vibrational modes (frequency changes) present in the system. Since this frequency is specific to molecular vibration and phonon within a crystal lattice, the Raman spectrum can be used to analyse a material's composition or obtain information about its crystalline structure.

In this study, Renishaw in Via Raman Microscope (Plate 3.11) was utilised to evaluate the chemical composition, chemical bonding, and phase of the carbon-copper composite, both before and after the post-baking process.



Plate 3.11 Renishaw Raman Microscope

3.10.4 ImageJ Software for Powder Particle Analysis

ImageJ is an image analysis software that was employed in this research to examine the size and shape characteristics of the powder particles of the raw materials. SEM images of the powder particles were captured and saved in a compatible format. After launching the ImageJ software, the saved SEM images were selected and imported into the software for analysis (Plate 3.12 and Plate 3.13).

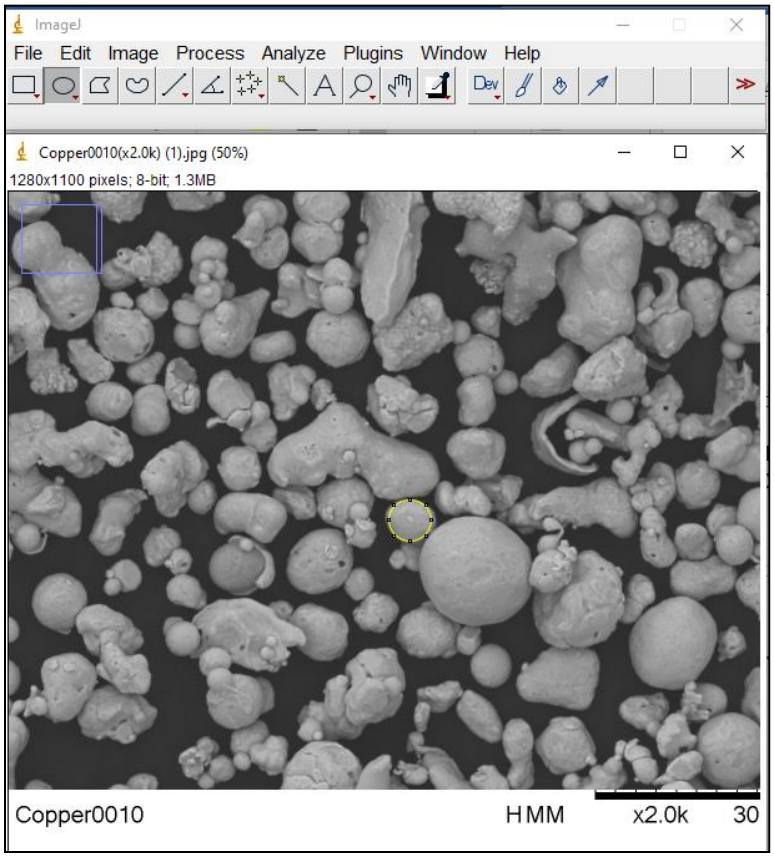

Plate 3.12 ImageJ Software Interface used to Measure Particle Size of Powder Samples

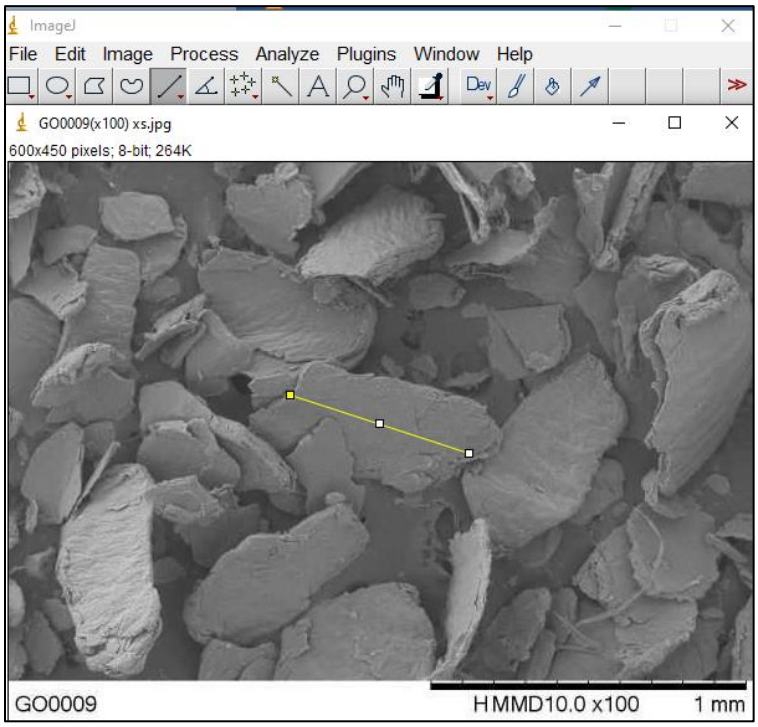

Plate 3.13 ImageJ Software Interface used to Measure Irregular Shape Powder Particles

When the image was opened, the brightness and contrast of the image was adjusted accordingly. When necessary, noise reduction filters were applied and between 50 and 100 particles were selected and measured. The data were exported to Microsoft Excel for analysis. The mean and standard deviation of the particle sizes were calculated and used to generate histograms and distribution curves. For non-spherical particles, such as flaky or irregular shapes, measurement was taken using ImageJ; however, the data represented the average size of the flakes (length of particles) rather than the diameter. For CNT, only the tube diameter was measured. All measurements were compared with the specifications provided by the manufacturer.

3.10.5 Density

The density of the sample was determined using a densitometer, following the ASTM D792 [142]. In this method, the mass of the sample was first determined in air, then the sample was immersed in water to determine its apparent mass while submerged, allowing the specific gravity to be calculated. The density measurements were conducted to evaluate differences before and after the post-baking process, as well

as before and after the incorporation of fillers. Electronic densimeter (MD-300S) was used, applying the Archimedes drainage method. The sample was placed on the top stage of the equipment, and the mass was recorded. The sample was then immersed in water, and the submerged mass was recorded. By pressing the Enter button, the density was calculated and displayed on the screen, and the value was recorded. The average of three samples was taken for each set.

The density test was conducted using the original-sized specimens (1 inch x 1 inch), as shown in Plate 3.14. Water was filled in the tank to the designated line, and the specimen was placed on top of the densimeter. The calculation of the sample density for the carbon-copper composite is shown in Equation (3.2).

$$\text{Density, } \rho(g/cm^3) = \frac{m_1}{m_1 - m_2} \times \rho_{water} \tag{3.2}$$

where ρ is the density, m is the mass of the specimen, and V is the volume. Using this densitometer, the density was automatically calculated.

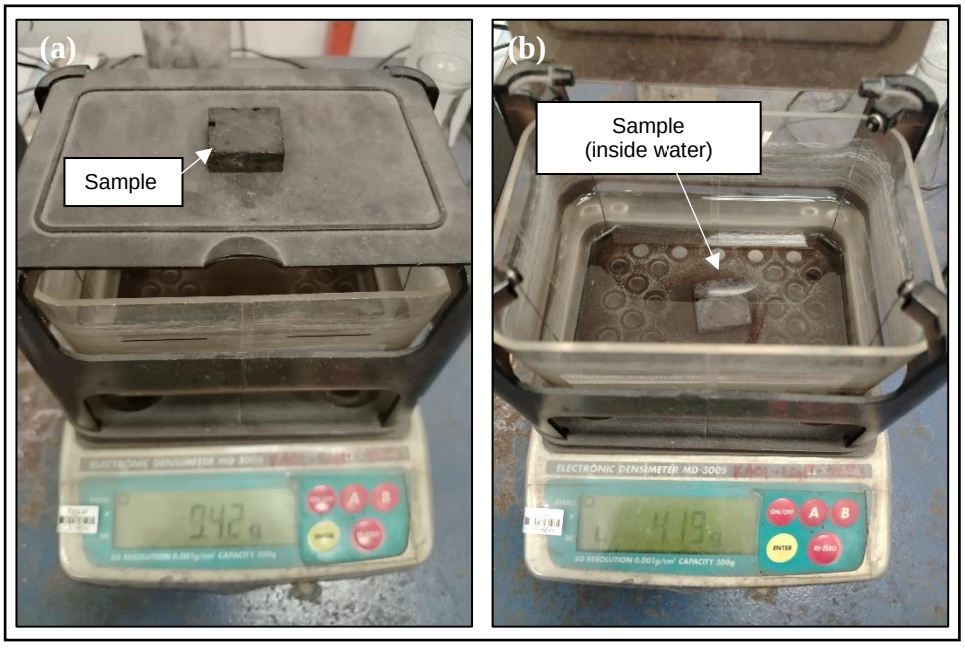

Plate 3.14 Densitometer for Density Measurement of the Composite

3.10.6 Hardness

A hardness test provides information on the material's ability to resist wear and deformation, ensuring durability and a longer service life. Hardness test was performed using Rockwell hardness tester (Mitutoyo model HR-430MR) shown in Plate 3.15. According to Procedure B in ASTM D785 [143], a 60 kgf load and ½ inch (12.7bcm) ball size was used. The sample was placed on the stage, and five hardness tests were conducted on the material. The average value was calculated and recorded.

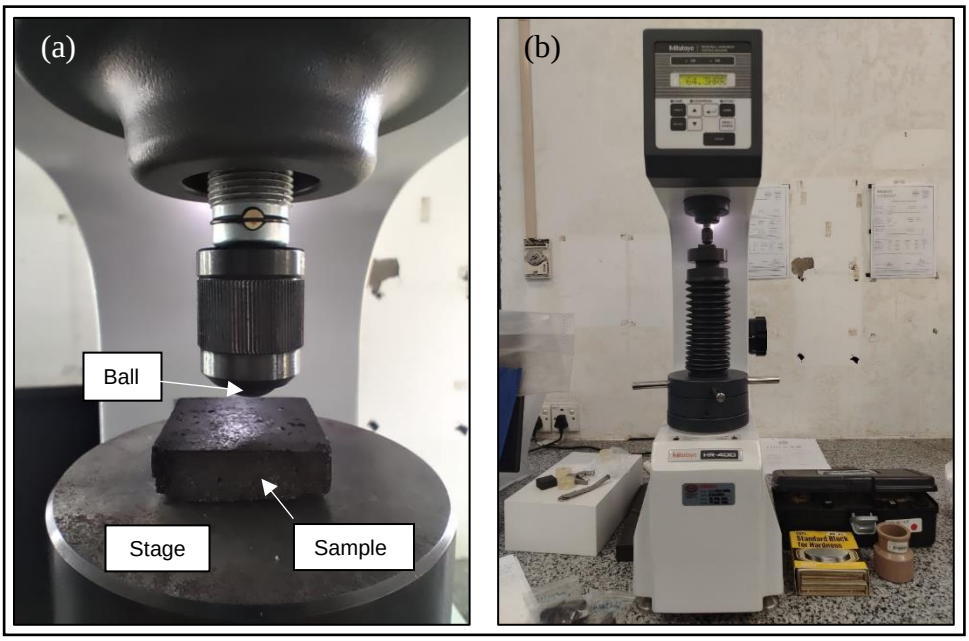

Plate 3.15 Rockwell Hardness Tester

3.10.7 Transverse Rupture Strength (TRS)

The TRS test assesses the material's ability to endure bending or flexural stresses. It is a measure of a material's ability to resist breaking under a bending load, providing valuable data for optimising processing parameters. The three-point bend test was performed to obtain the TRS using an Instron Universal Tensile Machine (model 3369) with INSTRON Series IX/s Automated Materials Tester software version 8.33.00 as shown in Plate 3.16.

The test was conducted following the ASTM D790 [144]. A 25.4 cm x 25.4 cm specimen was sliced using Struers Secotom equipped with an alumina blade to produce three sample pieces, as described in Section 3.9.

The three-point bending test method was used for the TRS evaluation. The specimen was placed on the support, and a load was applied at the midpoint. The crosshead speed was set according to the test requirements, and the span or distance between the supports was set to 20 mm. The maximum yield strength was recorded, together with the length, width, and thickness of the sample, to calculate the TRS value.

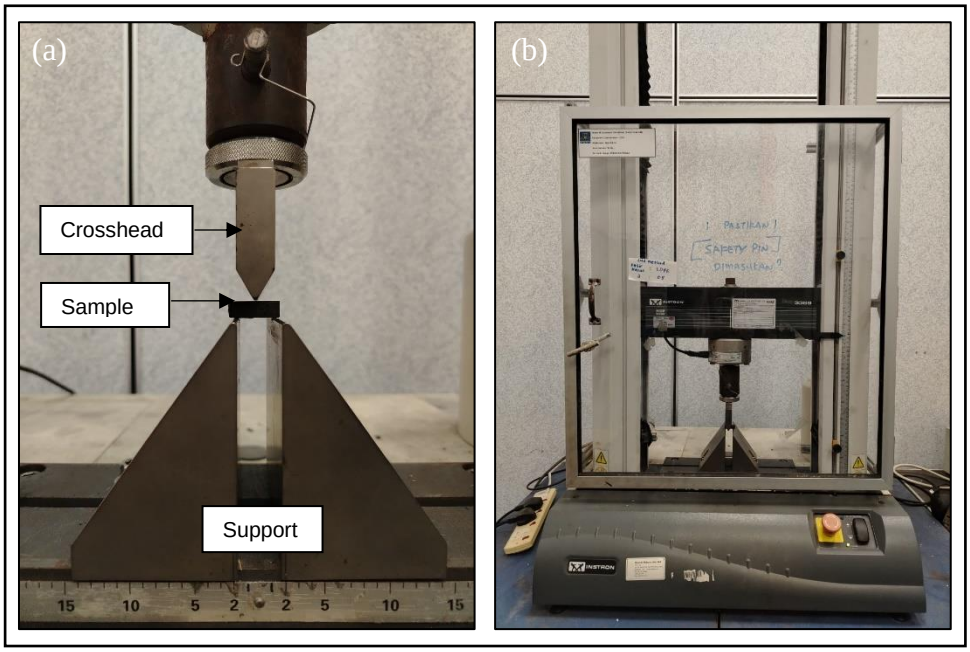

Plate 3.16 INSTRON Series IX/s Automated Materials for TRS Tests

In the three-point bending test, the TRS is determined and calculated using Equation (3.3):

$$TRS = \frac{3PL}{2bh^2} \tag{3.3}$$

where P is the maximum load applied, L is the span between the supports, b is the width of the specimen, and h is the thickness of the specimen. The width and thickness of the sample is measured using a digital calliper.

3.10.8 Electrical Resistivity

By measuring electrical resistivity, the electrical conductivity of the material can be indirectly assessed. Knowledge of the resistivity also helps predict the contact

resistance of the material, which is essential since the pantograph slide is in continuous contact with the contact wire during operation. The test was conducted following the procedure outlined in ASTM B193 [142]. According to this standard, a minimum sample length of 300 mm was required. However, the developed sample has a maximum length of only 25.5 mm. Therefore, modifications were made to obtain reliable data. A two-probe measurement method was applied to measure the resistivity, as shown in Figure 3.11 [145].

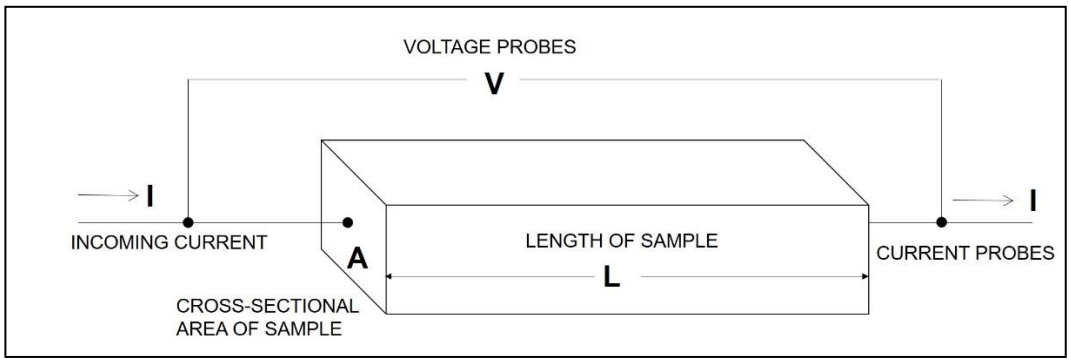

Figure 3.11 Electrical Resistivity Measurement by Two-Probe Method

In this method, the voltage drop, *V*, across the sample and the current passing through it were measured. The electrical resistivity is then calculated using Equation 3.4 [145].

$$\rho_E = \frac{VA}{Il} \tag{3.4}$$

where ρ is the resistivity, *A* is the cross-sectional area of the sample, *l* is the length of the sample, *V* is the voltage, and *I* is the current. Using the Automotive Meter, resistance (*R*) was measured, when *R* is equal to *V/I*, the resistivity can be expressed in Equation (3.5).

$$\rho_E = \frac{RA}{l} \tag{3.5}$$

The sample was sliced into three pieces using the Struers Secotom precision cutter with an alumina blade to obtain a bar measuring 25.5 mm in length, approximately 8mm in width, and 8 mm in depth. The actual size is measured using a

digital calliper. The details of the cutting process are explained in the Subtopic 3.9. The electrical resistivity of the sample was measured using the Automotive Meter Fluke 88 (Plate 3.17).



Plate 3.17 Automotive Meter for Electrical Resistance Test

3.10.9 Confocal Microscopy

To characterise the surface topography and quantify the surface roughness of copper disks following tribological wear testing, confocal laser scanning microscopy (CLSM) was employed. This non-contact optical technique provides high-resolution three-dimensional surface profiling, enabling accurate measurement of surface features, such as wear scars, grooves, and pits. In this study, Zeiss confocal laser scanning microscope (Model LSM800) (Plate 3.18) was used to evaluate the worn surface of copper disks subjected to sliding wear against composite pin materials. Wear tracks were examined, and roughness parameters, such as the average roughness (R_a), were measured using MountainMaps Version 7 software. These analyses provided insights into the dominant wear mechanisms and surface deformation patterns. These observations complement the morphological and elemental analyses conducted via SEM and EDX, offering a comprehensive understanding of the tribological interaction at the contact interface.

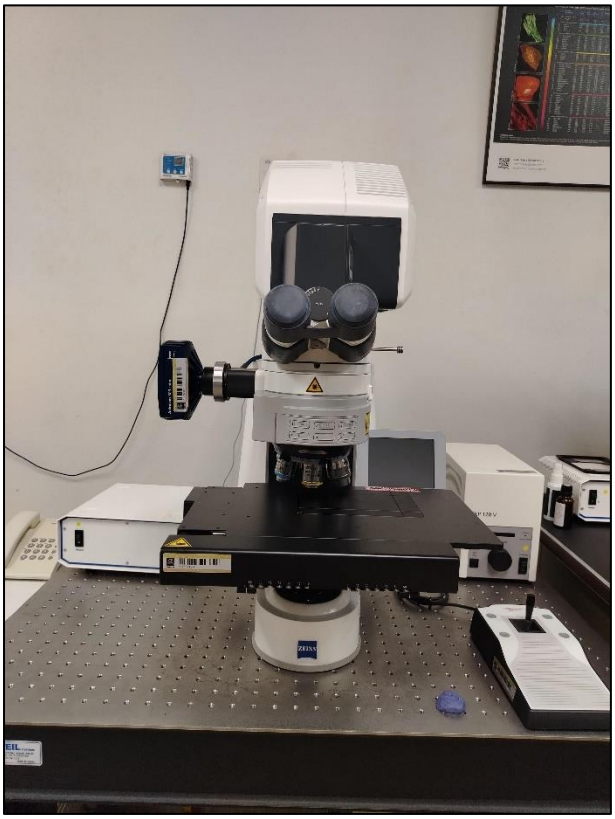

Plate 3.18 Confocal Laser Scanning Microscope

CHAPTER 4
RESULTS AND DISCUSSION

4.1 Introduction

This chapter presents and discusses the results obtained from the tests and analyses conducted in this study. To address the objectives of this study, this chapter is organised into four major phases. Phase 1 studies the effects of graphite/palm kernel shell (PKS) ratio on the properties of carbon-copper composite. Phase 2: studies the effects of filler addition on the properties of carbon-copper composite. In Phase 3, optimisation of warm compaction process parameters is conducted, and in Phase 4 the wear characterisation of carbon-copper composite is studied.

Phase 1 covers Objective 1 and is discussed in Sections 4.3 and 4.4. Phase 2 presents the results related to Objective 2 and is discussed in Sections 4.5 and 4.6. Phase 3 addresses Objective 3 and is discussed in Sections 4.7 and 4.8. Finally, Phase 4 covers Objective 4 and is discussed in Section 4.9. Before the detailed discussion of experimental results, this chapter also presents and discusses the findings of the preliminary study, which include the characterisation of the raw materials, selection of carbon composition, and selection of filler. This chapter also presents the necessity of the post-baking process after the warm compaction.

4.2 Raw Materials Characterisation and Analysis

The characterisation and analysis of the raw materials are essential to understand the behaviour of each element before and after mixing. The materials underwent physical and chemical analyses to comprehend and evaluate the findings during the development of the carbon-copper composites. The following sections discuss these characteristics thoroughly.

4.2.1 Powder Structure and Particle Size Analysis

Scanning electron microscope (SEM) micrographs of the raw powder materials were captured to analyse the particle morphology and determine the particle size. The obtained data were verified against the raw material specifications provided by the manufacturer, as presented in Chapter 3 (Table 3.1). The SEM micrographs of PKS-derived carbon powder at 100x and 2500x magnifications (Plates 4.1(b) and 4.1(b)) showed the surface morphology of the powder. The PKS-derived carbon powder exhibited natural irregularities in shape, consisting mainly of irregularly shaped particles. The particle size of PKS-derived carbon was observed to be less than 50µm, as displayed in Plate 4.1 (b). This observation is consistent with the manufacturer's specification, stating that the PKS-derived carbon powder is less than 200 mesh, equivalent to approximately 74 µm according to ASTM 11-95 [146].

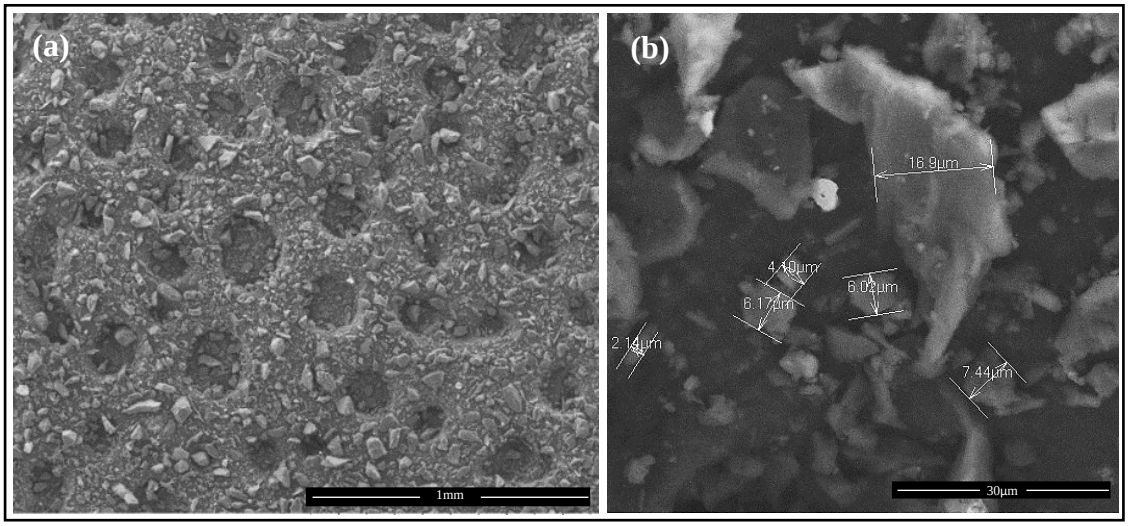

Plate 4.1 Particle Morphology of PKS-derived carbon at magnifications of (a) 100x and (b) 2500x

The SEM micrograph (Plate 4.2) of the graphite powder showed visible individual graphite particles, exhibiting a distinctive combination of bulk and flat plate-like morphologies. The layered structure of the graphite indicated the formation of stacked sheets. According to the manufacturer's specifications, the particle size is less than 500 µm.

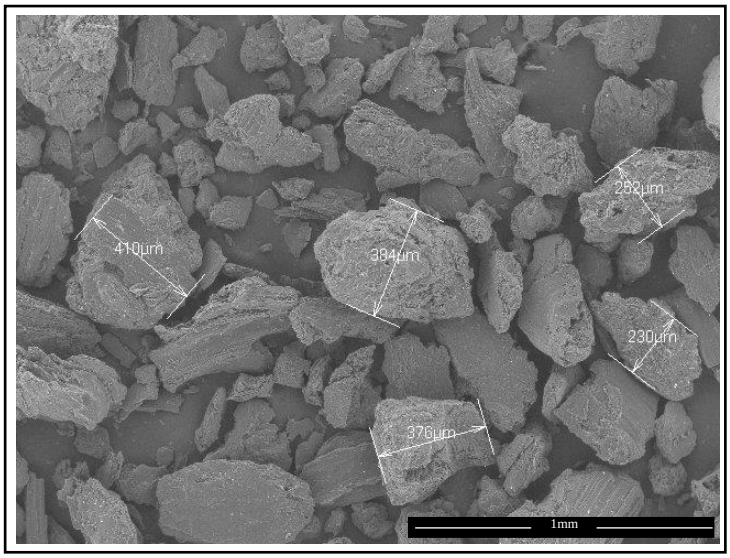

Plate 4.2 Particle Morphology of Graphite at magnification of 100x

The spherical form of copper powder was not visible at 100x magnification (Plate 4.3 (a)) due to its tiny size of 10µm to 25µm, as specified by the manufacturer. Plate 4.3(b) shows a larger magnification at 2000x. In the micrograph, it can be clearly seen that the copper powder is in spherical shape with some agglomeration. The particle size distribution of the spherical-shaped copper particles is analysed using ImageJ analysis software. ImageJ revealed a dispersion of particles from around 5µm to 25µm (Figure 4.1).

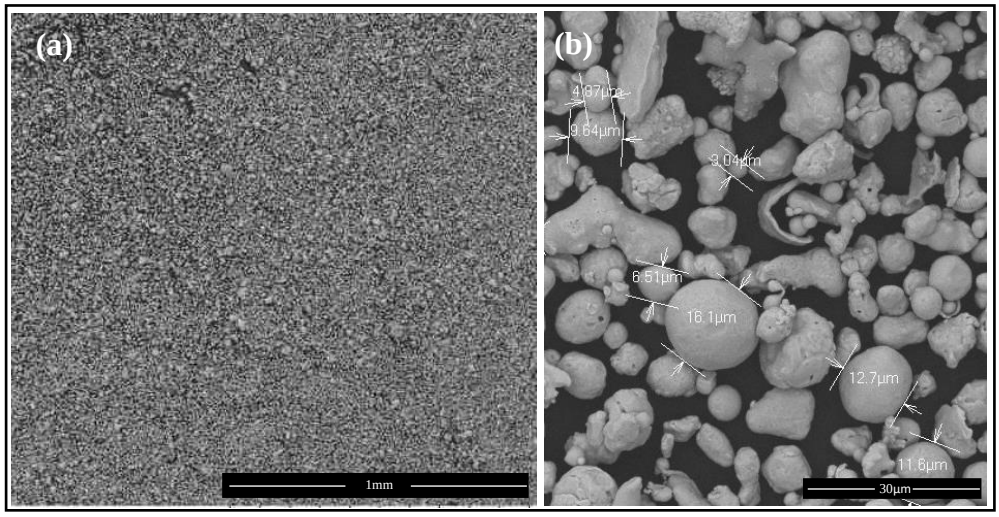

Plate 4.3 Particle Morphology of Copper Powder at magnifications of (a) 100x and (b) 2000x

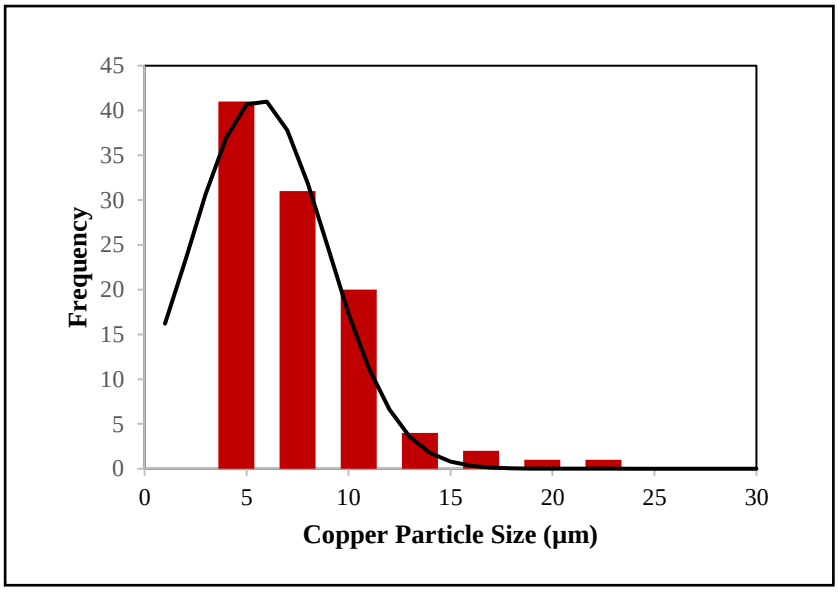

Figure 4.1 Size Distribution of Copper Powder

The particle shape of the phenolic resin powder was not visible under 100x magnification (Plate 4.4 (a)). At 500x magnification, the powder appeared agglomerated, as shown in Plate 4.4(b). The phenolic resin powder is granular in form, consisting of small, irregularly shaped particles rather than spherical particles. According to the manufacturer's specifications, the particle size of the phenolic resin is less than 100 µm, which is consistent with the observation in n Plate 4.4 (b).

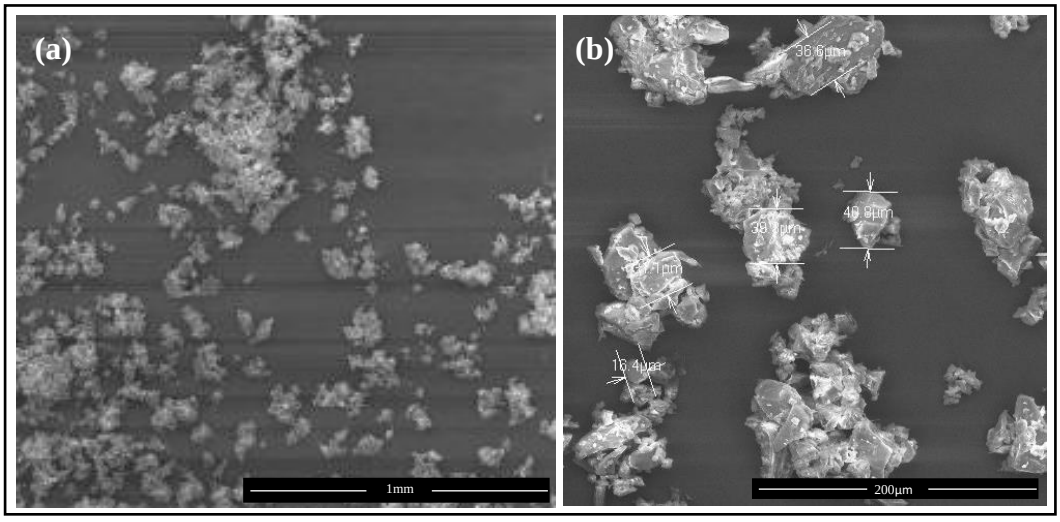

Plate 4.4 Particle Morphology of Phenolic Resin (a) 100x magnification and (b) 500x magnification

The SEM micrographs of the graphene oxide (GO) powder in Plates 4.5 (a) and (b) revealed the distinctive morphology of individual GO particles. In these images, the

GO appeared as thin, wrinkled platelets, exhibiting a layered structure. This is a typical morphology of GO, which is also observed by Lakshani et. al. [147]. The edges of the sheets exhibited irregularities and variations in shape. From the manufacturer's specifications, the particle size of the powders ranges from 200 µm to 500 µm.

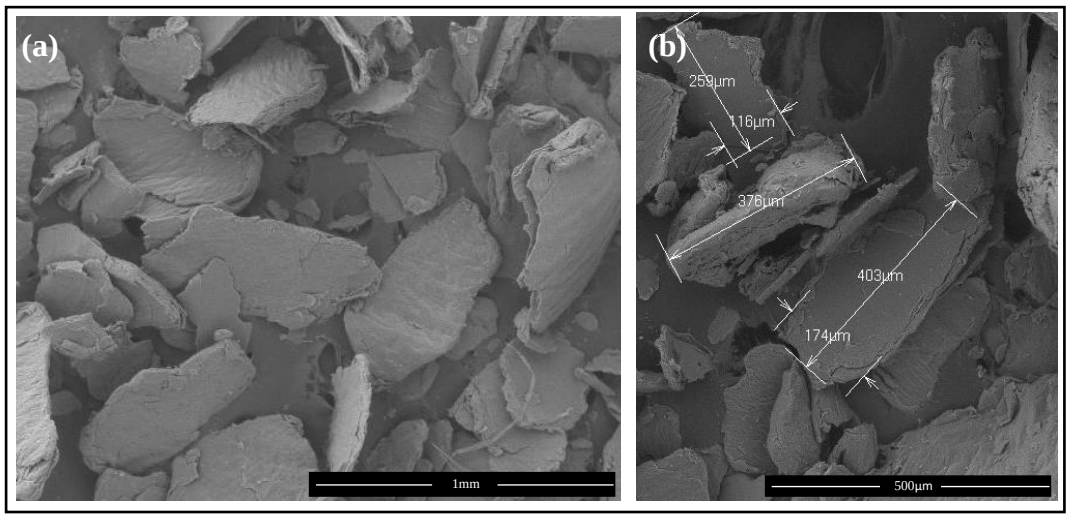

Plate 4.5 Particle Morphology of Graphene Oxide at (a) 100x Magnification and (b) 200x Magnification

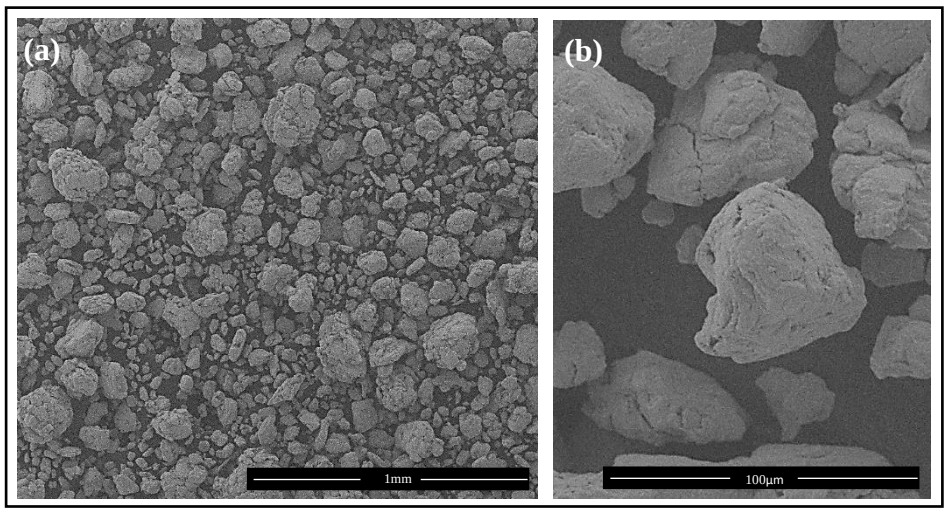

Plate 4.6 Particle Morphology of Cu-CNT at (a) 100x Magnification and (b) 1000x Magnification

The copper-carbon nanotube (Cu-CNT) powder was in small granular form, consisting of irregularly shaped particles, as shown in Plate 4.6 (a) and (b). According

to the manufacturer's specifications, the particle diameter is approximately 20 µm. The appearance of larger particles may be due to agglomeration of the powder.

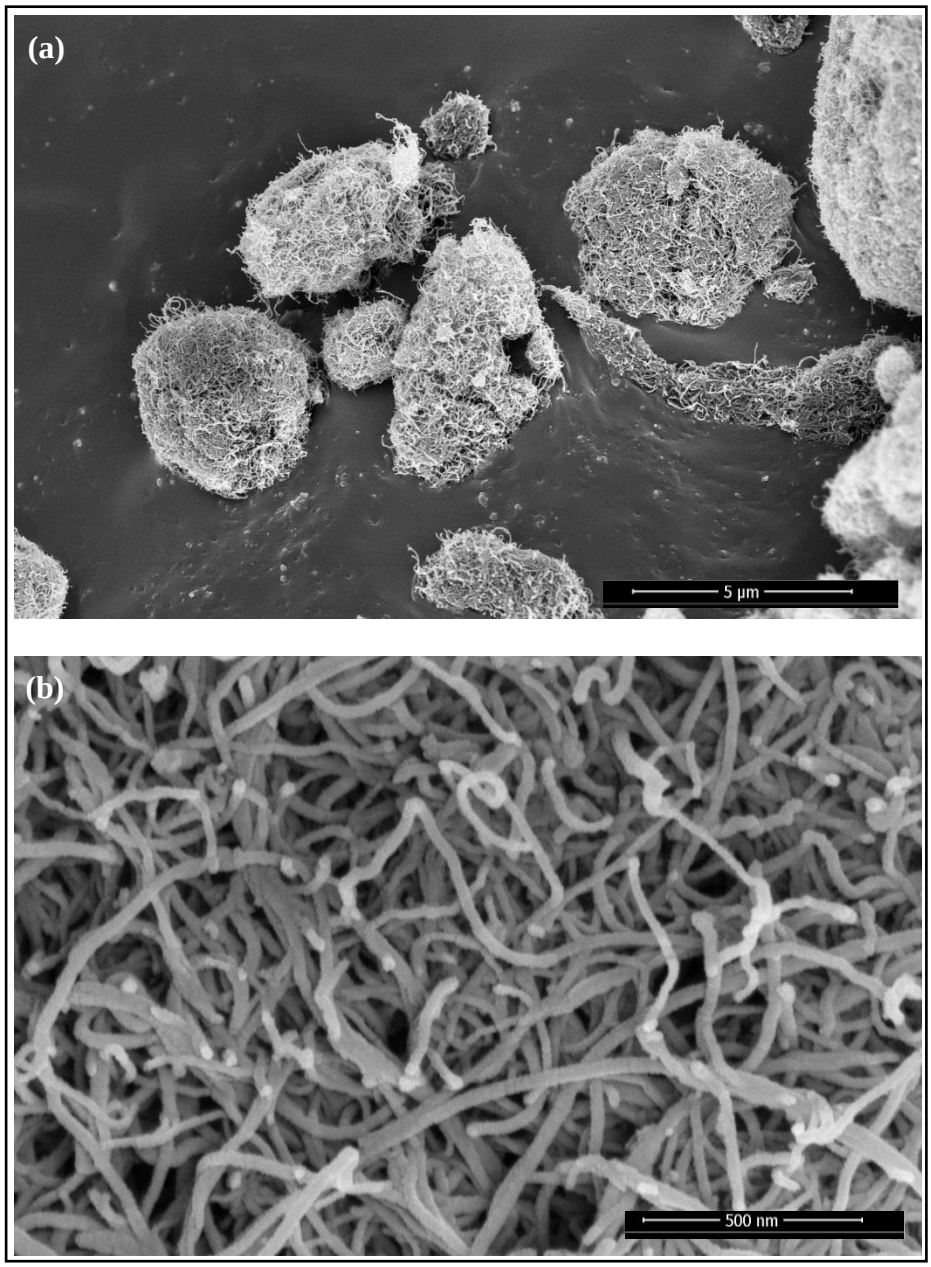

Plate 4.7 Particle Morphology of CNT

The lower-magnification image of the CNT sample in Plate 4.7 (a) revealed irregularly shaped particles, which is the agglomerated CNT. At higher magnification, as shown in Plate 4.7 (b), the individual CNT became visible, revealing that they were agglomerated but homogeneous within these particles. According to the manufacturer, the CNT diameter ranges from 8 nm to 15 nm, which is consistent with the measurement

obtained from the SEM micrographs.

These diverse particle sizes and shapes facilitate effective interlocking among the powder particles during consolidation processes, including cold pressing and warm compaction. According to Hlosta et al. [148], powder compressibility is influenced by the shape and size distribution of the particles. In this study, the particle shape of the powders exhibited a mixture of rounded shapes (copper) and irregular shapes (PKS, graphite, resin); therefore, this diversity may enhance interlocking.

Conversely, the fine copper particles are the most compressible, and their inclusion enhances the compressibility of the powder [148]. Irregular particle shapes, combined with the flaky morphology observed in some powders, promote greater interparticle contact and enhanced packing density, thereby facilitating consolidation and ensuring uniform distribution of the constituents within the composite structure. This morphology also contributes to a lower breakage rate and higher compressive strength [149]. Consequently, it improves the mechanical properties and structural integrity of the resulting carbon-copper composite. However, other factors, such as equipment limitations and process parameters, may also influence the development of the carbon-copper composite, as discussed in the subsequent section.

4.2.2 Powder Phase Composition

X-ray diffraction (XRD) analysis of the as-received raw materials was performed to determine their phases and interlayer spacing. XRD analysis provides information on the crystallographic structure of the materials, enabling the identification of the crystalline phases present in the raw materials and providing data on their crystal structure, orientation, and grain size [150]. This information is particularly important for predicting the mechanical properties, thermal stability, and potential phase transformations that may occur during the warm compaction process.

Figure 4.2 shows the XRD pattern of PKS-derived carbon powder. The pattern appeared noisy, with no distinct diffraction peaks observed. This behaviour may be attributed to the presence of amorphous regions within the PKS-derived carbon , which did not produce distinct XRD peaks. Low crystallinity or heterogeneous composition of PKS-derived carbon could contribute to the poorly defined pattern [12]. Further analysis is required to identify the phases present in the material.

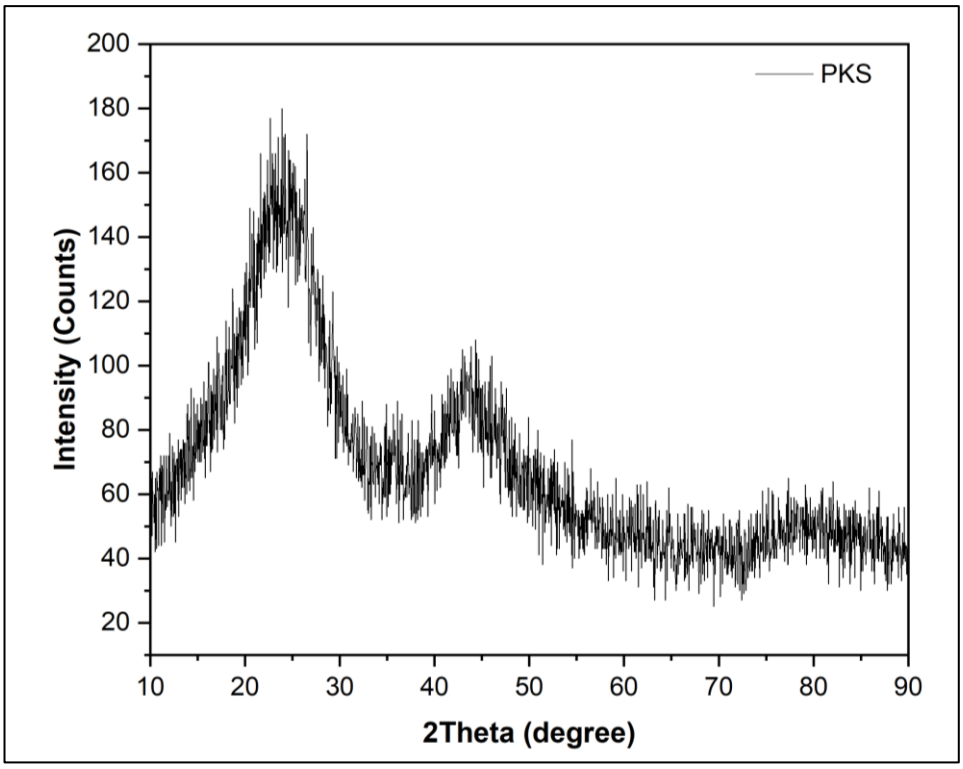

Figure 4.2 XRD Pattern of PKS-derived Carbon Powder

Figure 4.3 shows the XRD pattern of graphite, exhibiting a distinct and well-defined series of sharp peaks. Graphite has a highly ordered crystal structure composed of stacked layers that are held together by weak van der Waals forces. The characteristic XRD peaks correspond to the crystallographic planes within these layers. The most prominent peak was observed around 26.5° (2θ), representing the (002) plane of the hexagonal lattice, as also reported by Salvatore et al. [151]. The high degree of crystallinity and the regular arrangement of carbon atoms in graphite contribute to the clarity of the XRD pattern. Meanwhile, the absence of impurities or structural defects further enhances the visibility of the graphite peaks.

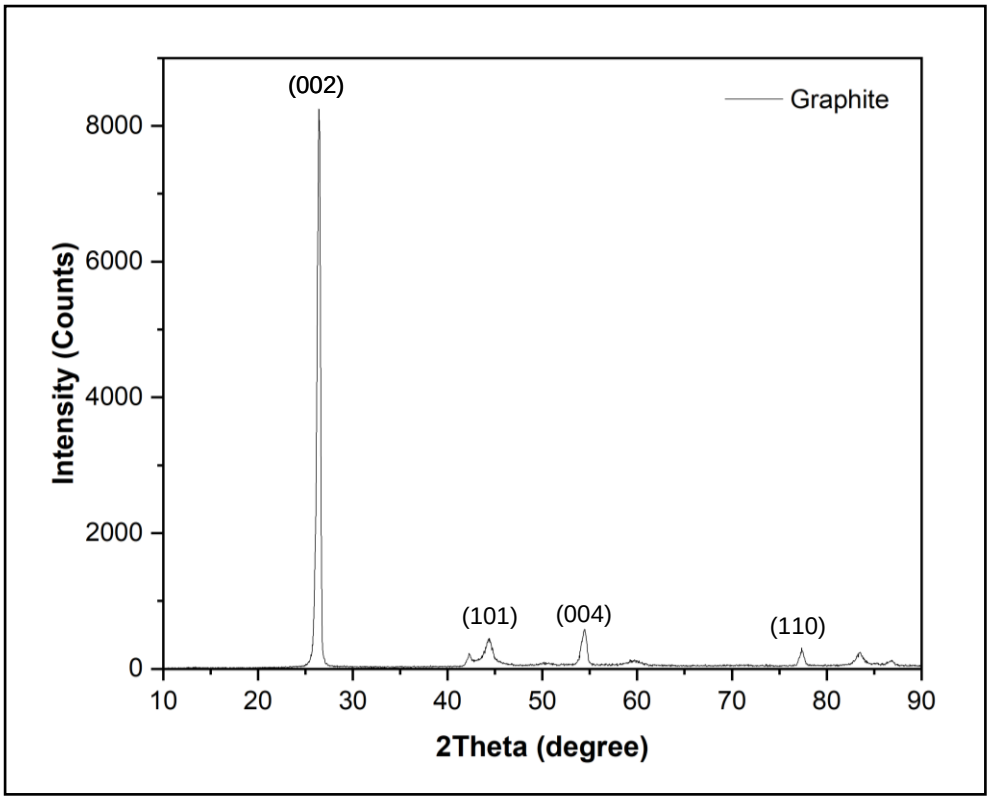

Figure 4.3 XRD Pattern of Graphite Powder

The XRD pattern of copper powder displayed a series of sharp and intense peaks to indicate crystalline structure, as shown in Figure 4.4. Copper has a face-centred cubic (FCC) crystal lattice, and the XRD peaks correspond to various crystallographic planes within this lattice. The most prominent peak was observed around 43° (2θ), corresponding to the (111) plane. The well-defined peaks in the XRD pattern indicate a high degree of crystallinity and a regular arrangement of copper atoms. XRD analysis of copper powder is essential for confirming its crystalline nature, determining its crystallographic orientation, and assessing the quality of the material for various applications, particularly in metallurgy and electronics [152].

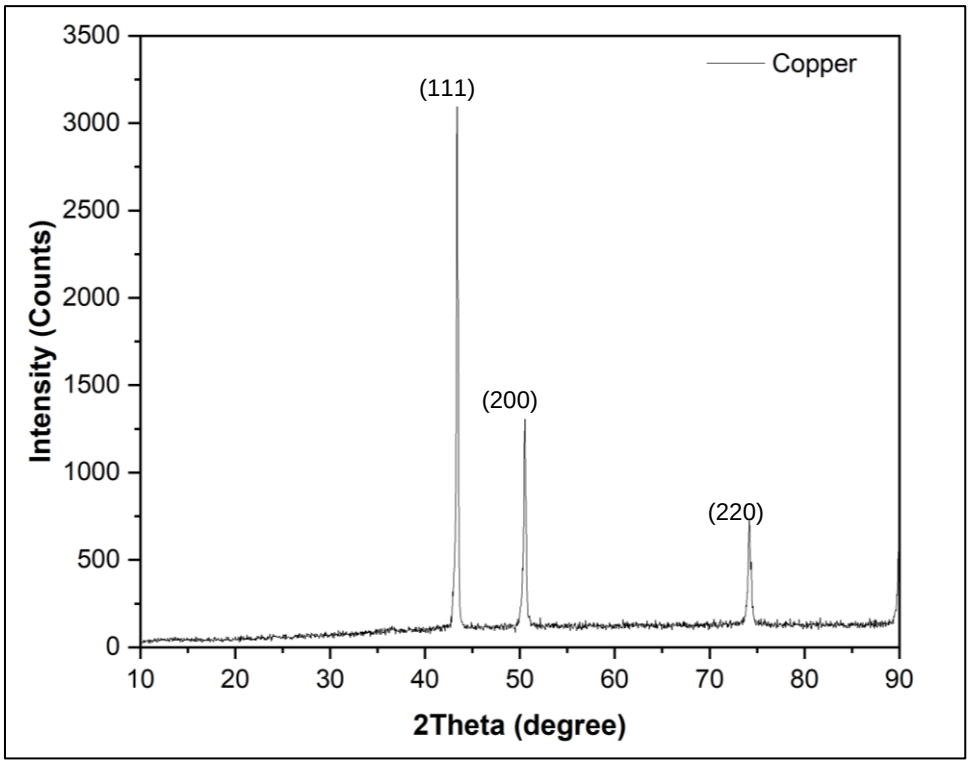

Figure 4.4 XRD Pattern of Copper Powder

Phenolic resin is generally known for its amorphous nature, which is reflected in its XRD patterns. As depicted in Figure 4.5, phenolic resin exhibited a broad peak rather than sharp diffraction peaks. This behaviour indicates that phenolic resin is predominantly an amorphous polymer with limited crystallinity. Consequently, the XRD pattern appeared broad and featureless, resembling a diffuse halo instead of sharp peaks. A broad peak was observed around 18° (2θ), confirming the high degree of amorphousness in the material. The absence of sharp peaks suggests that the material does not possess a well-defined crystalline structure, which is common in thermosetting polymers. However, there is a sudden peak appearance at around 29° (2θ), which suggests the presence of calcite ($CaCO_3$) or silica, most likely from the raw materials or the process of producing the resin [153]. The amorphous nature of phenolic resin contributes to its excellent thermal stability, making it suitable for various applications, including as a matrix in composites, as reported by Yu et al. [154].

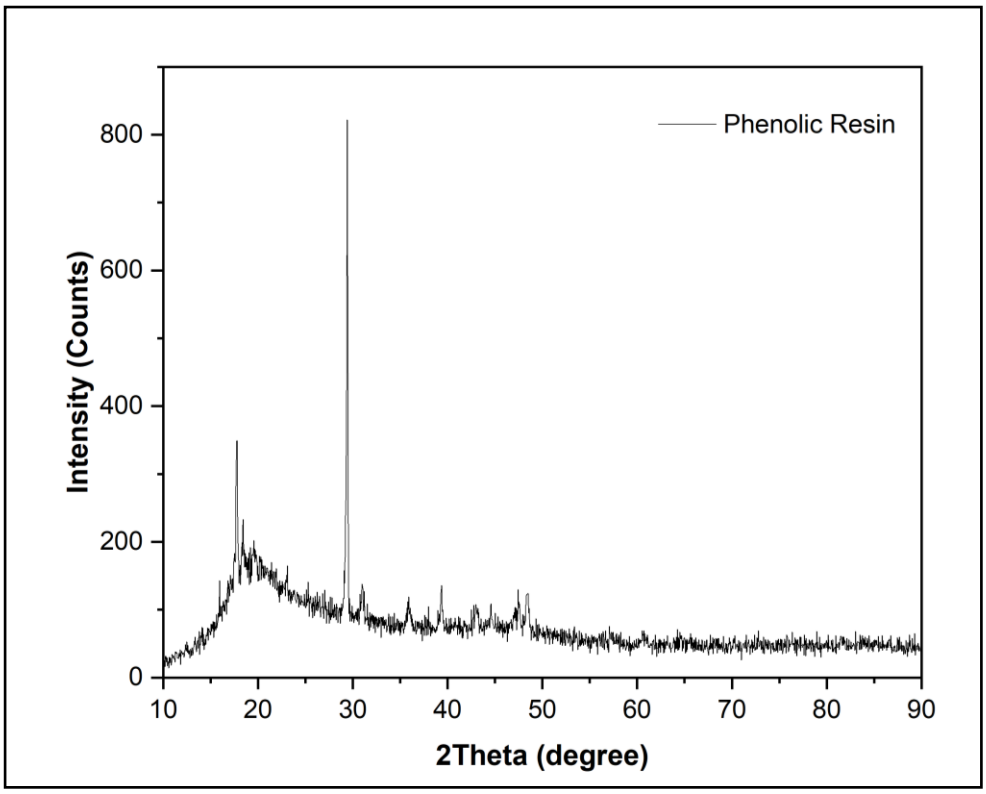

Figure 4.5 XRD Pattern of Phenolic Resin

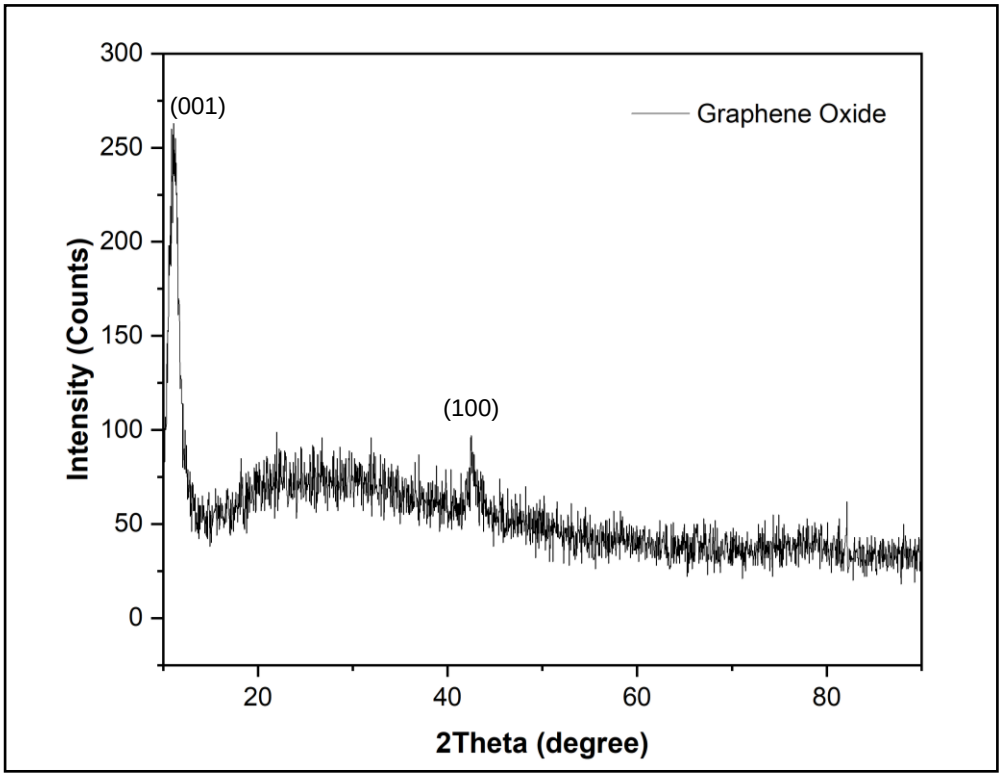

Figure 4.6 XRD Pattern of GO Powder

Figure 4.6 shows the XRD pattern of GO powder. The XRD pattern exhibited a prominent peak at around 10°-12° (2θ), corresponding to the (001) plane, while a less intense peak was observed around 43°-44°, attributed to the (100) plane of GO. A similar observation was reported in a previous study [155]. The XRD pattern can reveal information about the degree of crystallinity in GO. Compared to graphite, GO exhibited broader peaks, reflecting a more disordered structure due to the presence of various functional groups such as hydroxyls and carboxyl [156].

Figure 4.7 shows the XRD pattern of Cu-CNT powder. As the CNT was coated with copper, the diffraction pattern closely resembled that of copper powder. A prominent peak was observed at approximately 43° (2θ), corresponding to the (111) plane. The well-defined peaks in the XRD pattern indicate good crystallinity and a regular arrangement of copper atoms [157].

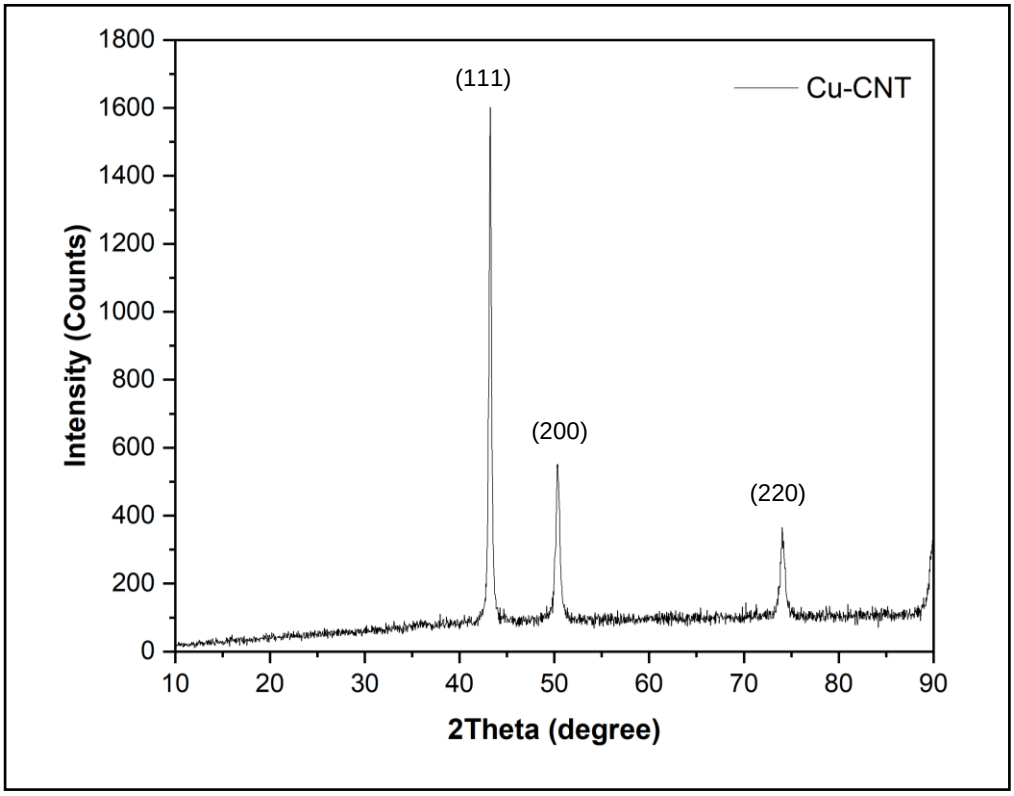

Figure 4.7 XRD Pattern of Cu-CNT Powder

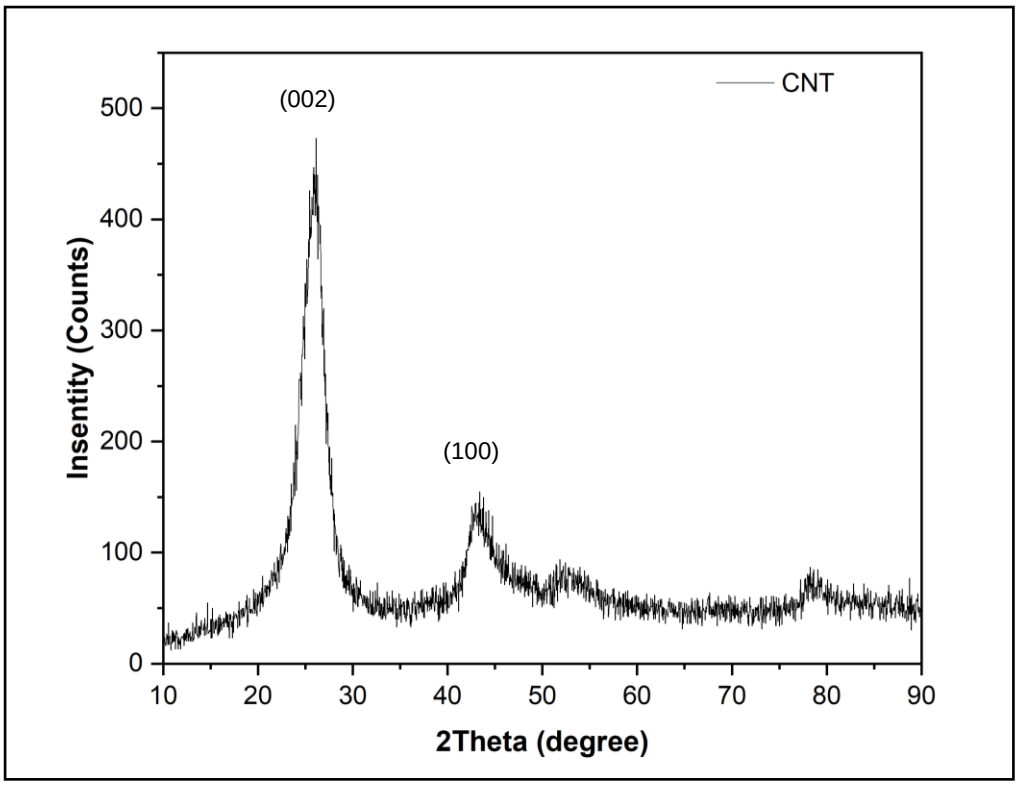

Figure 4.8 XRD Pattern of CNT

Figure 4.8 depicts the XRD pattern of the CNT used in this study. A high reflection was observed at around 25°–26° (2θ), indicating the graphite nature of CNT, and corresponded to the (002) plane of graphite. However, the peak was neither sharp nor intense, suggesting lower crystallinity. The broad, amorphous-like peaks suggest that CNT contains defects, partial disorder, or residual amorphous carbon. CNT synthesised via chemical vapour deposition (CVD) or other chemical routes commonly exhibit such patterns due to imperfect graphitic stacking and the presence of mixed carbon phases. A broad reflection was observed around 42°–46° (2θ), corresponding to the (100) plane. According to Soleimani et al. [158], the main features of the XRD pattern of CNT are close to those of graphite, which is also shown in Figure 4.3.

4.3 Effects of PKS-derived Carbon Content on the Properties of Carbon-Copper Composite

4.3.1 Formation of the Carbon-Copper Composite

From the five selected compositions, only two carbon-copper composites with carbon compositions of 6 5wt% (A03) and 70 wt% (A04) were effectively formed through the cold pressing process, as shown in Plate 4.8.

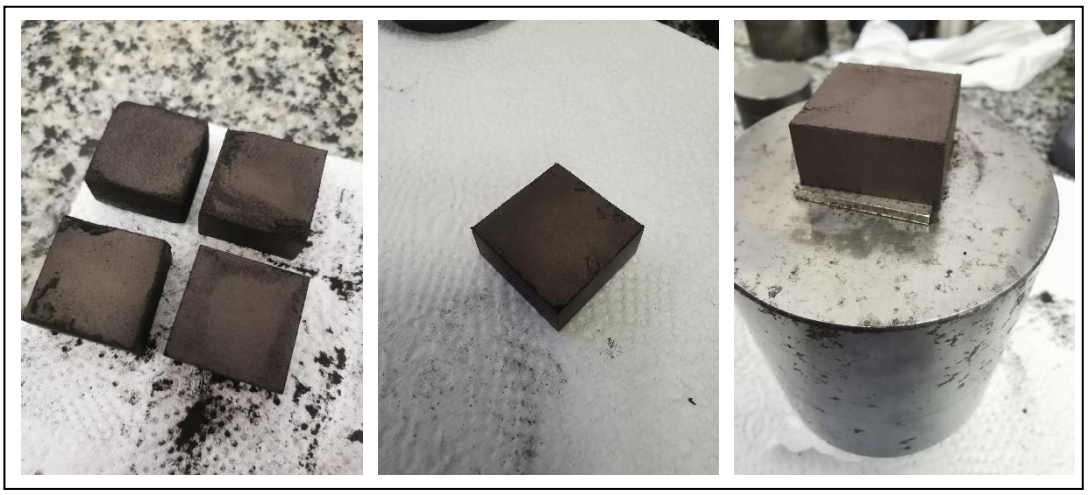

Plate 4.8 Successful Cold-Pressed Powder for 65 wt% PKS-derived carbon and 70 wt% PKS-derived carbon

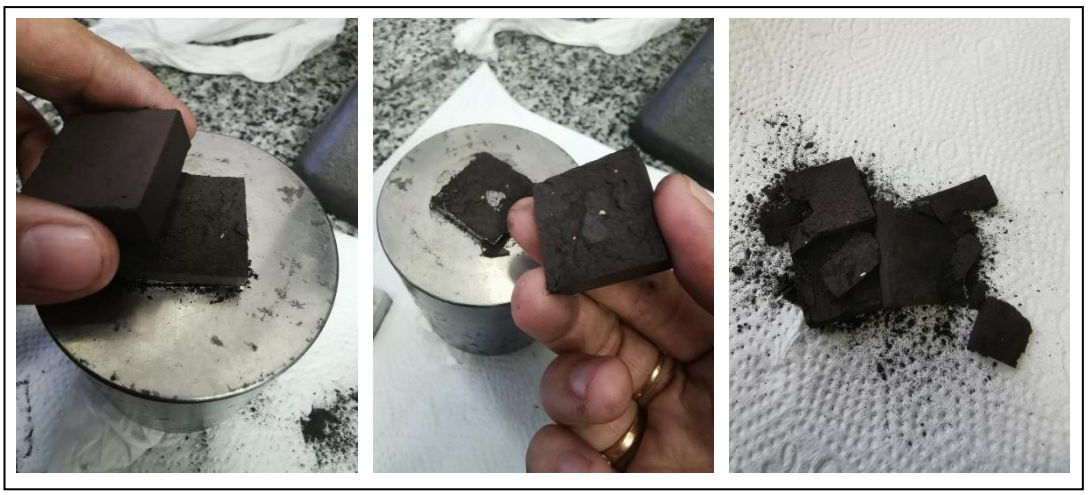

Plate 4.9 Failed Cold-Pressed Powder for A01, A02, and A05

On the other hand, as seen in Plate 4.9, the powder mixture with carbon compositions of 55 wt%, 60 wt%, and 75 wt% were found to be extremely brittle and fractured easily upon removal from the mould. Despite numerous trials, these

compositions could not be successfully formed. Therefore, only two variants of carbon content were selected for further examination in Phase 1(a).

The unsuccessful formation of carbon-copper composites with lower (55 wt% and 60 wt%) and higher (75 wt%) PKS-derived carbon content can be attributed to several factors related to the composition and properties of the mixture components. At 55 wt% and 60 wt% PKS-derived carbon, the carbon matrix may not have been sufficient to provide the necessary structural integrity. With inadequate carbon, the composite may lack the required reinforcement, leading to brittleness and cracking [159]. Furthermore, at lower carbon contents, the copper content was relatively higher. The microstructure of the composite is crucial for its performance. A previous study has found that a decrease in strength with increasing copper content may be due to two main reasons: the formation of voids caused by poor compatibility between the matrix and reinforcement, and the agglomeration of particles [160]. Although the copper particles were smaller, at higher copper concentrations, they may have filled the voids between the larger carbon particles without effectively bonding to the carbon. This can create a composite where copper acts more as a filler than as an integral part of the reinforcing matrix. Consequently, the resulting structure can remain highly porous, even if the smaller copper particles seem to fill the available space. Smaller copper particles may not have interlocked effectively with the irregular surfaces of the larger activated carbon particles. Effective interlocking is crucial for mechanical strength [161], if copper merely occupies the voids without strong adhesion, the green body remains weak. Thus, higher copper content may disrupt the balance needed for a cohesive structure.

A schematic illustration of the mixture of activated carbon, copper, and phenolic resin is shown in Figure 4.9. Previous research has demonstrated that increasing the concentration of copper particles in a composite can lead to the agglomeration of copper, which adversely affects the mechanical properties. The presence of agglomerates caused inhomogeneous deformation, resulting in void formation between the particles [160]. This clustering can prevent effective interlocking with the carbon particles, thereby leading to structural weaknesses in the composite.

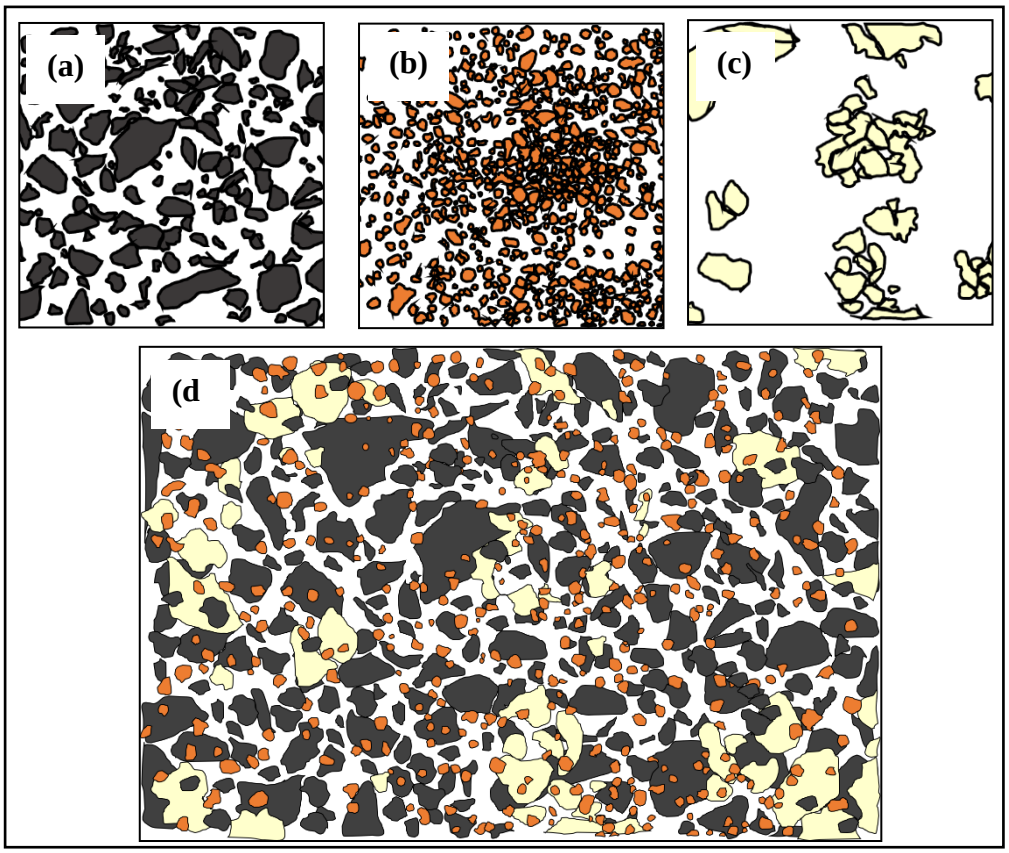

Figure 4.9 Schematic Illustration of (a) PKS, (b) Copper, (c) Resin, and (d) the Mixtures

Activated carbon has a large specific surface area and varied porosity. The high surface area may lead to increased stresses within the composite, especially when the resin or copper does not fill the pores [162]. The pressure applied during the pressing step may not be sufficient to force the smaller copper particles into intimate contact with the carbon particles, especially when there is insufficient resin to act as a lubricant and binder [163]. This resulted in a loosely packed, porous green body, which was brittle and easily broke or split when removed from the mould. The wettability of carbon by copper and resin is critical for achieving good interfacial bonding [163]. Poor wettability may have led to weak interfaces and reduced composition strength [95]. Nurul Hadi et. al. [46] reported that 55 wt% carbon content in carbon-copper composite was the optimised composition in their study. However, they used a larger PKS-derived carbon powder size (90 µm to 150 µm) compared to the 200 mesh (around 75 µm). Differences in particle size and the presence of irregular shapes may also have affected the ability to form a coherent shape under the applied pressure. It has been shown that

compressibility is mostly determined by particle size [164]. They also noted that spherical particles, such as copper in this study, exhibited better flowability and lower porosity than irregular particles. Therefore, the ratio of carbon to copper may have significantly affected the successful formation of the composite.

At 75 wt% PKS, the composite likely experienced agglomeration of carbon defects, leading to cracking, which is detrimental to the performance [159]. Activated carbon has a large specific surface and varied porosity. The high surface area may lead to increased internal stresses within the composite, especially when the resin and copper do not adequately fill the pores. As the carbon content exceeds a certain threshold, phase separation within the composite may have occurred. The irregular shape and size of the activated carbon particles likely contributed to uneven distribution within the composite matrix. This can create stress concentration points, making the composite more prone to breaking or splitting [8]. According to the US Patent Application Publication on Copper-Carbon Composite, high carbon concentrations may create a discontinuous phase that does not effectively bond with copper, resulting in weak points susceptible to fracture [165].

As a result, only carbon-copper composites with carbon compositions of 65 wt% and 70 wt% were successfully formed. This finding is consistent with the findings reported by Selamat et al. [8] and Ibrahim et al. [14]. Both studies reported that a carbon composition of 65 wt% was optimal for developing carbon-copper composites for a current collector in third-rail applications. Similarly, Nurul Hadi et al. [46] also developed composites with 65 wt% carbon and compared them with 55 wt% and 60 wt%. In all these studies, activated carbon derived from PKS-derived carbon with particle sizes of 90 µm to 150 µm was used, and epoxy resin served as the binder. The cold-pressing pressure employed in their studies was 18 tonnes, while in this study, only 12 tonnes of pressure was applied.

The development of the carbon-copper composite in this study was significantly impacted by the particle sizes and shapes of the materials, the composition, and equipment limitations. Composites with 65 wt% and 70 wt% carbon were more stable, allowing better interfacial bonding and mechanical integrity. The effectiveness of load transfer between copper and carbon particles is critical for composite performance, as carbon and copper exhibit low solubility and poor wettability [14]. Weak bonding at higher carbon contents could result in stress concentrations at the interfaces, leading to early failure under mechanical loads [166]. The fracture toughness of a material reflects

its ability to resist crack propagation. Composites with certain carbon content (such as 65 wt% and 70 wt%) likely exhibited higher toughness due to the more uniform distribution and improved bonding between carbon and copper powder particles [155].

4.3.2 Characterisation of the Carbon-Copper Composite

The green bodies or preforms containing 65 wt% and 70 wt% carbon underwent further processing, including warm compaction and post-baking produce the final carbon-sopper composite samples. Subsequently, the samples were characterised for density, hardness, resistivity, and transverse rupture strength (TRS). The properties of the successfully formed carbon-composites are summarised in Table 4.1. The development of this composite aimed to utilise activated carbon derived from PKS, a natural resource, and to demonstrate a simplified approach for producing a composite at low temperature while achieving sufficient performance for application as a pantograph slide in railway systems. The properties investigated in this study were compared with a pure carbon pantograph slide from the literature.

Table 4.1
Properties of Carbon-Copper Composite Samples in Phase 1 (Effect of Carbon Composition)

	Raw material composition (wt%)		Density	Hardness	Resistivity	TRS
Sample	**PKS**	**Copper**	**g/cm^3**	**HRR**	**μΩ.m**	**MPa**
A03	65	20	1.443	120	4884	46
A04	70	15	1.379	120	5900	35

The carbon-copper composite with 65 wt% PKS, 20 wt% copper, and 15 wt% phenolic resin exhibited superior qualities compared to the other sample. This sample showed a density of 1.443 g/cm^3, whereas the 70wt% carbon sample (A04) had lower density of 1.379 g/cm^3. The higher density of the 65 wt% PKS-derived carbon composite was likely due to more optimal packing of particles. Higher carbon content in the 70 wt% can lead to increased porosity due to insufficient resin or copper to fill the voids between carbon particles [167]. This porosity negatively impacted the overall

density, which is crucial for mechanical performance. Additionally, at 65wt% PKS-derived carbon, the particles likely interlocked more effectively, facilitating stronger interactions among carbon particles and with the copper and phenolic resin powders [168]. In contrast, at 70 wt% PKS-derived carbon, the interaction among carbon particles was less effective due to overcrowding, weakening the interparticle bonds and reducing the mechanical strength [169]. The application of 12 tonnes of pressure during pressing is significant and appropriate to shape the composite.

The microstructure of the composite can significantly influence its properties. The 65 wt% PKS-derived carbon composite exhibited a more uniform distribution of copper within the carbon matrix, leading to improved load transfer and reduced void formation, as shown in Plate 4.10 (a). In contrast, the 70 wt% PKS-derived carbon composite displayed a less homogeneous structure, resulting in areas of weakness. Figure 4.25 shows the micrographs of the 65 wt% and 70 wt% carbon composites. The darker region represented the PKS-derived carbon material, while the brighter areas indicated the presence of copper particles. Both micrographs revealed voids, suggesting high porosity and low density of the composites. Although the differences in void and copper distribution between the two samples were subtle, these microstructural variations likely impacted the properties of the composites.

Plate 4.10 (a) exhibits fewer and smaller voids compared to Plate 4.10 (b), indicating lower porosity in Sample A03. Porosity directly influences density, as a higher number of voids increases empty spaces within the material, leading to lower density [170]. Therefore, the micrograph in Plate 4.10 (a) for the carbon-copper composite with 65 wt% PKS-derived carbon supports the higher density compared to Plate 4.10 (b) for the 70 wt% PKS-derived carbon composite. The copper particles in (a) appeared more finely and evenly dispersed throughout the composite, contributing to the uniform distribution of stress under load and reducing localised stress concentrations that could cause premature failure. Although interfacial bonding was not visible from the micrograph, the finer copper distribution in Sample A03 suggests improved interaction between copper particles and the surrounding carbon matrix. Stronger interfacial bonding is essential for effective load transfer and higher TRS value, which is consistent with the superior performance of the 65 wt% PKS-derived carbon composite. The interfacial bonding between copper and carbon is critical for effective load transfer. In contrast, higher carbon content in the 70 wt% PKS-derived carbon composite may have caused poor wettability or inadequate resin coverage,

weakening the interfaces and compromising mechanical properties [95].

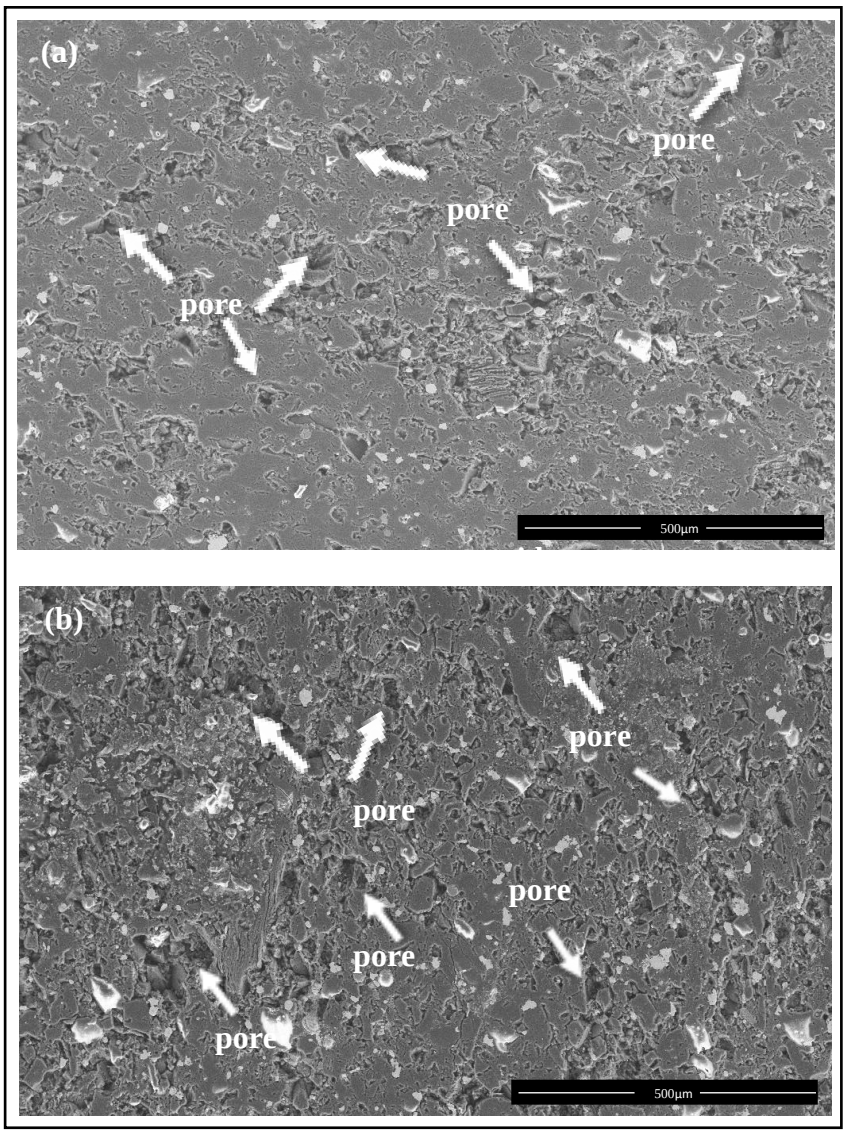

Plate 4.10 SEM Micrograph of Carbon-Copper Composite Cross-Section at 50X Magnification: (a) 65 wt% PKS-derived carbon and (b) 70 wt% PKS-derived carbon

The hardness and TRS of the composites are also influenced by their composition and microstructure [171]. The lower porosity and better interfacial bonding in the 65 wt% carbon composites likely contributed to its superior hardness compared to the 70 wt% composite. Increased porosity in the latter could reduce load-bearing capacity and increase brittleness [169]. Electrical resistivity is also affected by the arrangement of components within the composite. A more uniform distribution of copper within the 65 wt% composite provided improved conductivity pathways compared to the segregated

structure in the 70 wt% composite.

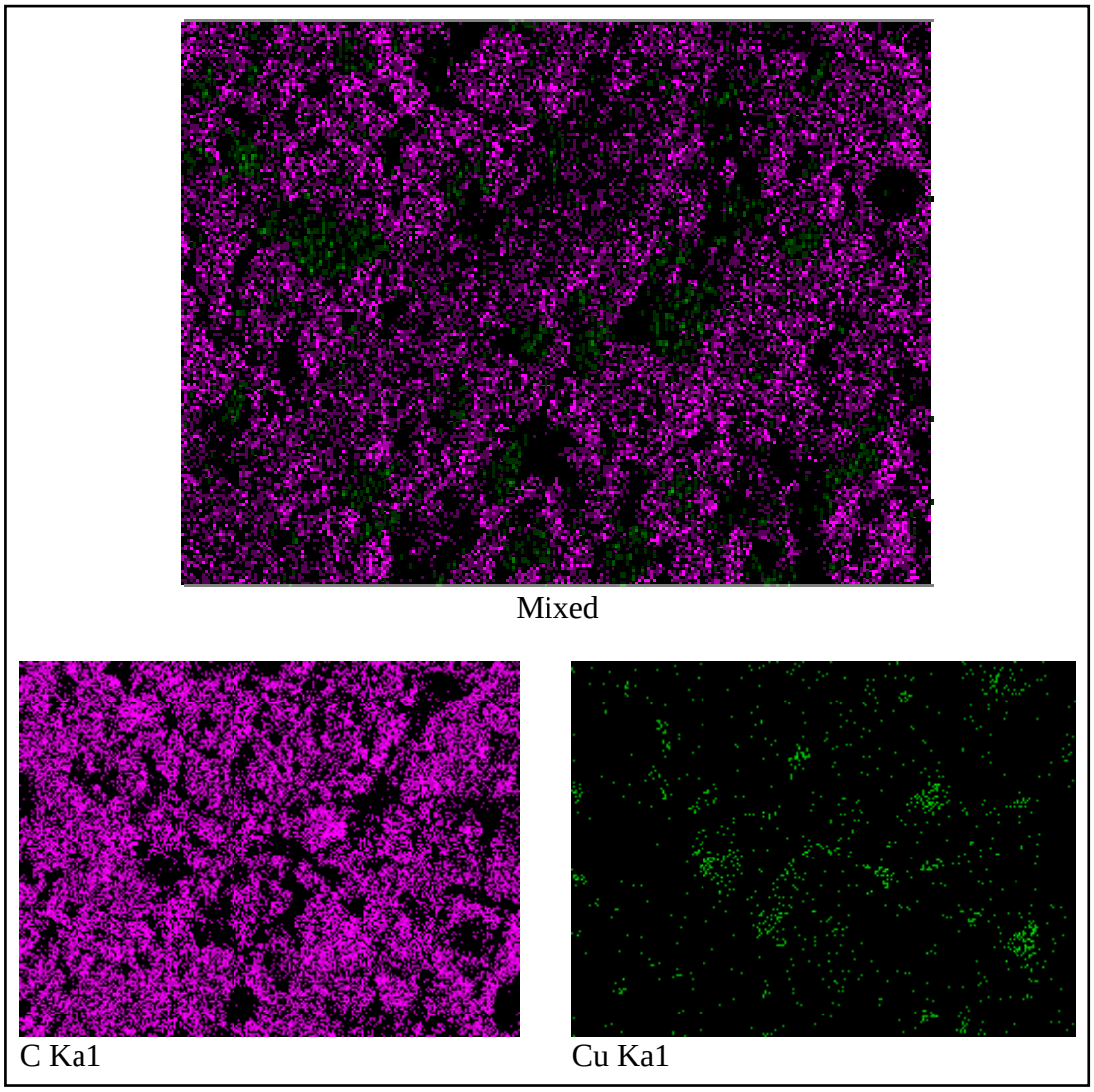

Plate 4.11 EDX image of Sample A03 (65 wt% PKS-derived Carbon, 20 wt% Copper, 15 wt% Resin)

During the post-baking process at elevated temperatures, from room temperature to 200℃, residual stresses and voids within the composites influenced their final properties. The thermal treatment may have caused differential expansion or contraction within the two composites, further affecting their structural integrity [172]. The curing dynamics of the resin were more effective at lower carbon content due to improved flow and infiltration into the voids between particles, resulting in a stronger matrix for the 65wt% PKS-derived carbon composite compared to that with higher carbon content [173]. In summary, the superior properties of the composite with 65 wt% PKS-derived carbon activated carbon, compared to the 70 wt% PKS-derived carbon , can be

attributed to several factors, including optimal packing density, improved microstructural integrity, better interfacial bonding, and more effective curing dynamics during processing. These factors collectively enhanced mechanical performance indicators such as hardness, density, resistivity, and TRS.

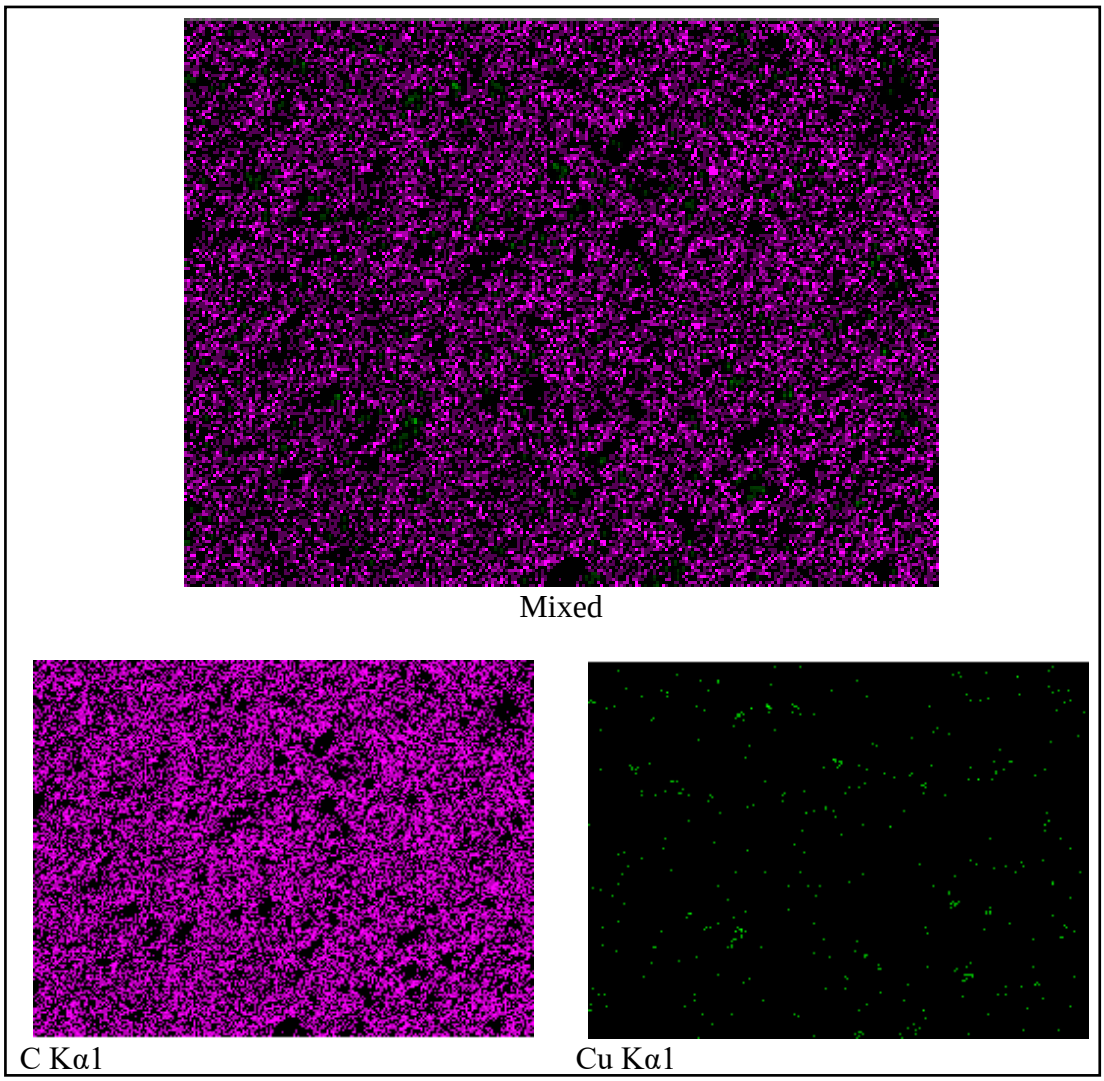

Plate 4.12 EDX image of Sample A04 (70 wt% PKS, 15 wt% Copper, 15 wt% Resin)

Plates 4.11 and 4.12 show the EDX images of the carbon-copper composites containing 65 wt% and 70 wt% PKS-derived carbon, respectively. In the EDX mapping, carbon (PKS-derived carbon) was represented by the magenta colour, while copper was indicated in green. Plate 4.11 demonstrates a relatively uniform distribution of both carbon and copper throughout the matrix compared to Plate 4.12. Although some areas indicated higher concentrations of one element, there were no large, distinct clumps or

segregations. This indicates effective mixing and processing during the development of the composite [174]. The carbon and copper appeared in the form of small domains rather than a large, continuous phase [175]. This is crucial for achieving the desired properties.

Plate 4.12 shows a slightly less uniform distribution of copper (green) compared to carbon (magenta), which remained relatively well-dispersed throughout the matrix. Noticeable areas with reduced copper concentration and slight clustering can be observed. In addition, the presence of larger white areas suggests higher porosity or voids within this sample. This could be due to the increased carbon content, affecting the compaction or processing. As expected, with the increased carbon proportion, the image was more dominated by the magenta (carbon) regions. Based on these images, the composite in Plate 4.11 (65 wt% carbon) exhibited a more desirable microstructure. The more uniform distribution of both carbon and copper, combined with lower porosity, suggests that this composite exhibited better and more consistent properties in terms of density, hardness, conductivity, and TRS.

Consequently, this composition was selected for further investigation in the following section. Previous research has also reported similar findings, although with variations in the size of PKS-derived carbon particles used [8][14][176]. In these studies, activated carbon was derived from PKS sourced from Malaysian Palm Oil Berhad (MPOB). The activated carbon was crushed and sieved, with particle sizes between 95μm and 150μm selected for use. The compositions employed consisted of 65 wt% carbon, 20 wt% copper (<10 μm) and 15 wt% commercial epoxy resin powder (65C-20Cu-15ER).

4.4 Effects of Graphite/PKS-derived Carbon Ratio on the Properties of Carbon-Copper Composite

From the findings in the previous section, the copper and resin compositions for this phase were fixed at 20 wt% and 15 wt%, respectively. The total carbon content remained at 65 wt%, consisting of varying proportions of PKS-derived carbon and graphite. The effects of different graphite-to-PKS-derived carbon ratios (20:80, 30:70, 50:50, 70:30, and 80:20) were examined. The addition of graphite is expected to produce composites with improved performance characteristics compared to those containing only PKS-activated carbon. After mixing the different sets of powders, the

samples were cold-pressed and then warm-compacted to produce the carbon-copper composites. The properties of the composites developed with varying graphite-to-PKS-derived carbon ratios are presented and discussed in the following sections.

4.4.1 Density

Figure 4.10 shows the density values of the carbon-copper composites at different graphite-to-PKS-derived carbon ratios. The addition of at least 50% graphite led to an improvement in density compared to the composites containing only PKS. Graphite has layered structures that allow for better packing efficiency compared to PKS-derived carbon. Graphite particles fill the voids between PKS-derived carbon particles, leading to a denser composite. Since the graphite particles are larger than the PKS-derived carbon particles, a ratio above 50:50 is required for them to effectively occupy the spaces between them, further enhancing the packing density.

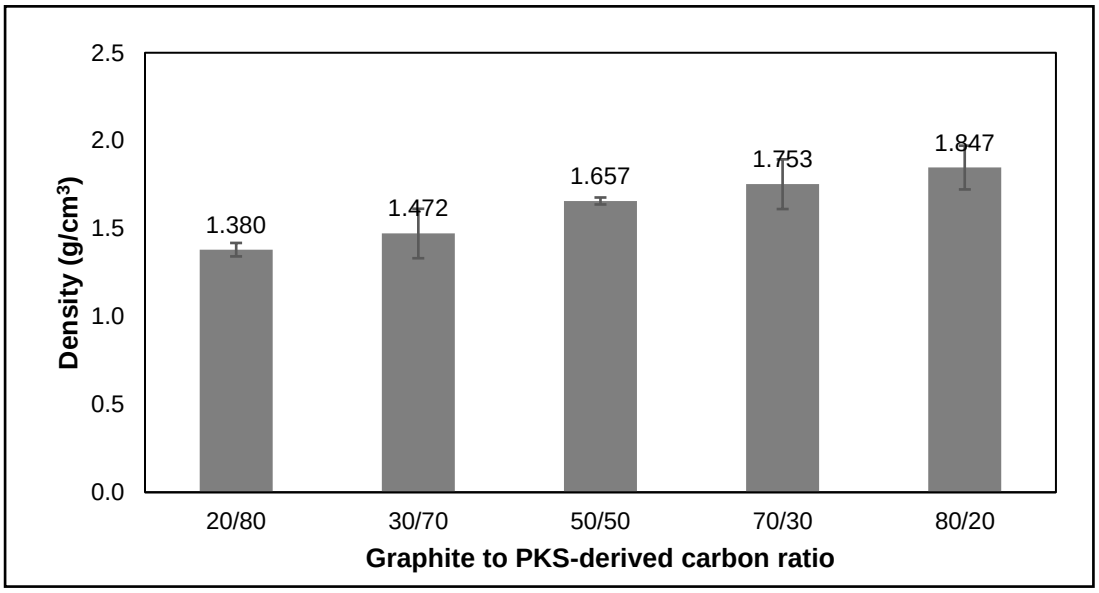

Figure 4.10 Density of Carbon-Copper Composite at Different Graphite to PKS-derived Carbon Ratio

Choi et al. [177] also reported in their research, when mixing particles of different sizes, smaller particles fill the voids between larger particles, increasing packing density. However, an optimal ratio, often beyond 50:50 proportion, is needed

to maximise this effect. As the graphite content increases, the overall density of the composite improves because graphite adds mass without significantly increasing porosity, resulting in a more compact structure. Tafere et al. [178] and Smole et al. [179] also found that increasing graphite content raised the densities of the composites. Though smaller graphite particles increased porosity slightly, overall graphite addition raised density due to mass contribution.

Liu et al. [175] adopted the spark plasma sintering (SPS) method to fabricate copper-graphite composites and reported that the relative density decreased with increasing graphite content. They added only 1% to 2.5% graphite and found that the highest density occurred at the lowest graphite content (1%). On the other hand, this study exhibited an increase in density with increasing graphite content. This finding aligns with the findings of Nasser et al. [180], who incorporated 0–35 vol% graphite flakes into ZrB2-SiC-graphite composite. In their study, composites were fully densified under hot-pressing conditions at a temperature of 1800℃ and a uniaxial pressure of 40 MPa for 1 hour. They also reported that adding up to 10 vol% of graphite, the relative density increased gradually, and fully densified composites were achieved at 7.5 and 10 vol% graphite. They employed the hot-pressing method in a vacuum chamber. Although the matrix system in this study was different, the trend observed here is consistent with Nasser et al. [180], as the densification mechanism assisted by graphite appears to apply across different composite systems. The flaky graphite particles occupy the interstitial spaces among the composite particles, enhancing the compact layering between the flakes. This is also supported by Aguiar et al. [181], who studied the densification of graphite. The layered structure (lamellar) of graphite allows the particles to slide under applied pressure, facilitating particle rearrangement during pressing (hot or warm), making compaction more efficient [182].

SEM micrographs in Plate 4.13(a) showed Sample B05 (80:20 graphite/PKS-derived carbon ratio) with a density value of 1.874 g/cm^3, while Figure 4.29(b) shows Sample B01 (20:80 graphite/PKS-derived carbon ratio) with a density value of 1.380 g/cm^3. Larger sizes of voids were found in Sample B01 (20:80 graphite/PKS-derived carbon ratio), contributing to its lower density. Smaller densities, higher porosities, and larger void ratios are generally associated with irregular particle shapes, as reported by Ulusoy et al. [183]. The highest density value of 1.847 g/cm^3 was achieved at the 80:20 graphite/PKS-derived carbon ratio, demonstrating that the inclusion of graphite, in a specific ratio with PKS, effectively enhanced the density of the carbon-copper

composites. Similar findings were reported by Magampa et al. [184], who observed that increasing graphite content in composites improved bulk density and reduced open porosity. This improvement could be attributed to the malleability of the natural graphite flakes, which deform more readily under pressure, forming a denser, more compact structure during pressing.

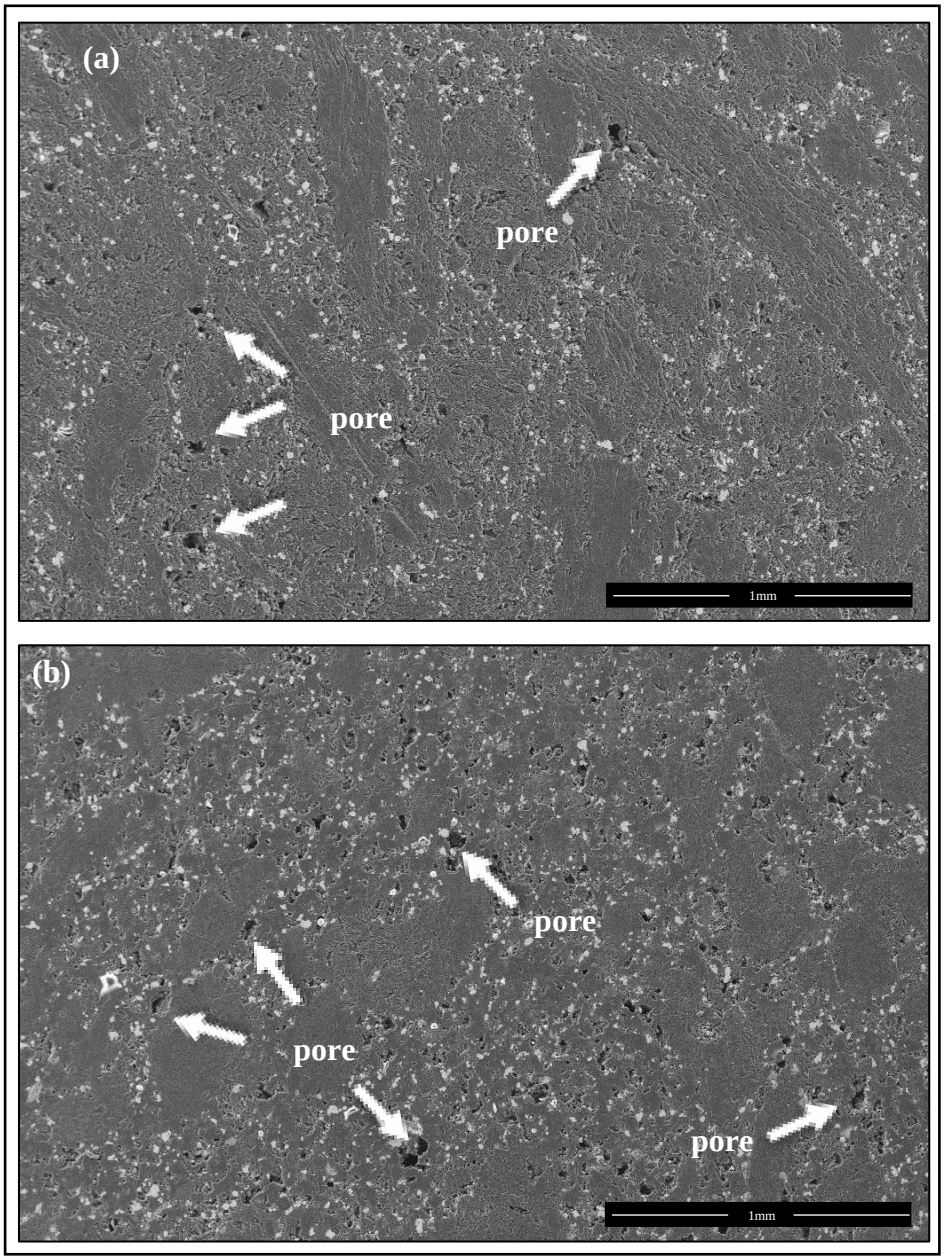

Plate 4.13 SEM Micrographs for Carbon-Copper Composite Sample (a) B05 (20:80 Graphite/PKS-derived carbon ratio) and (b) B01 (80:20 Graphite/PKS-derived carbon ratio)

4.4.2 Hardness

The hardness values of the carbon-copper composites at different graphite-to-PKS-derived carbon ratios are presented in Table 4.3. The highest hardness value of 118 HRR was obtained for the composite with a graphite/PKS-derived carbon ratio of 20:80. The hardness values of the developed composites were within the range of both pure carbon and metal-impregnated pantograph slides. Wu et al. [2] reported hardness values for pure carbon pantograph slides from different countries in the range of 65–92 HS, while Kuznar et al. [67] reported 90-110 HRD for commercial slides. Approximate relations suggest that these ranges correspond broadly to approximately 100–125 HRR. Hardness conversion was based on ASTM E140 tables, noting that direct equivalence for carbon-based composites is approximate, as the standards were originally developed for metallic materials. In this study, the developed carbon-copper composites exhibited hardness values of 86–112 HRR, which fell within and are comparable to the commercial ranges. This indicates that the material produced is mechanically suitable for pantograph slide applications. These hardness values were lower than those of the composite containing only PKS-derived carbon without graphite, as reported in the previous section. According to Kuznar et al. [67], the maximum hardness value is 125 HRB, as higher hardness values could risk damaging the catenary wire during contact.

Table 4.2
Hardness Values of Carbon-Copper Composite at Different Graphite/PKS-derived carbon Ratios

Sample	Graphite/PKS-derived carbon ratio, %		Hardness, HRR (Mean ± SD)*
	Graphite	PKS	
B01	20	80	112 ± 6
B02	30	70	99 ± 4
B03	50	50	105 ± 1
B04	70	30	86 ± 2
B05	80	20	93 ± 4

* Values are expressed as mean ± standard deviation (SD) from the three replicate measurements (n=3)

PKS-derived carbon is a natural material with relatively high intrinsic hardness due to its lignocellulosic composition and structure [5][21]. As reported in the previous section, where PKS-derived carbon was the sole carbon source, the composite exhibited

a hardness value exceeding 120 HRR, which is higher than the values obtained after adding graphite. Without graphite, the matrix material maintains its integrity, providing a more uniform structure that can better resist deformation. This uniformity contributes to higher hardness values. In contrast, the absence of graphite in the matrix indicates fewer soft regions within the composite, leading to an increase in hardness.

From Table 4.3, the hardness values fluctuated with increasing graphite content and decreasing PKS-derived carbon content. A higher proportion of PKS-derived carbon in the composite, such as the 80:20 ratio, could contribute to a higher hardness value. This may be due to several factors, such as the inconsistency of natural PKS-derived carbon [186], non-uniform dispersion, interfacial bonding between the materials [187], and the fibrous nature of PKS-derived carbon. Although the addition of graphite tends to lower the hardness, the values obtained remain acceptable and within the range suggested in the literature.

Liu et al. [175] studied copper-graphite composites and reported that an increase in graphite content showed a reduction in hardness. This was due to the softness of graphite, as well as the potential formation of porosity due to graphite agglomeration, which further reduced hardness. Similarly, research on graphite-reinforced aluminium composites has shown that adding graphite could decrease mechanical properties, such as hardness, due to its lubricating nature. For example, Papabathina et al. [188] investigated the effect of graphite on the mechanical properties of Al6061/SiC composite and reported that hardness increased with graphite addition up to 6 wt%. However, further addition of graphite caused a decline in hardness. This decrease in hardness can be attributed to the superior lubricating properties of graphite.

In an investigation by Omrani et al. [189], it was reported that increasing graphite nanoplatelet content (0.5–3 wt%) led to an increase in hardness, followed by a decrease at higher contents. Composites containing more than 1 wt% graphite nanoplatelets exhibited more porosity, negatively affecting the hardness of the composites. Similarly, Somayaji et al. [190]. Graphite, being a solid lubricant, increased the material's malleability under the indenter of the hardness tester, enhancing ductility. They also reported that there was a practical limit to the amount of graphite that could be added to the composite to enhance its mechanical properties, due to the monotonic decrease in hardness as the graphite content increased. Since graphite is inherently soft, the overall hardness of the composite decreased with higher graphite content. However, the rate of this decrease can vary depending on how well the graphite particles are

dispersed and bonded within the matrix. The lubricating properties of graphite can also influence hardness measurements. In some cases, the presence of graphite reduced friction during hardness testing, which could lead to inconsistent or fluctuating hardness values. As graphite is a soft material, a significant reduction in hardness was observed in a study conducted by Liu et al. [191]. The easy sliding of graphite layers resulted in lower resistance to deformation. When graphite was incorporated into the composite, its layered structure allowed the sheets to slide past each other under applied stress, thereby reducing the overall resistance to indentation or deformation, which is typically measured as hardness. Li et al. [192] reported that increasing the graphite content in yttria-stabilised zirconia coating further reduced the hardness but increased the toughness. Although this improvement in toughness led to a greater stress relaxation effect, it also reduced the deformation resistance of the coating, resulting in easier crack formation.

Changes in the microstructure of the composite, such as porosity or particle agglomeration, can also affect hardness. Increased graphite content might introduce more voids or alter the microstructure of the matrix, leading to variations in hardness. Plate 4.14 shows the SEM micrographs of the carbon-copper composites with 20:80 and 80:20 graphite-to-PKS-derived carbon ratios. When the graphite content was lower, as in the 20:80 graphite-to-PKS-derived carbon ratio, the microstructure appeared more porous and less uniform, possibly due to incomplete bonding between particles and the uneven dispersion of the PKS-derived carbon within the copper matrix. The increased porosity reduced the effective load-bearing area and weakened the matrix continuity, which contributed to lower hardness. In contrast, when the graphite content was increased to 80:20 ratio, the microstructure became denser and more compact. The higher graphite content promotes better particle packing and smoother interfaces between carbon and copper. The reduced presence of voids and improved bonding may enhance the matrix integrity, resulting in higher hardness values. This was also reported by Sulaymon et al. [193] in their research on copper-graphite composites. Low graphite content composites showed more voids caused by incomplete particle bonding and uneven dispersion of carbon phases. Increasing the graphite content promotes better particle packing, thereby reducing voids and improving hardness.

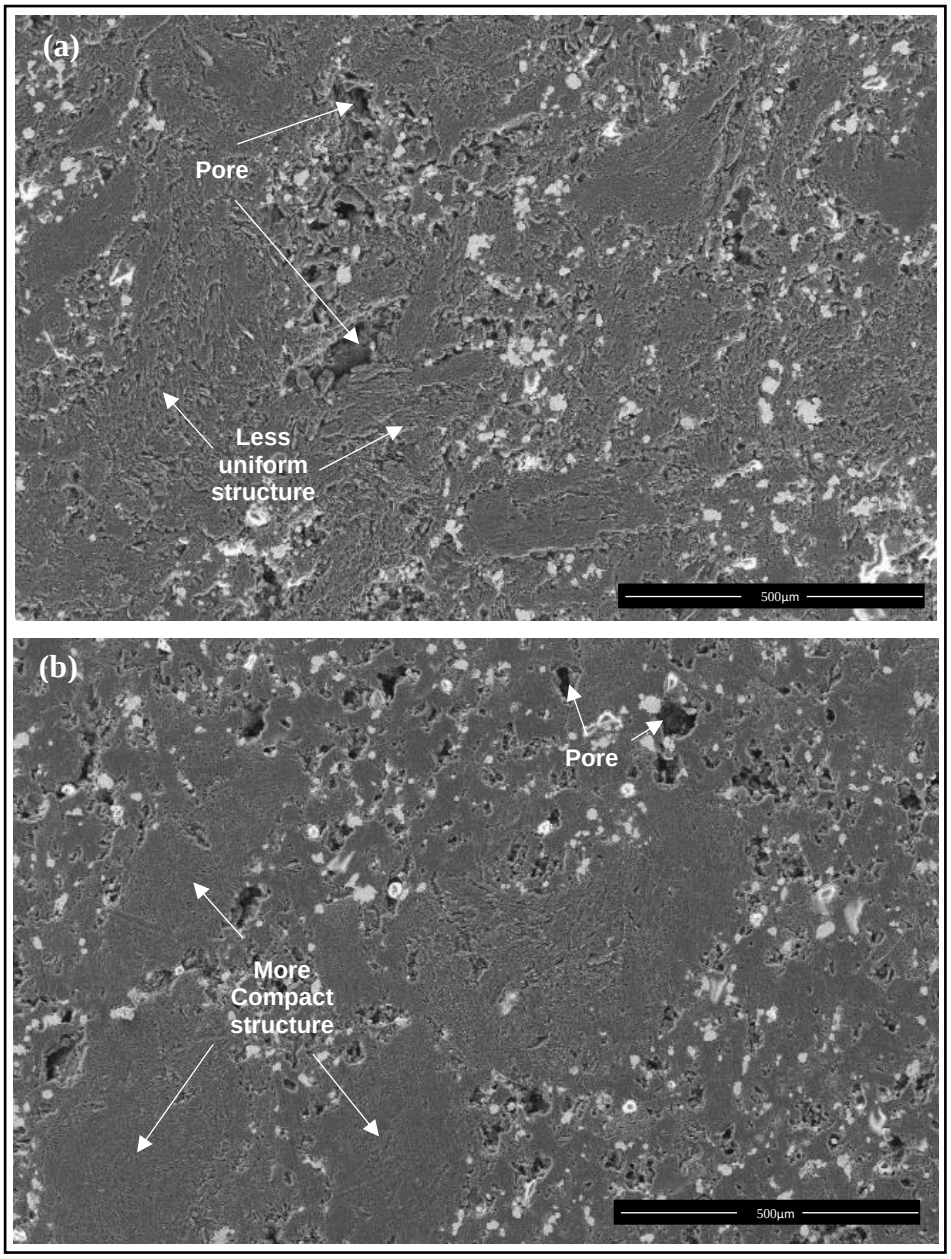

Plate 4.14 SEM Micrograph of Carbon-Copper Composite with Graphite to PKS-derived carbon Ratios of (a) 20:80 and (b) 80:20

4.4.3 Transverse Rupture Strength

The TRS values of the carbon-copper composites at different graphite-to-PKS-derived carbon ratios are presented in Table 4.7. Despite some fluctuations in the data, TRS results showed an increasing trend as the graphite content increased. The highest TRS value was obtained for the composite with 80:20 graphite-to-PKS-derived carbon ratio. However, the TRS value of the composite containing only PKS-derived carbon as

the carbon source, as discussed in the previous section, was higher (46 MPa) compared to the composites developed with the addition of graphite. In the absence of graphite, other reinforcement mechanisms or particles might have been more effective due to better interfacial bonding or a more uniform distribution of stress within the composite [194]. Without graphite, there were fewer potential stress concentrations caused by irregularly shaped particles or weak interfaces [195]. This reduction in stress concentration could have led to higher TRS values for the composite without graphite.

Table 4.3
TRS of Carbon-Copper Composite at Different Graphite/PKS-derived carbon Ratios

Sample	Graphite/PKS-derived carbon ratio, %		TRS, MPa (Mean ± SD)
	Graphite	PKS	
B01	20	80	28 + 5
B02	30	70	27 ± 5
B03	50	50	35 ± 6
B04	70	30	34 ± 6
B05	80	20	36 ± 7

* Values are expressed as mean ± standard deviation (SD) from the three replicate measurements (n=3)

The fluctuation in TRS with the addition of graphite can be attributed to several factors, including changes in the microstructure, interfacial bonding, and the inherent properties of graphite. The distribution of graphite particles within the composite can significantly affect TRS. A uniform distribution enhances strength, while particle agglomeration can lead to stress concentration and a reduction in TRS. Such fluctuations in TRS may occur due to variations in particle distribution among different samples. Furthermore, increasing the graphite content can introduce more voids or pores within the composite, particularly when the graphite particles do not blend well with the matrix. The presence of these voids can weaken the composite structure, thereby contributing to the observed fluctuations in TRS.

The bonding between graphite and the matrix material is crucial for achieving high TRS. Weak interfacial bonding can lead to reduced strength, as stress cannot be efficiently transferred between the graphite particles and the surrounding matrix [196]. In composites, failure often initiates at the interfaces or within the matrix rather than through the reinforcement itself. If graphite particles debonded from the matrix under stress, premature failure could occur, resulting in fluctuations in the measured TRS. The

inherent softness and lubricating nature of graphite may also facilitate easier deformation under stress, thereby reducing the TRS. Although the layered structure of graphite can provide some mechanical reinforcement, it may not be as effective as other reinforcement materials under certain orientations or loading conditions.

When mixed with graphite, a higher proportion of PKS-derived carbon can introduce weaker interfaces due to the inconsistency in grain size and shape. In addition, the irregular shapes and flake-like structure of graphite can act as reinforcements within the composite, potentially enhancing mechanical properties such as TRS. However, the effectiveness of this reinforcement depends on factors such as particle size, distribution, and interfacial bonding with the matrix. Irregularly shaped particles can create stress concentrations within the composite. These stress concentrations occur when the irregular shapes or sharp edges of the particles disrupt the uniform distribution of stress, potentially leading to reduced mechanical strength. The orientation of the flake-shaped graphite particles may also have influenced the TRS. When the flakes are aligned in a manner that allows them to bear the applied load effectively, they can enhance strength. However, when the flakes are randomly oriented or perpendicular to the load direction, their reinforcement effect is less pronounced. This may potentially lead to crack initiation and propagation under stress, as reported by Fu et al. [197]. They found that particle size had a significant effect on fracture toughness, and higher fracture toughness often leads to higher TRS. Similarly, Liu et al. [175] emphasised that particle distribution and interfacial bonding are crucial for achieving improved strength of the composite.

The dispersion among PKS, graphite, and copper was observed to be poor, as shown in Plate 4.15. The dark regions were likely carbon-based particles (labelled as C), including both graphite and PKS, while the brighter areas represented the copper matrix (labelled as Cu). The micrograph revealed the presence of a porous region surrounding the dark area, which may have corresponded to the PKS-derived carbon particles. This observation indicated poor particle packing and weak interfacial bonding, both of which could reduce the TRS of the composite [198]. In addition, porosity was also observed between the carbon and the copper areas due to poor wetting [199].

Although the TRS of the composite without graphite was higher, the values for the composite with graphite were still comparable to commercial standards. This suggests that, while graphite may not enhance TRS, it does not significantly degrade it

either, making the composite suitable for applications where other properties, such as electrical conductivity, are prioritised. The addition of graphite often involves trade-offs between different properties. While TRS may decrease, other properties, such as electrical resistivity or wear resistance, can improve, thereby making the composite more versatile for specific applications.

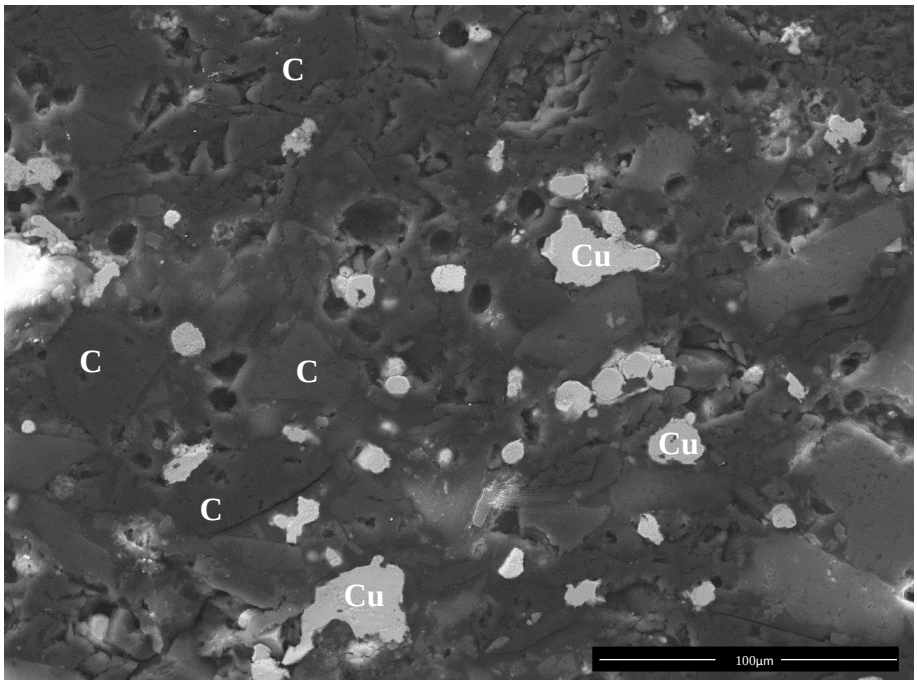

Plate 4.15 SEM Micrograph of Cross-Section of Developed Composite

4.4.4 Electrical Resistivity

Figure 4.11 presents the electrical resistivity values of carbon-copper composites at different graphite-to-PKS-derived carbon ratios. A lower electrical resistivity value is desired for pantograph slide applications, and the lowest value was obtained at a higher ratio. Overall, all carbon-copper composites exhibited relatively high resistivity values, which is undesirable for this application. As a result, further research is needed to improve this attribute.

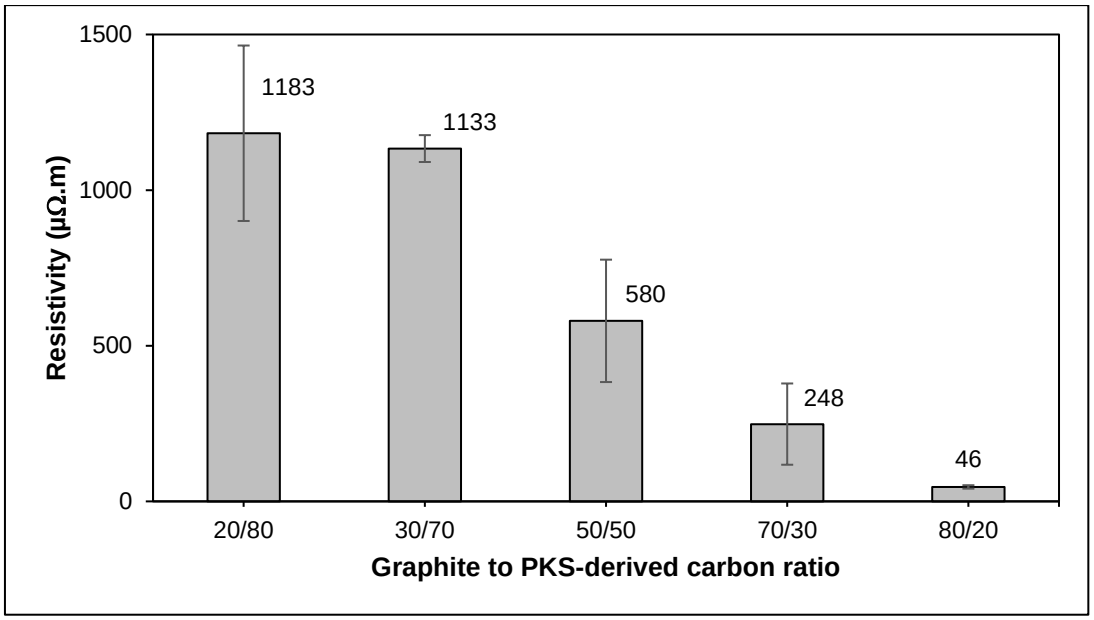

Figure 4.11 Electrical Resistivity of Carbon-Copper Composite at Different Graphite to PKS-derived carbon Ratios

PKS-derived carbon, as a natural material, is primarily composed of carbon in a non-graphitic form, which is less conductive than graphite [185]. Higher PKS-derived carbon ratios introduce more insulating material into the composite, increasing the resistivity. On the other hand, graphite consists of conductive particles and is naturally an excellent electrical conductor due to its delocalised electrons [200]. The addition of graphite into the composite showed a decrease in electrical resistivity of the composite, as shown in Figure 4.11. The lowest resistivity was achieved at 80:20 graphite-to-PKS-derived carbon ratio. Lower electrical resistivity is favourable in this context since the developed materials are intended for use as pantograph slides in railway applications, where they transfer electrical power from the traction substation to the moving train. Therefore, low resistivity, or high conductivity, is crucial to ensure seamless transmission of power to the propulsion system of the train.

Graphite is an excellent conductor of electricity due to its delocalised π-electron system. The addition of graphite to a composite creates more conductive pathways within the composite [201] and improves electrical connectivity between copper and carbon particles, reducing the resistivity. The increased surface area provided by graphite also contributes to improved conductivity. Rovnanik et al. [202] investigated the effect of graphite addition as a conductive admixture on Portland cement and alkali-activated slag mortars. They reported that the resistivity decreased gradually with

increasing graphite content until the percolation threshold was reached. In a study reported by Szczepanik et al. [203], composites with different graphite compositions (3–12 vol%) as filler and epoxy resin as a matrix were cast. Their results highlighted that adding 3–6 vol% graphite to epoxy resin decreased the resistivity of these materials. Higher filler content (9–12 vol%) in polymeric composite caused a rapid, non-linear decrease in resistivity. They concluded that the most pronounced decrease in resistivity was achieved for specimens with the highest graphite content, indicating the formation of a spatial conductive network within the composite.

Rew et al. [204] investigated the effect of different graphite types and compositions on the electrical resistivity of asphalt mastic. They found that the resistivity of mastics (resin used in construction) containing flake graphite decreased gradually with increasing graphite content in the composite. They concluded that flake-type graphite is the most suitable for multifunctional applications, considering its efficiency in enhancing both conductivity and mechanical strength. The finding is in line with this study, where flaky graphite was incorporated into the carbon-copper composite with the expectation of achieving similar improvements in both electrical resistivity and mechanical performance of the composite.

The SEM images in Plate 4.16 showed carbon-copper composite with different proportions of graphite and PKS-derived carbon as the carbon source. The darker grey areas (labelled C) corresponded to carbon-rich areas, including graphite and PKS, while the brighter areas represented the copper phase. The resin, being a polymer, was not distinguishable in these SEM images. They revealed a relatively dispersed distribution of the copper phase (bright areas) within the carbon matrix (dark areas).

However, noticeable agglomerations or larger clusters of carbon and copper were observed in some regions. The non-uniform distribution of copper is a key factor contributing to the high resistivity. Although copper is a good conductor, its effectiveness in lowering overall resistivity is limited by its distribution. The agglomerations of copper may not form a continuous conductive network throughout the material, thereby hindering electron flow [205]. In addition, the disruption of conductive pathways by the insulating resin matrix and PKS-derived carbon may also have affected the resistivity of the composite.

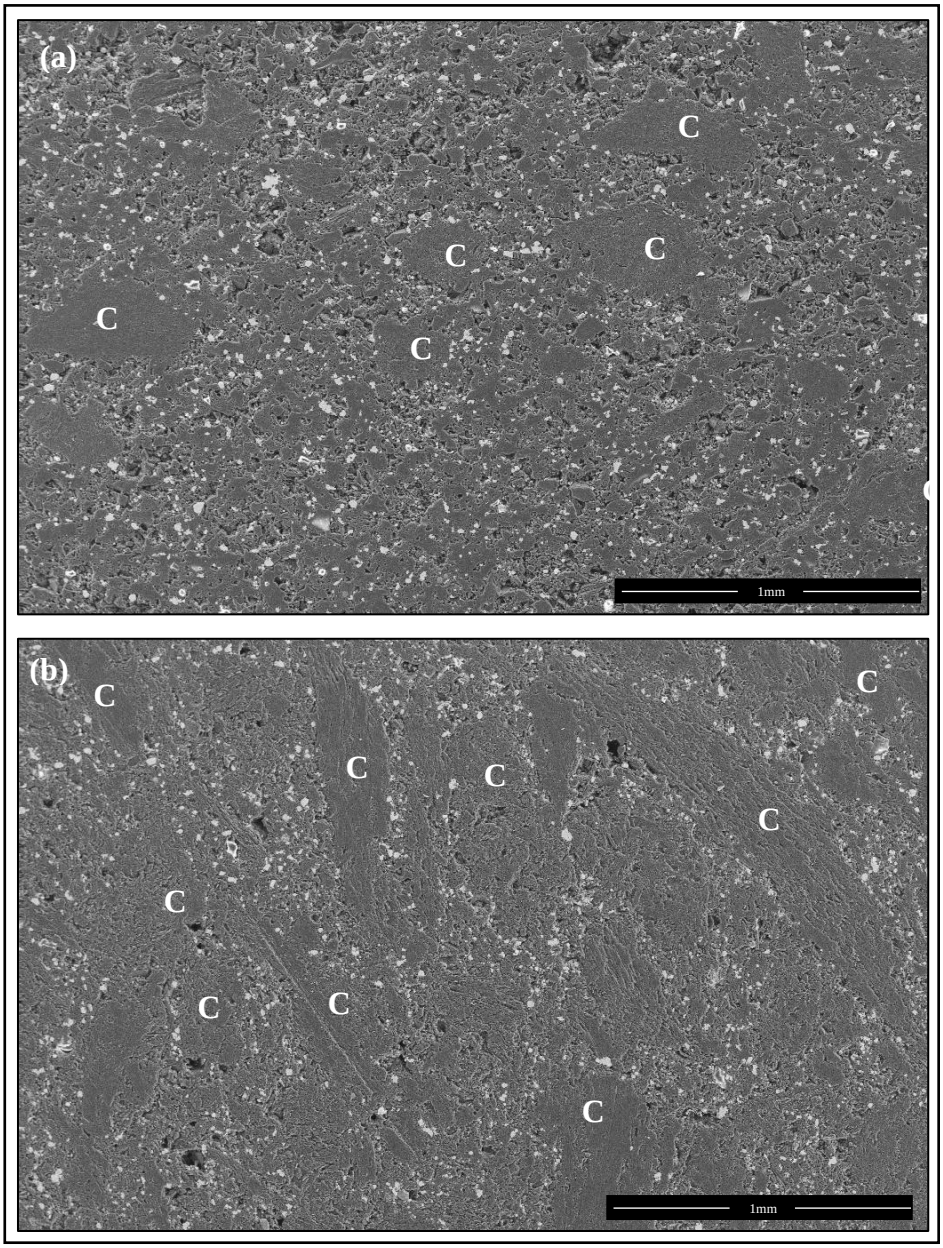

Plate 4.16 Micrograph of Carbon-Copper Composites with Graphite-to-PKS-derived carbon Ratios of (a) 20:80 and (b) 80:20

Lower proportion of PKS-derived carbon minimised its negative impact on resistivity, resulting in a lower resistivity value at 80:20 graphite-to-PKS-derived carbon ratio (Sample B05). Graphite has a highly crystalline structure with delocalised π- electrons, enabling excellent electrical conductivity [191]. The interconnected graphite regions form efficient conductive pathways for electron flow, thereby reducing the resistivity. The layered structure of graphite allows for efficient electron transport, forming a continuous conductive matrix within the composite matrix. Radzuan et al. [206] highlighted the importance of interconnected graphite particles for forming

conductive networks. They reported that the presence of voids within the conductive composite could eventually decrease electrical conductivity.

4.5 Effects of Different Filler Addition on the Properties of Carbon-Copper Composite

To increase conductivity effectively, other types of conductive material, such as graphene, copper, and CNT, can be incorporated to produce a multi-phase conductive matrix, as suggested by a previous study [81]. The study suggested different types of conductive fillers, including graphite paste, graphene, CNT, carbon fibres (CFs), and carbon black (CB), to reduce the electrical resistivity of cement-based materials and to improve electrical conductivity.

In the subsequent stage, the influence of different fillers on the characteristics of the carbon-copper composite was evaluated. To increase electrical resistivity, several types of filler were considered, including CNT, copper-based fillers, and GO. CNT and copper-based fillers are well known for their excellent electrical conductivity properties. However, further investigation is required to understand their characteristics within the composite. In addition to improving resistivity, the incorporation of GO was suggested, as it could potentially improve TRS due to its high mechanical strength, which could increase the original strength of a material by up to five times [207], [207], as well as its ability to bridge microcracks [208]. High TRS is essential for pantograph slides to withstand mechanical stresses encountered during operation, such as bending and friction [32].

CNT are known for their exceptional electrical conductivity, which can significantly enhance the conductivity of the composite. Their high aspect ratio allows the formation of efficient conductive pathways within the material. In addition, CNT provide mechanical reinforcement, improving properties such as hardness and tensile strength. However, achieving uniform dispersion is crucial to maximise these benefits. Previous research has shown that CNT can improve both the mechanical and electrical properties of copper composites [209]. Nonetheless, high CNT content can occasionally compromise conductivity due to agglomeration or interfacial issues [210]. Meanwhile, GO can exhibit high electrical conductivity similar to graphene, with easier dispersibility, which facilitates a more uniform distribution within the composite. Graphene-based materials are recognised for their excellent electrical conductivity and

mechanical strength, making them suitable for enhancing composite properties [211].

Hybrid reinforcement using Cu-CNT powder combines the benefits of copper and CNT. Copper provides a conducive pathway, while CNT enhances mechanical properties and further improves conductivity. Although specific studies on Cu-CNT powder are limited, the concept leverages the established benefits of CNT in enhancing composite properties, with copper facilitating better dispersion and conductivity [212].

Three different fillers were selected to investigate the effects of incorporating different fillers into carbon-copper composite material: GO, Cu-CNT, and CNT. Each filler was added at a consistent concentration of 1 wt% to the carbon-copper powder mixture. The resulting composites were subjected to a series of characterisation tests to evaluate their mechanical, electrical, and other relevant properties. Analysis of these results provides valuable insights into the influence of each filler type on the overall performance of the carbon-copper composite.

The composition of the materials for the development of the carbon-copper composite is presented in Table 4.5 in the previous section, consisting of 65 wt% carbon (80% graphite: 20% PKS), 20 wt% copper, and 15 wt% resin. In this study, the addition of 1wt% filler is proposed. For instance, for every 100 g of the mixed materials, 1 g of filler was added. The mixture was processed following the same procedure as described in the previous section, including mixing, cold pressing, warm compaction, post-baking, and composite characterisation.

4.5.1 Density

Figure 4.12 shows the density data for composites containing different types of fillers, compared to the composite without any filler from the previous section. The composite without filler exhibited the highest density, as the absence of additional fillers may have minimised void formation and ensured better particle packing within the matrix. The second-highest density was observed in the composite containing CNT. Although CNT has a relatively low density (~1.3–1.4 g/cm^3) compared to copper and graphite, their high aspect ratio allows them to integrate into the matrix without introducing significant voids. Consequently, CNT may slightly reduce the density compared to the composite without filler, but their dispersion likely maintains good packing efficiency

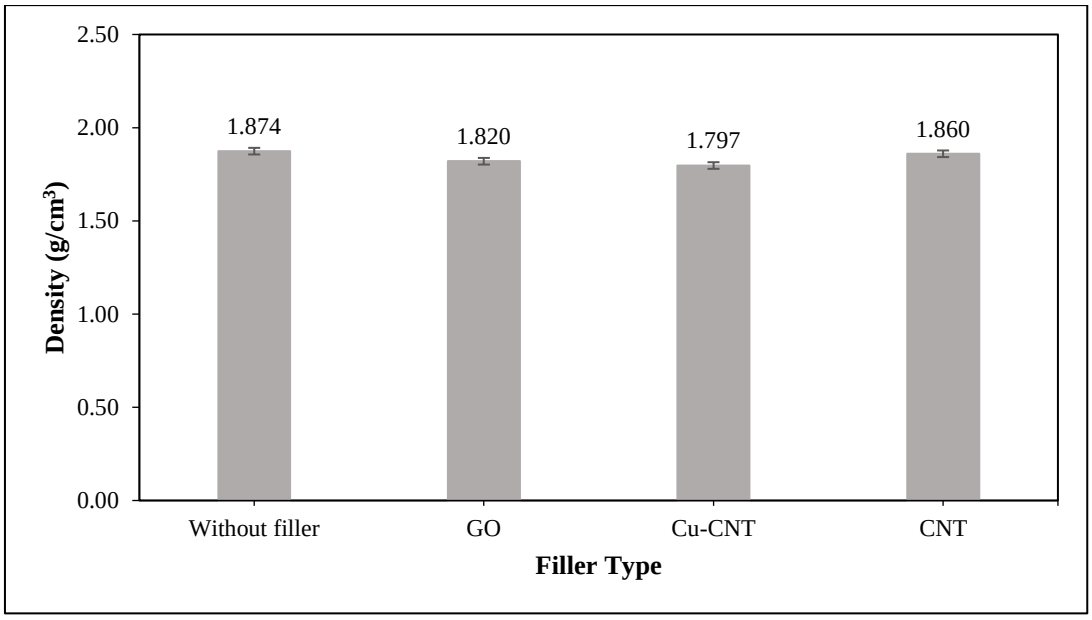

Figure 4.12 Density of Carbon-Copper Composites with Different Types of Fillers

GO has a slightly higher intrinsic density (~2.2 g/cm^3) than CNT; however, it may have introduced more voids due to its flake-like structure and tendency to agglomerate during mixing. The presence of oxygen-containing functional groups in GO may also have disrupted particle bonding within the matrix, contributing to the reduction in density. The Cu-CNT powder combined copper and CNT but typically exhibited a lower effective density than pure copper due to the inclusion of low-density Cu-CNT. The hybrid structure of Cu-CNT may also lead to agglomeration or uneven dispersion, generating microvoids that reduce overall packing efficiency and density.

A study on the production and characterisation of Cu-CNT nanocomposites also reported that the addition of CNT reduced the relative density of the nanocomposites [213]. In their study, copper nanocomposites reinforced with CNT were produced by ultrasonication and conventional sintering. The resulting nanocomposites demonstrated potential candidate for electrical and electronic applications.

4.5.2 Hardness

Figure 4.13 presents the hardness values of the carbon-copper composites with different types of fillers. CNT are among the hardest known materials due to their strong covalent sp^2 bonds arranged in a hexagonal lattice structure [214]. Their tubular morphology provides exceptional reinforcement, resisting deformation under applied

loads. The high aspect ratio of CNT allows effective stress distribution throughout the matrix, thereby enhancing the hardness. Proper dispersion of CNT within the matrix ensures uniform reinforcement without introducing significant voids or defects. Studies on CNT-reinforced composites consistently report improved hardness due to the load transfer capability of CNT and their ability to strengthen weak points within the matrix. Nurazzi et al., [215] reported that CNT improved interfacial bonding and load-transfer mechanisms in the composite. Functionalised CNT enhance dispersion and bonding with the matrix, leading to significant improvement in mechanical properties, including hardness.

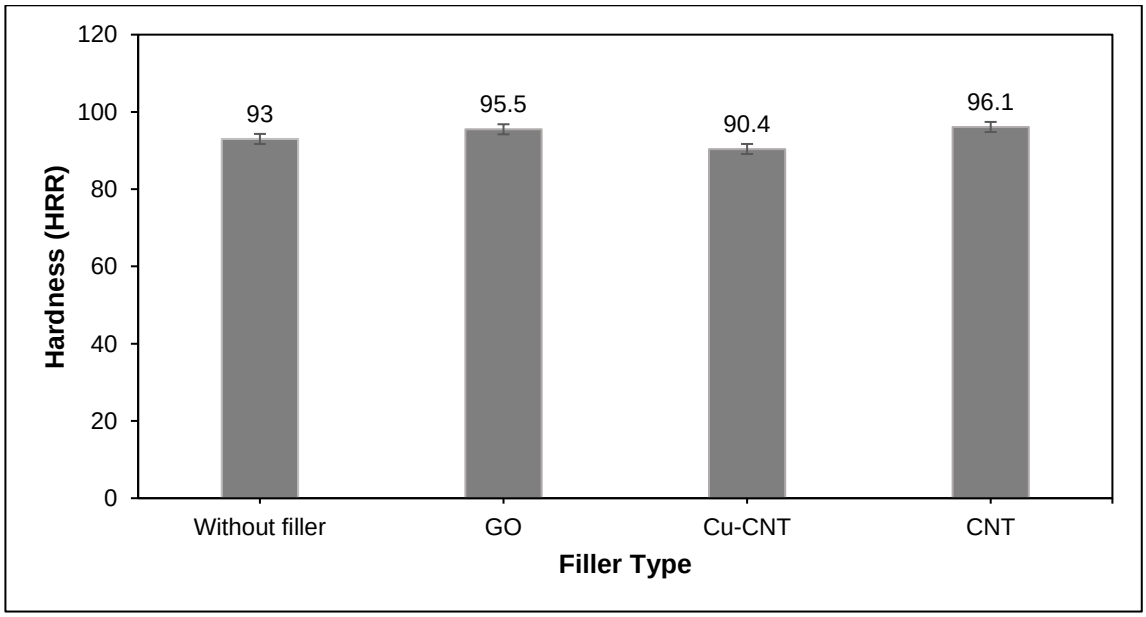

Figure 4.13 Hardness of Carbon-Copper Composite with Different Type of Fillers

GO also contributes to the improvement of hardness due to its layered structure and ability to enhance interfacial bonding within the matrix. However, the presence of oxygen-containing functional groups in GO may disrupt the structural integrity of the composite when dispersion is inadequate, thereby limiting its effectiveness compared to CNT. The flake-like morphology of GO can also promote slide agglomeration, which reduces its reinforcing efficiency. Aoyang et al. [216] investigated several methods for dispersing graphene-based filler within the composite. They discussed how weak interfacial bonding and poor dispersion of GO can hinder improvements in mechanical properties such as hardness. They also reported that the addition of GO increased the hardness value of the composite.

The Cu-CNT hybrid fillers combined copper and CNT, but their performance depended on dispersion quality and interfacial bonding. In this study, the addition of Cu-CNT may have introduced voids or agglomerates within the matrix, reducing its reinforcing efficiency and leading to lower hardness. Hybrid fillers such as Cu-CNT may compromise mechanical properties due to agglomeration or weak interfacial bonding.

4.5.3 Transverse Rupture Strength (TRS)

Figure 4.14 displays the TRS values of the carbon-copper composites with different types of fillers. The composites reinforced with CNT showed the highest TRS values. As discussed in the previous section, CNT is known for their exceptional mechanical properties, including high tensile strength and modulus. When incorporated into a composite, CNT acts as reinforcement by bridging gaps within the matrix and improving load transfer. Their high aspect ratio and tubular structure effectively distribute stress throughout the matrix, thereby reducing localised stress concentrations and enhancing TRS. Proper dispersion of CNT ensures uniform reinforcement without introducing significant defects or voids. Zihong et al. [217] reported that CNT-reinforced composites exhibited improved mechanical properties, including high TRS, due to their ability to form strong interfacial bonds with the matrix and to reinforce weak points. In their study, the mechanical performance of the fibre-reinforced polymer composite was enhanced through CNT incorporation. In another study conducted by Preethi et al. [218], Al-CNT composites fabricated via powder metallurgy showed significant improvements in compressive strength and hardness to CNT reinforcement. They also highlighted the ability of CNT to impede crack propagation and enhance the mechanical properties of the composite.

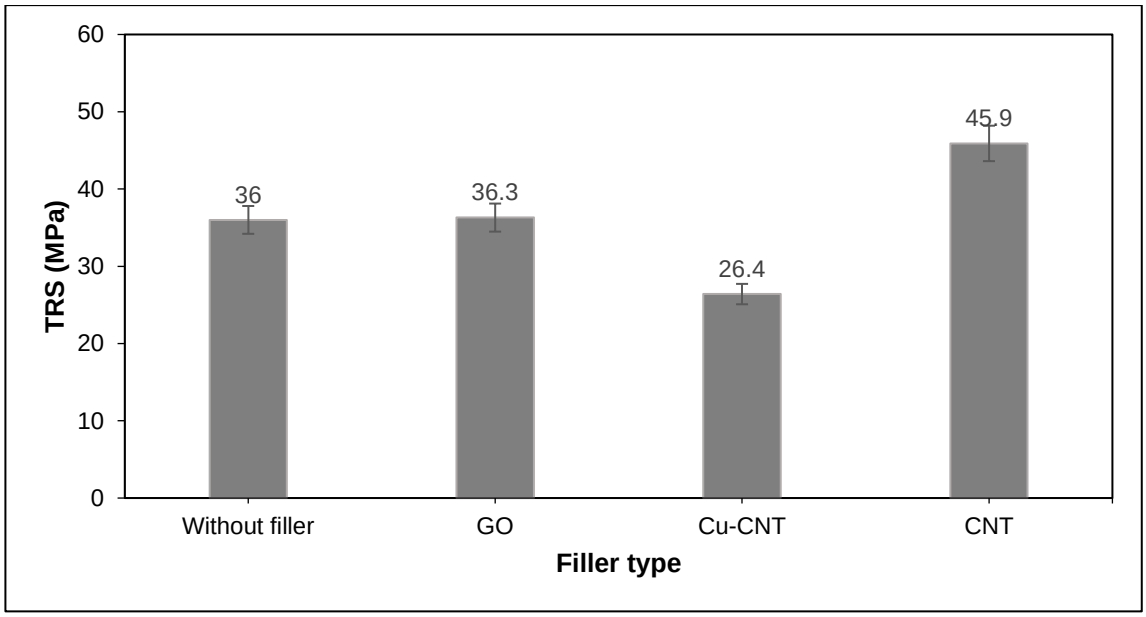

Figure 4.14 TRS of Carbon-Copper Composite with Different Types of Fillers

The addition of GO also showed a moderate improvement in TRS value. GO has a layered structure that can enhance mechanical properties by strengthening interfacial bonding within the composite matrix. However, the presence of oxygen-containing functional groups in GO may have disrupted the structural integrity of the matrix when dispersion was inadequate. This could have led to agglomeration, creating weak points and limiting its reinforcing effect compared to CNT [218]. The flake-like morphology of GO provides some reinforcement but may be less effective at distributing stress compared to the tubular structure of CNT [219].

The Cu-CNT hybrid filler combined copper and CNT but may have introduced agglomeration or weak interfacial bonding within the matrix. These issues create stress concentration points that reduce the overall mechanical performance of the composite. Additionally, poor dispersion of Cu-CNT particles may have led to localised defects or voids within the composite, thereby reducing the TRS value.

4.5.4 Electrical Resistivity

Figure 4.15 shows the resistivity of the composites with different types of fillers, along with a comparison to the composite without any filler. The composite from the previous section, which contained no filler, exhibited a moderate resistivity value due to the presence of copper and graphite. However, the absence of additional conductive

fillers limited the formation of continuous conductive pathways within the matrix. The matrix likely contained voids or interruptions in the copper-carbon network, thereby increasing the electrical resistivity.

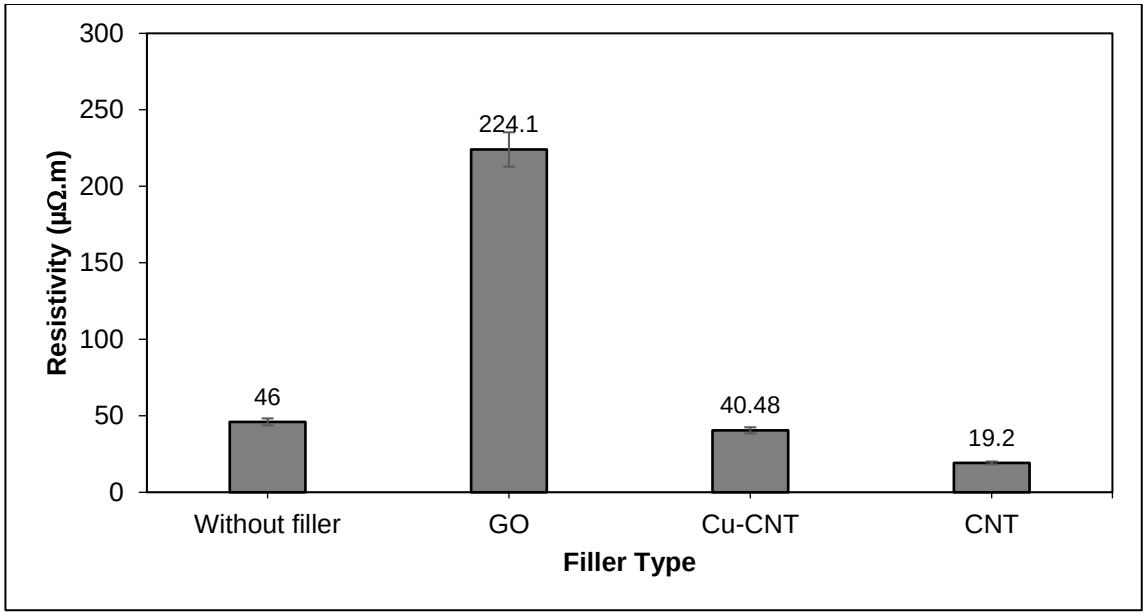

Figure 4.15 Resistivity of Carbon-Copper Composite

Among all fillers, GO exhibited the highest resistivity, indicating that it significantly increased the resistivity compared to the sample without filler. GO contains oxygen functional groups, which could disrupt electron mobility and act as insulating barriers. Its flake-like structure may lead to agglomeration, creating voids and further hindering conductivity. Previous studies on GO-reinforced composites consistently reported increased resistivity due to its insulating nature, unless it was converted into reduced graphene oxide (rGO). In addition, poor dispersion of GO may have worsened these effects by preventing the formation of efficient conductive networks [220].

Cu-CNT reduced resistivity compared to the baseline composite. The hybrid structure of Cu-CNT combines the excellent conductivity of copper with the ability of CNT to form interconnected conductive pathways. However, agglomeration of Cu-CNT particles may create localised regions of poor conductivity, thereby preventing further reductions in resistivity [221]. Previous research on Cu-CNT composites reported that they enhanced electrical conductivity by forming hybrid conductive networks [222]. They also found that the hybrid network formed by CNT within the

copper matrix provided additional conductive pathways, thus enhancing overall conductivity.

Among all fillers, the addition of CNT into the composite resulted in the lowest resistivity, demonstrating its superior ability to enhance electrical conductivity. Its high aspect ratio allows the formation of interconnected conductive pathways even at low concentrations (1wt%), significantly reducing resistivity [223]. Proper dispersion ensures uniform distribution, minimising voids, and maximising conductive network formation. CNT-reinforced composites are widely recognised for their ability to reduce electrical resistivity. Previous studies showed that even small amounts of CNT can drastically improve conductivity by creating percolation pathways. Silva et al. [224] and Paleari et. al. reported that the addition of small amounts of CNT (0.5–2 wt%) to thermoplastic composite resulted in a percolation threshold, significantly increasing electrical conductivity through the formation of interconnected networks.

Figures 4.16 and 4.17 show the EDX line scanning results for the carbon-copper composites without and with CNT incorporation, respectively. In the composite with CNT, the carbon signal exhibited a higher baseline and a more extended region of spatial overlap with copper. In contrast, the composite without CNT showed a lower carbon baseline. Quantitative peak analysis revealed that the composite with CNT has 20–30% higher carbon baseline. This finding suggests that the presence of CNT promotes the formation of a more continuous carbon network and increases C-Cu bonding. The oxygen signal remained low for both samples; however, localised oxygen (O) peaks coinciding with copper indicated possible surface oxidation of the copper particles.

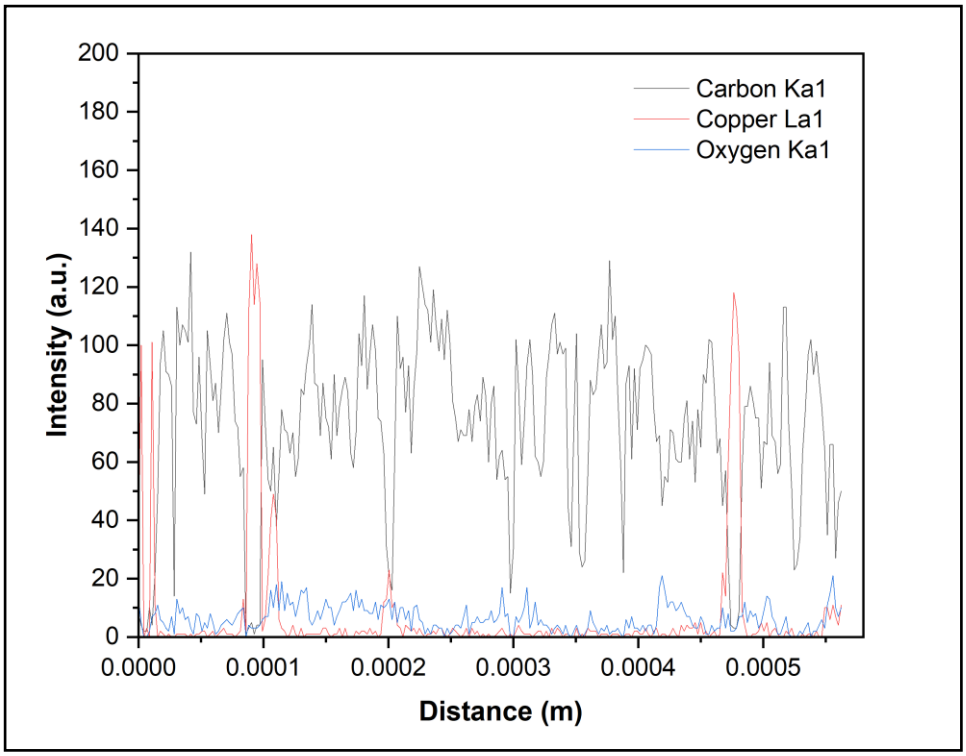

Figure 4.16 EDX Line Scanning for Carbon-Copper Composite without CNT

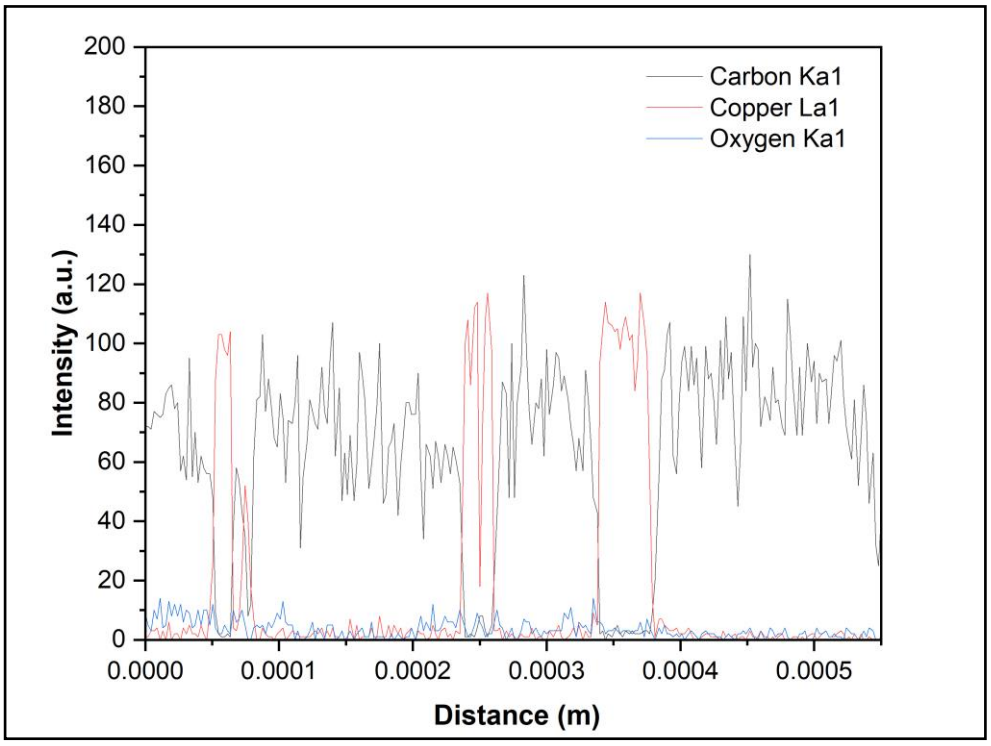

Figure 4.17 EDX Line Scanning for Carbon-Copper Composite with CNT Addition

Increased carbon continuity and larger contact length between carbon and copper phases may reduce the effective contact resistance, thereby improving electrical conductivity [222]. Moreover, densification and enhanced interfacial bonding enhance TRS by facilitating load transfer [225]. Therefore, these findings indicate that CNT addition enhanced both electrical and mechanical performance through microstructural connectivity.

4.6 Effects of CNT Addition on the Properties of Carbon-Copper Composite

As CNT was chosen as the filler for the carbon-copper composite, the effect of varying filler content was investigated. From the previous sections, the properties of the carbon-copper composite without filler and with 1 wt% CNT were obtained and recorded. Further investigation was conducted for the addition of 2 wt% and 3 wt% CNT to examine their influence on the properties of the carbon-copper composite. While higher CNT content may improve the carbon-copper composite, excessive amounts could hinder enhancement due to poor dispersion and agglomeration of the materials. The mixed materials underwent the same processing steps as described previously, including mixing, cold pressing, warm compaction, post-baking, and composite characterisation. The data were recorded and are discussed in this section.

4.6.1 Density

Figure 4.18 shows the change in density of the carbon-copper composite with increasing CNT content (0 wt%, 1 wt%, 2 wt%, and 3 wt%). The density decreased steadily from 1.874 g/cm^3 (0 wt%) to 1.836 g/cm^3 at 1 wt%, 1.790 g/cm^3 at 2 wt%, and 1.732 g/cm^3 at 3 wt%. This decrease was attributed to the low intrinsic density of CNT (~1.3-1.4 g/cm^3) compared to copper (~8.96 g/cm^3) and carbon (~2.2 g/cm^3). Shaari et al. [226] also reported that, as CNT content increased in the copper composite, the density decreased owing to the low density of the CNT.

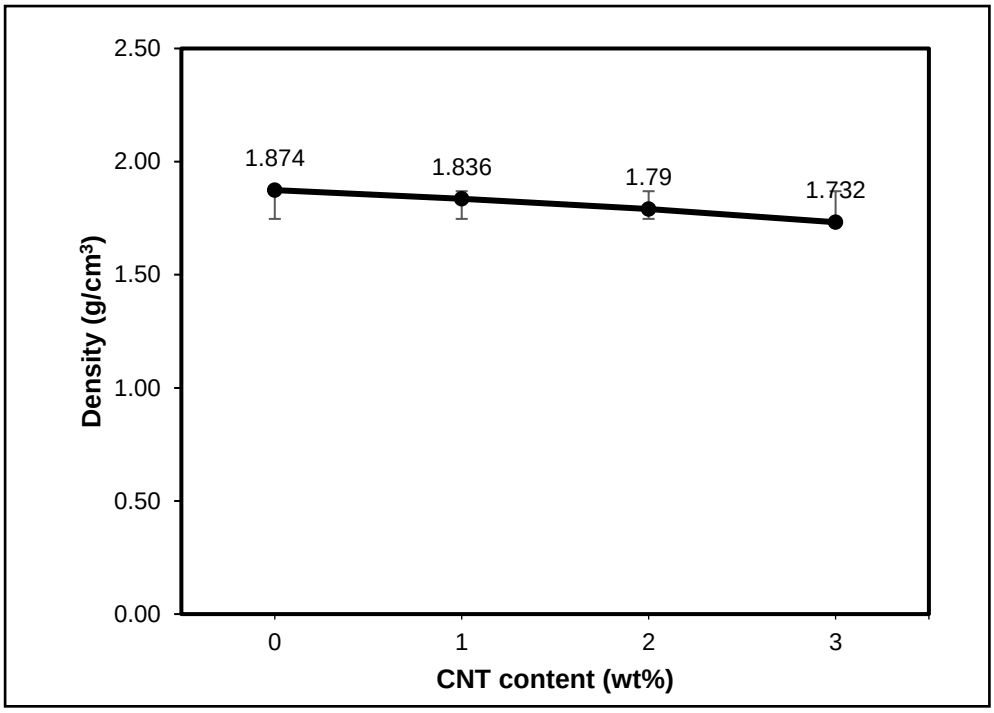

Figure 4.18 Density of Carbon-Copper Composite at Different CNT Contents

A similar finding was reported by Soleymani et. al. [227], who highlighted that increasing the volume of dense CNT clusters as reinforcing particles decreased the density of the composite material. The agglomeration of CNT within the composite led to non-uniformity and void formation, thereby reducing the density and mechanical properties. They also discussed the challenges of achieving uniform dispersion in CNT-reinforced composites. Elbakyan et al. [228] reported that CNT-reinforced polypropylene composites exhibited reduced density due to the lightweight nature of CNT. They noted that agglomerates occupied less than 3% of the total area but could significantly impact structural properties if the CNT was not dispersed properly. On the other hand, Jagannthan et al. [229] observed 5.7% increase in density when 2 wt% CNT were added to high-density polyethylene (HDPE). The increase was attributed to the formation of interfacial layers between CNT and polymer matrix, as well as homogeneous dispersion without agglomeration. Proper dispersion of CNT is crucial, as it can increase density by improving matrix packing and reducing voids. Ding et al. [230] also reported that increasing CNT content reduced agglomeration, improved bonding, and refined the microstructural arrangement, which decreased porosity and improved the density value.

Figure 4.19 shows the XRD patterns, displaying the crystallographic

characteristics of carbon-copper composites with varying CNT content (0-3 wt%).

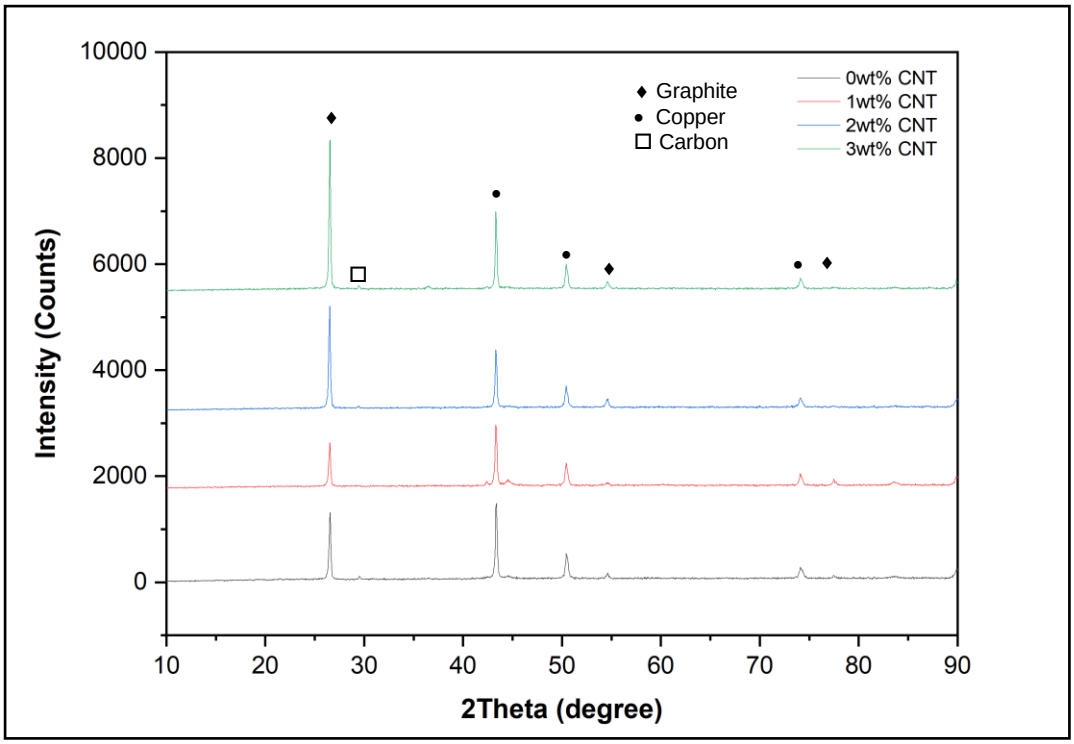

Figure 4.19 XRD Pattern of Carbon-Copper Composites with Different CNT Contents

Distinct peaks corresponding mainly to copper appeared at around 43°, 50°, and 74°, which can be indexed to the (111), (200), and (220) planes, respectively. These peaks were consistently observed in all samples, confirming that copper remains in its metallic state regardless of CNT content. The results also indicated that CNT addition did not induce the formation of new crystalline phases. A broad peak associated with graphitic carbon appeared in the region of 26°–28°, and its intensity became more pronounced with increasing CNT loading, indicating successful incorporation of CNT into the composite. The gradual increase in the carbon peak relative to the copper peaks suggests both a higher fraction of graphitic material and a possible dilution or surface coverage effect on the copper crystallites. No new diffraction peaks attributable to copper oxides or carbide phases were detected, confirming that no significant chemical reaction occurred between copper and carbon during processing and CNT addition. This structural stability is beneficial, as it ensures that both metallic copper and graphitic CNT additions contribute to the electrical and mechanical performance of the composite. This observation aligns with previous research on CNT-reinforced metal

matrix composites, where the absence of CNT-specific diffraction peaks at low concentrations is often reported due to their limited volume fraction and minimal reaction with the matrix material [231]. Similar findings have been reported in another research, where dominant copper peaks remain after CNT addition, indicating that the copper matrix retains its metallic and crystalline nature [232].

4.6.2 Hardness

The hardness values of the carbon-copper composites with different CNT contents are depicted in Figure 4.20. The addition of CNT resulted in a decrease in hardness value from 110 HRR (without filler) to 105 HRR at 1 wt%, 102 HRR at 2wt%, and 101 HRR at 3 wt%. Despite the high mechanical strength of CNT, the composite with 1wt% CNT exhibited higher hardness than those with 2 wt% and 3 wt% CNT. This result can be attributed to microstructural differences and the behaviour of CNT in the composites.

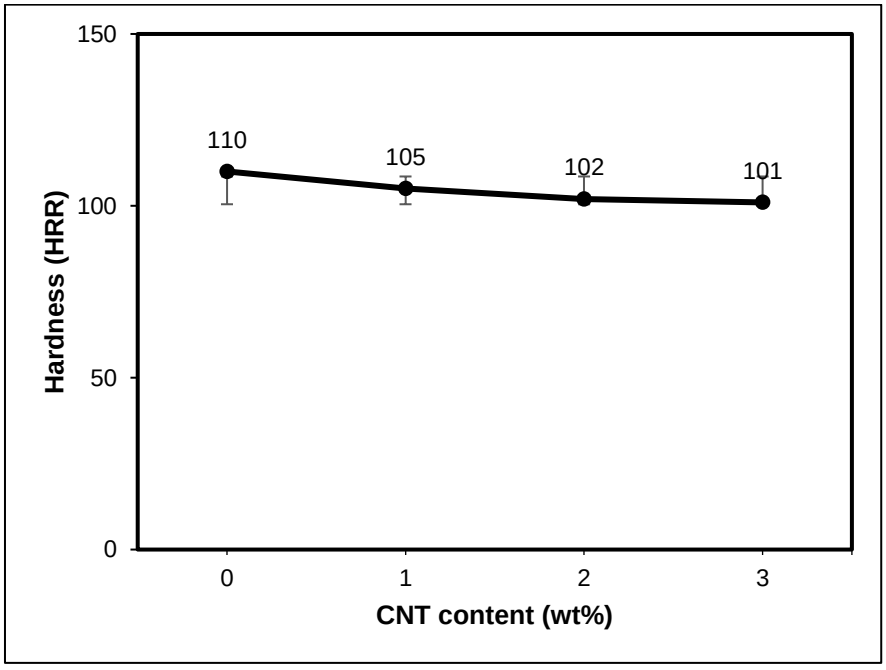

Figure 4.20 Hardness Carbon-Copper Composites with Different CNT Contents

Plates 4.17 (a) and (b) show the micrographs of the carbon-copper composite containing 1 wt% and 3 wt% CNT, respectively. In Plate 4.17 (a), the bright copper

particles appeared moderately dispersed across the darker carbon matrix, with fewer visible voids or defects in the matrix. A more uniform distribution of components and fewer agglomerations was also observed. In contrast, Plate 4.17 (b) shows more visible clustering or agglomeration zones.

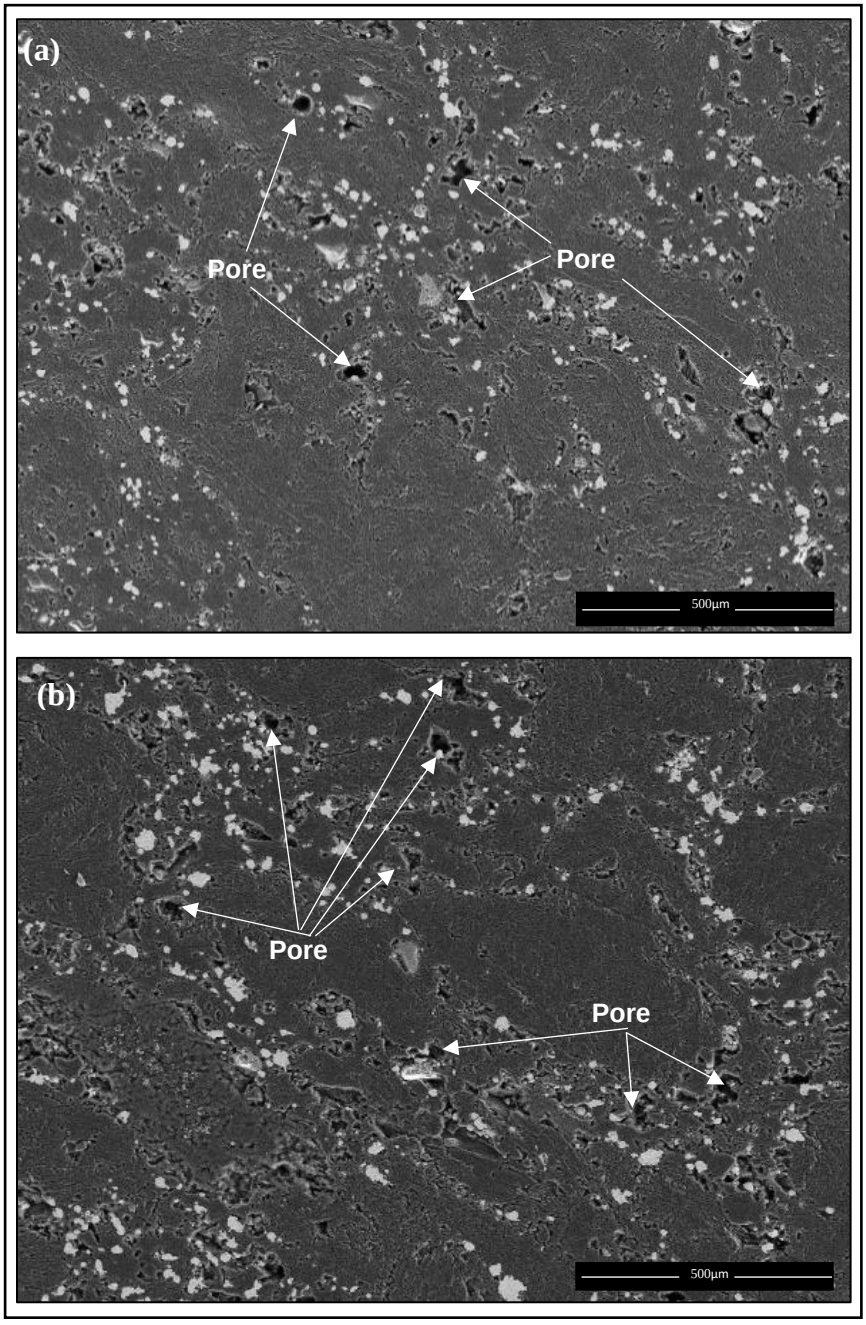

Plate 4.17 SEM Micrographs of Carbon-Copper Composite with (a) 1 wt% CNT and (b) 3 wt% CNT

The increased presence of darker regions may represent CNT clusters or voids. This was also reported by Zhao et al. [232], who reported that dark regions in SEM micrographs correspond to pores, indicating increased porosity following CNT

addition. The dispersion appeared less uniform in the micrograph, with clustering likely creating voids or stress concentration points that further reduced hardness. Agglomerated CNT may have also disrupted the matrix continuity, thus weakening the composite structure. This observation is supported by Punera [233], who reported a significant reduction in material stiffness and natural frequency with increasing degrees of agglomeration, causing non-uniform material properties.

Higher CNT content may have also introduced porosity into the composite due to poor packing efficiency. Hu et al. [234] reported that the porosity of mortar increased significantly when the CNT fraction increased to 0.5%. Increased porosity reduces the overall density and mechanical integrity of the material, thereby contributing to lower hardness. This was also reported by Cherry et al. [235], who found that increased porosity led to a decrease in material hardness. Takahashi et. al. [236] reported that when CNT content exceeded 2 wt%, the hardness of PPS prepared using solution mixing remained constant and decreased. At 5 wt% CNT, the hardness was significantly lower compared to the optimal value obtained at 2 wt% CNT addition. This low hardness of the melt-blended samples was attributed to insufficient mixing of PPS and CNT owing to the localisation of CNT. On the other hand, Yuan et. al. [237] revealed that the microhardness of Ti/Mg composites increased with increasing CNT content. Pasha et. al. [238] reported that as multi-walled CNT (MWCNT) content increased, hardness also increased due to uniform mixing between MWCNT and AlSi matrix. Both studies employed lower CNT content, ranging between 0.25 wt% and 1 wt%. The hardness of the composite was influenced by the amount of CNT added. Nonetheless, the hardness value remained adequate for the intended application when compared to those of commercial products reported in the literature.

4.6.3 Transverse Rupture Strength (TRS)

Figure 4.21 illustrates the effect of CNT addition on the TRS of the carbon-copper composites. The TRS exhibited a non-linear relationship with CNT content, initially increasing from 36 MPa at 0 wt% to a maximum value of 47 MPa at 1 wt% CNT, representing 28% enhancement in mechanical strength. This improvement can be attributed to the reinforcing effect of well-dispersed CNT, which effectively transferred the load throughout the matrix. However, at higher CNT additions, the TRS progressively decreased to 38 MPa at 2 wt% and 31 MPa at 3 wt%, falling below the

baseline value. The decline suggests that excessive CNT content leads to agglomeration, creating stress concentration points rather than reinforcement. The observed behaviour indicated that 1 wt% is the optimal CNT concentration for maximising the TRS of the carbon-copper composite, beyond which diminishing returns occur, a threshold effect commonly reported in nanoparticle-reinforced composites.

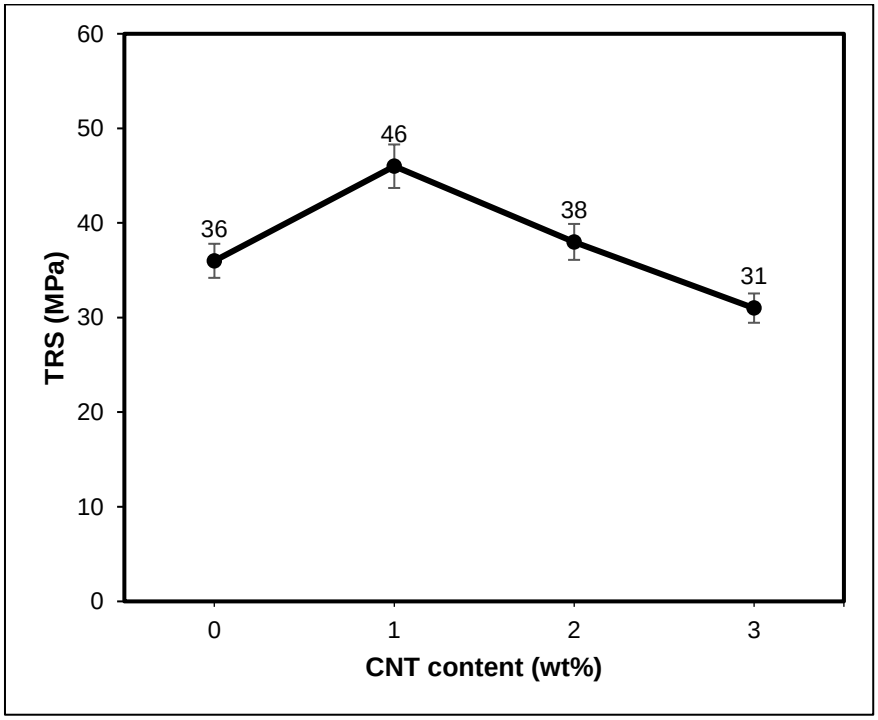

Figure 4.21 TRS of Carbon-Copper Composites with Different CNT Contents

With the addition of CNT, dispersion challenges may have led to agglomeration, introducing weak points within the matrix. These weak points reduce the ability of the composite to resist deformation, resulting in lower flexural strength. Poor bonding between the CNT and the matrix could have also limited the effective load transfer. As CNT content increases, agglomeration becomes more pronounced due to the van der Waals forces between the nanotubes [237]. Yang et.al. [239] tested four different CNT concentrations (0.00 wt%, 0.02 wt%, 0.04 wt%, and 0.05 wt% by mass of cement) in their study and demonstrated that the relationship between CNT content and strength properties depended significantly on dispersion quality rather than on CNT quantity alone.

Research by Hu et. al. [234] indicated that the addition of 0.05% CNT enhanced the average strength of concrete by 67.2%. When the proportion of CNT increased to

0.10 wt% and 0.15 wt%, the tensile strength increased by only 5.5% and 1.1%, respectively. However, excessive CNT incorporation resulted in agglomeration, which reduced the bridging effect between the CNT and the foamed concrete matrix. Consequently, a weak region was developed in the agglomerated area, diminishing the strength of the composite.

4.6.4 Electrical Resistivity

Figure 4.22 shows the electrical resistivity of carbon-copper composites at different CNT additions. The resistivity exhibited a non-linear relationship with CNT loading, initially decreasing from 46 μΩ.m at 0 wt% to a minimum of 19 μΩ.m at 1 wt%, followed by an increase to 30 μΩ.m at 2 wt% and a slight further increase to 32 μΩ.m at 3 wt%.

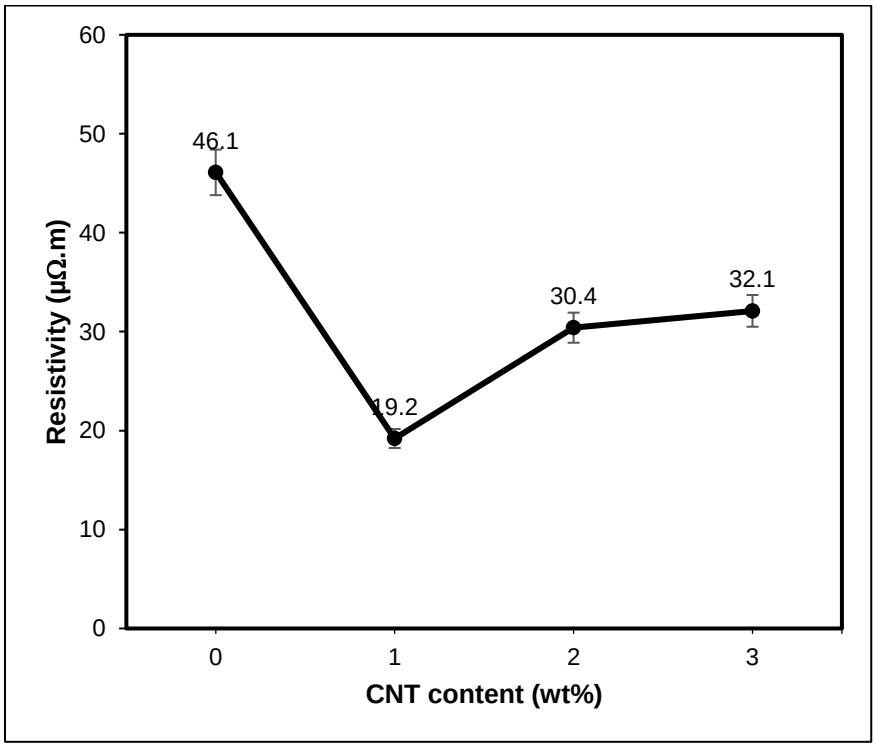

Figure 4.22 Resistivity of Carbon-Copper Composite at Different CNT Contents

This behaviour can be attributed to competing mechanisms governing electrical transport in the CNT-reinforced composite. The significant reduction in resistivity at 1 wt% CNT indicates the formation of efficient conductive networks,

where well-dispersed CNT create percolative pathways for electron transport throughout the matrix. However, the subsequent increase in resistivity at higher CNT loadings (2-3 wt%) suggests the onset of agglomeration, as van der Waals interactions between CNT cause clustering rather than uniform dispersion. These agglomerates disrupt the continuity of conductive pathways and create interfacial resistance points, compromising the electrical performance despite the higher CNT content. This percolation-dominated behaviour establishes 1 wt% as the optimal CNT concentration for maximising electrical conductivity in the carbon-copper composite system.

A study by Earp et. al. [240] demonstrated that CNT-polymer composite exhibited a dramatic decrease in resistivity at low CNT loadings (0.1–1 wt%), followed by diminishing returns or even increases in resistivity at higher loadings. This behaviour was attributed to the formation of a percolative network at low loadings, while subsequent CNT agglomeration disrupted efficient electron transport pathways at higher loadings. In another research by Earp et al. [241], it was reported that epoxy-CNT samples showed a clear reduction in resistivity as the CNT content increased from 0.014 wt% to 0.05 wt%, with consistent decreasing trends observed within this range.

4.7 Effects of Post-baking Process

Before investigating the effects of warm compaction process parameters, namely temperature, time, and pressure, the overall process for developing the carbon-copper composites was investigated and finalised. As described in the previous section, the process comprised mixing, cold-pressing, warm compaction, and post-baking. Using the best composition (Table 4.6) obtained from the previous section (Phase 2), a comparison was conducted between carbon-copper composites with and without post-baking. The results of the characterisation tests are shown in Table 4.7. Both composites, with and without post-baking, exhibited acceptable values of density, hardness, TRS, and resistivity when compared to the properties of commercial pantograph slide material.

Table 4.4
Characterisation of Carbon-Copper Composites With and Without Post-baking Process

Process for developing carbon-copper composite	Density (g/cm^3)	Hardness (HRR)	TRS (MPa)	Resistivity ($\mu\Omega.m$)
With Post-baking (200°C)	1.85	96	45.93	16.7
Without Post-baking	1.79	92	46.25	19.2

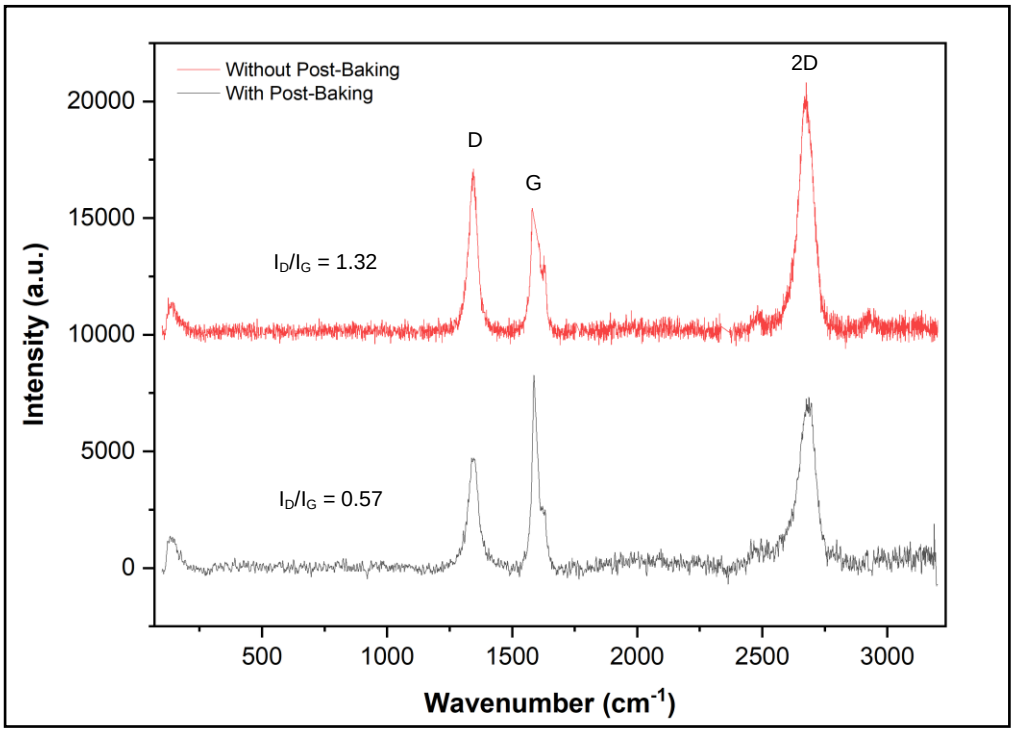

Figure 4.23 Raman Spectra of Carbon-Copper Composite with Post-baking and without Post-baking

The Raman spectra of carbon-copper composites with and without post-baking are depicted in Figure 4.23. Distinct differences were observed in the intensity and sharpness of the D and G bands, located at approximately 1350 cm^{-1} and 1580 cm^{-1}, respectively. The WPB sample showed a more pronounced G band and a reduced D/G intensity ratio compared to the XPB sample. This indicates that the post-baking promotes structural ordering and graphitisation within the carbonaceous phase. The reduced D/G ratio corresponds to a lower degree of disorder and fewer defect-induced vibrations in the sp^2 carbon lattice, consistent with thermal annealing effects that facilitate the rearrangement of amorphous carbon into more ordered graphitic domains [242].

In contrast, the XPB sample retained broader peaks, suggesting a higher proportion of amorphous carbon structures. The persistence of defects in the XPB composite can be advantageous by maintaining certain interfacial contrast areas with copper, potentially improving electron transport pathways. The trade-off between structural order and interfacial connectivity is a key characteristic of a hybrid metal-carbon composite. Similar behaviour was reported by Xiu et al. [243], who observed that moderate annealing enhances graphitisation while simultaneously creating distinct carbon-metal boundaries, which can increase interfacial resistance. Therefore, the Raman results indicate that although post-baking enhances the order of the carbon phase, it may compromise the electronic percolation network by promoting phase segregation at the Cu-C interface.

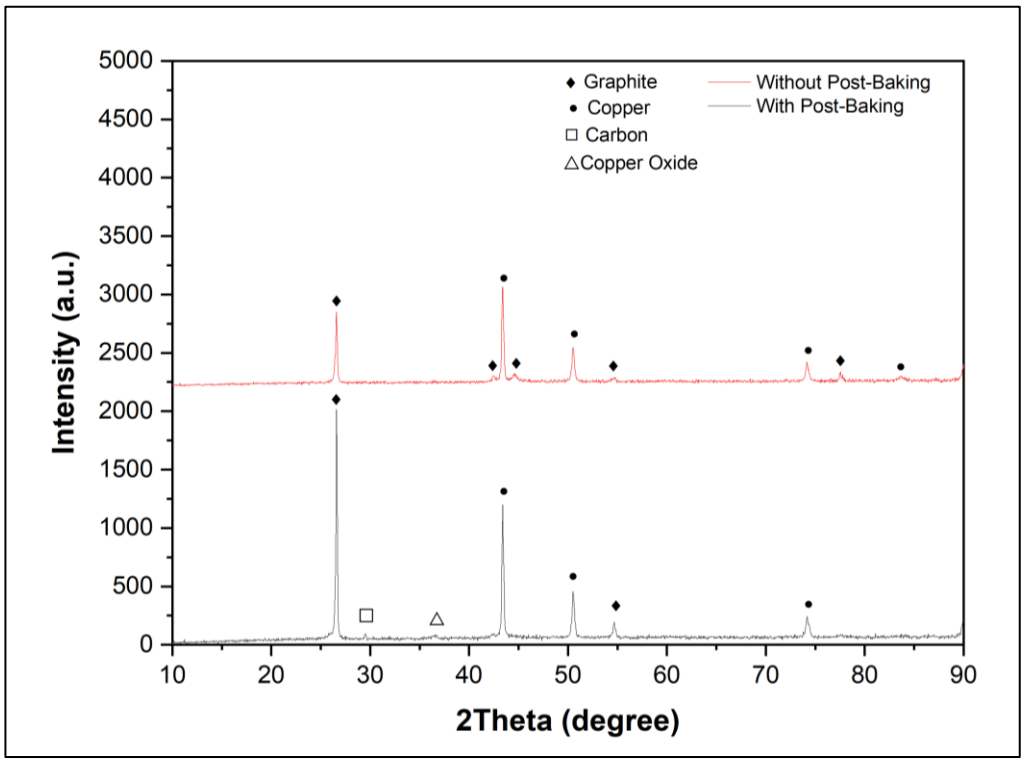

Figure 4.24 XRD Spectrum of Carbon-Copper Composite with and without Post-baking

Figure 4.24 shows the XRD spectra of the carbon-copper composites with (WPB) and without (XPB) post-baking. The graphite peak at approximately $2\theta = 26°$ appeared significantly intense in the WPB sample compared to the XPB sample. This suggests that the post-baking process enhanced the crystallinity of the graphitic structure in the

composite. In both samples, copper peaks were clearly visible (marked in red). The relative intensity of these peaks compared to the carbon peaks differed between the two samples, reflecting the effect of post-baking on crystallinity. The sharpness of the copper peaks in both samples suggests the presence of well-crystallised copper phases.

The post-baking process significantly improved the overall crystallinity of the composite, as indicated by the more defined and intense peaks in the WPB sample. The graphite (002) reflection at approximately $2\theta \approx 26$ ° became sharper and more intense, suggesting larger crystalline sizes and reduced lattice defects. No significant new phases, such as copper oxides or carbides, were apparent. The WPB sample also exhibited slightly sharper peaks compared to the XPB sample, indicating that thermal treatment reduces lattice strain and increases crystallite size. This is consistent with annealing effects typically observed in thermal post-processing of composite materials. A small peak around 34° in the WPB sample suggests the presence of copper oxide, commonly formed during processing at moderate temperatures.

Although post-baking clearly enhanced the crystallinity of the graphitic carbon phase, it did not lead to better electrical conductivity in the composite system, as shown in Table 4.8. Despite the improved structural order, the electrical resistivity increased from 16.7 μΩ.m to 19.2 μΩ.m after post-baking. This apparent contradiction can be attributed to the formation of well-defined Cu-C interfaces during heat treatment, which can act as electron scattering sites and disrupt conduction pathways. Similar observations were reported by Nepal et al. [244], where poorly conducting interfaces, caused by collapsed voids lined with elemental carbon, reduced the conductivity of the carbon-copper composite. In carbon-copper composites, interfacial resistance often dominates the overall electrical conductivity, as also highlighted by Daoush et al. [245]. The post-baking process may have created more distinct phase boundaries between copper and carbon and acted as barriers to electron transport. Moreover, it may have altered the dispersion pattern of carbon within the copper matrix. Optimal conductivity requires uniform distribution without agglomeration or phase separation. Even with better crystallinity, poor distribution can reduce overall conductivity.

This finding is consistent with previous reports showing that the behaviour of carbon-copper composites is often unconventional or non-linear. Improvements in structural order do not necessarily correspond to enhanced electrical or mechanical performance. Although higher crystallinity improves electrical properties, in a composite system, the interfaces and phase distributions play a dominant role in

determining overall electrical behaviour. The XPB sample likely retained better interfacial contact between carbon and copper phases, with fewer scattering and a more favourable carbon distribution pattern for electron transport, despite exhibiting lower carbon crystallinity. The difference in resistivity value is relatively small. Even in the post-baking process, the values remained within an acceptable range. For applications requiring optimal electrical conductivity, these findings suggest that carefully controlled processing conditions that maintain favourable interfacial properties are more critical than solely maximising the crystallinity of the carbon phase.

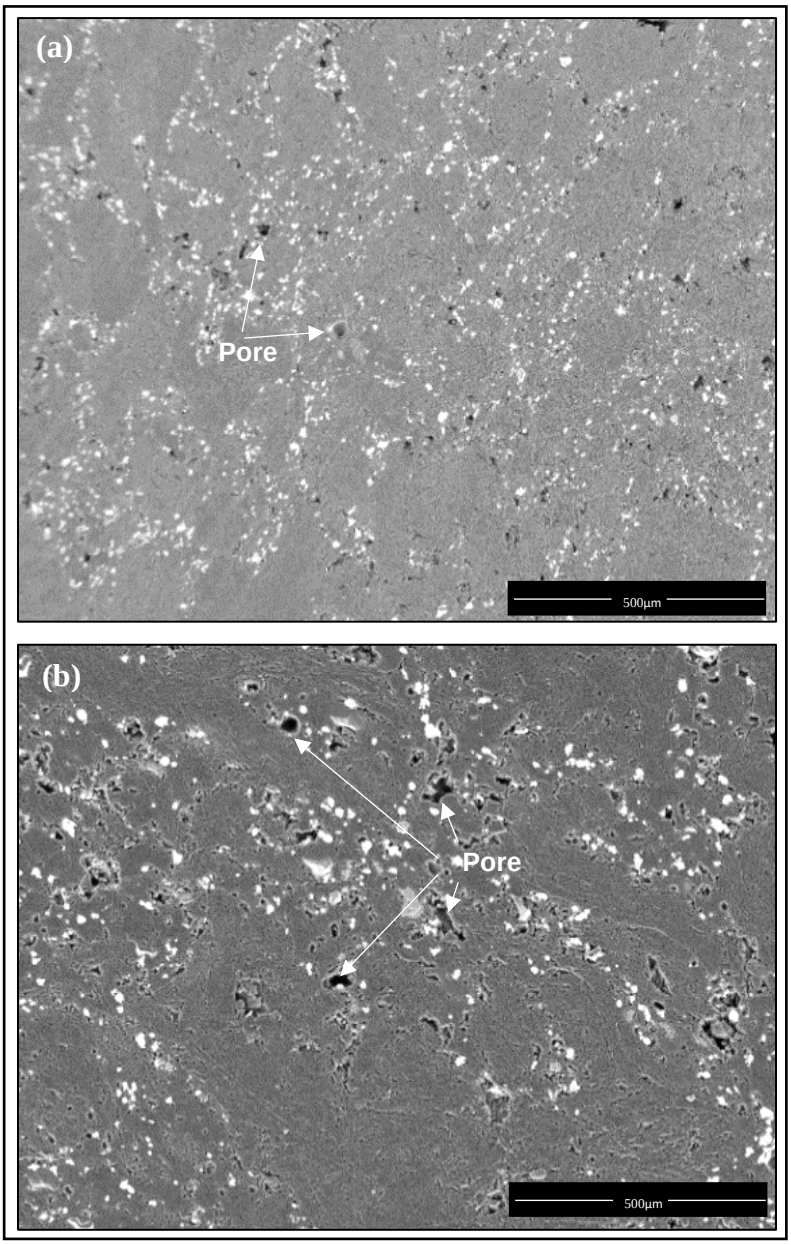

Plate 4.18 SEM Micrographs of Carbon-Copper Composite (a) with (WPB) and (b) without Post-baking (XPB)

Plate 4.18 depicts the SEM micrographs of WPB and XPB carbon-copper composites. The micrograph of the WPB showed a relatively compact microstructure with fewer and smaller pores, as indicated by the dark black region. The distribution of bright spots, representing copper, appeared to be more uniform, and the matrix also seemed to be denser and more consolidated. On the other hand, the micrograph of the XPB sample revealed a more porous structure, with larger and more frequent pores. The distribution of copper-rich material remained uniform, and the matrix appeared to be consolidated. While the post-baking process promotes densification, it may also induce composite brittleness due to the formation of microcracks or weakened interfaces between copper and carbon due to thermal stresses and binder loss. Conversely, the XPB sample, although less dense, may retain greater ductility and better stress distribution, leading to higher TRS. The microstructural densification observed in the WPB sample could also have limited the continuity of conductive carbon pathways, as excessive consolidation may isolate graphitic domains within the copper matrix. Similar findings were reported by Canturk et al. [222], who observed that densification and interface quality in Cu-C composites affected both mechanical and electrical properties. They highlighted that increased densification tended to improve mechanical strength, but electrical resistivity was sensitive to interfacial bonding, porosity, and continuity of the conductive path, thereby reducing electrical performance.

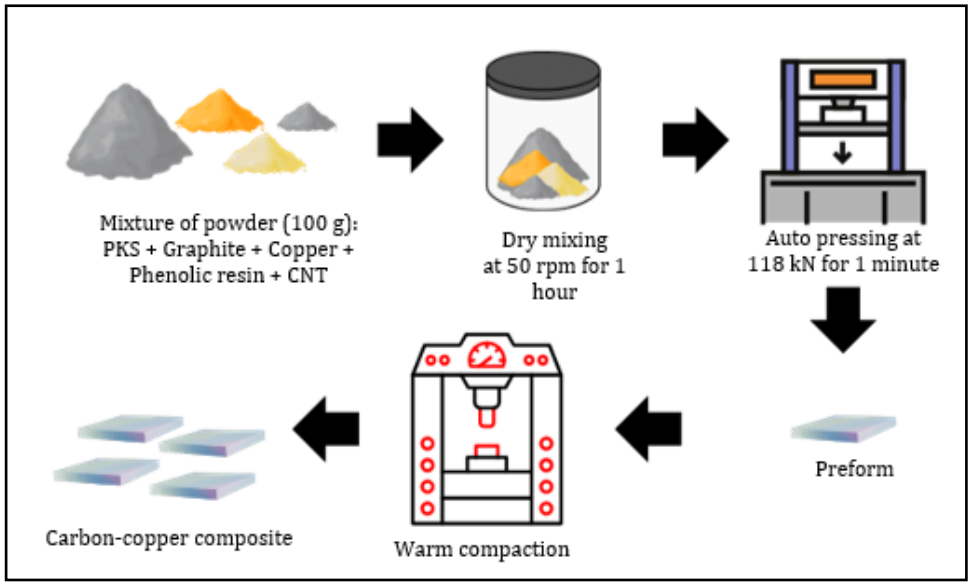

Figure 4.25 Altered Process Route for Developing Carbon-Copper Composite

Based on the collected data, it can be concluded that the carbon-copper

composite developed for pantograph slide in rail applications can be effectively manufactured without the post-baking process. The composite produced without post-baking exhibited superior electrical resistivity and mechanical strength compared to the post-baked sample. Moreover, eliminating the post-baking step makes the manufacturing process more cost-effective and time efficient. Therefore, the composite without post-baking was selected for further detailed investigation in the subsequent section. The altered process route to develop the carbon-copper composite is illustrated in Figure 4.25. The optimum condition identification focused only on the warm compaction process, where temperature, time, and pressure were varied.

4.8 Optimum Condition of Warm Compaction Process Parameter using the Taguchi Method

This section presents the optimum condition of the warm compaction process parameters using the Taguchi method. In this study, key process variables, such as compaction temperature, pressure, and time, were systematically varied according to an orthogonal array experimental design. This approach minimises the number of experiments required while efficiently identifying parameter settings that yield optimal composite performance with minimal variability. The analysis focuses on evaluating the influence of each parameter on the critical material properties to establish processing conditions that meet commercial pantograph slide standards based on mean values. As identified in the previous section, resistivity and TRS were the primary focus areas due to observed instability in these values within the required range.

The analysis revealed that all three process parameters affected the composite the final properties, although their influence varied significantly. Pressure was identified as the most dominant factor, followed by time, with temperature having the least effect. The collective results from the response tables, analysis of variance (ANOVA), and main effects plots highlighted that the optimal conditions of 150℃, 50 tonnes, and 5 minutes yielded the highest TRS value (OPT1). On the other hand, compaction at 200℃, 50 tonnes, and 5 minutes yielded the lowest resistivity value (OPT2). Both compaction conditions produced resistivity and TRS values within the acceptable range for commercial pantograph slides, suggesting some flexibility in processing conditions for industrial scalability.

The identification of the optimum condition of the process parameters using the Taguchi method resulted in two distinct sets of optimal conditions, each targeting specific targets as follows:

a) OPT1 – optimum condition in achieving maximum TRS, and
b) OPT2 – optimum condition in achieving minimum electrical resistivity.

4.8.1 Experimental Data

All experimental data are tabulated in Table 4.5, organised according to the Taguchi L_9 (3^3) orthogonal array designed in the Minitab 22 software. The resistivity and TRS of each sample were measured following the procedures described in Chapter 3. To minimise experimental error, each condition was tested in duplicate, and the average values were calculated for further analysis.

Table 4.5
Experimental Data from Taguchi Design

Sample	Temperature	Time	Pressure	Resistivity	TRS
	℃	s	ton	μΩ.m	MPa
1	150	2.5	40	62.30	14.705
2	150	5	50	17.00	50.770
3	150	10	60	88.75	21.635
4	200	2.5	50	26.40	39.477
5	200	5	60	41.55	23.325
6	200	10	40	54.45	21.230
7	250	2.5	60	60.50	19.302
8	250	5	40	39.75	16.415
9	250	10	50	28.79	35.855

4.8.2 Data Analysis

The experimental data were analysed using Minitab 22 software, focusing on two responses: electrical resistivity and TRS. The processing variables influenced the continuity of the conductive network and interparticle contact, governing electrical resistivity, as well as interfacial bonding, matrix cohesion, and binder carbonisation, governing TRS performance. The analysis was deliberately restricted to the

identification of optimum condition of these two responses. In contrast, density and hardness remained within acceptable limits and were treated as constraints rather than competing objectives.

The identification of the optimum condition of warm compaction parameters using the Taguchi method successfully identified the most influential factors controlling both the electrical and mechanical performance of the carbon-copper composite. ANOVA, response tables, and main effects plots revealed that pressure was the dominant variable for both resistivity and TRS, followed by time and temperature. This ranking highlights the critical role of consolidation mechanics in achieving a balance between conductivity and mechanical integrity.

4.8.3 Main Effects and S/N Ratio Analysis

The Taguchi signal-to-noise (S/N) ratio analysis was employed to determine the optimal warm compaction parameter levels for electrical resistivity and transverse rupture strength (TRS). Since the objective for electrical resistivity is minimisation, the smaller-the-better S/N criterion was applied, whereas the larger-the-better S/N criterion was used for TRS. The S/N ratio transforms the experimental responses into a robustness-based performance index, enabling the identification of parameter combinations that simultaneously improve performance and reduce variability.

Table 4.6
Response Table for Mean Resistivity

Level	Temperature	Time	Pressure
1	-33.20	-33.34	-34.21
2	-31.87	-29.70	-27.47
3	-32.27	-34.30	-35.66
Delta	1.33	4.60	8.19
Rank	3	2	1

Table 4.6 presents the response table of the S/N ratios for electrical resistivity at different levels of temperature, time, and pressure. Among the three parameters, pressure had the most pronounced effect, with 50 tonnes producing the lowest resistivity. Compaction time shows a moderate influence, with 5 minutes giving the

lowest resistivity. Temperature has a smaller effect, with 200 °C being slightly more favourable. The corresponding main effects plot in Figure 4.26 shows that the S/N ratio increases markedly when the compaction pressure decreases from 40 to 50 tonnes and subsequently increases at 60 tonnes, indicating that the most robust resistivity performance is achieved at the intermediate pressure level. A similar trend is observed for compaction time, with the highest S/N ratio obtained at 5 minutes.

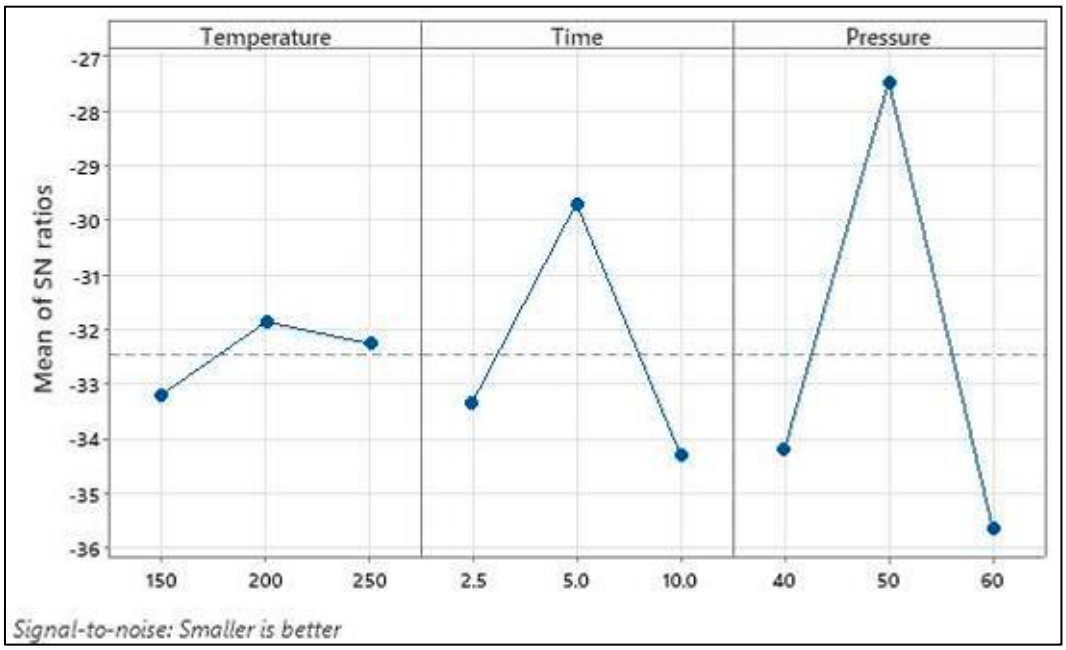

Figure 4.26 Main Effects Plot for S/N Ratio in Resistivity

For TRS, Table 4.7 indicates that pressure is again the most influential factor, followed by time and temperature. The main effects plot in Figure 4.27 shows a pronounced increase in the S/N ratio at 50 tonnes, confirming that this pressure level provides the most stable and robust strength performance. The S/N ratio of TRS also reaches its maximum at the intermediate compaction time of 5 minutes, whereas temperature exhibits a comparatively smaller effect.

Table 4.7
Response Table for S/N Ratio

Level	Temperature	Time	Pressure
1	27.99	26.97	24.67
2	28.58	28.56	32.36
3	27.01	28.05	26.54
Delta	1.57	1.59	7.68
Rank	3	2	1

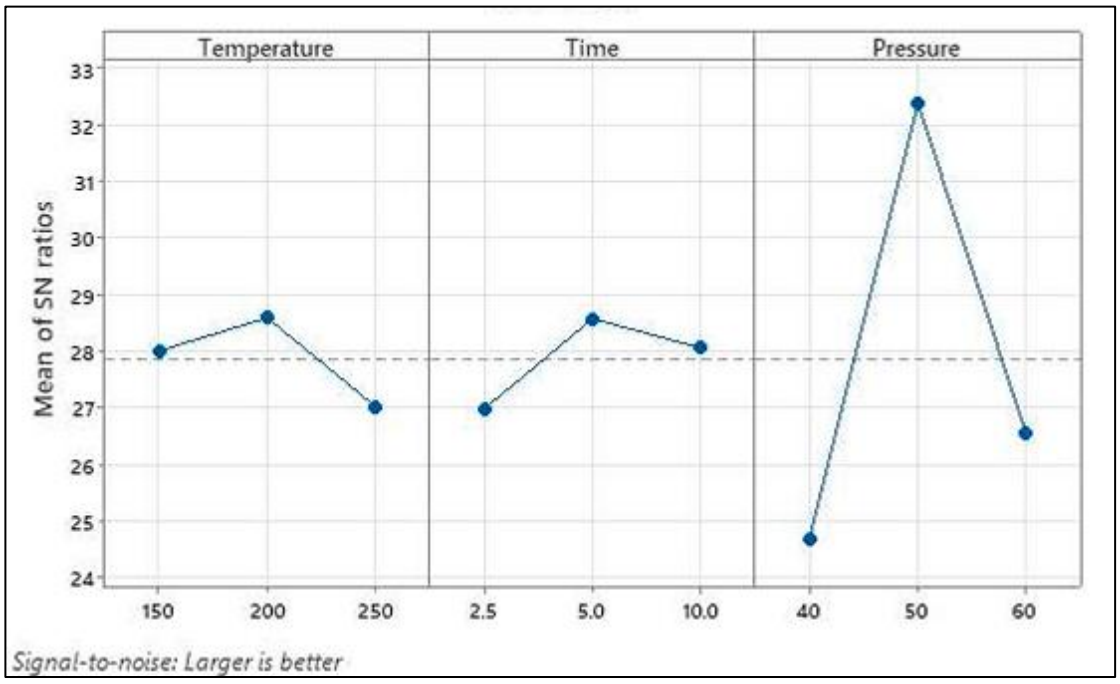

Figure 4.27 Main Effects Plot for S/N Ratio in TRS

Based on the S/N ratio analysis, two distinct optimal parameter combinations were obtained according to the targeted performance characteristics. The optimum condition for maximising TRS (OPT1) was identified as 150 °C, 5 minutes and 50 tonnes, while the optimum condition for minimising electrical resistivity (OPT2) was identified as 200 °C, 5 minutes and 50 tonnes. These results indicate that compaction pressure and holding time govern the robustness of both mechanical and electrical responses, whereas temperature mainly determines the trade-off between strength and conductivity.

The main effects plots of the S/N ratios further reveal a non-linear response with respect to pressure, characterised by an inverted-V trend. This behaviour indicates that

excessive pressure deteriorates both electrical and mechanical robustness, even though higher pressure generally promotes densification. At 50 tonnes, sufficient plastic deformation of copper particles promotes intimate interparticle contact and pore closure, leading to the formation of a continuous conductive network while maintaining mechanical cohesion. In contrast, further increase to 60 tonnes is likely to induce elastic–plastic recovery and micro-damage at particle interfaces, disrupting conductive pathways and weakening the load-bearing skeleton. Similar over-compaction behaviour has been reported for carbon–metal systems, where excessive hydrostatic pressure induced interfacial stresses and localised delamination, leading to degraded electrical performance [246].

Compaction time exhibits a moderate influence on the S/N ratios of both responses. The S/N trends indicate that insufficient holding time leads to unstable consolidation and higher scatter in resistivity and TRS, whereas excessive holding time provides no further improvement and may even reduce robustness due to microstructural degradation and binder deterioration [247]. The optimum compaction time of 5 minutes therefore represents a balance between adequate stress relaxation, binder redistribution and microstructural stability. A similar optimum short holding time has been reported by Tokita et al. [248], where short dwell times were shown to preserve fine microstructures and enhance performance stability.

Temperature shows the least influence on the S/N ratios compared with pressure and time. Nevertheless, the S/N trend indicates that moderate temperatures improve robustness by facilitating binder softening and particle rearrangement, whereas excessive temperature leads to a reduction in both strength and conductivity robustness. The decreasing S/N ratio of TRS at 250 °C suggests degradation of binder integrity and weakening of interfacial bonding. These observations are consistent with previous findings that optimal warm compaction temperatures promote carbon–metal interfacial bonding, while excessive thermal input accelerates binder decomposition and microstructural instability [249][250].

4.8.4 ANOVA for Factor Significance

The ANOVA results for resistivity (Table 4.8) showed that the regression model was statistically significant at the 90% confidence level (F = 8.33, P = 0.056). This suggests that variations in resistivity are effectively explained by the warm compaction parameters, namely temperature, time, and pressure, including their quadratic terms. Among these parameters, pressure (P =0.015) and its quadratic term (pressure^2, P = 0.015) exhibited the most significant impact, highlighting the dominant role of compaction pressure in determining the electrical resistivity of the carbon-copper composite.

Table 4.8
ANOVA for Resistivity

Source	DF	Adj SS	Adj MS	F-Value	P-Value
Regression	5	3685.9	737.19	8.33	0.056
Temperature	1	253.5	253.53	2.86	0.189
Time	1	610.3	610.27	6.89	0.079
Pressure	1	2203.2	2203.21	24.89	0.015
Time*Time	1	733.3	733.32	8.28	0.064
Pressure*Pressure	1	2287.2	2287.23	25.84	0.015
Error	3	265.5	88.51		
Total	8	3951.5			

This strong dependence on pressure can be attributed to enhanced particle densification and improved contact between the copper and carbon phase, which facilitates electron conduction through the composite. Higher compaction pressures reduce void content and interfacial resistance, thereby lowering overall resistivity. Temperature (P = 0.189) and compaction time (P = 0.079) exerted moderate effects, reflecting the role of thermal energy in enhancing plastic flow and binder softening. Moderate heating promotes improved interfacial bonding, while excessive temperature may cause oxidation or stress relaxation that increases the electrical connectivity.

Table 4.9
Optimum Condition for Smaller is Better for Resistivity

Warm compaction parameter	Level	Values
Temperature (℃)	2	200
Time (minutes)	2	5
Pressure (ton)	2	50

The optimum condition for minimum resistivity, as presented in Table 4.9, corresponded to 200℃, 5 minutes, and 50 tonnes. This condition was outside the Taguchi L9 orthogonal array. Under these conditions, the temperature is sufficiently high to activate binder softening and promote interparticle adhesion, while the applied pressure ensures good compaction density without causing structural damage [251].

Among the individual terms, pressure exhibits a very small *P-value* ($P = 0.006$), indicating a statistically dominant influence on TRS. This is consistent with the high F-value (50.82) and reflects the strong role of compaction pressure in governing green density, particle rearrangement and inter-particle contact, which directly control load transfer during bending. In contrast, temperature ($P = 0.255$) and time ($P = 0.213$) are statistically insignificant within the investigated processing window, implying that changes in thermal conditions do not produce a measurable direct effect on TRS compared with experimental noise. The quadratic term for pressure (Pressure×Pressure, $P = 0.006$) is also significant, revealing a pronounced non-linear relationship between pressure and strength, and suggesting the existence of an optimum pressure range beyond which further densification no longer yields proportional mechanical improvement. Conversely, the quadratic term for time (Time×Time, $P = 0.215$) remains insignificant, indicating that prolonging the holding time does not introduce a meaningful curvature in the TRS response. The increase in TRS with higher pressure could result from the enhanced bonding, reduced porosity, and improved stress transfer across particle boundaries [252]. Higher compaction pressure leads to better packing of copper and carbon particles, thus forming a more cohesive and load-bearing structure [253].

Therefore, although moderate temperature still assists binder curing and improves particle adhesion indirectly, its statistical insignificance confirms that, for this warm-compaction system, TRS is primarily governed by the compaction state rather than the thermal cycle. This statistical interpretation supports the selection of 150 °C, 5 min and

50 tonne as the optimum condition for maximising TRS (Trial 2 in the L9 array), and explains why the optimum differs from that obtained for electrical resistivity, where thermal effects play a more direct role.

Table 4.10
Analysis of Variance (ANOVA) for TRS

Source	DF	Adj SS	Adj MS	F-Value	P-Value
Regression	5	1135.99	227.20	11.15	0.037
Temperature	1	40.24	40.24	1.97	0.255
Time	1	50.66	50.66	2.49	0.213
Pressure	1	1035.97	1035.97	50.82	0.006
Time*Time	1	50.04	50.04	2.45	0.215
Pressure*Pressure	1	1021.39	1021.39	50.11	0.006
Error	3	61.15	20.38		
Total	8	1197.14			

In contrast, temperature (P = 0.255) and time (P = 0.213) showed weaker influence, indicating that within the investigated range, mechanical strength was primarily governed by compaction density rather than the thermal process. However, moderate temperature still assists binder curing and enhances particle adhesion, indirectly contributing to TRS improvement [254].

The optimum conditions for maximum TRS, shown in Table 4.14, were 150℃, 5 minutes, and 50 tonnes, corresponding to Taguchi L9 orthogonal array (Trial 2). Compared to the optimum resistivity condition, the lower temperature suggests that excessive heat may soften the binder excessively or induce residual stresses upon cooling, thereby reducing mechanical performance [249][250].

Table 4.11
Optimum Condition for Larger is Better for TRS

Warm compaction parameter	Level	Values
Temperature (℃)	1	150
Time (minutes)	2	5
Pressure (ton)	2	50

The optimum results revealed a temperature-dependent trade-off between electrical and mechanical properties. Minimum resistivity was achieved at 200℃, whereas maximum TRS occurred at 150℃, with both sharing identical compaction time and pressure (5 minutes, 50 tonnes). This highlights that densification governs both properties, but thermal responses differ. The results demonstrate that the warm compaction process can be tailored for both mechanical and electrical performance through careful selection of pressure and temperature combinations. Both conditions were validated experimentally.

4.8.5 Experimental Data Validation

To validate the optimised warm compaction conditions, a comparative evaluation was conducted using commercial pantograph slide data from the literature as a reference standard. Samples fabricated under both OPT1 (A1B2C2) and OPT2 (A2B2C2) were tested for TRS and electrical resistivity. Each test was repeated three times to calculate the mean and standard deviation. The results were then compared with the properties of the commercial pantograph slide, as summarised in Table 4.15.

Table 4.12
Comparison of TRS and Resistivity of Optimised Samples with Commercial Pantograph Slide Data

Properties	**A1B2C2 (OPT1)**	**A2B2C2 (OPT2)**	**Commercial Data**
TRS (MPa)	50.72 ± 1.33	45.64 ± 1.18	35 - 50
Resistivity (μΩ.m)	18.7 ± 0.8	14.2 ± 0.3	23.8 – 34.5

Both optimised samples demonstrated competitive or superior performance when compared with the commercial material. OPT1 achieved higher TRS, suggesting improved mechanical strength and structural reliability. Meanwhile, OPT2 showed lower resistivity value, indicating improved electrical performance. Both conditions showed values within the acceptable range relative to the commercial sample. These findings validate the practical relevance of the optimised process parameters and support their selection for further investigation.

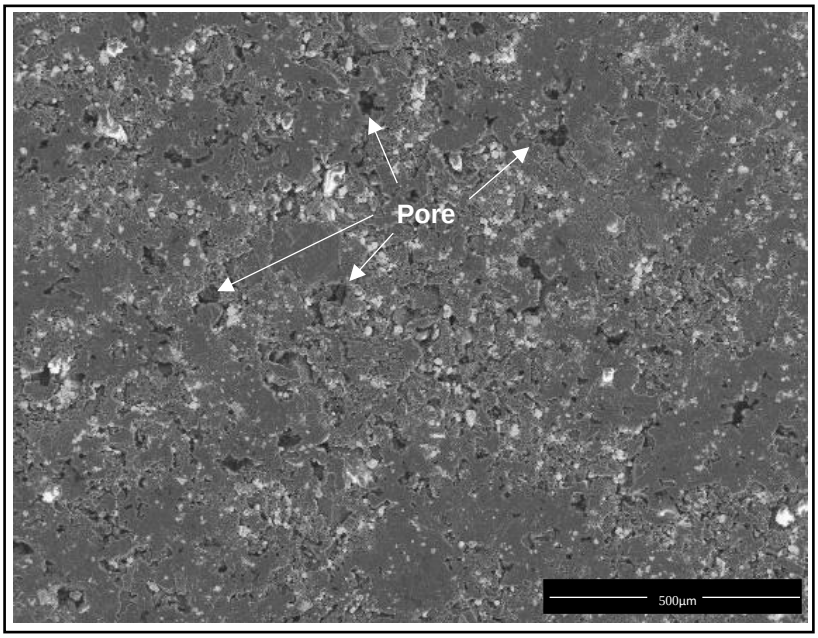

Plate 4.19 SEM Micrographs of OPT1 (Mag. 50x)

Plate 4.19 and 4.20 depict the cross-sectional SEM micrographs of OPT1 and OPT2, the composites optimised for TRS and resistivity, respectively. At 50x magnification (Plate 4.19), OPT1 exhibited a relatively homogeneous surface morphology with large, agglomerated regions and irregular particle dispersion. These microstructural features may contribute to mechanical interlocking, enhancing load-bearing capability and resistance to crack propagation. The sample also displayed coarser particulates and a more porous structure compared to OPT2. Although these features could increase stress concentration in some cases, they appear to promote more effective stress distribution, likely contributing to the higher TRS measured in this sample.

The morphological differences observed via SEM align well with the functional performance: OPT1, optimised for TRS, exhibited a rougher, more agglomerated structure with features that enhanced mechanical strength, while OPT2, optimised for electrical resistivity, showed a denser and more homogeneous surface, facilitating efficient electron transport.

Plate 4.20 reveals that OPT2 has a uniform and compact cross-section, likely due to improved material densification and better particle dispersion during processing at a higher temperature of 200℃. The microstructure of the OPT2 appeared finer and denser, with fewer visible voids and cracks. These characteristics reduce the electron-scattering sites and interfacial boundaries, thereby promoting lower electrical

resistivity. The bright spots represented the distribution of copper within the matrix, and the continuous conductive pathways observed were consistent with the resistivity results.

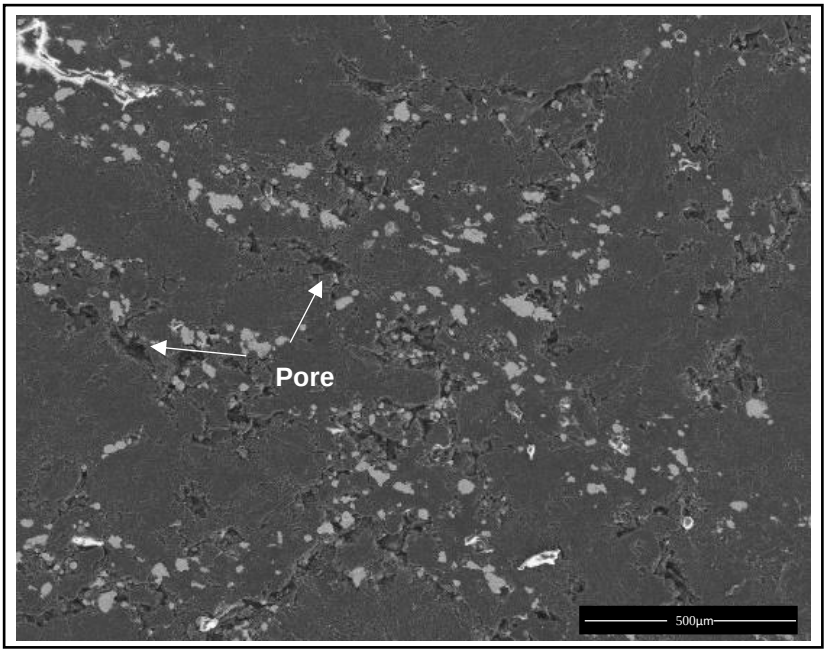

Plate 4.20 SEM Micrographs of OPT2 (Mag. 50x)

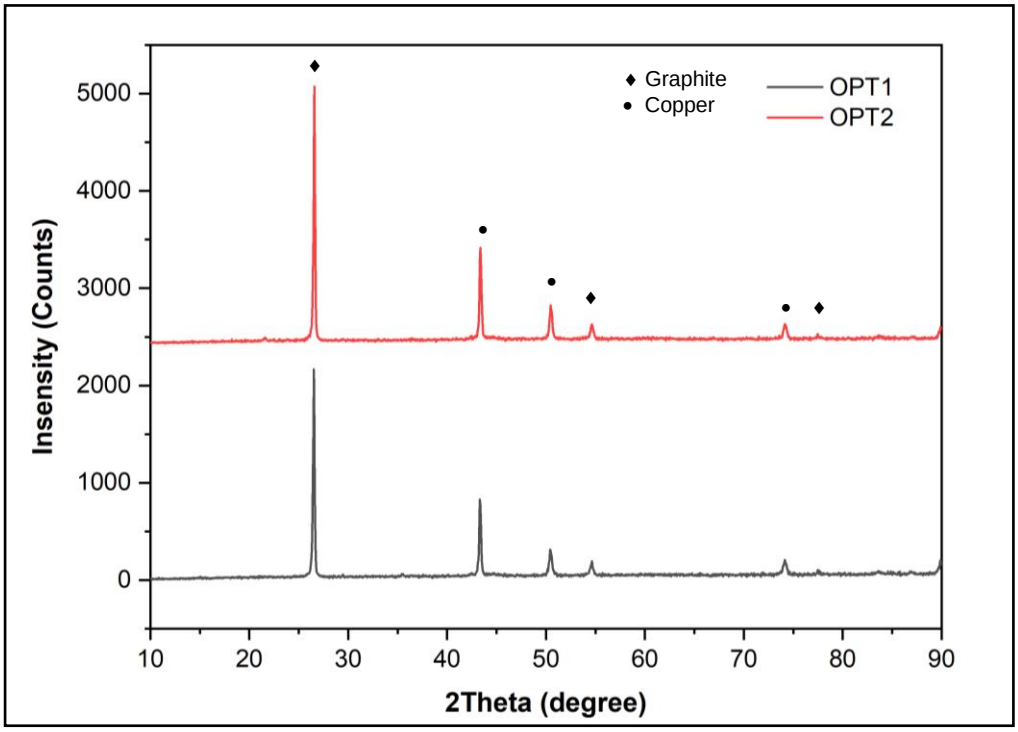

Figure 4.28 XRD spectra for OPT1 and OPT2

Figure 4.28 shows the XRD spectra of OPT1 and OPT2 samples compacted under different warm compaction temperatures. Both spectra exhibited characteristic diffraction peaks corresponding to metallic copper (Cu) at $2\theta \approx 43.3°$, 50.4°, and 74.1°, associated with the (111), (200), and (220) planes, respectively (PDF-3-065-9026). The presence of these peaks confirms that the copper matrix maintained its crystalline metallic phase after warm compaction.

The spectra did not depict any phase changes despite the difference in warm compaction temperatures between the two samples. No additional peaks indicative of new phase formation, such as Cu_2O, CuO, or Cu-C compounds, were detected, suggesting that the warm compaction process did not induce oxidation or intermetallic formation. The processing temperature, limited to 200℃, was insufficient to trigger significant solid-state diffusion or reactions between copper and carbonaceous phases. However, the intensity of the Cu peaks in OPT2 was noticeably higher and sharper than in OPT1, indicating improved crystallinity and reduced lattice strain. This improvement can be attributed to enhanced particle rearrangement and densification under the optimised Taguchi parameters (200℃, 50 tonnes, 5 minutes). Improved compaction reduces voids and dislocation density, leading to more uniform diffraction peaks.

The phenolic resin used as a binder may have undergone crosslinking and curing at these temperatures, but it did not form new crystalline phases detectable by XRD. Instead, it transitions from a thermosetting polymer to a more rigid network without altering the crystalline phases of the other components [255]. Overall, the XRD data confirmed that the structural stability of the composite was maintained while microstructural refinement occurred, consistent with the Taguchi-optimised conditions (OPT1 and OPT2), yielding superior electrical and mechanical performance.

The Raman spectra of OPT1 and OPT2, shown in Figure 4.29, exhibited characteristic D-band (~ 1350 cm^{-1}) and G-band (~ 1580 cm^{-10}) peaks, corresponding to disordered (sp^3) and graphitic (sp^2) carbon structures, respectively. The presence of both bands indicated that the carbon derived from the phenolic resin and any added graphite phases contained both amorphous and graphitic domains.

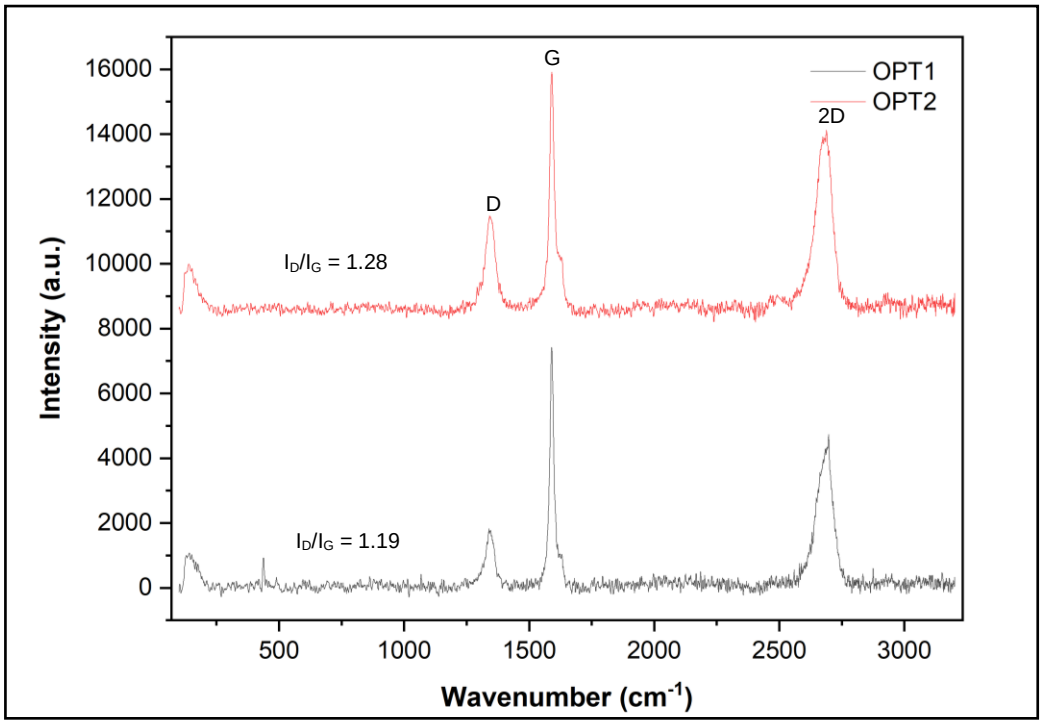

Figure 4.29 Raman Spectra of OPT1 and OPT2

A clear intensity difference was observed between the two samples: the OPT2 spectrum showed more intense and well-defined D and G peaks compared to OPT1, reflecting higher overall carbon content and improved graphitic ordering. The I_D/I_G ratio for OPT2 was slightly lower, suggesting a higher degree of graphitisation and reduced disorder after warm compaction under the optimised conditions at 200°C.

The enhanced graphitic ordering in the OPT2 condition can be attributed to thermally assisted rearrangement of carbon atoms and better interfacial bonding between carbon and copper, which promotes graphitic layer alignment. These effects contributed to the improved electrical conductivity and mechanical integrity observed in the resistivity and the TRS results [95].

4.9 Tribological Characterisation on the Carbon-Copper Composite

The wear performance of carbon-copper composites is crucial for sliding electrical contact applications, such as pantograph slides in railway systems. A balance between electrical conductivity and mechanical as well as tribological durability is essential.

The tribological performance of the developed carbon-copper composites (OPT1 and OPT2) was evaluated using a pin-on-disc test against a copper disc simulating the catenary contact surface. As shown in Figure 4.42, the wear rates of both samples were nearly identical. However, significant differences were observed in the coefficient of friction (CoF) and friction force. OPT2 exhibited a substantially lower CoF (0.761) and friction force (1.7607 N) compared to OPT1 (0.2936 and 2.9361 N, respectively), indicating a more stable and less resistive sliding interface. This reduction in CoF is often associated with the formation of a uniform, lubricative tribofilm and reduced asperity interlocking during sliding, as reported in similar copper-carbon composite systems by Grandin et al. [256] and Han et. al. [69].

4.9.1 Wear Rate

Figure 4.30 shows the wear rates of OPT1 and OPT2. The volumetric wear rates of OPT1 and OPT2 were nearly identical at 0.0000250mm^3/Nm and 0.0000251 mm^3/Nm, respectively, with a marginal difference of only 0.0000001 mm^3/Nm. This indicated that increasing the warm compaction temperature from 150℃ (OPT1) to 200℃ (OPT2) had a negligible effect on the volumetric material loss per unit load and distance. Both compaction conditions provided excellent wear resistance, reflecting sufficient cohesion between the copper and the carbon phases to resist material detachment, which is desirable for applications such as pantograph slides. The comparable wear rates suggest that changes in compaction temperature primarily influence frictional stability rather than bulk wear resistance [257]. While the wear rate is within acceptable limits, the vibration and impact loads of a moving train are not yet accounted for.

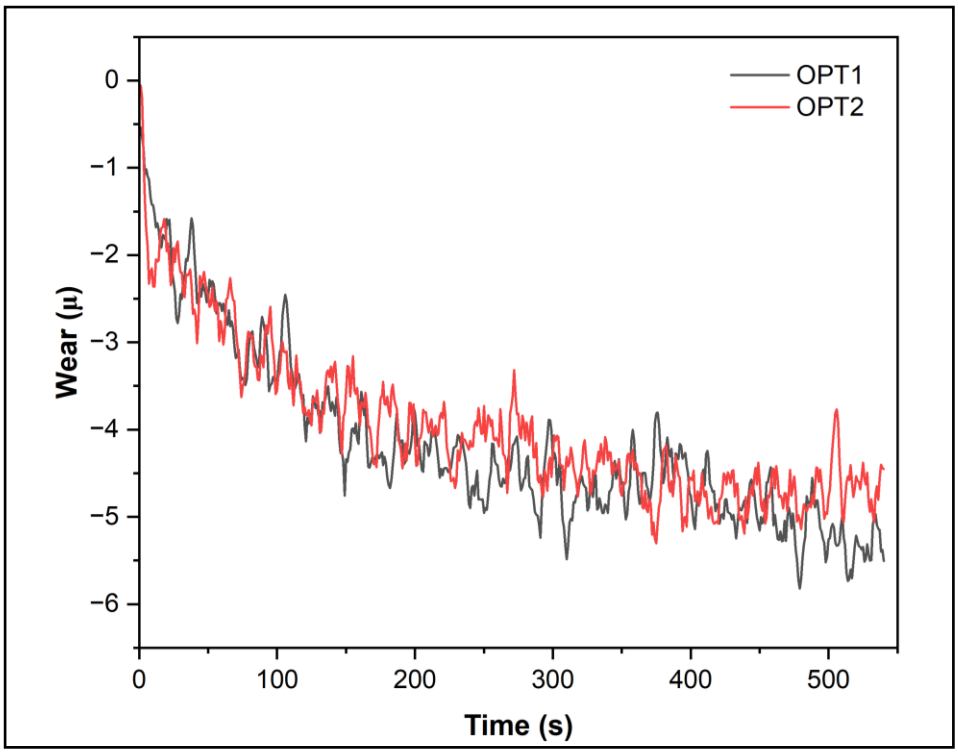

Figure 4.30 Wear Rates for OPT1 and OPT2

4.9.2 Coefficient of Friction

OPT2 exhibited a significantly lower CoF of 0.176 compared to OPT1 (0.294), as shown in Figure 4.31. The lower CoF indicated that the surface of OPT2 was smoother or had better lubricating characteristics, possibly due to improved densification, reduced porosity, or enhanced carbon-copper bonding achieved at the higher compaction temperature. This reduction may also result from the enhanced formation of a carbonaceous tribofilm that separated the mating surfaces and minimised adhesion, consistent with the findings of Li et al. [258] and Ma et al. [243]. Both studies reported that well-bonded Cu-graphite composites and the development of graphite-rich tribofilms effectively reduced friction and wear by forming continuous lubricating layers during sliding. The reduction of nearly 40% in CoF suggested a significant improvement in the sliding interface, which could be attributed to microstructural densification and enhanced bonding achieved at the higher compaction temperature. Improved densification reduced open porosity and void content, resulting in smoother load transfer and decreased asperity interlocking during sliding. Similar behaviour was

reported in Cu-C systems optimised through hot-pressing or sintering, where improved bonding promoted the generation of lubricative films that suppressed frictional spikes [191].

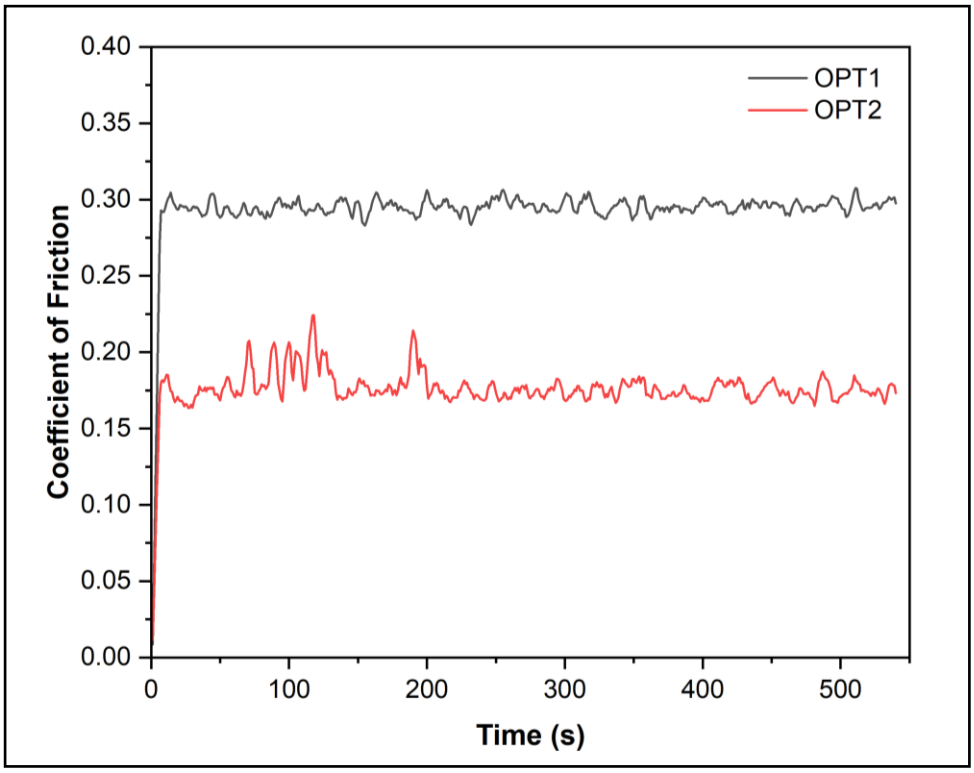

Figure 4.31 Coefficient of Friction for OPT1 and OPT2

4.9.3 Friction Force

Consistent with the lower CoF, OPT2 also showed a much lower friction force (1.7607 N) compared to OPT1 (2.9261 N), as shown in Figure 4.32. This reduction confirmed that the higher compaction temperature produced a more stable and less resistive sliding interface. The lower friction force minimises energy dissipation and heat generation during contact, preventing localised softening or oxidation that often accelerates wear in copper-based composites. The result aligns with that of Grandin et al Grandin et al. [257] who demonstrated that dense Cu-C composites exhibited smoother sliding and reduced frictional fluctuations due to the presence of cohesive tribofilms. This finding also further supported the discussion that compaction at 200°C

temperature led to a surface that interacted more favourably under sliding conditions, resulting in less resistance and consequently less wear-related heating and stress [258].

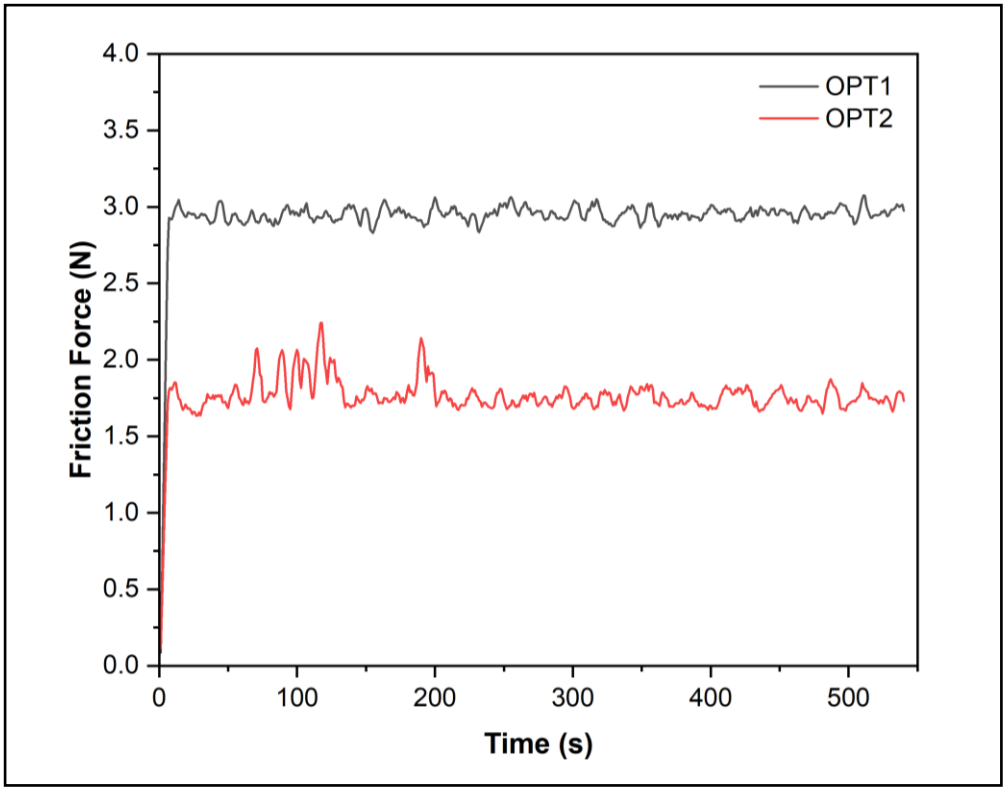

Figure 4.32 Friction Force of OPT1 and OPT2

4.9.4 Morphology of Pin and Disc Worn Surface

To support the data collected and to enhance the understanding of the tribological differences, the worn pin surface and copper plate were examined using SEM and EDX, as illustrated in Plates 4.21 to 4.25. Both OPT1 and OPT2 samples displayed distinct bright and dark regions, reflecting compositional variations that developed during the sliding process.

Plate 4.21 presents the SEM micrographs of the pin surfaces for OPT1 and OPT2. The analysis of the worn pin revealed distinct differences in its wear mechanisms. Clear parallel grooves were observed along the sliding direction in OPT1, accompanied by loose wear debris and evidence of localised delamination.

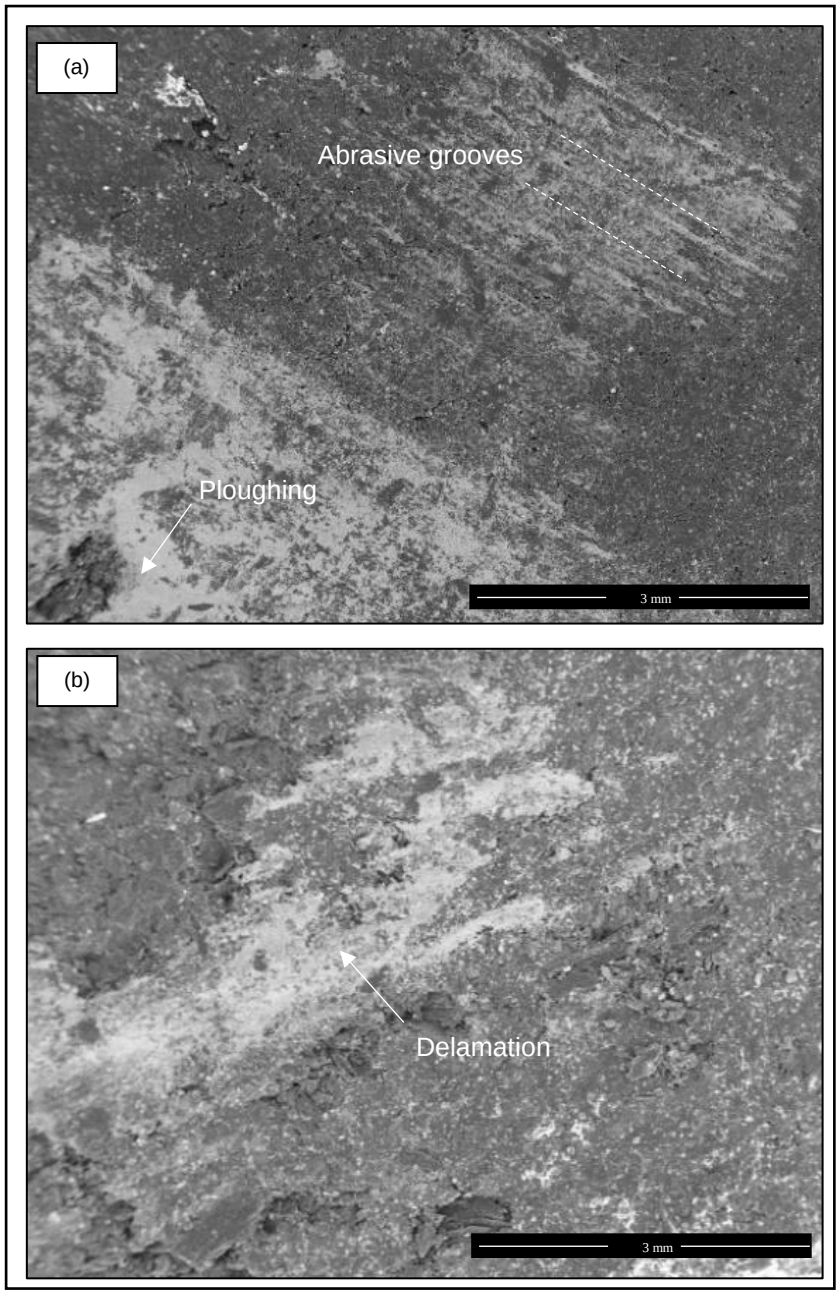

Plate 4.21 SEM Micrograph of Worn Surface of Pin Specimen
(a) OPT1 and (b) OPT2

The parallel grooves and striations indicated abrasive wear caused by sliding contact during the wear test, likely caused by harder asperities or loose wear particles ploughing through the pin surface. These features are commonly observed in copper-carbon composites under insufficient tribofilm formation, as also reported by Tang et al. [69].The debris-assisted micro-cutting observed in OPT1 was consistent with the higher CoF and friction force recorded (0.2936; 2.9361 N), as well as with the EDX indications of oxygen-rich zones, suggesting the presence of brittle oxide fragments contributing to the ploughing action (Plate 4.21). In contrast, the OPT2 pin exhibited a

comparatively smoother worn surface with fewer debris agglomerations, suggesting more effective load distribution and reduced abrasive action.

EDX spectra obtained from the worn pin surfaces confirmed material transfer from the copper disc. OPT1 showed higher copper content within the wear grooves, indicating adhesive interaction and metallic transfer, possibly due to higher localised contact temperatures and shear stress. For OPT2, the copper signal was less intense and more evenly distributed, which was consistent with more stable sliding and reduced adhesion. Similar trends have been reported in optimised copper-graphite composites, where reduced CoF is associated with lower metallic transfer and minimal surface damage [259].

The worn surfaces of the pin specimens after the tribological test revealed significant differences between OPT1 and OPT2, reflecting the influence of processing parameters on their wear response and surface chemistry. As shown in Plate 4.22, both samples exhibited distinct bright and dark regions, indicating compositional and topographical heterogeneity formed during sliding contact [260].

The surface of OPT1 displayed a relatively rough and uneven morphology. EDX spectra from these zones revealed a dominant copper signal, confirming that localised delamination had removed the carbon-rich surface layer and exposed the metallic matrix. Conversely, the dark regions contained a higher concentration of carbon and oxygen, as evidenced by their strong peaks in the EDX spectrum. These features suggested the formation of a tribofilm or carbonaceous transfer layer composed of compacted debris and phenolic degradation products. The coexistence of both metallic and carbonaceous zones on the worn surface indicated an intermittent protection mechanism, where the tribofilm was repeatedly formed and removed during sliding.

In contrast, the worn surface of OPT2 appeared smoother and more uniform. The bright areas were less pronounced, suggesting that the copper matrix remained better protected during the test. EDX analysis of these regions still indicated the presence of copper, but with a notably higher carbon content than OPT1, implying that the carbonaceous film was more stable and continuous. The dark regions on OPT2 show stronger C and O peaks than those of OPT1, indicating a more developed carbon-based film, possibly enriched with oxidised wear debris. The presence of oxygen in both samples supported the occurrence of mild oxidative wear.

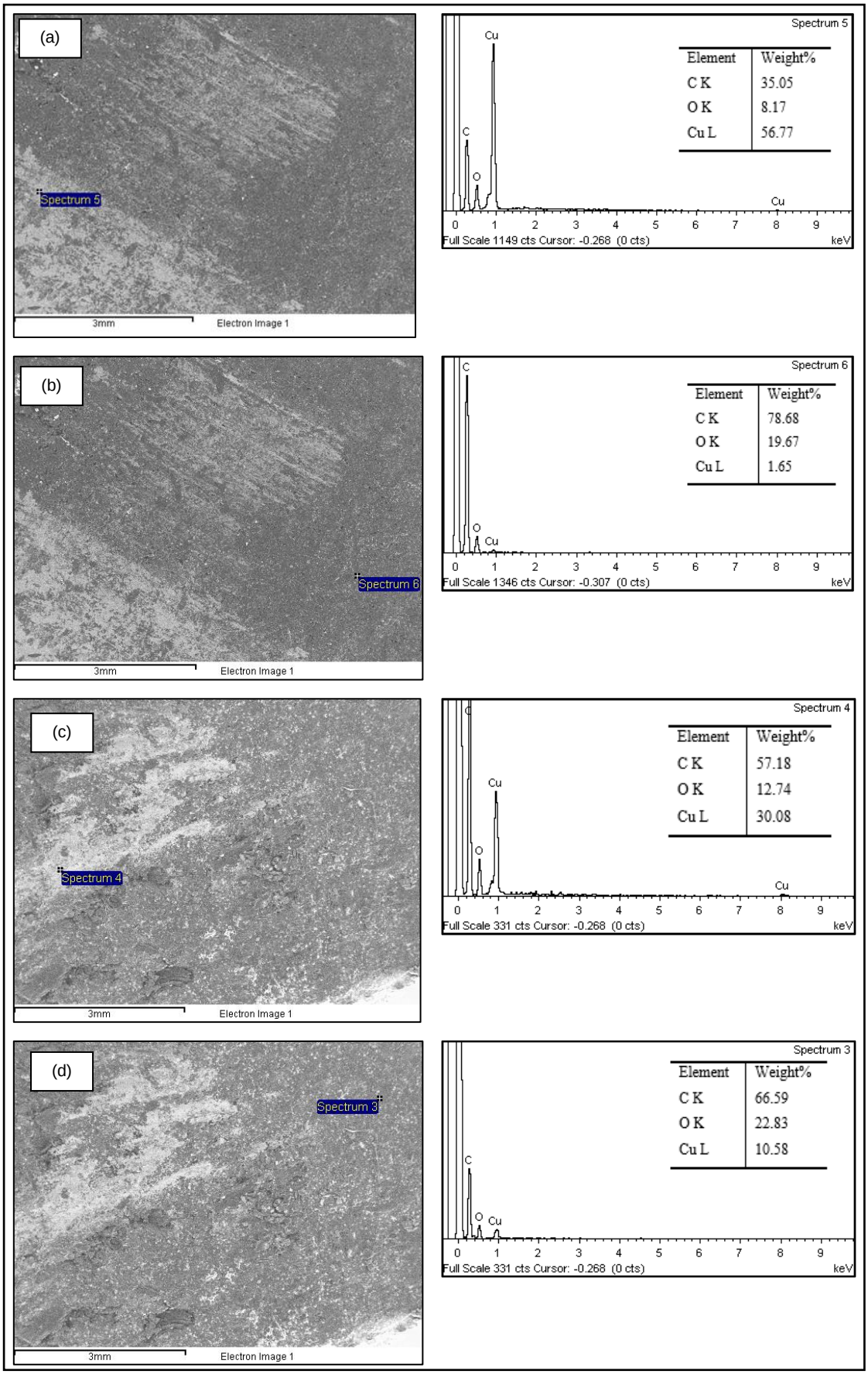

Plate 4.22 EDX Spots and Spectrum for Pin Surface of Sample OPT1 (a,b) and OPT2 (c,d) on Bright Area and Dark Area

However, the smoother texture and more uniform carbon distribution on OPT2 indicated that oxidation was minimal and that a stable tribofilm layer had formed during sliding. Such behaviour was also reported by Guo et al. [261] who observed that dense composites promoted the formation of continuous carbonaceous tribofilms that reduced friction and wear rate.

Overall, the EDX and morphological evidence of the pin surfaces suggested that OPT2 experienced a more controlled wear process dominated by mild oxidation and the formation of a tribofilm. The enhanced carbon coverage and reduced metallic exposure in OPT2 corresponded well with its lower CoF and smaller wear scar observed during testing. These findings confirmed that microstructural densification and improved carbon-copper bonding, achieved through optimised warm compaction parameters, directly enhanced tribofilm stability and, consequently, the tribological performance. The copper disc surface was also examined to further understand the material transfer and surface interactions during dry sliding. The EDX and SEM results of the copper plates are shown in Plates 4.23 and 4.24.

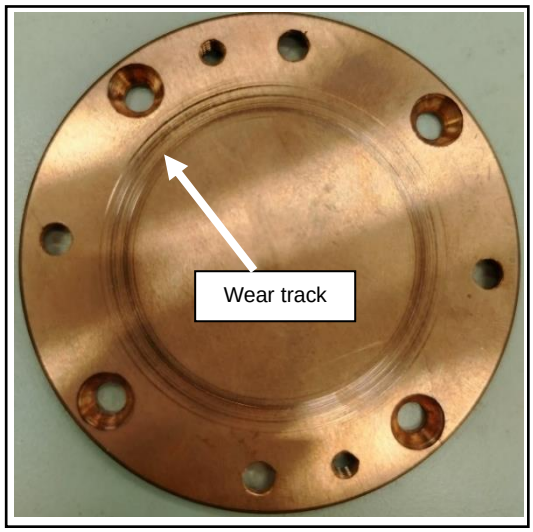

Plate 4.23 Wear Track on Copper Disk

The copper disc (Plate 4.23) also demonstrated a clear difference in wear track morphology. The OPT1 disc surface exhibited deeper grooves and irregular wear tracks following the sliding path (Plate 4.24). EDX analysis confirmed the presence of embedded carbon particles originating from the pin, suggesting that severe asperity interaction and particle ploughing had occurred, which supported the higher CoF and friction force recorded. In contrast, the disc used against OPT2 showed shallower wear

tracks with a more continuous and uniform tribofilm. EDX mapping indicated a balanced presence of copper and carbon, implying a stable transfer film that reduced direct metal-metal contact. These observations are consistent with previous findings by Li et al [262] and Wu et. al [263], where the presence of a uniform transfer film on copper reduced both friction and wear.

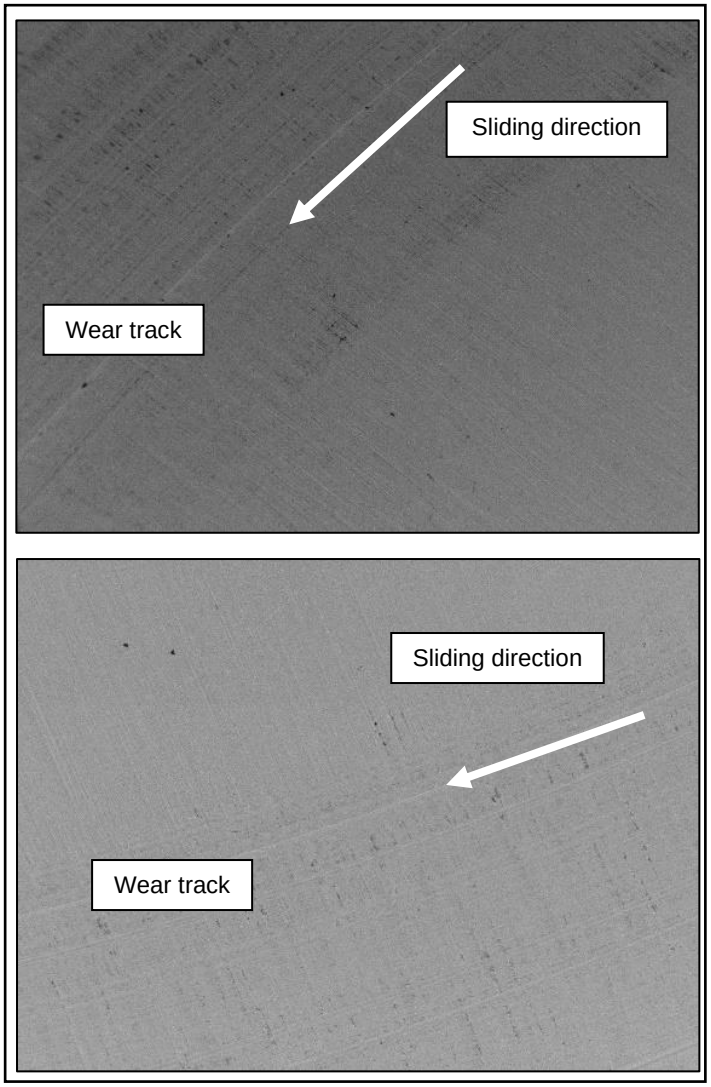

Plate 4.24 SEM micrograph of the Wear Track on the Copper Disk for the Sample (a) OPT1 and (b) OPT2

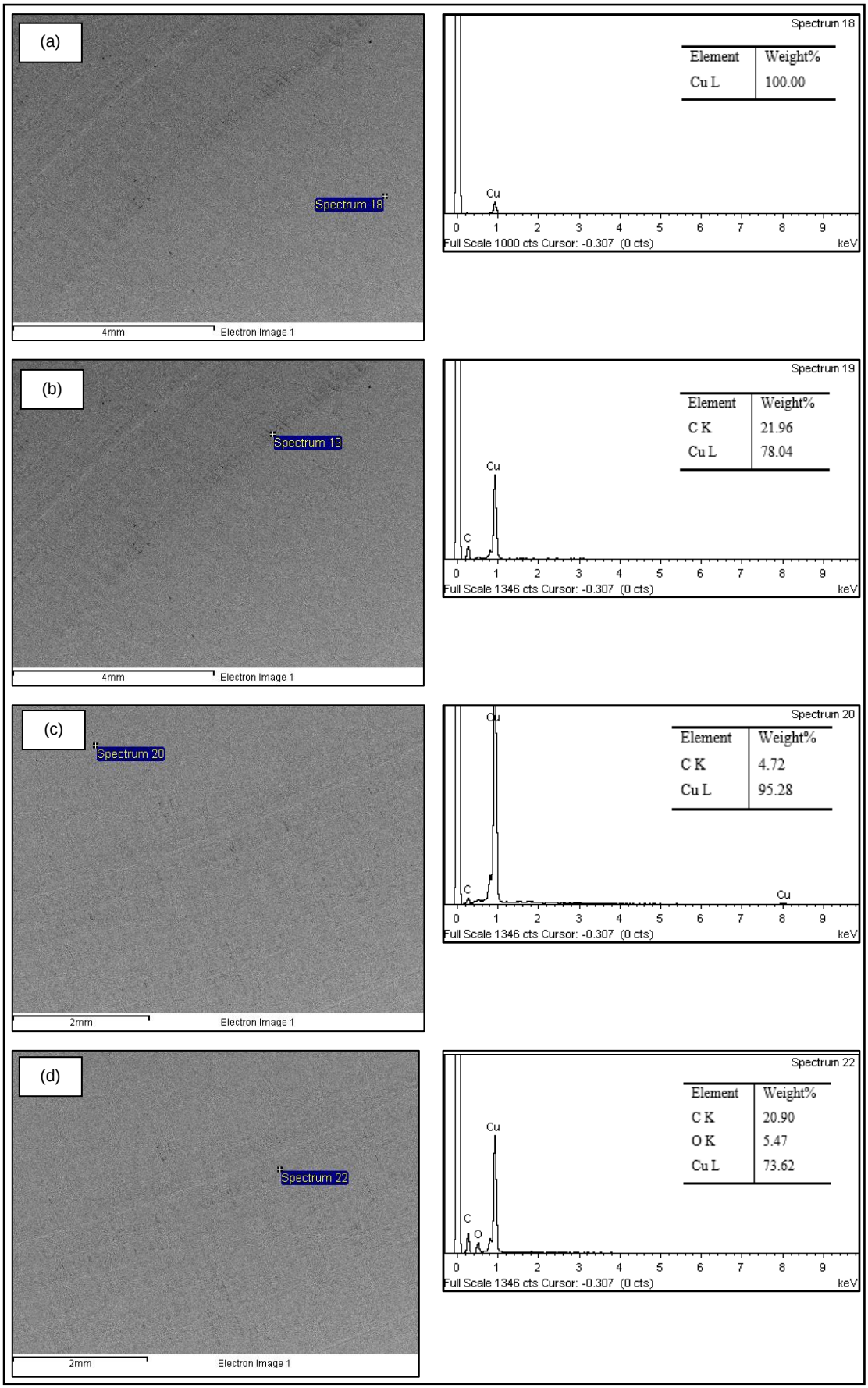

Plate 4.25 EDX Spots and Spectrums for Disk Surface of OPT1 (a,b) and OPT 2 (c,d)

Plate 4.25 represents the EDX spots and spectra of the disc surface for OPT1 (a-b) and OPT2 (c-d). The lighter area represented the copper plate, while the darker area showed the carbon-copper composite wear tracks and scars left on the copper plate after completion of the wear test, as confirmed by the EDX spectra.

For OPT1, the dark regions on the copper layer showed a moderate carbon signal with higher copper intensity, indicating that the transferred layer was discontinuous and uneven. These observations were consistent with the pin surface of OPT1, which showed partial film coverage. The copper plate worn against OPT2 also exhibited a moderate carbon signal and high copper intensity. The presence of oxygen in these regions suggests mild oxidation of the copper substrate, possibly due to the film removal and formation during sliding. The stable film was likely formed through consistent material transfer from the pin throughout the sliding process. These findings aligned with the smoother and more uniform pin surface of OPT2 and its lower CoF.

By comparing the EDX results from both the pin and copper plate, a consistent interaction mechanism was revealed. For OPT2, a stable carbon-rich tribofilm was formed on both surfaces, reducing adhesive wear and promoting steady friction behaviour. For OPT1, although a carbon layer developed, it was less continuous, leading to non-continuous metal exposure and slightly higher friction force.

Surface roughness, R_a, was measured using the confocal microscope. The confocal surface measurements provided further evidence of the improved performance of OPT2. Before testing, the initial R_a values for the discs were 0.586 μm (OPT1) and 0.528 μm (OPT2). After the wear test was conducted, the R_a values on the wear tracks were measured. The R_a of the OPT1 disc increased to 0.881 μm, as shown in the roughness profile in Figure 4.33, reflecting significant surface degradation. In contrast, the R_a of OPT2 disc only increased to 0.653 μm, as shown in the roughness profile in Figure 4.34, indicating smoother wear tracks and less severe material removal. Lower post-test R_a has been directly linked to the presence of protective films and reduced abrasive action in prior studies on the carbon-copper system. Previous studies have also shown that the metal-catalysed formation of carbon-rich tribofilms at the sliding interface reduces abrasive action and surface degradation, leading to lower post-test surface roughness and reduced wear rates. Shirani et al. [264] also reported that the formation of carbonaceous tribofilms in hydrocarbon environments supported the reduction in wear and surface degradation that occurred when such films were formed.

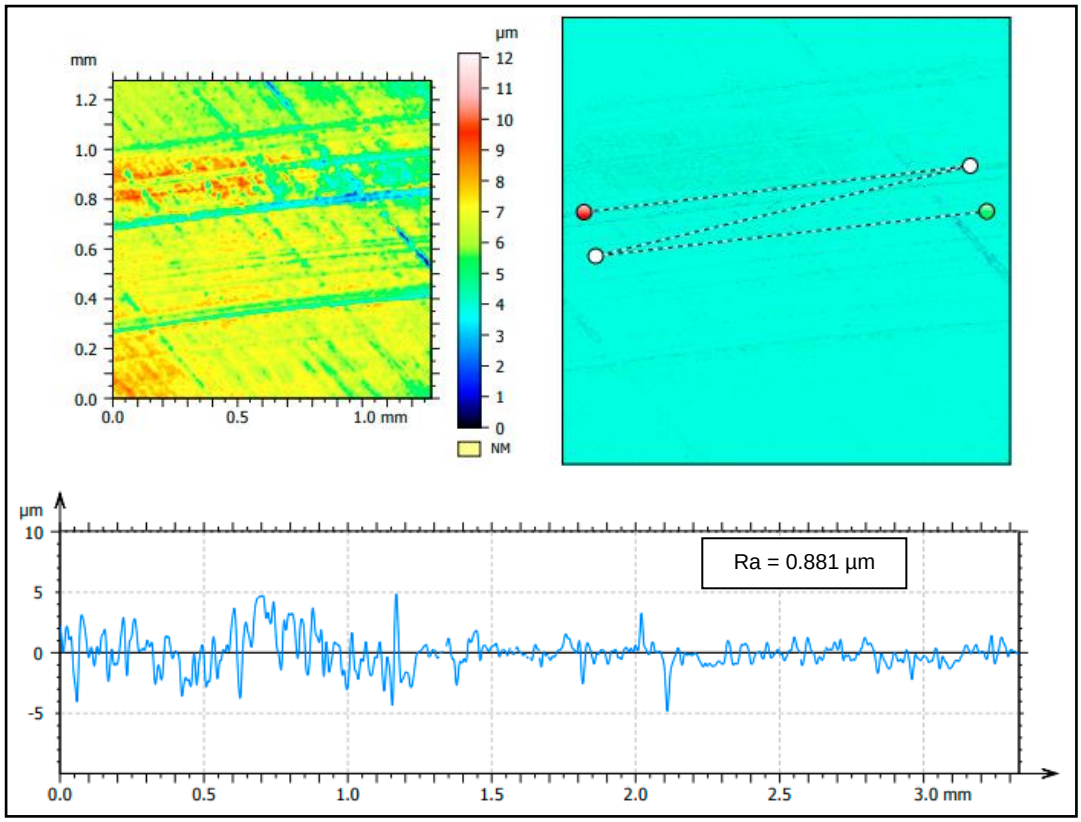

Figure 4.33 Roughness Profile for OPT1

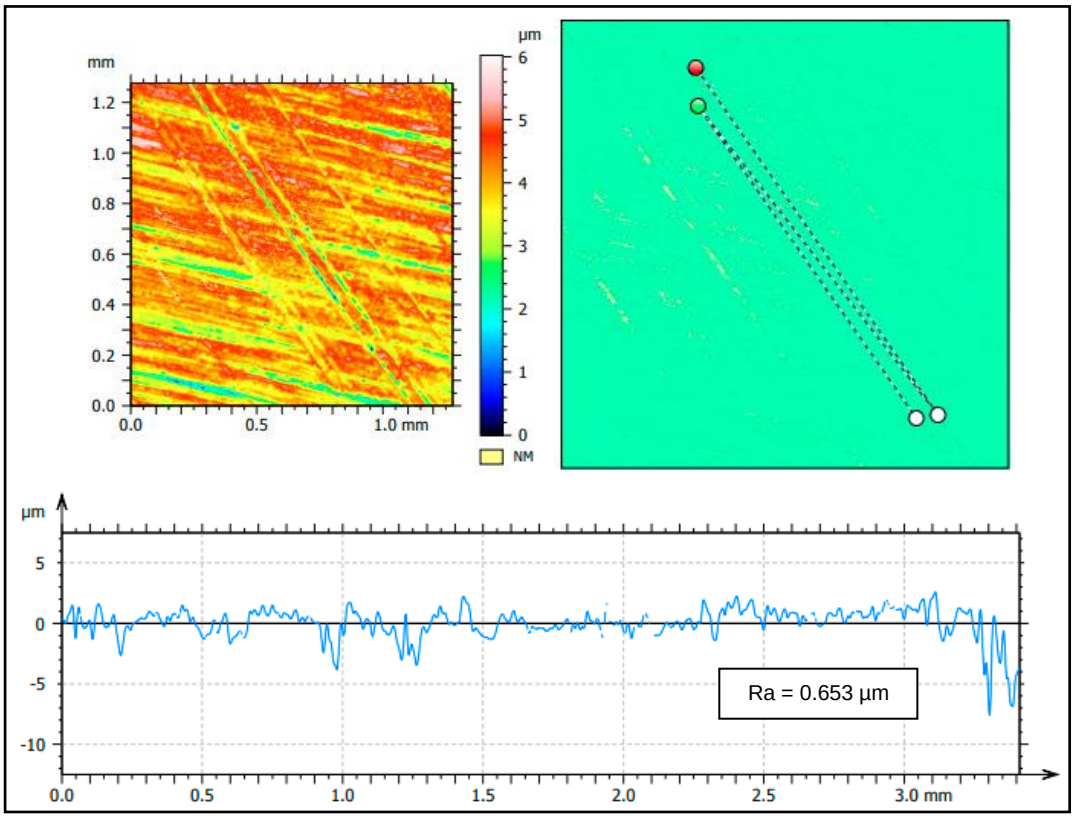

Figure 4.34 Roughness Profile for OPT2

4.10 Summary

In Phase 1, it was found that PKS-activated carbon alone could not produce a carbon-copper composite with the required properties, especially in terms of density and resistivity, for use as a pantograph slide in railway applications. The hardness value of the composite was 120 HRR, exceeding the commercial pantograph slide range of 65–92 HRR, while the TRS value was 46 MPa, which fell within the commercial range of 35–50 MPa. Therefore, the incorporation of graphite into the carbon-copper composite was suggested in this study to improve the properties, specifically density and electrical resistivity, to at least meet the minimum requirements of a commercial pantograph slide. Graphite was selected because its flaky morphology and high carbon content enable better particle packing and conductive network formation, which can improve composite density and electrical conductivity, both of which are critical for pantograph slide applications. Table 4.13 demonstrates the best formulation of carbon-copper composite, and its properties. It was found that at the graphite/PKS-derived carbon ratio of 80:20 (52 wt% graphite and 13 wt% PKS-derived carbon), both the density and resistivity values were improved compared to the previous formulation without graphite. The density value of the composite surpassed that of the commercial pantograph slide. By reducing the amount of PKS-derived carbon in the composite, the presence of fibrous materials decreased, lowering the hardness and TRS values. Despite these reductions, the hardness and TRS values remained within the recommended range relative to commercial pantograph slides.

Table 4.13
New Formulation of Carbon-Copper Composite at a Graphite/PKS-derived carbon Ratio of 80:20

Material				**Properties**			
PKS wt%	**Graphite wt%**	**Copper wt%**	**Resin wt%**	**Density g/cm^3**	**Hardness HRR**	**Resistivity μΩ.m**	**TRS MPa**
13	52	20	15	1.874	93	46	36
Commercial Pure Carbon Pantograph Slide				1.65 – 1.70	65 – 92	23.8 – 34.5	35 – 50
Meet/Exceed requirement*				Yes	Yes	No	Yes

*The requirement refers to data from the commercial pantograph slide from the literature

Improvement of the resistivity is still crucial, as the current values have not yet achieved the recommended range. Lower resistivity is desired to achieve higher conductivity. Although graphite is composed of conductive particles and is naturally an excellent electrical conductor due to its delocalised electrons, it may not form conductive networks within the composite matrix, leading to high resistivity value.

From the findings in Phase 2, CNT demonstrated better improvement in electrical conductivity (resistivity) and a moderate improvement in mechanical strength (TRS) compared to the baseline and other fillers. Cu-CNT exhibited a trade-off: while it improved conductivity to some extent, it reduced mechanical strength (TRS) and hardness significantly. GO increased hardness and TRS, but severely degraded electrical conductivity due to its insulating properties. These insights are essential for tailoring the properties of carbon-copper composite to specific application requirements, such as pantograph slides in railway systems. Although material agglomeration can hinder the improvement of the properties, based on the targeted values compared to conventional and commercial pantograph, CNT appears to be the most promising filler among those tested. The addition of CNT at different weight percentages significantly affected the properties of the carbon-copper composites. As the CNT content increased, both density and hardness decreased gradually, likely due to the low intrinsic density of CNT and their tendency to agglomerate. This can introduce porosity and hinder uniform particle packing during compaction. In contrast, TRS and electrical resistivity showed a clear optimum at 1 wt% CNT. At this composition, the CNT is sufficiently dispersed to enhance interfacial bonding between the carbon matrix and the copper phase, facilitating effective load transfer and the formation of conductive pathways. Beyond this level, excessive CNT may agglomerate at grain boundaries, disrupting the continuity of the metallic matrix and increasing interfacial resistance. Therefore, the 1 wt% CNT formulation was identified as the most balanced composition, combining adequate mechanical integrity with improved electrical performance, and was selected for subsequent stages of warm compaction and optimum condition identification.

In Phase 3, the results showed that although post-baking improved the crystallinity of the graphitic carbon phase and densified the microstructure, it did not enhance electrical conductivity but led to a slight increase in resistivity. The improved crystallinity and denser structure in the post-baked sample were offset by increased electron scattering at more defined carbon-copper interfaces and potential

microcracking and interfacial weakening due to thermal stresses. In contrast, the non-baked sample exhibited lower resistivity and slightly higher mechanical strength, making it more suitable for applications requiring both conductivity and durability. Based on these findings, the process route was optimised by eliminating the post-baking step, thereby enhancing production efficiency without compromising composite performance. The findings confirm that eliminating the post-baking process preserves the mechanical-electrical balance while enhancing production efficiency. The non-baked composite demonstrated comparable performance with lower electrical resistivity and slightly higher mechanical strength, making it more suitable for railway pantograph applications that demand both optimal conductivity and durability. This setup will be used for future improvements to the carbon-copper composite.

The study on optimum condition of warm compaction in Phase 3 employed the Taguchi L_9 orthogonal array to systematically optimise the warm compaction parameters, namely temperature, time, and pressure, using the orthogonal array design. Analysis revealed that pressure was the most influential factor affecting both electrical resistivity and TRS, followed by compaction time, while temperature had the least effect within the tested range. Optimal resistivity was achieved at intermediate levels of all parameters, while TRS was maximised at the lowest temperature with intermediate time and pressure. These findings were validated and showed that the optimised process parameters produced composites with properties meeting or exceeding the commercial standards for pantograph slides. For resistivity, the optimal condition was achieved at intermediate levels of temperature, time, and pressure, minimising electrical resistance. In contrast, TRS was maximised at the lowest temperature with intermediate time and pressure. These findings suggest a trade-off in optimising both properties simultaneously, which is critical for meeting commercial standards. Main effects plots and statistical analysis consistently highlighted the dominance of pressure; however, the limited temperature range and absence of interaction effects in the analysis may restrict the applicability of these findings to broader processing conditions. Validation results confirmed that both optimised conditions, OPT1 and OPT2, provided performance comparable to or better than the commercial pantograph slide, making them suitable for the evaluation of wear resistance.

Table 4.15 summarises the tribological characteristics of the optimised carbon-copper composites in Phase 4, OPT1 and OPT2. Both samples demonstrated excellent wear resistance, making them suitable for demanding applications. The negligible

difference in wear rates suggested that the compaction temperature was effective in minimising material loss. OPT2 outperformed OPT1 in terms of frictional behaviour. The lower CoF and friction force indicated a more favourable tribological surface, likely due to a denser microstructure and an improved carbon-copper interface at the higher temperature. This observation was supported by morphological evidence showing minimal debris, shallow grooves, and uniform material transfer, while the disc surfaces exhibited reduced roughness and well-formed tribofilms. Although both compaction temperatures resulted in low wear rates, the superior frictional performance of OPT2 made it more attractive for applications where reduced friction and energy loss are critical, such as in railway pantograph slides or other sliding electrical contacts.

Table 4.14
Wear Test Results

	OPT1	**OPT2**
Wear Rate (mm^3/Nm)	0.0000250	0.0000251
Coefficient of Friction	0.293606	0.176074
Friction Force (N)	2.9361	1.7607
R_a of Copper Disc (before wear test) (μm)	0.586	0.528
R_a of Copper Disc (after wear test) (μm)	0.881	0.653

The overall properties performance of the optimised carbon-copper composite developed using PKS-derived carbon, graphite, copper, resin and CNT as filler is compared to the commercial pantograph as shown in Table 4.15. The developed carbon–copper composite fabricated using PKS-derived carbon, graphite, copper, resin and CNT via the warm compaction process demonstrates overall performance that is comparable to, and in several aspects superior to, the commercial pure carbon pantograph slide. The developed composite exhibits a higher density (1.898 g/cm^3) than the commercial range (1.65–1.70 g/cm^3), indicating improved compaction and reduced porosity, which are beneficial for mechanical integrity and electrical stability. Its hardness (93 HRR) is at the upper limit and slightly exceeds the commercial range (65–92 HRR), suggesting enhanced surface durability and resistance to mechanical damage during sliding contact. In terms of electrical performance, the developed composite shows a significantly lower electrical resistivity (14.2 μΩ·m) compared with the commercial slide (23.8–34.5 μΩ·m), reflecting the positive contribution of copper and

CNT fillers in forming more efficient conductive pathways. The transverse rupture strength (TRS) of the developed material (45 MPa) falls within the upper range of the commercial product (35–50 MPa), confirming that the mechanical load-bearing capability is maintained. Most importantly, the wear rate of the developed composite (2.5×10^{-5}) is substantially lower than that of the commercial slide (7.0×10^{-5}), indicating superior tribological performance. Overall, the combined improvements in hardness, electrical resistivity and wear resistance demonstrate that the PKS-based carbon–copper composite with CNT filler can meet or exceed the functional requirements of a commercial pantograph slide material.

Table 4.15
Comparison of Properties of Developed Carbon-Copper Composite and Commercial Pure Carbon Pantograph Slide

	Density g/cm^3	**Hardness HRR**	**Resistivity μΩ.m**	**TRS MPa**	**Wear**
Developed Carbon-Copper Composite using PKS-derived Carbon, Graphite, Copper, Resin and CNT using Warm Compaction Process	1.898	94.5	14.2	45.6	2.5×10^{-5}
Commercial Pantograph Slide	1.65 – 1.70	65 – 92	23.8 – 34.5	35 – 50	7.0×10^{-5}
Meet/Exceed requirement*	Yes	Yes	Yes	Yes	Yes

*The requirement refers to data from the commercial pantograph slide from the literature

CHAPTER 5
CONCLUSION AND RECOMMENDATION

5.1 Conclusion

This study was undertaken to address the national challenge of dependence on imported pantograph slides for electric railway systems in Malaysia by developing a locally manufacturable carbon-copper composite using sustainable raw materials and optimised processing techniques. Through the research methodologies, this study successfully identified the best composition, filler addition, and optimum processing conditions to achieve validated material performance through comprehensive physical, mechanical, electrical, and tribological characterisation.

This study examined thoroughly the effects of carbon type and the graphite-to-PKS-derived carbon ratio on the properties of carbon-copper composites intended for pantograph slide applications. Only composites with 65 wt% and 70 wt% PKS-derived carbon were successfully formed, but they exhibited resistivity values higher than those desired for electrical applications. The findings indicated that, although PKS-based activated carbon contributed to mechanical reinforcement, it alone did not provide the necessary balance of density, electrical conductivity, and mechanical properties required for pantograph slide applications. This study identified the composition containing 65 wt% carbon, 20 wt% copper, and 15 wt% phenolic resin as the most promising variant. It also emphasised the importance of incorporating 80% graphite and 20% PKS-derived carbon in the 65 wt% carbon composition to meet the specific requirements of the intended application thereby fulfilling the first objective of the research which is to determine the composite formulation including local natural carbon for pantograph slide development.

This study investigated the effects of three different fillers, namely graphene oxide (GO), carbon nanotube (CNT), and copper-coated CNT (Cu-CNT), on the mechanical and electrical properties of carbon-copper composites intended for pantograph slide applications. The incorporation of 1 wt% of each filler into the baseline composite (65 wt% carbon, 20 wt% copper, and 15 wt% resin) had notable effects on composite performance. Among the fillers evaluated, CNT exhibited the most significant improvement in both electrical conductivity and mechanical strength. CNT-

reinforced composites (1 wt%) demonstrated the lowest electrical resistivity (19 μΩ.m) and the highest flexural strength (47 MPa) and hardness (105 HRR). These improvements were due to the superior intrinsic conductivity, elevated aspect ratio, and effective load transfer capability of uniformly dispersed CNT within the matrix. Overall, these results deliver the second objective by demonstrating the comparative influence of different fillers on the electrical and mechanical performance of the developed carbon-copper composite, by identifying CNT as the most effective reinforcement for enhancing the properties required for pantograph slide.

The post-baking study showed that, although some differences existed between the composites with and without post-baking, their properties remained within acceptable ranges for commercial pantograph slides. XRD and Raman analyses also indicated no significant phase changes. Therefore, it can be concluded that the carbon-copper composite developed for pantograph slides can be adequately manufactured without the need for a post-baking process. Eliminating this step is more cost-effective and time efficient.

While wear rates were similar, OPT2 exhibited a significantly lower coefficient of friction (CoF) and friction force, as supported by scanning electron microscope (SEM) and energy dispersive X-ray (EDX) evidence of a stable tribofilm with minimal abrasive wear. In contrast, OPT1 showed more severe surface damage and debris formation. OPT2 demonstrated superior frictional performance, with a lower CoF (0.1761) and friction force (1.7607 N) compared to OPT1, indicating a more stable sliding interface. EDX analysis also confirmed higher copper transfer on OPT1. Complementary analysis of the worn copper discs supported these findings, with discs paired to OPT2 exhibiting shallower wear tracks and less adhered debris. Overall, the wear study confirmed that the optimised process parameters in OPT2 not only reduced friction but also promoted a more protective wear mechanism, thereby enhancing operational efficiency and surface preservation in simulated pantograph-catenary contact. These results directly address the final objective by demonstrating the tribological behaviour of the developed composites under dry sliding condition.

5.2 Recommendation

As the objectives of this research were successfully achieved, several recommendations for further research are suggested for future work as follows:

i. To investigate chemical or physical surface treatments of PKS-derived carbon to improve its compatibility with copper and resin matrices. Techniques such as functionalisation or coating could enhance the interfacial adhesion and electrical pathways. In this study, only activated carbon from PKS-derived carbon was utilised as the raw material. Improvement of the raw materials may further increase the performance of the carbon-copper composite for the intended application.
ii. To develop and test advanced dispersion techniques for CNT and other advanced fillers, such as ultrasonication, surfactant-assisted mixing, or in-situ polymerisation, to minimise agglomeration and achieve uniform distribution at higher filler loadings. This also includes exploring other emerging nanofillers or functionalised variants, such as doped CNT or reduced GO, which may offer improved performance or greater cost-effectiveness

compared to conventional CNT and GO. Achieving uniform dispersion of CNT within the matrix could improve the properties of the composites.

iii. To investigate the wear resistance of the material under current-carrying load to imitate actual operational conditions. A deeper understanding of how the composite performs in the presence of current load is crucial to evaluate the potential of the natural-based carbon-copper composite for deployment as the main material for pantograph slides in local production in Malaysia.

REFERENCES

[1] A. B. Perumal, R. B. Nambiar, P. Selvam, and E. R. Sadiku, "Handbook of Nanomaterials and Nanocomposites for Energy and Environmental Applications," in *Springer Link*, Springer Link, 2020, ch. Carbon Fib, pp. 1–32.

[2] G. Wu, K. Dong, Z. Xu, S. Xiao, W. Wei, H. Chen, J. Li, Z. Huang, J. Li, G. Gao, G. Kang, C. Tu, and X. Huang, "Pantograph–catenary electrical contact system of high-speed railways: recent progress, challenges, and outlooks," *Railway Engineering Science*, 30(4), pp. 437–467, 2022.

[3] F. Shang, S. Wei, Q. Bin, Y.-Q. He, and H.-Q. Li, "Research status and development trend of pantograph contact strip materials," *MATEC Web of Conference*, 67(06040), pp. 1–5, 2016.

[4] J. Huang, M. Wang, Y. Li, E. Xu, K. Jiang, M. Li, H. Zhong, J. Liu, and Y. Jiang, "Effect of flake graphite content on wear between behavior between P/M copper-based pantograph slide and contact wire," *Materials Research Express*, 7(076510), pp. 1–13, 2020.

[5] N. A. Omar, R. A. Ghani, S. M. Ramly, N. Aqilah, H. Mohd, and M. A. Nazri, "Keretapi Tanah Melayu (KTMB) Services: The Role of Service Quality and Recovery Towards Satisfaction and Loyalty.," *Journal of International Business, Economics and Entrepreneurship*, 7(1), pp. 79–90, 2022.

[6] K. I. A. Isai, V. Kadiresan, N. Jayabalan, Z. K. Mohamed Makhbul, M. N. A. Ibrahim, H. Sio Ching, V. Naidu Kanan, and S. Ramalingam, "Customer Satisfaction and Commuter Service: An Evaluation of Intercity Keretapi Tanah Melayu Berhad (KTMB) Performance Delivery," *Malaysian Journal of Social Sciences and Humanities (MJSSH)*, 5(5), pp. 95–124, 2020.

[7] Y. Kubota, S. Nagasaka, T. Miyauchi, C. Yamashita, and H. Kakishima, "Sliding wear behavior of copper alloy impregnated C/C composites under an electrical current," *Wear*, 302(1–2), pp. 1492–1498, 2013.

[8] M. A. Selamat, A. A. Mahaidin, M. A. Nurul Hadi, Z. S. Sulaiman, and M. I. Abdul Razak, "Fabrication of carbon-copper composites using local carbon material: microstructure, mechanical, electrical and wear properties," *Advanced Materials Research*, 1133, pp. 171–174, 2016.

[9] G. F. Bocchini, "The warm compaction process. Basics, advantages and limitations," *International Congress and Exposition*, 1998.

[10] A. Simchi and A. Nojoomi, "Warm compaction of metallic powders," *Advances in Powder Metallurgy: Properties, Processing and Applications*, pp. 86–108, 2013.

[11] M. Chouhan, L. Thakur, and P. Kumar, "Parametric optimization and impact behaviour of AA7075/SiC FGM fabricated by hot compaction powder metallurgy process," *Materials Today Communications*, 38, pp. 107833, 2024.

[12] I. Uchegbulam, E. O. Momoh, and S. A. Agan, "Potentials of palm kernel shell derivatives: a critical review on waste recovery for environmental sustainability," *Cleaner Materials*, 6, pp. 100154, 2022.

[13] X. He, W. Jia, Y. Dong, and M. Siahkouhi, "The application of bamboo in the railway industry: a sustainable solution for track construction," *Infrastructures*, 8(12), pp. 1–18, 2023.

[14] M. H. I. Ibrahim, M. A. Razak, N. Mustafa, and M. A. Selamat, "Carbon-Copper composites using local carbon material through warm compaction process for potential electrical and electronic application," *ARPN Journal of Engineering and Applied Sciences*, 11(18), pp. 11117–11123, 2016.

[15] H. Zuo, W. Wei, Z. Yang, X. Li, J. Ren, Y. Xian, Q. Liao, G. Yin, G. Gao, and G. Wu, "Performance enhancement of carbon/copper composites based on boron doping," *Journal of Alloys and Compounds*, 876, pp. 160213, 2021.

[16] B. Ren, C. Gao, W. Wu, J. He, J. Liu, H. Zhong, and Y. Jiang, "Enhanced mechanical and current-carrying wear performances of copper/carbon-matrix composites via interfacial reaction of chromium," *Journal of Materials Science*, 58(4), pp. 1538–1553, 2023.

[17] Y. Li, Z. Xue, Y. Luan, L. Wang, D. Zhao, F. Xu, Y. Xiao, Z. Guo, and Z. Wang, "Improved mechanical performance of graphene oxide based artificial nacre composites by regulating the micro-laminated structure and interface bonding," *Composites Science and Technology*, 179, pp. 63–68, 2019.

[18] K. Bilisik and M. Akter, "Graphene nanocomposites: A review on processes, properties, and applications," *Journal of Industrial Textiles*, 51(3), pp. 3718S-3766S, 2022.

[19] N. Zhou, Y. Cheng, X. Zhang, X. Zhi, and W. Zhang, "Wear rate and profile prediction of Cu-impregnated carbon strip for high-speed pantograph," *Wear*, 530–531, pp. 205056, 2023.

[20] "BS EN 50405-2015+A1-2016 Railway Applications - Current collection

systems - Pantographs, testing methods for contact strips," 2016.

[21] G. Wu, G. Gao, W. Wei, and Z. Yang, "The current collection approach of high-speed train—pantograph and catenary system," in *The Electrical Contact of the Pantograph-Catenary System*, Springer Singapore, 2019, pp. 1–16.

[22] I. Yusoff, B. K. Ng, and S. A. Azizan, "Towards sustainable transport policy framework: A rail-based transit system in Klang Valley, Malaysia," *Plos One*, 16, pp. 1–30, 2021.

[23] P. Nileon, "Overhead vs third rail: how does rail electrification work?" Accessed: Mar. 03, 2026. [Online]. Available: https://rail.nridigital.com/future_rail_jul23/overhead_vs_third_rail_electrification

[24] KTM Berhad, "ETS - Malaysia's Fast Track Journey," KTM Berhad. Accessed: Mar. 03, 2026. [Online]. Available: https://www.ktmb.com.my/ETS.html

[25] Express Rail Link Sdn Bhd, "KLIA Express." Accessed: Mar. 03, 2026. [Online]. Available: https://www.kliaekspres.com/about-us/

[26] Prasarana Malaysia Berhad, "Kelana Jaya Line," Prasarana Malaysia Berhad. Accessed: Mar. 03, 2026. [Online]. Available: https://myrapid.com.my/

[27] A. Mańka, A. Hełka, and J. Ćwiek, "Influence of copper content on pantograph contact strip material on maximum temperature of railroad wire," *Scientific Journal of Silesian University of Technology. Series Transport*, 106, pp. 97–105, 2020.

[28] H. Nagasawa and K. Kato, "Wear mechanism of copper alloy wire sliding against iron-base strip under electric current," *Wear*, 216, pp. 179–183, 1998.

[29] M. Li, B. Ren, W. Wu, K. Jiang, J. Zhang, E. Xu, J. Liu, H. Zhong, G. Tong, and Y. Jiang, "Copper fiber reinforced needle-coke/carbon composite for pantograph slide and its current-carrying wear performance," *Materials Research Express*, 9(5), 2022.

[30] G. Wu, G. Guoqiang, W. Wei, and Z. Yang, "The electrical contact of the pantograph-catenary system," in *The Electrical Contact of the Pantograph-Catenary System*, Springer Nature Singapore Pte Ltd., 2019, ch. 5, pp. 195–220.

[31] M. Wang, M. Li, K. Jiang, E. Xu, J. Liu, H. Zhong, and Y. Jiang, "Full density graphite/copper-alloy matrix composite fabricated via hot powder forging for pantograph slide," *Materials Research Express*, 8(6), 2021.

[32] Z. Liu, H. Wang, H. Chen, X. Wang, Y. Song, and Z. Han, "Active pantograph

in high-speed railway: Review, challenges, and applications," *Control Engineering Practice*, 141, 2023.

[33] F. Shuhadah, M. Ramli, H. Hashim, A. Othman, H. Mamat, and M. A. Yusoff, "IJIE Effect of The Staggering of a Contact Wire on Wear Behaviour in Malaysian Railway Traction Power Supply," 16(9), pp. 366–384, 2024.

[34] W. Wei, X. Li, Q. Liao, H. Zuo, Z. Yang, and G. Wu, "Electro-mechanical performance improvement of pantograph strip for high-speed railway," *ICEMPE 2021 - 3rd International Conference on Electrical Materials and Power Equipment*, pp. 1–4, 2021.

[35] X. Wei, S. Jiang, Y. Li, C. Li, L. Jia, and Y. Li, "Defect detection of pantograph slide based on deep learning and image processing technology," *IEEE Transactions on Intelligent Transportation Systems*, 21(3), pp. 947–958, 2020.

[36] J. Wang and G. Mei, "Effect of pantograph's main structure on the contact quality in high-speed railway," *Shock and Vibration*, 2021, 2021.

[37] P. Kwasniewski, G. Kiesiewicz, K. Franczak, B. Tomiczek, G. Matula, T. Knych, S. Kordaszewski, A. Mamala, W. Sciezor, and R. Wycisk, "Research of Sn and Zn impregnated carbon materials for railway sliding strip," *Metal*, pp. 1708–1713, 2017.

[38] S. Ma, E. Xu, Z. Zhu, Q. Liu, S. Yu, J. Liu, H. Zhong, and Y. Jiang, "Mechanical and wear performances of aluminum/sintered-carbon composites produced by pressure infiltration for pantograph sliders," *Powder Technology*, 326, pp. 54–61, 2018.

[39] Y. Li, J. Huang, M. Wang, J. Liu, C. Wang, H. Zhong, and Y. Jiang, "Microstructure and current carrying wear behaviors of copper/sintered–carbon composites for pPantograph sliders," *Metals and Materials International*, 27(9), pp. 3398–3408, 2021.

[40] X. Fu, Y. Hu, G. Peng, and J. Tao, "Effect of reinforcement content on the density, mechanical and tribological properties of Ti3SiC2/Al2O3 hybrid reinforced copper-matrix pantograph slide," *Science and Engineering of Composite Materials*, 24(6), pp. 807–815, 2017.

[41] C. Panoiu and G. Militaru, "Real-Time Video Processing for Measuring Zigzag Length of Pantograph – Catenary Systems Based on GPS Correlation," *Applied Sciences*, 14(9252), pp. 1–26, 2024.

[42] H. J. Yang, G. X. Chen, G. Q. Gao, G. N. Wu, and W. H. Zhang, "Experimental

research on the friction and wear properties of a contact strip of a pantograph – catenary system at the sliding speed of 350 km/h with electric current," 333, pp. 949–955, 2015.

[43] B. Zhang, Z. Zhang, and W. Li, "Mechanical properties , electrical conductivity and microstructure of CuCrZr alloys treated with thermal stretch process," *Transactions of Nonferrous Metals Society of China*, 25(7), pp. 2285–2292, 2015.

[44] N. Selvakumar and K. Gangatharan, "Electrical resistivity, tribological behaviour of multiwalled carbon nanotubes and nanoboron carbide particles reinforced copper hybrid composites for pantograph application," *Advances in Materials Science and Engineering*, 2016, 2016.

[45] S. Budin, M. A. N. Hadi, T. R. Jaafar, and M. A. Selamat, "Optimization of warm compaction process parameters in synthesizing carbon-copper composite using Taguchi method," *Key Engineering Materials*, 701, pp. 112–116, 2016.

[46] M. A. Nurul Hadi, M. A. Selamat, S. Budin, T. Ria Jaafar, A. A. Mahaidin, Z. Syazwan Sulaiman, A. Z. Omar, and M. B. Mohd Hijazi, "Physical and mechanical properties of warm compacted carbon-copper composite by different powder formulation," *Advanced Materials Research*, 1133, pp. 146–150, 2016.

[47] H. Mou, S. Ma, E. Xu, X. Wang, B. Zhang, T. Zhang, H. Zhong, and Y. Jiang, "Effect of aging treatment on microstructure and properties of urban rail transit copper-based pantograph slider," *Materials Science and Engineering of Powder Metallurgy*, 22(3), pp. 435–442, 2017.

[48] J. Yin, H. Zhang, X. Xiong, H. Tao, P. Wang, and C. Deng, "Influence of applied load on wear behavior of C/C-Cu composites under electric current," *Progress in Natural Science: Materials International*, 27(2), pp. 192–196, 2017.

[49] G. Wu, Y. Zhou, G. Gao, J. Wu, and W. Wei, "Arc erosion characteristics of Cu-impregnated carbon materials used for current collection in high-speed railways," *IEEE Transactions on Components, Packaging, and Manufacturing Technology*, 2018.

[50] P. Wang, G. Deng, H. Zhang, J. Yin, X. Xiong, X. Zhang, and H. Zhu, "Microstructural feature and tribological behaviors of pyrolytic carbon-coated copper foam/carbon composite," *Journal of Materials Science*, 54(21), pp. 13557–13568, 2019.

[51] E. Xu, J. Huang, Y. Li, Z. Zhu, M. Cheng, D. Li, H. Zhong, J. Liu, and Y. Jiang,

"Graphite cluster/copper-based powder metallurgy composite for pantograph slider with well-behaved mechanical and wear performance," *Powder Technology*, 344, pp. 551–560, 2019.

[52] J. Huang, M. Wang, Y. Li, E. Xu, K. Jiang, M. Li, H. Zhong, J. Liu, and Y. Jiang, "Effect of flake graphite content on wear between behavior between P/M copper-based pantograph slide and contact wire," *Materials Research Express*, 7(076510), pp. 1–13, 2020.

[53] Q. Deng, W. Wei, G. Yin, W. Xie, Z. Huang, J. Ren, Y. Yang, Q. Chen, and G. Wu, "The effect of thermal shock temperature difference on the structural, dynamics and mechanical properties of carbon materials characterized by ultrasonic test technology," *Journal of Materials Science*, 56(33), pp. 18522–18533, 2021.

[54] Q. Liao, W. Wei, H. Zuo, X. Li, Z. Yang, S. Xiao, and G. Wu, "Interfacial bonding enhancement and properties improvement of carbon/copper composites based on nickel doping," *Composite Interfaces*, 28(6), pp. 637–649, 2021.

[55] Y. Li, J. Huang, M. Wang, J. Liu, C. Wang, H. Zhong, and Y. Jiang, "Microstructure and current carrying wear behaviors of copper/sintered–carbon composites for pantograph sliders," *Metals and Materials International*, 27(9), pp. 3398–3408, 2021.

[56] P. Wang, L. Wang, K. Kang, J. Yin, X. Xiong, and H. Zhang, "Microstructural, mechanical and tribological performances of carbon fiber reinforced copper/carbon composites," *Composites Part A: Applied Science and Manufacturing*, 142, 2021.

[57] P. Wang, Y. Jia, Y. Li, Y. Liu, Z. Hao, G. Deng, and L. Wang, "Microstructural, mechanical and tribological performances of copper foam modified CFRP composite for pantograph strip," *Journal of Applied Polymer Science*, 138(36), 2021.

[58] F. Morimoto and Y. Kubota, "Evaluation of material properties of contact strip by microscopic structure model performance improvement of pantograph fuel cell hybrid powered test railway vehicle," *Quarterly Report of Railway Technical Research Institute*, 63(3), pp. 1–6, 2022.

[59] J. Zou, H. Wei, and C. Xiao, "Effect of sintering temperature and hydrophobic treatment on the microstructure and properties of copper-graphite composites," *Journal Wuhan University of Technology, Materials Science Edition*, 37(3), pp.

305–313, 2022.

[60] W. Wu, J. X. He, B. Y. Ren, C. Y. Gao, J. W. Liu, H. H. Zhong, and Y. Jiang, “Current-carrying wear behavior of Bi-containing graphite/copper-matrix composites via hot powder forging,” *Journal of Materials Engineering and Performance*, 2023.

[61] P. Wang, F. Xie, D. Wexler, J. Yin, H. Zhang, and H. Zhu, “Tribological behaviors of copper modified carbon/carbon composites for pantograph strip under electric current conditions,” *Tribology International*, 185, 2023.

[62] H. Li, Y. Liu, B. Zheng, S. Wang, Y. Yi, Y. Zhang, and W. Li, “On the tribological behaviors of Cu matrix composites with different Cu-coated graphite content,” *Journal of Materials Research and Technology*, 25, pp. 83–94, 2023.

[63] S. Zhang, C. Tu, T. Song, Y. Xian, X. Liu, H. Sun, and Y. Chen, “Sulfonated graphene improve the wear resistance of pantograph carbon slider materials under normal and wet conditions,” *New Carbon Materials*, 38(2), pp. 378–384, 2023.

[64] P. Wang, H. Song, K. Li, Y. Guo, C. Deng, G. Deng, and H. Zhu, “Fabrication and tribological properties of carbon fiber and copper fiber reinforced carbon-based composite by hot pressing,” *Tribology International*, 192, pp. 109224, 2024.

[65] J. Li, Y. Zhang, Z. Chen, H. Wei, and J. Zou, “Microstructure and tribological properties comparison of Cu – Ti2 SnC composite and Cu – Ti2 SnC-graphite composite,” 337, 2025.

[66] P. Wang, Y. Jia, Y. Li, Y. Liu, Z. Hao, G. Deng, and L. Wang, “Microstructural, mechanical and tribological performances of copper foam modified CFRP composite for pantograph strip,” *Journal of Applied Polymer Science*, 138(36), 2021.

[67] M. Kuznar, A. Lorenc, and G. Kaczor, “Pantograph sliding strips failure — reliability assessment and damage reduction method based on decision tree model,” *Materials*, 14(5743), 2021.

[68] A. Jamwal, P. Prakash, D. Kumar, N. Singh, K. K. Sadasivuni, K. Harshit, S. Gupta, and P. Gupta, “Microstructure, wear and corrosion characteristics of Cu matrix reinforced SiC–graphite hybrid composites,” *Journal of Composite Materials*, 53(18), pp. 2545–2553, 2019.

[69] H. Xiao-Ming, G. Fei, S. Lin-Lin, F. Rong, and Z. En, “Effect of graphite content

on the tribological performance of copper-matrix composites under different friction speeds," *Journal of Tribology*, 139(4), 2017.

[70] P. Wang, L. Wang, K. Kang, J. Yin, X. Xiong, and H. Zhang, "Microstructural, mechanical and tribological performances of carbon fiber reinforced copper/carbon composites," *Composites Part A: Applied Science and Manufacturing*, 142, 2021.

[71] Y. Hu, P. Huang, C. Cheng, M. Zhang, and R. Ma, "Influence of arc discharge on the temperature and wear behaviors of the contact strip in pantograph-rigid catenary systems under AC conditions," *Wear*, 546–547(March), pp. 205368, 2024.

[72] J. Yin, H. Zhang, C. Tan, and X. Xiong, "Effect of heat treatment temperature on sliding wear behaviour of C/C-Cu composites under electric current," *Wear*, 312(1–2), pp. 91–95, 2014.

[73] M. Kuźnar, "Damage caused by material defects of carbon composites used on various types of railway pantographs," *Materials*, 16(5), 2023.

[74] H. Zuo, W. Wei, Z. Yang, X. Li, W. Xie, Q. Liao, Y. Xian, J. Ren, G. Gao, and G. Wu, "Synchronously improved mechanical strength and electrical conductivity of Carbon/Copper composites by forming Fe3C interlayer at C/Cu interface," *Materials Today Communications*, 28, pp. 102661, 2021.

[75] B. Guo, Y.-P. Jin, E.-D. Wang, and D.-B. Shan, "Influence of sintering on physical properties of high-carbon copper matrix pantograph slider sinters," *Transactions of Nonferrous Metals Society of China (English Edition)*, 13, pp. 206–212, 2003.

[76] R. C. Dante, "Carbon Materials," in *Handbook of Friction Materials and their Applications*, Boston: Woodhead Publishing, 2016, pp. 93–103.

[77] M. S. Dresselhaus and I. L. Thomas, "Alternative energy technologies," 414, 2001.

[78] D. Pantea, H. Darmstadt, S. Kaliaguine, and C. Roy, "Electrical conductivity of conductive carbon blacks : influence of surface chemistry and topology," 217, pp. 181–193, 2003.

[79] Z. Chen, X. Jiang, Y. Boyjoo, L. Zhang, W. Li, L. Zhao, Y. Liu, Y. Zhang, J. Liu, and X. Li, "Nanoporous Carbon Materials Derived from Biomass Precursors: Sustainable Materials for Energy Conversion and Storage," *Electrochemical Energy Reviews*, 7(1), pp. 26, 2024.

[80] K. Liang, Y. Chen, D. Wang, W. Wang, S. Jia, N. Mitsuzakic, and Z. Chen, “Post-modified biomass derived carbon materials for energy storage supercapacitors: a review,” *Sustainable Energy Fuels*, 7(15), pp. 3541–3559, 2023.

[81] T. Luo and Q. Wang, “Effects of graphite on electrically conductive cementitious composite properties: A review,” *Materials*, 14(17), 2021.

[82] Y. Liu, J. Chen, B. Cui, P. Yin, and C. Zhang, “Design and Preparation of Biomass-Derived Carbon Materials for Supercapacitors : A Review,” 2018.

[83] S. Supercapacitors, K. Lee, M. Shyan, W. Lim, Z. Hong, S. Chong, T. J. Tiong, G. Pan, and C. Huang, “Coconut Shell-Derived Activated Carbon for High-Performance,” 2021.

[84] C. Sato, N. E. Paucar, S. Chiu, M. Z. I. M. Mahmud, and J. Dudgeon, “Single-Chamber Microbial Fuel Cell with Multiple Plates of Bamboo Charcoal Anode : Performance Evaluation,” 2021.

[85] M. P. Chavhan, M. Khandelwal, S. Arya, T. Das, and A. Singh, “A review of nanocomposites / hybrids made from biomass-derived carbons for electrochemical capacitors,” *Chemical Engineering Journal*, 500(July), pp. 157267, 2024.

[86] R. Haider, S. Sagadevan, N. R. Cameron, and M. Rafie, “Biomass-derived activated carbon for high-performance energy storage devices,” *Journal of Power Sources*, 633(December 2024), pp. 236404, 2025.

[87] P. Nawangsari, Jamasri, and H. S. B. Rochardjo, “Effect of phenolic resin on density, porosity, hardness, thermal stability, and friction performance as a binder in non-asbestos organic brake pad,” *IOP Conference Series: Materials Science and Engineering*, 547(1), 2019.

[88] Q. Wang, J. Tao, H. Shan, T. Cui, J. Ding, and J. Wang, “Effect of heat treatment under different atmospheres on the bonding properties and mechanism of ceramiziable heat-resistant adhesive,” *Polymers*, 16(4), 2024.

[89] H. Lee and K. Neville, Handbook of Epoxy Resins. in McGraw-Hill classic handbook reissue. McGraw-Hill, 1967. [Online]. Available: https://books.google.com.my/books?id=3kVqAAAAMAAJ

[90] C. May, Epoxy Resins: Chemistry and Technology, Second Edition,. CRC Press, 2018. [Online]. Available: https://books.google.com.my/books?id=YlQPEAAAQBAJ

[91] A. Gardziella, L. A. Pilato, and A. Knop, “Phenolic Resins: Chemistry, Reactions, Mechanism,” in *Phenolic Resins: Chemistry, Applications, Standardization, Safety and Ecology*, A. Gardziella, L. A. Pilato, and A. Knop, Eds., Berlin, Heidelberg: Springer Berlin Heidelberg, 2000, pp. 24–82.

[92] A. Gardziella, L. A. Pilato, and A. Knop, “Chemical, Physical and Application Technology Parameters of Phenolic Resins,” in *Phenolic Resins: Chemistry, Applications, Standardization, Safety and Ecology*, A. Gardziella, L. A. Pilato, and A. Knop, Eds., Berlin, Heidelberg: Springer Berlin Heidelberg, 2000, pp. 488–513.

[93] S. Irie and J. Rappolt, “Phenolic Resin for Refractories,” in *Phenolic Resins: A Century of Progress*, L. Pilato, Ed., Berlin, Heidelberg: Springer Berlin Heidelberg, 2010, pp. 503–515.

[94] N. A. Ismail, N. W. M. Zulkifli, Z. Z. Chowdhury, and M. R. Johan, “Functionalization of graphene-based materials: Effective approach for enhancement of tribological performance as lubricant additives,” *Diamond and Related Materials*, 115, 2021.

[95] S. B. Cantürk and J. Kováčik, “Review of recent development in copper/carbon composites prepared by infiltration technique,” *Energies*, 15(14), pp. 1–22, 2022.

[96] P. Y. Feng, C. J. Tu, Z. K. Chen, G. Wei, and Z. P. Gu, “The effect of sulfonated graphene oxide on the current-carrying wear characteristics of a resin matrix carbon brush,” *Xinxing Tan Cailiao/New Carbon Materials*, 32(4), pp. 352–357, 2017.

[97] P. Hidalgo-Manrique, X. Lei, R. Xu, M. Zhou, I. A. Kinloch, and R. J. Young, “Copper/graphene composites: a review,” *Journal of Materials Science*, 54(19), pp. 12236–12289, 2019.

[98] L. Sun, L. Bai, H. Chang, J. Liu, and Z. Li, “Research progress on copper-carbon/carbon composites,” *Composite Interfaces*, 32(3), pp. 321–347, 2025.

[99] Y. Chen, C. Tu, Y. Liu, P. Liu, P. Gong, G. Wu, X. Huang, J. Chen, T. Liu, and J. Jiang, “Microstructure and mechanical properties of carbon graphite composites reinforced by carbon nanofibers,” *Carbon Letters*, 33(2), pp. 561–571, 2023.

[100] A. Duhain, “Copper – CNT interfacing with Cu-doped and resistance decrease upon soft annealing,” pp. 11900–11909, 2021.

[101] B. J. Kim, S. Y. Oh, H. S. Yun, J. H. Ki, C. J. Kim, S. Baik, and B. S. Lim,

"Synthesis of Cu-CNT nanocomposite powder by ball milling.," *Journal of nanoscience and nanotechnology*, 9(12), pp. 7393–7397, 2009.

[102] H. Jiang, L. Cooke, K. Srivilliputhur, M. A. McGuire, H. M. I. I. I. Meyer, M. Yoon, J. Haynes, K. Nawaz, A. R. Lupini, K. Li, and T. Aytug, "Copper–Carbon Nanotube Composites Enabled by Brush Coating for Advanced Conductors," *ACS Applied Nano Materials*, 7(10), pp. 11176–11183, 2024.

[103] O. A. Afolabi and N. Ndou, "Synergy of hybrid fillers for emerging composite and nanocomposite materials—a review," *Polymers*, 16(13), 2024.

[104] S. Z. Al Sheheri, Z. M. Al-Amshany, Q. A. Al Sulami, N. Y. Tashkandi, M. A. Hussein, and R. M. El-Shishtawy, "The preparation of carbon nanofillers and their role on the performance of variable polymer nanocomposites," *Designed Monomers and Polymers*, 22(1), pp. 8–53, 2019.

[105] A. Ketema and D. Worku, "Results in chemistry recent advances of graphene-based materials for emerging technologies," *Results in Chemistry*, 5, pp. 100971, 2023.

[106] L. N. Dyachkova and E. E. Feldshtein, "Journal of Materials Science & Technology Microstructures , Strength Characteristics and Wear Behavior of the Fe-based P / M Composites after Sintering or Infiltration with Cu – Sn Alloy," *Journal of Materials Science & Technology*, 31(12), pp. 1226–1231, 2015.

[107] P. C. Angelo, R. Subramanian, and B. Ravisankar, "Powder metallurgy, second edition: science, technology and applications," PHI Learning Pvt. Ltd., 2022.

[108] Q. Porter, X. Li, and C. Ma, "Pressing and Infiltration of Metal Matrix Nanocomposites," 2021.

[109] J. Long, W. Guan, H. Qiu, H. Yin, and M. Yin, "Synergistic effect of steam and sand grains on sliding wear properties of metal-impregnated pantograph strip," *Journal of Materials Engineering and Performance*, 33(24), pp. 14150–14160, 2024.

[110] C. P. Samal, J. S. Parihar, and D. Chaira, "The effect of milling and sintering techniques on mechanical properties of Cu – graphite metal matrix composite prepared by powder metallurgy route," *Journal of Alloys and Compounds*, 569, pp. 95–101, 2013.

[111] S. K. Sharma, S. Gajević, L. K. Sharma, D. G. Mohan, Y. Sharma, M. Radojković, and B. Stojanović, "Significance of the powder metallurgy approach and its processing parameters on the mechanical behavior of magnesium-based

materials," *Nanomaterials*, 15(2), 2025.

[112] N. B. Pradeep, S. Parameshwara, S. G. Chethan, V. Lokesh, T. S. Harish, S. Basavarajappa, and K. B. Girisha, "Mechanism of ball milling and the factors affecting the process of milling," in *Mechanically alloyed novel materials: processing, applications, and properties*, S. Rajendrachari, Ed., Singapore: Springer Nature Singapore, 2024, pp. 1–10.

[113] S. Shrestha, B. Wang, and P. Dutta, "Nanoparticle processing : Understanding and controlling aggregation," *Advances in Colloid and Interface Science*, 279, pp. 102162, 2020.

[114] G. Shiju, "Warm compaction of powder," in *The ECPH Encyclopedia of Mining and Metallurgy*, X. Kuangdi, Ed., Singapore: Springer Nature Singapore, 2024, pp. 2298–2299.

[115] P. Wang, Z. Zhu, J. Liu, H. Wang, J. Pang, and J. Zhang, "Finemet nanocrystalline magnetic powder cores: Application of binder and warm compaction process," *Journal of Magnetism and Magnetic Materials*, 596(171985), 2024.

[116] W. D. Callister and D. G. Rethwisch, Materials Science and Engineering an Introduction, Eighth. John Wiley & Sons, Ltd, 2009.

[117] Y. Zhao, Y. Li, F. Ma, X. Xing, S. Wang, T. Hong, C. Zhang, and X. Jing, "Optimization of crosslinked network structure of cured phenolic resin with high char yield," *Polymer Degradation and Stability*, 231, pp. 111073, 2025.

[118] J.-P. Corriou and C. Azzaro-Pantel, "Process optimization strategies," in *Green Process Engineering*, (January), 2015, pp. 27–48.

[119] B. Durakovic, "Design of experiments application, concepts, examples: State of the art," *Periodicals of Engineering and Natural Sciences*, 5(3), pp. 421–439, 2017.

[120] M. Tanco, N. Costa, and E. Viles, "Experimental design selection: Guidelines for practitioners," *International Journal of Productivity and Quality Management - Int J Prod Qual Manag*, 4, 2009.

[121] D. C. Montogomery, Design and Analysis of Experiments, Eighth. John Wiley & Sons, Inc, 2012.

[122] P. Ravindran, K. Manisekar, P. Narayanasamy, N. Selvakumar, and R. Narayanasamy, "Application of factorial techniques to study the wear of Al hybrid composites with graphite addition," *Materials and Design*, 39, pp. 42–54,

2012.

[123] G. P. Jadhav, “Optimization of EDM process withTaguchi, Grey relational analysis and fuzzy logic technique,” *International Journal of Scientific Development and Research*, 2(11), pp. 104–109, 2017.

[124] J. Antony and M. Kaye, “The Taguchi Approach to Quality Improvement,” in *Experimental Quality*, Kluwer Academic Publishers, 2000, pp. 17–46.

[125] R. Petersen, R. Link, and R. Rushforth, “Review of design experiments using the Taguchi approach: 16 steps to product and process improvement,” *Journal of Testing and Evaluation*, 29(6), pp. 588, 2001.

[126] T. P. Bagchi and T. Fearn, Taguchi Methods Explained: Practical Steps to Robust Design, 12. Prentice-Hall of India, 1993.

[127] C. Hamzaçebi, “Taguchi Method as a Robust Design Tool,” *Quality Control - Intelligent Manufacturing, Robust Design and Charts*, 2021.

[128] M. S. Phadke, Quality Engineering Using Robust Design. in Prentice-Hall International editions. Prentice Hall, 1989. [Online]. Available: https://books.google.com.my/books?id=TZoQAQAAMAAJ

[129] D. C. Montgomery, Introduction to Statistical Quality Control. in EMEA edition. Wiley, 2019. [Online]. Available: https://books.google.com.my/books?id=YWLNEAAAQBAJ

[130] T. Zhang, Q. Cheng, Z. Xu, B. Jiang, C. Wang, and Y. Huang, “Improved interfacial property of carbon fiber composites with carbon nanotube and graphene oxide as multi-scale synergetic reinforcements,” *Composites Part A*, 125, pp. 105573, 2019.

[131] X. Zhao, X. Ren, Z. Chen, and C. Ge, “Materials characterization enhancement of mechanical and electrical properties of copper matrix composites by different types of carbon nanotubes,” *Materials Characterization*, 218(P2), pp. 114575, 2024.

[132] H. Yang, K. Wang, Y. Liu, L. Fu, X. Cui, G. Jiang, and B. Hu, “The formation of the delamination wear of the pure carbon strip and its influence on the friction and wear properties of the pantograph and catenary system,” *Wear*, 454–455, 2020.

[133] M. Freschi, A. Arrigoni, O. Haiko, L. Andena, J. Kömi, C. Castiglioni, and G. Dotelli, “Physico-mechanical properties of metal matrix self-lubricating composites reinforced with traditional and nanometric particles,” *Lubricants*,

10(3), 2022.

[134] Y. Li, J. Huang, M. Wang, J. Liu, C. Wang, H. Zhong, and Y. Jiang, "Microstructure and current carrying wear behaviors of copper/sintered–carbon composites for pantograph sliders," *Metals and Materials International*, 27(9), pp. 3398–3408, 2021.

[135] K. Shibata, T. Yamaguchi, J. Mishima, and K. Hokkirigawa, "Friction and wear properties of copper/carbon/RB ceramics composite materials under dry condition," *Tribology Online*, 3(4), pp. 222–227, 2008.

[136] K. Shibata, T. Yamaguchi, and K. Hokkirigawa, "Friction and wear properties of copper/carbon/rice bran ceramics composite under water-lubricated condition," *Tribology Online*, 6(4), pp. 180–184, 2011.

[137] P. Wang, F. Xie, D. Wexler, J. Yin, H. Zhang, and H. Zhu, "Tribological behaviors of copper modified carbon/carbon composites for pantograph strip under electric current conditions," *Tribology International*, 185, pp. 108483, 2023.

[138] X. Guo, Y. Yang, K. Song, and L. Shaolin, "Arc erosion resistance of hybrid copper matrix composites reinforced with CNTs and micro-TiB2 particles," *Journal of Materials Research and Technology*, 11, pp. 1469–1479, 2021.

[139] X. Jiang, H. C. Fang, P. Xiao, T. Liu, J. M. Zhu, Y. C. Wang, P. F. Liu, and Y. Li, "Influence of carbon coating with phenolic resin in natural graphite on the microstructures and properties of graphite/copper composites," *Journal of Alloys and Compounds*, 744, pp. 165–173, 2018.

[140] A. Gomez-Sanchez, V. A. Franco-Luján, H. M. Alfaro-López, L. Hernández-Sánchez, H. Cruz-Martínez, and D. I. Medina, "Carbon material-reinforced polymer composites for bipolar plates in polymer electrolyte mmembrane fuel cells," *Polymers*, 16(5), pp. 1–24, 2024.

[141] N. C. I. S. Furuvik, L. Wang, R. Jaiswal, R. Thapa, M. S. Eikeland, and B. M. E. Moldestad, "Experimental study and SEM-EDS analysis of agglomerates from gasification of biomass in fluidized beds," *Energy*, 252, pp. 124034, 2022.

[142] "ASTM B193-20 Standard Test Method for Resistivity of Electrical Conductor Materials."

[143] "ASTM D785-23 Standard Test Method for Rockwell of Plastics and Electrical Insulating Materials."

[144] "ASTM D790-17 Standard Test Methods for Flexural Properties of Unreinforced

and Reinforced Plastics and Electrical Insulating Materials."

[145] Y. Singh, "Electrical resistivity measurements: a review," *International Journal of Modern Physics: Conference Series*, 22(October), pp. 745–756, 2013.

[146] ASTM Internacional, "Standard Specification for Wire Cloth and Sieves for Testing Purposes ASTM 11-95," 1995.

[147] S. D. M. Lakshani, D. B. H. I. Bandara, and R. C. L. De Silva, "Mass scale production and purification of graphite oxide from Sri Lankan vein graphite and spectroscopic characterization," 24(2), pp. 98–109, 2023.

[148] J. Hlosta, D. Žurovec, L. Jezerská, J. Zegzulka, and J. Nečas, "Effect of particle shape and size on the compressibility and bulk properties of powders in powder metallurgy," *METAL 2016 - 25th Anniversary International Conference on Metallurgy and Materials, Conference Proceedings*, pp. 1394–1399, 2016.

[149] C. Ma, R. Qu, C. Zhu, H. Liu, and T. Wang, "Microscopic study of the impact of particle morphology on the compressibility of calcareous sands," *Powder Technology*, 433, 2024.

[150] A. A. Bunaciu, E. gabriela Udriştioiu, and H. Y. Aboul-Enein, "X-Ray Diffraction: Instrumentation and Applications," *Critical Reviews in Analytical Chemistry*, 45(4), pp. 289–299, 2015.

[151] M. Salvatore, G. Carotenuto, S. De Nicola, C. Camerlingo, V. Ambrogi, and C. Carfagna, "Synthesis and characterization of highly intercalated graphite bisulfate," *Nanoscale Research Letters*, 12(1), 2017.

[152] N. D. Nikolic, L. Avramovic, E. R. Ivanovic, V. M. Maksimovic, Z. Bascarevic, and N. Ignjatovic, "Comparative morphological and crystallographic analysis of copper powders obtained under different electrolysis conditions," *Transactions of Nonferrous Metals Society of China*, 29(6), pp. 1275–1284, 2019.

[153] Z. Jia, Y. X. Liu, and G. L. Li, "Preparing Phenolic Resin / Calcium Carbonate Nanocomposites by Polymerization In Situ," in *Environment Materials and Environment Management, EMEM2011*, in Advanced Materials Research, vol. 281. Trans Tech Publications Ltd, 2011, pp. 267–269.

[154] Z.-L. Yu, Y.-C. Gao, B. Qin, Z.-Y. Ma, and S.-H. Yu, "Revitalizing traditional phenolic resin toward a versatile platform for advanced materials," *Accounts of Materials Research*, 5(2), pp. 146–159, 2024.

[155] W. Gul and H. Alrobei, "Effect of graphene oxide nanoparticles on the physical and mechanical properties of medium density fiberboard," *Polymers*, 13(11), pp.

1–15, 2021.

[156] C. Monteserín, M. Blanco, E. Aranzabe, A. Aranzabe, J. M. Laza, A. Larrañaga-Varga, and J. L. Vilas, “Effects of graphene oxide and chemically-reduced graphene oxide on the dynamic mechanical properties of epoxy amine composites,” *Polymers*, 9(9), pp. 1–16, 2017.

[157] S. Nasiri, M. Rabiei, A. Palevicius, G. Janusas, A. Vilkauskas, V. Nutalapati, and A. Monshi, “Modified Scherrer equation to calculate crystal size by XRD with high accuracy, examples Fe2O3, TiO2 and V2O5,” *Nano Trends*, 3, pp. 100015, 2023.

[158] S. H, “Synthesis of carbon nanotubes for oil-water interfacial tension reduction,” *Oil & Gas Research*, 1(1), pp. 1–6, 2015.

[159] B. Ya, Y. Xu, L. Meng, B. Zhou, J. Zhao, X. Chen, and X. Zhang, “Fabrication of Copper Matrix Composites Reinforced with Molecular-Level-Mixing Method,” *Materials*, 115(6488), pp. 1–11, 2022.

[160] M. I. M. Ahmad, M. A. M. Muzafa, M. F. M. Tahir, M. S. Rahmat, M. A. M. Sabri, and M. Selamat, “Physical and mechanical properties of local carbon materials and warm compaction method on the production of current collectors for Light Rail Transit (LRT) applications,” *Journal of Mechanical Engineering*, 21(3), pp. 319–331, 2024.

[161] K. Yaman and Ö. Taga, “Thermal and electrical conductivity of unsaturated polyester resin filled with copper filler composites,” *International Journal of Polymer Science*, 2018, 2018.

[162] Y. Yim and B. Kim, “Preparation and Characterization of Activated Carbon / Polymer Composites : A Review,” pp. 1–14, 2023.

[163] V. Casalegno, M. Salvo, and M. Ferraris, “Surface modification of carbon / carbon composites to improve their wettability by copper,” *Carbon*, 50(6), pp. 2296–2306, 2012.

[164] Powder Characteristics Guidebook. Ltd., Bettersize Instrument, 2025.

[165] J. V Shugart and R. C. Scherer, “United States Patent Application Publication. Pub. No.: US 2010/0327233 A1. Copper-Carbon Composition,” 2010

[166] A. Joulain, V. Audurier, P. Gadaud, J. Bonneville, C. Azina, Y. Lu, and J. F. Silvain, “Correlation of the mechanical properties of Cu/C composite materials with the chemistry of Cu C interfacial zone,” *Materials Characterization*, 179, 2021.

[167] M. Cerny, J. Petrus, and I. Chamradova, “The Influence of Porosity on Mechanical Properties of PUR-Based Composites : Experimentally Derived,” *Polymers*, 15(1960), pp. 1–19, 2023.

[168] A. Manalo and W. Ferdous, “Mechanical and Durability Characteristics of Particulate-Filled Recycled Thermoplastic Composites (RTCs): A Comprehensive Review,” pp. 1–35, 2025.

[169] M. Li and R. Luo, “Effect of carbon fiber content on mechanical and tribological properties of carbon/phenolic resin composites,” *Proceedings of the 5th International Conference on Information Engineering for Mechanics and Materials*, 21, pp. 539–542, 2015.

[170] A. E. Pramono, Y. Patrickr, and N. Indayaningsih, “MBI The electrical properties of composite fabricated of carbon- phenol formaldehyde,” 01(04), pp. 1–10, 2023.

[171] Z. Z. Fang, “Correlation of transverse rupture strength of WC-Co with hardness,” *International Journal of Refractory Metals and Hard Materials*, 23(2), pp. 119–127, 2005.

[172] P. Geffroy, J. Silvain, and J. Heintz, “Elaboration and properties of carbon fibre reinforced copper matrix composites,” in *Advances in Composite Materials - Ecodesign and Analysis*, 2023.

[173] A. I. Rudskoy, A. G. Nasibulin, T. S. Koltsova, and O. V. Tolochko, “Novel metal matrix/carbon composites for airspace applications,” *29th Congress of the International Council of the Aeronautical Sciences, ICAS 2014*, (September), 2014.

[174] Z. Chen, H. C. Fang, J. M. Zhu, J. W. Li, Y. X. Xu, Z. Sun, F. Chen, and P. Xiao, “Effect of carbon type and morphology on the microstructure and properties of carbon / copper composites,” 461(August), 2020.

[175] J. Liu, K. Sun, L. Zeng, J. Wang, X. Xiao, and J. Liu, “Microstructure and properties of copper–graphite composites fabricated by spark plasma sintering based on two-step mixing,” *Metals*, 10(1506), 2020.

[176] M. A. Selamat and A. A. Mahaidin, “Method for fabrication of C-Cu composites using local oil palm kernel shell material,” *World Journal of Engineering Research and Technology*, 3(3), pp. 397–407, 2017.

[177] Y. Choi, Y. Lee, and J. Kim, “Optimization of Pore Characteristics of Graphite-Based Anode for Li-Ion Batteries by Control of the Particle Size Distribution,”

Materials, 16(6896), 2023.

[178] A. G. Tafere and A. G. Gerezgiher, "Effect of graphite additive on physical , mechanical , and wearing properties of Al 2 O 3 / E-glass / phenol formaldehyde hybrid composite grinding wheel," *Composites and Advanced Materials*, 33, pp. 1–10, 2024.

[179] J. Smole, P. Olesik, K. St, M. Miku, H. Myalska-g, M. Engineering, M. Miku, H. Myalska-głowacka, and A. Gawron, "Properties of Epoxy Composites The Influence of Graphite Filler on the Self-Lubricating," *Materials*, 17(1308), 2024.

[180] N. Pourmohammadie, M. Ghassemi, and M. Shahedi, "Advantages and disadvantages of graphite addition on the characteristics of hot-pressed ZrB 2 – SiC composites," *Ceramics International*, 46(7), pp. 8561–8566, 2020.

[181] J. A. Aguiar, S. Kwon, B. D. Coryell, E. Eyerman, A. A. Bokov, R. H. R. Castro, D. Burns, H. T. Hartmann, and E. P. Luther, "Densification of graphite under high pressure and moderate temperature," *Materials Today Communications*, 22(100821), 2020.

[182] S. Zhou, S. Zhang, H. Xiang, W. Xu, K. Sun, C. Fang, W. Xie, H. Wang, and Y. Zhou, "Ultrasonic-Assisted Hot-Press Sintering: A Novel Method to Reduce the Densification Temperature and Enhance the Mechanical and Tribological Properties of Cu–Graphite Composites," *Lubricants*, 13(8), pp. 1–26, 2025.

[183] U. Ulusoy, "A review of particle shape effects on material properties for various engineering applications: from macro to nanoscale," *Minerals*, 13(1), 2023.

[184] P. P. Magampa, N. Manyala, and W. W. Focke, "Properties of graphite composites based on natural and synthetic graphite powders and a phenolic novolac binder," *Journal of Nuclear Materials*, 436(1–3), pp. 76–83, 2013.

[185] E. Baffour-Awuah, S. A. Akinlabi, T. C. Jen, S. Hassan, I. P. Okokpujie, and F. Ishola, "Characteristics of palm kernel shell and palm kernel shell-polymer composites: a review," *IOP Conference Series: Materials Science and Engineering*, 1107(1), pp. 012090, 2021.

[186] H. Y. Saw, J. Janaun, S. Kumaresan, and C. M. Chu, "Characterization of the physical properties of palm kernel cake," *International Journal of Food Properties*, 15(3), pp. 536–548, 2012.

[187] O. Issakah, A. Kayaba, Y. Fiabge, S. Akromah, J. Kpare, and E. Asare, "Effect of partial replacement of CaCO3 with palm kernel shell particles on the mechanical properties of PKS/CaCO3/HDPE hybrid composites," 2024.

[188] M. R. Papabathina, S. Sankara, B. Chinka, N. R. Putta, and M. Vijaya, “Effect of graphite on mechanical and tribological properties of Al6061 / SiC hybrid composites,” *Annales de Chimie - Science des Matériaux*, 47(3), pp. 125–132, 2023.

[189] E. Omrani, A. D. Moghadam, A. K. Kasar, P. Rohatgi, and P. L. Menezes, “Tribological performance of graphite nanoplatelets reinforced Al and Al/Al2O3 self-lubricating composites,” *Materials*, pp. 1–17, 2021.

[190] A. Somayaji, M. Nagaral, C. Anjinappa, M. Q. Alkahtani, R. K. Billady, N. Kumar, V. Auradi, S. Islam, J. R. R. Chowdary, A. Razak, M. A. Khan, and C. K. Naik, “Influence of graphite particles on the mechanical and wear characterization of Al6082 alloy composites,” *ACS Omega*, 8, pp. 26828–26836, 2023.

[191] Q. Liu, M. Castillo-Rodríguez, A. J. Galisteo, R. G. de Villoria, and J. M. Torralba, “Wear behavior of copper–graphite composites processed by field-assisted hot pressing,” *Journal of Composites Science*, 3(1), 2019.

[192] Q. Li, L. Shi, Y. Cai, X. Wang, L. Li, Z. Yuan, W. Tang, and Z. Zhan, “Effect of graphite on microstructure and friction-wear properties of yttria-stabilized zirconia coatings,” *Ceramics International*, 50, pp. 54116–54124, 2024.

[193] S. Sulaymon, I. Raxmatjon, M. Otabek, A. Bunyod, and S. Kim, “Optimization of Copper-Graphite Composite Materials through Spark Plasma Sintering: Impact of Varied Powder Sizes on Physical, Mechanical, and Electrical Properties,” *International Scientific Journal*, 2(11), pp. 185–191, 2023.

[194] Y. Zhou, Z. Huang, J. Wang, and Y. Wang, “Tensile strength of particle reinforced composite with interfacial debonding,” *Engineering Fracture Mechanics*, 303(April), pp. 110110, 2024.

[195] M. M. Ibrahim, N. S. M. El Tayeb, M. Shazly, and M. M. E. S. Seleman, “An experimental study on the effect of graphite microparticles on the mechanical and tribological properties of epoxy matrix composites,” *Functional Composite Materials*, 2024.

[196] D. M. Jarząbek, “The impact of weak interfacial bonding strength on mechanical properties of metal matrix - ceramic reinforced composites,” *Composite Structures*, 2018.

[197] S. Y. Fu, X. Q. Feng, B. Lauke, and Y. W. Mai, “Effects of particle size, particle/matrix interface adhesion and particle loading on mechanical properties

of particulate-polymer composites," *Composites Part B: Engineering*, 39(6), pp. 933–961, 2008.

[198] C. Zuo, L. Xu, Y. Sun, H. Xia, Z. Tang, and G. Zheng, "Effect of interface bonding and properties of graphite / copper composites by microwave pressure sintering," *Journal of Alloys and Compounds*, 976(November 2023), pp. 173009, 2024.

[199] B. Kong, T. Fan, and J. Ru, "Diamond & Related Materials Improved wetting and thermal properties of graphite-Cu composite by Cr-solution immersion method," *Diamond & Related Materials*, 65, pp. 191–197, 2016.

[200] C. Ayyappadas, O. S. Shanu, A. Vijayan, I. A. Mohammed, V. Vishnu, and M. Shamnadh, "Effect of graphene, SiC and graphite addition on hardness, microstructure and electrical conductivity of microwave sintered copper MMCs fabricated by powder metallurgy route," *Journal of Physics: Conference Series*, 1355(1), pp. 1–14, 2019.

[201] L. Ren, Y. Ren, Y. Zhang, K. Orzechowski, K. Kułacz, M. Pocheć, and S.-L. Bai, "Graphite films/carbon fiber fabric/ polyurethane composites with ultrahigh in-plane thermal conductivity and enhanced mechanical properties," *Nanotechnology*, 31(47), 2020.

[202] P. Bayer, P. Rovnaník, and I. Kus, "Effect of water saturation on the electrical properties of cement and alkali-activated slag composites with graphite conductive admixture," *Construction and Building Materials*, 361, 2022.

[203] J. Stabik, "Influence of graphite on electrical properties of polymeric composites," *Archives of Materials Science and Engineering*, 37(1), pp. 37–44, 2009.

[204] Y. Rew, A. Baranikumar, A. V Tamashausky, S. El-tawil, and P. Park, "Electrical and mechanical properties of asphaltic composites containing carbon based fillers," *Construction and Building Materials*, 135, pp. 394–404, 2017.

[205] K. Zhou, Y. Jia, D. Jia, J. Wang, W. Sun, Y. Wang, X. Kong, R. Zhang, and Y. Fu, "Progress of highly conductive graphene-reinforced copper matrix composites: a review," *Journal of Materials Research and Technology*, 33, pp. 7546–7571, 2024.

[206] N. A. Mohd Radzuan, A. B. Sulong, and Iswandi, "Effect of multi-sized graphite filler on the mechanical properties and electrical conductivity," *Sains Malaysiana*, 50(7), pp. 2025–2034, 2021.

[207] A. T. Smith, A. M. LaChance, S. Zeng, B. Liu, and L. Sun, “Synthesis, properties, and applications of graphene oxide/reduced graphene oxide and their nanocomposites,” *Nano Materials Science*, 1(1), pp. 31–47, 2019.

[208] R. Mowlaei, J. Lin, F. Basquiroto de Souza, A. Fouladi, A. Habibnejad Korayem, E. Shamsaei, and W. Duan, “The effects of graphene oxide-silica nanohybrids on the workability, hydration, and mechanical properties of Portland cement paste,” *Construction and Building Materials*, 266, pp. 121016, 2021.

[209] Z. Xiu, J. Sun, X. Li, Y. Chen, Y. Yan, P. Shao, H. Li, B. Ju, W. Yang, and G. Chen, “Study on mechanical and electrical properties of high content CNTs/Cu composites,” *Materials*, 17(3866), 2024.

[210] S. Kumar, “Mechanics of Materials Investigating effect of CNT agglomeration in CNT / polymer nanocomposites using multiscale finite element method,” *Mechanics of Materials*, 183, pp. 104706, 2023.

[211] C. Pan, A. P. S. Gaur, M. Lynn, M. P. Olson, G. Ouyang, and J. Cui, “Enhanced electrical conductivity in graphene–copper multilayer composite,” *AIP Advances*, 12(015310), 2022.

[212] W. A. D. M. Jayathilaka, A. Chinnappan, and S. Ramakrishna, “A review on properties influencing on the conductivity of CNT/Cu composites and their applications in wearable/flexible electronics,” *Journal of Materials Chemistry C*, 2017.

[213] Í. Carneiro, B. Monteiro, B. Ribeiro, and J. V Fernandes, “Production and characterization of Cu/CNT nanocomposites,” *Applied Sciences*, 13(3378), pp. 1–17, 2023.

[214] S. Rathinavel, K. Priyadharshini, and D. Panda, “A review on carbon nanotube: An overview of synthesis, properties, functionalization, characterization, and the application,” *Materials Science and Engineering: B*, 268, pp. 115095, 2021.

[215] N. M. Nurazzi, M. R. M. Asyraf, A. Khalina, N. Abdullah, C. L. Lee, H. A. Aisyah, M. Nor, F. Norrrahim, R. A. Ilyas, M. M. Harussani, and M. R. Ishak, “Nanotube-reinforced polymer composite : an overview,” *Polymers*, 13(7), pp. 1047, 2021.

[216] M. Mirzapour, P. Cousin, M. Robert, and B. Benmokrane, “Dispersion characteristics, the mechanical, thermal stability, and durability properties of epoxy nanocomposites reinforced with carbon nanotubes, graphene, or graphene oxide,” *Polymers*, 16(1836), 2024.

[217] Z. Wu, Y. Zhao, K. Yang, J. Guan, S. Wang, Y. Gu, M. Li, Y. Feng, W. Feng, and R. O. Ritchie, “Enhancing the mechanical performance of fiber-reinforced polymer composites using carbon nanotubes as an effective nano-phase reinforcement,” *Advanced Materials Interfaces*, 10(3), 2023.

[218] K. Preethi, T. N. Raju, and H. A. Shivappa, “Development and Characterization of Carbon Nanotube Reinforced Aluminium-6061 Metal Matrix Composites,” *Journal of Minerals and Materials Characterization and Engineering*, 09(03), pp. 290–300, 2021.

[219] C. A. Amadei, P. Arribas, and C. D. Vecitis, “Graphene oxide standardization and classification: Methods to support the leap from lab to industry,” *Carbon*, 133(March), pp. 398–409, 2018.

[220] R. Chen, C. Feng, J. Yang, Z. Hang, Y. Fan, and J. Zhang, “Data-driven prediction of electrical resistivity of graphene oxide/cement composites considering the effects of specimen size and measurement method,” *Buildings*, 14(8), 2024.

[221] A. Ghorbani, S. Sheibani, and A. Ataie, “Microstructure and mechanical properties of consolidated Cu-Cr-CNT nanocomposite prepared via powder metallurgy,” *Journal of Alloys and Compounds*, 732, pp. 818–827, 2018.

[222] Z. Zheng, A. Yang, J. Tao, J. Li, W. Zhang, X. Li, and H. Xue, “Mechanical and conductive properties of Cu matrix composites reinforced by oriented carbon nanotubes with different coatings,” *Nanomaterials*, 12(266), 2022.

[223] D. Janas and B. Liszka, “Copper matrix nanocomposites based on carbon nanotubes or graphene,” *Materials Chemistry Frontiers*, 2(1), pp. 22–35, 2018.

[224] S. Silva, J. M. Barbosa, J. D. Sousa, M. C. Paiva, and P. F. Teixeira, “High-performance PEEK/MWCNT nanocomposites: combining enhanced electrical conductivity and nanotube dispersion,” *Polymers*, 16(5), 2024.

[225] S. Bagchi, A. Harpale, and H. B. Chew, “Interfacial load transfer mechanisms in carbon nanotube-polymer nanocomposites,” *Proceedings of the Royal Society A: Mathematical, Physical and Engineering Sciences*, 474(2216), 2018.

[226] N. S. Shaari, M. H. Ismaill, A. Jumahat, and R. Goodall, “Sintering and dimensional analysis of Cu/CNTs via a powder metallurgy route,” *Journal of Mechanical Engineering*, 17(3), pp. 117–130, 2020.

[227] M. Soleymani, A. R. Ghasemi, and B. Moslemi-Abyaneh, “Agglomerated carbon nanotubes effects on buckling behavior of fiber metal laminated nanocomposite

shells," *Polymers and Polymer Composites*, 30, pp. 1–16, 2022.

[228] L. Elbakyan and I. Zaporotskova, "Polypropylene modified with carbon nanomaterials: structure, properties and application (a review)," *Polymers*, 17(4), pp. 1–28, 2025.

[229] D. Jagannathan, H. Adarsha, K. Ramaiah, and R. Neralur, "A systematic study on mechanical properties of CNT reinforced HDPE composites developed using 3D printing," *Iranian Journal of Materials Science and Engineering*, 20(3), pp. 1–16, 2023.

[230] Y. Ding, Z. Shi, Z. Li, S. Jiao, J. Hu, X. Wang, Y. Zhang, H. Wang, and X. Guo, "Effect of CNT content on microstructure and properties of CNTs/refined-AZ61 magnesium matrix composites," *Nanomaterials*, 12(2432), 2022.

[231] M. Gholami-Kermanshahi, Y. C. Hsiao, G. Lange, and S. H. Chang, "Effects of carbon nanotube addition on the microstructures, martensitic transformation, and internal friction of Cu–Al–Ni shape-memory alloys," *Scientific Reports*, 13(1), pp. 1–12, 2023.

[232] K. M. Joseph, K. Brittingham, V. K. R. Kondapalli, M. Khosravifar, A. A. Raut, B. D. Karsten, H. J. Kasparian, N. Phan, A. Kamath, A. S. Almansour, M. Lizcano, D. Santiago, D. Mast, and V. Shanov, "Lightweight copper–carbon nanotube core–shell composite fiber for power cable application," *Journal of Carbon Research*, 9(43), 2023.

[233] D. Punera, "The effect of agglomeration and slightly weakened CNT–matrix interface on free vibration response of cylindrical nanocomposites," *Acta Mechanica*, 232(6), pp. 2455–2477, 2021.

[234] S. Hu, Y. Xu, J. Wang, P. Zhang, and J. Guo, "Modification effects of carbon nanotube dispersion on the mechanical properties, pore structure, and microstructure of cement mortar," *Materials*, 13(5), 2020.

[235] J. A. Cherry, H. M. Davies, S. Mehmood, N. P. Lavery, S. G. R. Brown, and J. Sienz, "Investigation into the effect of process parameters on microstructural and physical properties of 316L stainless steel parts by selective laser melting," *International Journal of Advanced Manufacturing Technology*, 76(5–8), pp. 869–879, 2015.

[236] T. Takahashi, S. Tsubo, K. Inoue, R. Suzuki, H. Murata, and M. Tachibana, "Effect of dispersibility of carbon nanotubes on the hardness and thermal properties of polyphenylene sulphide/carbon nanotube composites obtained

using solution mixing and melt blending methods," *Materials Science and Engineering: B*, 295(May), pp. 116579, 2023.

[237] X. Yuan, H. Zhu, H. Ji, and Y. Zhang, "Effect of CNT contents on the microstructure and properties of CNT/TiMg composites," *Materials*, 12(1620), pp. 1–9, 2019.

[238] A. Pasha and B. M. Rajaprakash, "Effect of CNT content on microstructure and hardness of AlSi/MWCNT nano composite," *Materials Today: Proceedings*, 49, pp. 1345–1350, 2021.

[239] J. Kang, S. Al-Sabah, and R. Théo, "Effect of single-walled carbon nanotubes on strength properties of cement composites," *Materials*, 13(6), pp. 1–12, 2020.

[240] B. Earp, J. Simpson, J. Phillips, D. Grbovic, S. Vidmar, J. McCarthy, and C. C. Luhrs, "Electrically conductive CNT composites at loadings below theoretical percolation values," *Nanomaterials*, 9(4), pp. 1–17, 2019.

[241] B. Earp, J. Phillips, D. Grbovic, S. Vidmar, M. Porter, and C. C. Luhrs, "Impact of current and temperature on extremely low loading epoxy-CNT conductive composites," *Polymers*, 12(4), pp. 1–17, 2020.

[242] A. Inam, R. Brydson, and D. V. Edmonds, "Raman spectroscopy study of the crystallinity of graphite formed in an experimental free-machining steel," *Materials Characterization*, 163, 2020.

[243] W. Ma, Y. Liu, X. Wang, and B. Su, "Friction and wear properties of spark plasma sintered Cu-15Ni-8Sn/graphite self-lubricating composites," *Mocaxue Xuebao/Tribology*, 44(4), pp. 509–518, 2024.

[244] K. Nepal, C. Ugwumadu, F. Kraft, Y. Al-Majali, and D. A. Drabold, "The effects of crystal orientation and common coal impurities on electronic conductivity in copper–carbon composites," *Carbon*, 231, 2025.

[245] W. Daoush, A. Swidan, G. A. El-Aziz, and M. Abdelhalim, "Fabrication, microstructure, thermal and electrical properties of copper heat sink composites," *Materials Sciences and Applications*, 07, pp. 542–561, 2016.

[246] A. Eiling and J. S. Schilling, "Pressure and temperature dependence of electrical resistivity of Pb and Sn from 1-300K and 0-10 GPa-use as continuous resistive pressure monitor accurate over wide temperature range; Superconductivity under pressure in Pb, Sn and in," *Journal of Physics F: Metal Physics*, 11(3), pp. 623–639, 1981.

[247] P. S. Liu, T. F. Li, and C. Fu, "Relationship between electrical resistivity and

porosity for porous metals," 268, pp. 208–215, 1999.

[248] M. Tokita, "Progress of spark plasma sintering (SPS) method, systems, ceramics applications and industrialization," *Ceramics*, 4, pp. 160–198, 2021.

[249] P. C. Verma, P. Aswath, G. Straffelini, and S. Gialanella, "Carbonaceous decomposition products at high temperatures and their interfacial role in the friction behaviour of composite brake material," *Lubricants*, 12, pp. 1–15, 2024.

[250] S. S. Feng, H. R. Geng, and Z. Q. Guo, "Effect of lubricants on warm compaction process of Cu-based composite," *Composites Part B: Engineering*, 43(3), pp. 933–939, 2012.

[251] C. X. Hu, T. L. Ngai, J. J. Zheng, Z. Y. Xiao, and Y. Y. Li, "Warm flow compaction forming of complex part by using binder-treated powder," *Materials Science Forum*, 628–629, pp. 581–586, 2009.

[252] M. Tian, J. Xu, S. Yang, J. Wang, T. Yang, G. Li, Q. Chen, and X. Liu, "Effects of heat treatment and compaction pressure on the microstructure and magnetic properties of core-shell structured FeSiBNbCu/SiO2 soft magnetic composites," *Journal of Alloys and Compounds*, 923, pp. 166394, 2022.

[253] Y. Mahani and H. Zuhailawati, "Effect of compaction pressure on microstructure and properties of copper-based composite prepared by mechanical alloying and powder metallurgy," *Advanced Materials Research*, 795, pp. 343–346, 2013.

[254] I. V. Terekhov and E. M. Chistyakov, "Binders used for the manufacturing of composite materials by liquid comsposite molding," *Polymers*, 14(87), pp. 101–136, 2021.

[255] H. Hu, W. Wang, L. Jiang, L. Liu, Y. Zhang, Y. Yang, and J. Wang, "Curing mechanism of resole phenolic resin based on variable temperature FTIR spectra and thermogravimetry-mass spectrometry," *Polymers and Polymer Composites*, 30(1), pp. 1–11, 2022.

[256] M. Grandin and U. Wiklund, "Wear phenomena and tribofilm formation of copper/copper-graphite sliding electrical contact materials," *Wear*, 398–399, pp. 227–235, 2018.

[257] B. R. Gupta, "Friction and wear mechanism of polymers, their composites and nanocomposites," in *Elsevier Series on Tribology and Surface Engineering*, T. of Polymers, Ed., Elsevier, 2023, pp. 51–117.

[258] Z. Li, J. Liu, S. Lu, F. Liu, G. Yang, and J. Wang, "Effect of graphite content on mechanical properties and high-temperature tribological behavior of Cu-Ni-Sn-

Mo-Gr self-lubricating composites," *Lubricants*, 13(10), pp. 428, 2025.

[259] Gamze Ispirlioglu Kara, Sinan Sezek, and Bunyamin Aksakal, "Enhanced mechanical, tribological and corrosion properties of graphite and carbon nanotube-reinforced copper-based hybrid composites," *Journal of Composite Materials*, 58(27), pp. 2915–2935, 2024.

[260] W. Camp, E. Diaz, and B. Wawak, Electron Microscopy of Shale Hydrocarbon Reservoirs. 2013.

[261] H. X. Guo and J. F. Yang, "Fabrication and tribological properties of mesocarbon microbead-Cu friction composites," *Materials*, 13(2), 2020.

[262] R. Li, Y. Yin, K. Zhang, R. Song, and Q. Chen, "Effects of ball milling and load on transfer film formation of copper-based composites," *Industrial Lubrication and Tribology*, 74(9), pp. 1056–1062, 2022.

[263] J. Wu, Z. Li, G. Wen, Z. Gao, Y. Li, and Y. Zhao, "Friction mechanism analysis of copper-based composites reinforced with ball-milled and modified composite ceramic powders," 529, 2023.

[264] A. Shirani, Y. Li, O. L. Eryilmaz, and D. Berman, "Tribocatalytically-activated formation of protective friction and wear reducing carbon coatings from alkane environment," *Scientific Reports*, 11(1), pp. 1–9, 2021.

AUTHOR'S PROFILE



Fazira Suriani Mohamed Fadzil obtained a Bachelor of Engineering (Honours) B.Eng. (Hons.) in Chemical Engineering in 2003 and a Master of Science (M.Sc) in Chemical Engineering in 2007 from Universiti Teknologi PETRONAS, Seri Iskandar, Malaysia. Her PhD thesis involves the development of a carbon-copper composite through the warm compaction method using different types of carbon and fillers for a pantograph slide in rail applications. The design of the experiment utilises the Taguchi Method for identification of optimum condition of the process parameters. Currently, she is also working on the development and field test of a current collector made of carbon-copper composite for the third-rail system, a project under the MOSTI grant at her workplace, SIRIM Berhad. Her research includes the development and characterisation of the carbon-copper composite from natural carbon (PKS-derived carbon) for localisation of the current collectors. The project has progressed to the prototype fabrication stage at laboratory scale, and the samples are scheduled for field testing with Prasarana as well as third-party evaluation in Thailand and Germany.

LIST OF PUBLICATION:

F. S. Mohamed Fadzil, K. M. Hyie, N. C. Maideen, N. A. M. Fohimi, N. S. Abdullah, and M. A. Abd Mutalib, "Influence of Carbon Nanotube (CNT) Addition and Post-Baking Process on the Mechanical and Electrical Properties of Carbon-Copper Composites," Solid State Phenomena, 2026. 392: pp. 53–62.

Hyie K.M., Fadzil F.S.M., Selamat M.A., Othman E.A., Mahaidin A.A., "Effect of palm kernel shell and graphene oxide incorporation on the physical, electrical, and wear properties of carbon-copper composite for railway pantograph slides", Jurnal Tribologi, 2025. 44: pp. 167 – 182.

Fadzil F.S.M., Hyie K.M., Selamat M.A., Othman E.A., Mahaidin A.A., "Effects of Carbon Type and Composition on the Properties of Carbon-Copper Composite as Pantograph Slide in Railway Application", Journal of Mechanical Engineering, 2024. 13: pp. 1 – 15.

Fadzil F.M., Hyie K.M., Selamat M.A., "Development And Characterisation Of Pantograph Slides For Railway Applications: A Short Review", Jurnal Mekanikal, 2023. 46: pp. 38 – 47.

AWARDS RECEIVED:

SIRIM Invention, Innovation, and Technology Expo (Si2TE) 2025
MyCarbonRail: Reinventing Rail with Local Carbon (Team Leader)
Gold Award

International Invention, Innovation, Technology Competition and Exhibition (ITEX) 2024
Pilot Manufacturing Process of Producing Local-Material-Based Current Collector for Rail Application (Team Member)
Gold Award

OTHER RELATED ACHIEVEMENT:

Outstanding Oral Presenter

2025 International Conference on Advanced Materials, Mechanical Engineering, and Manufacturing, Langkawi, Kedah, 19 – 21 November 2025. Title of Paper presented: Influence of Carbon Nanotube (CNT) Addition and Post-baking Process on the Mechanical and Electrical Properties of Carbon-Copper Composites.

2nd Place, Best Oral Presentation

SIRIM Scholastic Retreat, SIRIM Bukit Jalil, Selangor, 15 – 16 July 2024.

Top 10

Postgraduate Research Image Competition (PRIC) 2025.